DEVELOPMENT OF A NOVEL STIMULI RESPONSIVE FILTRATION MEMBRANE USING SELF-ASSEMBLING PEPTIDES

A thesis submitted in partial fulfilment of the requirements for the degree of

Doctor of Philosophy in Chemical and Process Engineering

University of Canterbury

by

PRASANNA PONNUMALLAYAN

Department of Chemical and Process Engineering,

University of Canterbury,

Christchurch, New Zealand

2014

Abstract

Membrane based separation of specific constituents from a complex mixture is a well-established technology. Numerous filtration membranes have been developed for separations based on size, charge and hydrophobicity. Alternatively, synthetic membranes have been modified using various materials (e.g. charged polymers), to induce stimuli responsiveness and achieve specific separation goals. However, controlling finer separations based on more complex properties has been a challenge. Further improvements in separations could be made with a universal membrane that could be used for a wide range of applications. This thesis describes the development of a novel stimuli-responsive membrane whose pores and surface are functionalised with self-assembling peptides (SAPs). SAPs are molecules that spontaneously organize into ordered structures through non-covalent interactions, in response to external stimuli. The use of reversible SAPs to control membrane permeability could possibly result in a more effective separation process, whereby a condition such as pH could be used to enable or block passage of certain solutes through the membrane. To progress towards achieving this goal, the following sub-objectives were addressed, i) to identify a suitable reversible SAP and examine the effect of conjugating it with a poly(ethylene glycol) (PEG) polymer spacer on self-assembly, ii) to functionalise a membrane surface and subsequently tether the SAP via the spacer molecule, whilst retaining the self-assembling behaviour on the membrane surface.

Initially, peptide P11-4 (QQRFEWEFEQQ) was chosen as the candidate for membrane tethering, because it can spontaneously switch molecular conformation from random coil at high pH to β sheet at low pH. P11-4 was conjugated to a 2 kDa N-hydroxy succinimide-activated PEG via N-terminal amine coupling to form P11-4-PEG-2K and the conjugation was validated using MALDI-tof spectrometry. However, P11-4-PEG-2K did not retain self-

assembly of the peptide P11-4 but instead retained its random coil structure at pH < 3, in contrast to the behaviour of native P11-4, which formed β sheets at similar pH. P11-4-PEG-2K retained its random coil conformation across various pH conditions (pH 2.5, 7 and 11) and incubation periods (2 min-20 days). Additional investigations on the effect of unreacted free PEG on P11-4 self-assembly indicated that the presence of free PEG in solution did not hinder self-assembly. Further, conjugation carried out in 3 mM sodium phosphate buffer and water also resulted in P11-4-PEG-2K that lost its ability to form β sheets at pH 2.5. Thus, P11-4-PEG-2K was deemed unsuitable for membrane modification and an alternative peptide EL-5F (ELELELELELF), with pH responsiveness, was used for further investigations on bioconjugate self-assembly in solution and upon being tethered to a membrane surface.

For the first time, rapid and reversible pH-regulated self-assembly of EL-5F and its conjugates with 2 and 5 kDa PEG (EL-5F-PEG-2K and EL-5F-PEG-5K) was demonstrated. Circular dichroism indicated the formation of β sheet structures at pH < 5.9, 5.8 and 5.4 and disassembly to random coils above those pH values for EL-5F, EL-5F-PEG-2K and EL-5F-PEG-5K, respectively. β sheets were confirmed by the thioflavin T assay and transmission electron microscopy revealed the existence of extended fibrillar structures below the above pH values. pH-induced secondary structure conversion in both directions was reproducible for over fifteen cycles, even at salt concentrations of up to 200 mM NaCl, and the amounts of β sheet formed were quantitatively related to pH below the transition points. Self-supporting hydrogelation after self-assembly was observed at concentrations as low as 0.2 wt%, which is 15-fold lower than previously reported concentrations with PEGylated SAPs.

Subsequent work, involving tethering of EL-5F-PEG-2K to an Anodisc alumina membrane surface and/or pores and investigations on the effect of reversible self-assembly on the permeability of the membrane was carried out. COOH groups were immobilised on the

membrane surface to prepare it for the coupling of EL-5F-PEG-2K, using multilayer deposition of poly(acrylic acid) (PAA) and poly(allylamine hydrochloride) (PAH). EL-5F-PEG-2K was then successfully amine-coupled to the COOH groups on the surface and this was confirmed using ATR-FTIR. Subsequent flux tests indicated no pH-dependant variation in buffer flux properties of the EL-5F-PEG-2K modified membrane. However, MWCO experiments using 72 and 29 kDa PEGs indicated reversible self-assembly of membrane tethered EL-5F-PEG-2K, upon changes in pH, thereby affecting macromolecule permeation. Furthermore, investigations on the reversible, pH-regulated self-assembly of peptide EL-5F and conjugate EL-5F-PEG-2K tethered to polystyrene nanoparticle (NP) surfaces, showed size transitions and aggregation of NPs upon changes in pH, indicating retention of peptide and bioconjugate self-assembly after surface tethering.

The results provide a tentative but consistent proof-of-concept, giving the first steps towards the development of a novel switchable SAP-based, stimuli-responsive membrane. Further investigations suggested to validate reversible peptide self-assembly on the membrane surface, are expected to pave the way towards achieving finely controlled membrane separations.

Deputy Vice-Chancellor's Office
Postgraduate Office

UNIVERSITY OF CANTERBURY
Te Whare Wānanga o Waitaha
CHRISTCHURCH NEW ZEALAND

Co-Authorship Form

This form is to accompany the submission of any thesis that contains research reported in co-authored work that has been published, accepted for publication, or submitted for publication. A copy of this form should be included for each co-authored work that is included in the thesis. Completed forms should be included at the front (after the thesis abstract) of each copy of the thesis submitted for examination and library deposit.

Please indicate the chapter/section/pages of this thesis that are extracted from co-authored work and provide details of the publication or submission from the extract comes:

Chapter 4 in this thesis is extracted from co-authored work, Ponnumallayan, P., Fee, C.J. (2014). Reversible and Rapid pH-Regulated Self-Assembly of a Poly(Ethylene Glycol)-Peptide Bioconjugate, *Langmuir, 30(47),14250-14256* .

Please detail the nature and extent (%) of contribution by the candidate:

This work was carried out in usual fashion as a lab-based research student, by the candidate. He wrote the draft of the paper and submitted to me for corrections, simiar to a fairly rigorous thesis chapter, I would say. I estimate 90% by the candidate and 10% by me (the latter in terms of feedback to meet the style and rigour required of peer-review standards.)

Certification by Co-authors:

If there is more than one co-author then a single co-author can sign on behalf of all
The undersigned certifys that:

- The above statement correctly reflects the nature and extent of the PhD candidate's contribution to this co-authored work
- In cases where the candidate was the lead author of the co-authored work he or she wrote the text

Name: *Conan Fee* Signature: Date: *28/11/2014*

Acknowledgements

First and foremost, I would like to express my sincere gratitude to my supervisor Professor Conan J Fee, for giving me an opportunity to work in his lab. His constant support, encouragement and invaluable guidance helped me grow as an independent researcher. I'm privileged to have been associated with a researcher like Conan, at a very early stage of my career.

I sincerely acknowledge the support and encouragement from my lab manager Rayleen Fredericks. I would like to thank Dr. Simone Dimartino for his support.

I also thank Professor Alison Downard and Mr. Kalib Bell (Department of Chemistry, UC) for their valuable contributions in surface chemistry work.

I would like to thank Dr. Celine Valery and Mr Rishi Pandey (School of Biological Sciences, UC) for their help with the ThT binding assay, Ms. Jackie Healy (School of Biological Sciences, UC) for assistance with TEM analysis, Drs. Stefan Clerens and Jessica Gathercole (AgResearch Ltd., Lincoln, New Zealand) for helping with MALDI-tof analysis, Dr. Mark Lay and Mrs. Helen Turner (University of Waikato, Hamilton, New Zealand) for their help with SEM analysis, Mr. Manfred Ingerfeld (School of Biological Sciences, UC) for assistance with fluorescence microscopy.

I would like to acknowledge the Biomolecular Interaction Centre, University of Canterbury for partially funding my research.

I wish to thank CAPE technical staffs, post-graduate students and administrators for their support and cooperation.

I wish to acknowledge my beloved friends Mr. Ramanathan Vaidyanathan, Dr. Kannan Subramanian, Mr. Lokesh Kumar, Mr. Ramanath Muthukrishnan, Mr. Vishanth Baburaj, Ms. Anitha Chellamuthu, Ms. Salini Devi Ramaraj, Dr. Balaji Somasundaram, Mr. Kishorekumar Gopalakrishnan, Dr. Neha Chandrasekaran, Ms. Shradha Chandrasekaran, Mr. Govind Pratap Singh, Mr. Vivek Balachandran, Dr. Abishek Muralidhar and Mr. Suzal Samuel Shukla for their unconditional support and constant encouragement.

My special thanks to Mr. Seenivasan Nagaraj for his timely advices and motivation throughout my life.

Finally, I would like to dedicate this thesis and all other achievements to my beloved parents Mr. Ponnumallayan Malliah and Mrs. Regina Ponnumallayan for their unconditional love and blessings.

Preface

List of the outcomes arising from this thesis are:

Ponnumallayan, P., Fee, C.J. (2014). Reversible and Rapid pH-Regulated Self-Assembly of a Poly(Ethylene Glycol)-Peptide Bioconjugate, Langmuir, 30(47), 14250-14256.

Ponnumallayan, P., Fee, CJ. (2013). Molecular self-assembly: Development of a novel switchable filtration membrane using self-assembling peptides. Chemeca, September 29-October 2, 2013, Brisbane, Australia (Poster presentation).

Ponnumallayan, P. (2013). ON/OFF Membrane. Thesis in three competition, University of Canterbury, New Zealand (University finalist).

Table of Contents

Abstract.....iii

Acknowledgements.....vi

Preface.....viii

Table of contents.....ix

List of figures.....xv

List of tables.....xxiv

Abbreviations.....xxv

1. INTRODUCTION.....1-1

1.1 BACKGROUND.....1-1

1.2 SELF-ASSEMBLING PEPTIDE (SAP) FUNCTIONALIZED MEMBRANES - A NOVEL APPROACH.....1-3

1.3 SIGNIFICANCE OF THIS RESEARCH.....1-6

1.4 OBJECTIVES.....1-7

1.5 THESIS ORGANIZATION.....1-8

2. REVIEW OF LITERATURE.....2-1

2.1 INTRODUCTION.....2-1

2.2 MOLECULAR SELF-ASSEMBLY.....2-1

2.3 SELF-ASSEMBLING PEPTIDES.....2-2

2.3.1 Type I SAPs.....2-4

2.3.2 Type II SAPs.....2-4

2.3.3 Type III SAPs.....2-5

2.3.4 Type IV SAPs.....2-6

2.3.5 Responsive peptide hydrogels.....2-7

2.3.6 Responsive peptide amphiphiles.....2-11
2.4 PEPTIDE-POLYMER BIOCONJUGATES.....2-13
2.4.1 PEG polymer spacers.....2-13
2.4.2 Strategies for peptide-PEG bioconjugation.....2-15
2.4.3 Self-assembly of peptide polymer bioconjugates.....2-18
2.4.4 Bioconjugate self-assembly on membrane surfaces.....2-22
2.5 STIMULI-RESPONSIVE MEMBRANES.....2-22
2.5.1 Surface-initiated modification.....2-24
2.5.2 'Grafting to' method.....2-25
2.5.3 pH responsive membranes.....2-26
2.5.4 Application of pH-sensitive pore-filled membrane.....2-31
2.5.4.1 *Extraction of specific proteins*.....2-33
2.5.4.2 *Rejection of proteins*.....2-35
2.6 ANODISC^{TM} ALUMINA MEMBRANES.....2-38
2.7 IMMOBILISATION OF CARBOXYLATE GROUPS (COOH) ON ALUMINA SURFACE.....2-39
2.7.1 Phosphonic acid chemistry.....2-40
2.7.2 Diazonium chemistry.....2-41
2.7.3 PEM adsorption.....2-43
2.8 SUMMARY OF LITERATURE REVIEW.....2-44
3. INVESTIGATION OF FACTORS INFLUENCING SELF-ASSEMBLY OF PEPTIDE P11-4-PEG BIOCONJUGATE..... 3-1
3.1 INTRODUCTION..... 3-1
3.2 EXPERIMENTAL SECTION.....3-3
3.2.1 Materials.....3-3

3.2.2 Conjugation and purification.....3-3

3.2.3 Effect of ethanolamine on conjugation.....3-3

3.2.4 Time course experiment.....3-4

3.2.5 Electrospray mass spectroscopy.....3-4

3.2.6 Matrix-assisted laser desorption/ionization time-of-flight (MALDI-TOF) mass spectrometry.....3-4

3.2.7 Circular dichroism spectroscopy.....3-5

3.2.8 Transmission electron microscopy.....3-5

3.3 RESULTS.....3-6

3.3.1 Secondary structure characterization of native P11-4.....3-6

3.3.2 Conjugation, purification and characterization of conjugate P11-4-PEG-2K.....3-7

3.3.2.1 *Effect of ethanolamine on conjugation*.....3-11

3.3.2.2 *Time course experiment*.....3-12

3.3.3 Secondary structure characterization of conjugate P11-4-PEG2K.....3-14

3.3.3.1 *Effect of salt (NaCl) on self-assembly of P11-4-PEG-2K*.....3-16

3.3.3.2 *Effect of free PEG on self-assembly of P11-4*.....3-17

3.3.3.3 *Effect of phosphate ions on self-assembly of P11-4*.....3-18

3.3.3.4 *Conjugation in 3 mM sodium phosphate buffer*.....3-20

3.3.3.5 *Conjugation in water*.....3-21

3.3.3.6 *Conjugation using equimolar concentrations of P11-4 and PEG*.....3-23

3.3.3.7 *Effect of residual by-products of EDC/NHS reaction on the self-assembly of P11-4*.....3-24

3.4 DISCUSSION AND CONCLUSION.....3-25

4. REVERSIBLE AND RAPID SELF-ASSEMBLY OF PEPTIDE-PEG BIOCONJUGATES EL-5F-PEG-2K AND EL-5F-PEG-5K..... 4-1

4.1 INTRODUCTION..... 4-1

4.2 EXPERIMENTAL SECTION....4-3
4.2.1 Materials....4-3
4.2.2 EL-5F concentration calibration curve....4-3
4.2.3 Conjugation and purification....4-3
4.2.4 Matrix-assisted laser desorption/ionization time-of-flight (MALDI-TOF) mass spectrometry....4-4
4.2.5 Circular dichroism spectroscopy....4-4
4.2.6 Transmission electron microscopy....4-5
4.2.7 Thioflavin T fluorescence binding assay....4-5
4.2.8 BOC deprotection....4-5
4.3 RESULTS AND DISCUSSION....4-6
4.3.1 Conjugation and purification....4-6
4.3.2 Secondary structure characterisation....4-9
4.3.3 Self-supporting hydrogelation....4-17
4.3.4 Characterisation of structural morphology....4-18
4.3.5 ThT binding assay....4-20
4.3.6 BOC deprotection....4-21
4.4 CONCLUSIONS....4-21
5. DEVELOPMENT OF A NOVEL STIMULI-RESPONSIVE FILTRATION MEMBRANE FUNCTIONALIZED WITH SELF-ASSEMBLING PEPTIDE-PEG BIOCONJUGATE....5-1
5.1 INTRODUCTION....5-1
5.2 EXPERIMENTAL SECTION....5-8
5.2.1 Materials....5-8

5.2.2 Immobilisation of carboxylic acid (COOH) groups on the Anodisc membrane surface.....5-8
5.2.2.1 *Phosphonic acid chemistry*.....5-9
5.2.2.2 *Diazonium chemistry*.....5-9
5.2.2.3 *PAA / PAH multilayers*.....5-11
5.2.3 Amine coupling.....5-11
5.2.4 Fluorescence microscopy.....5-11
5.2.5 Attenuated Total Reflectance - Fourier Transform Infrared Spectroscopy (ATR-FTIR).....5-12
5.2.6 Contact angle measurement (CAM).....5-12
5.2.7 X-ray Photoelectron Spectroscopy (XPS).....5-12
5.2.8 Atomic Force Microscopy (AFM).....5-13
5.2.9 Field Emission Scanning Electron Microscopy (FESEM).....5-14
5.2.10 Flux test.....5-14
5.2.11 Molecular weight cut-off (MWCO) experiment.....5-14
5.2.12 Coupling of EL-5F / EL-5F-PEG-2K to NPs.....5-15
5.2.13 DLS.....5-16
5.2.14 Transmission electron microscopy.....5-16
5.3 RESULTS AND DISCUSSION.....5-17
5.3.1 COOH groups immobilisation on the Anodisc surface.....5-17
5.3.1.1 *Phosphonic acid chemistry*.....5-17
5.3.1.2 *Diazonium chemistry*.....5-18
5.3.1.3 *PEM adsorption*.....5-36
5.3.2 Determination of flux of blank, PAA/PAH-modified and EL-5F-PEG-2K coupled Anodisc membranes at pH 3 and 8.....5-44

5.3.3 Determination of MWCO of EL-5F-PEG-2K coupled Anodisc membrane at pH 3 and 8.....5-46

5.3.4 Conjugation of EL-5F / EL-5F-PEG-2K to NPs.....5-53

5.3.4.1 *Coupling and purification*.....5-53

5.3.4.2 *Particle size characterisation*.....5-54

5.3.4.3 *Characterisation of structural morphology*.....5-60

5.4 CONCLUSIONS..... 5-62

6. CONCLUSIONS AND RECOMMENDATIONS FOR FUTURE WORK..... 6-1

6.1 FACTORS AFFECTING SELF-ASSEMBLY OF BIOCONJUGATE P11-4-PEG-2K..... 6-1

6.2 RAPID AND REVERSIBLE SELF-ASSEMBLY OF BIOCONJUGATES EL-5F-PEG-2K AND EL-5F-PEG-5K..... 6-2

6.3 STIMULI RESPONSIVE MEMBRANE FUNCTIONALISED WITH SAP-PEG BIOCONJUGATE.....6-3

References..... R-1

Appendix A.....A-1

Appendix B..... B-1

Appendix C..... C-1

Appendix D.....D-1

List of Figures

Figure 1-1	A characteristic diagram showing the retention (%) of a 2 kDa nominal molecular weight cut-off dialysis membrane. Image reproduced from (http://www.piercenet.com/previews/2013-articles/separation-characteristics-dialysis-membranes, 23rd Nov, 2014)	1-2
Figure 1-2	Schematic representation showing pH dependent reversible self-assembly of peptides tethered to membrane pores, A) top view, B) cross sectional view	1-6
Figure 2-1	Self-assembly (bottom up approach) of molecules under the influence of external stimuli	2-2
Figure 2-2	Timeline showing the development process and applications of SAPs spanning over 20 years. Image adapted from (Luo & Zhang, 2012)	2-3
Figure 2-3	TEM image showing surfactant like peptides forming nanotubes with diameter around 30-50 nm. Image reproduced from (Zhang, 2002)	2-6
Figure 2-4	The self-assembled and disassembled states of peptides P11-4 and P11-5 at low and high pH values. Image reproduced from (Aggeli et al., 2003)	2-9
Figure 2-5	Reversible self-assembly of peptide amphiphiles. Image adapted from (Hartgerinket al., 2002)	2-12
Figure 2-6	Peptide guided self-assembly of peptide-polymer bioconjugates. Image adapted from (Borner, 2009)	2-19
Figure 2-7	Schematic representation of membrane functionalization approaches, a) the grafting-to method, in which the functional end groups in a polymer chain are covalently coupled to active groups on the surface, b) the grafting-from method, in which the polymer chains grow from initiator sites tethered to the surface. Image adapted from (Jain et al., 2009)	2-24
Figure 2-8	Immobilisation of PLGA on gold coated polycarbonate membrane. Image adapted from (Ito et al., 2000)	2-26

Figure 2-9	Immobilisation of poly(acrylic acid) conjugated with cysteamines (PAA-SH) on gold coated polycarbonate membrane. Image adapted from (Zhang & Ito, 2001)	2-27
Figure 2-10	Schematic representation of pore-filled membrane showing changes in physical characteristics of the incorporated gel upon change of pH. Image reproduced from (Hu & Dickson, 2007)	2-30
Figure 2-11	Covalent capture of His-tagged protein by NTA-Ni^{2+} derivatised PHEMA brush inside a membrane pore. Image adapted from (Jainet al., 2007)	2-35
Figure 2-12	Schematic representation of PET membrane pore functionalized with stimuli responsive PNIPAAm via two different methods and the change in effective pore diameter with change in temperature. Image adapted from (Friebe & Ulbricht, 2007)	2-37
Figure 2-13	Anodisc pore structure. Image reproduced from (http://www.whatman.com/products.aspx?PID=193, 5th May, 2012)	2-39
Figure 2-14	Chemical structure of 6-PHA	2-41
Figure 2-15	Chemical structure of 16-phosphono-hexadecanoic acid	2-41
Figure 2-16	General chemical structure of aryl diazonium salts where R refers to range of substituents such COOH, NO_2 etc. and A^- is the counter anion	2-41
Figure 2-17	The carboxy benzene diazonium (CBD) reduction mechanism forming radical. Reduction is either done electrochemically or using reducing agents	2-17
Figure 2-18	Schematic diagram of layer-by-layer adsorption of polyelectrolytes on Anodisc surface. Image adapted from (Bruening et al., 2008)	2-44
Figure 3-1	CD spectra of native peptide P11-4 showing the repeated conformational shifts between β sheet and random coil upon changing the pH between 2.5 and 7	3-6
Figure 3-2	TEM images of negatively stained (A) P11-4 at pH < 3, (B) P11-4 at pH > 7	3-7

Figure 3-3	Size exclusion chromatograms of native P11-4 and NHS PEG-2K	3-8
Figure 3-4	Size exclusion chromatogram showing the separation of conjugate P11-4-PEG-2K from the unreacted peptide and EDC/NHS	3-9
Figure 3-5	Size exclusion chromatogram showing the desalting of sodium phosphate salts from conjugate P11-4-PEG-2K	3-10
Figure 3-6	Mass spectra of conjugate P11-4-PEG-2K	3-10
Figure 3-7	Mass spectra of conjugate P11-4-PEG-2K	3-11
Figure 3-8	Size exclusion chromatogram of conjugation mixtures in the presence and absence of ethanolamine	3-12
Figure 3-9	Size exclusion chromatogram of conjugation mixtures at different time intervals ranging from 0-120 min	3-13
Figure 3-10	Conjugate yield obtained from reaction mixtures obtained at different time intervals ranging from 0-120 min	3-14
Figure 3-11	CD spectra of conjugate P11-4-PEG-2K showing random coil conformation at both pH 2.5 and 7	3-15
Figure 3-13	CD spectra of peptide P11-4 showing β sheet conformation at pH 2.5 in the presence of PEG 2K at concentrations 5, 10 and 15 mg/mL	3-17
Figure 3-14	CD spectra showing secondary structure conformation of peptide P11-4 (0.25 mg/mL) in different concentrations of sodium phosphate buffer ranging from 3-50 mM at pH 2.5	3-19
Figure 3-15	CD spectra showing secondary structure conformation of peptide P11-4 (0.4 mg/mL) in different concentrations of sodium phosphate buffer ranging from 3- 20 mM at pH 2.5	3-19

Figure 3-16	Size exclusion chromatogram showing the separation of conjugate P11-4-PEG-2K from the unreacted peptide and EDC/NHS in 3 mM sodium phosphate buffer	3-20
Figure 3-17	CD spectra showing secondary structure conformation of P11-4-PEG-2K, unreacted P11-4 and P11-4 control at pH 2.5	3-21
Figure 3-18	Size exclusion chromatogram showing the separation of conjugate P11-4-PEG-2K from the unreacted peptide in water	3-22
Figure 3-19	CD spectra showing secondary structure conformation of P11-4-PEG-2K and unreacted P11-4 at pH 2.5	3-22
Figure 3-20	Size exclusion chromatogram showing the separation of conjugate P11-4-PEG-2K from the unreacted peptide and EDC/NHS in 3 mM sodium phosphate buffer	3-23
Figure 3-21	CD spectra of P11-4-PEG-2K showing random coil conformation at pH 2.5	3-24
Figure 3-22	Size exclusion chromatogram showing the separation of conjugate P11-4-PEG-2K from the unreacted peptide and EDC/NHS in 3 mM sodium phosphate buffer	3-25
Figure 4-1	Structural view of pH-regulated, reversible self-assembly of (A) peptide EL-5F, (B) EL-5F-PEG conjugates	4-2
Figure 4-2	Size exclusion chromatogram showing the separation of conjugates EL-5F-PEG-2K and EL-5F-PEG-5K from the unreacted peptide and EDC/NHS	4-6
Figure 4-3	MALDI-TOF mass spectrum of the EL-5F-PEG-2K conjugate confirming the successful coupling of peptide EL-5F (1376.5 Da) and PEG 2K	4-8
Figure 4-4	MALDI-TOF mass spectrum of the EL-5F-PEG-5K conjugate confirming the successful coupling of peptide EL-5F (1376.5 Da) and PEG 5K	4-8

Figure 4-5	CD spectra of (A) native peptide EL-5F, (B) EL-5F-PEG-2K and EL-5F-PEG-5K, showing the repeated conformational shifts between β sheet and random coil upon changing the pH between 5 and 7	4-10
Figure 4-6	CD spectra of native peptide EL-5F, showing similar β sheet intensities before and after 24 h incubation at pH 5	4-11
Figure 4-7	CD negative intensity at 215 nm, indicating the extent of β sheet (θ_{215nm} < -60 x 10^3) to random coil ($\theta_{215nm} \approx 0$) transition with 16 repeated secondary structure shifts of EL-5F-PEG-2K, mediated by corresponding changes in pH from below 5 to above 7	4-12
Figure 4-8	CD negative intensity at 215 nm, indicating the extent of β sheet-to-random coil transition of EL-5F after the addition of NaCl at concentrations ranging from 0 to 200 mM mediated by corresponding changes in pH between 5 and 7	4-13
Figure 4-9	The mean β sheet intensity at 215 nm for EL-5F at NaCl concentrations ranging from 0 to 200 mM	4-14
Figure 4-10	Circular dichroism adsorption at 215 nm (values > 0 indicating β sheet formation) for peptide EL-5F and conjugates over the pH range 3–7	4-16
Figure 4-11	Self-supporting hydrogel of EL-5F-PEG-2K at pH < 5.4 (0.2 wt%) and the dissociation of the gel at pH > 5.8	4-18
Figure 4-12	TEM images of negatively stained (A) EL-5F at pH < 5.7, (B) EL-5F at pH > 5.9, (C) EL-5F-PEG-2K at pH < 5.4, (D) EL-5F-PEG-2K at pH > 5.8, (E) EL-5F-PEG -5K at pH < 5.1, (F) EL-5F-PEG-5K at pH > 5.4	4-19
Figure 4-13	ThT binding assay of EL-5F, EL-5F-PEG-2K and EL-5F-PEG-5K at pH < 5.1 and pH > 5.9	4-20
Figure 5-1	Chemical structure of 6-PHA	5-4
Figure 5-2	General chemical structure of aryl diazonium salts where R refers to range of substituents such as COOH, OH and NO_2 and A^- is the counter anion	5-4

Figure 5-3	CBD reduction mechanism forming radical. Reduction is either done electrochemically or using reducing agents	5-5
Figure 5-4	General chemical structure of A) NBD and B) CMBD salts	5-6
Figure 5-5	Schematic representation of layer-by-layer adsorption of deprotonated PAA and protonated PAH on the Anodisc surface	5-7
Figure 5-6	FTIR spectra of 6-PHA, HPA and HA modified Anodisc surface in water and ethanol	5-18
Figure 5-7	FTIR spectra of the CBD modified Anodisc surface in basic and acidic conditions	5-19
Figure 5-8	FTIR spectra of CBD and NBD modified Anodisc surface using hypophosphoric acid as the reducing agent	5-20
Figure 5-9	FTIR spectra of powdered CBD and NBD modified Anodisc membrane using hypophosphoric acid as the reducing agent	5-21
Figure 5-10	CAMs of bare, control and CBD modified native alumina surface using water and pH 10 buffer	5-23
Figure 5-11	CAM images of A) water and B) pH 10 buffer droplet on CBD modified native alumina surface	5-23
Figure 5-12	FTIR spectra of control, NBD- and CBD-modified PC membrane surfaces using hypophosphoric acid as the reducing agent	5-24
Figure 5-13	FTIR spectra of CMBD ex situ and in situ modified Anodisc surface. Each method had a control sample, only CMBD immobilised sample and conjugate coupled sample	5-26
Figure 5-14	The Anodisc membrane appearing coloured due to azo linkages after CMBD in situ diazonium modification	5-26
Figure 5-15	Chemical structure of EDANS (5 - [(2 - aminoethyl)amino]naphthalene - 1 - sulfonic acid) fluorescent dye	5-27

Figure 5-16 Fluorescence microscopy images of EDANS dye coupled Anodisc surface modified using A) CBD control. B) CBD, C) CMBD control, D) CMBD, E) CMBD (DMSO) control, F) CMBD (DMSO). Fluorescence microscopy images of EDANS dye coupled carbon surface modified using G) CMBD control, H) CMBD (DMSO), I) CMBD (sodium phosphate) 5-30

Figure 5-17 Wide scan XPS spectrum of A) Anodisc blank, B) Anodisc – CMBD modified, C) Anodisc – CMBD + EL-5F-PEG-2K coupled (control), iv) Anodisc – CMBD + EL-5F-PEG-2K coupled 5-31

Figure 5-18 Deconvolution of the C1s carbon and N1s nitrogen XPS peaks of Anodisc surface modified with CMBD only (A and B) and CMBD + EL-5F-PEG-2K coupled (C and D) respectively 5-33

Figure 5-19 Flux data over a range of back pressures of the Anodisc modified using CMBD and CMBD + EL-5F-PEG-2K coupled at pH 3 and 8 5-36

Figure 5-20 FTIR spectra of blank, PAA/PAH modified and PAA/PAH modified + EL-5F-PEG-2K coupled Anodisc surface 5-37

Figure 5-21 FTIR spectra of PAA, (PAA/PAH), $(PAA/PAH)_2$ PAA and $(PAA/PAH)_3$ PAA-modified Anodisc surfaces 5-38

Figure 5-22 AFM images of permeate sides of the Anodisc blank membrane (A and B) and $(PAA/PA)_3$ PAA-modified membrane (C and D), filtrate sides of the Anodisc blank membrane (E) and $(PAA/PA)_3$ PAA-modified membrane (F) 5-40

Figure 5-23 FE-SEM images of filtrate and permeate sides of the Anodisc blank (A and B), $(PAA/PAH)_3$ PAA-modified (C and D), $(PAA/PAH)_3$ PAA-modified + EL-5F-PEG-2K coupled (pH 8) (E and F) and $(PAA/PAH)_3$ PAA-modified + EL-5F-PEG-2K coupled (pH 3) (G and H) membranes respectively 5-43

Figure 5-24 Flux data over a range of back pressures of the Anodisc blank, $(PAA/PAH)_3$ PAA-modified and $(PAA/PAH)_3$ PAA-modified + EL-5F-PEG-2K coupled membranes at pH 3 and 8 5-45

Figure 5-25	The permeation of PEG 72 kDa + 29 kDa mixture (2.5 mg/mL) through $(PAA/PAH)_3$ PAA-modified + EL-5F-PEG-2K coupled Anodisc membrane at pH 3 and 8	5-47
Figure 5-26	A) Size exclusion chromatogram showing the distinct peaks of PEG 72 and 29 kDa in the feed and permeate samples at pH 3 and 8, B) The retention (%) of PEG 72 and 29 kDa from the feed mixture by the $(PAA/PAH)_3$ PAA-modified + EL-5F-PEG-2K coupled Anodisc membrane at pH 3 and 8	5-49
Figure 5-27	The permeation of PEG 72 kDa + 29 kDa mixture (2.5 mg/mL) through $(PAA/PAH)_3$ PAA-modified + EL-5F-PEG-2K coupled Anodisc membrane at pH 3 and 8	5-50
Figure 5-28	A) Size exclusion chromatogram showing the distinct peaks of PEG 72 and 29 kDa in the feed and permeate samples at pH 3 and 8, B) The mean retention (%) of PEG 72 and 29 kDa from the feed mixture by the $(PAA/PAH)_3$ PAA-modified + EL-5F-PEG-2K coupled Anodisc membrane at pH 3 and 8	5-51
Figure 5-29	DLS measurement showing reversible transition in size of EL-5F coupled NPs with change in pH between 3 and 7	5-54
Figure 5-30	Correllogram showing reversible transition in size and aggregation of EL-5F coupled NPs with change in pH between 3 and 7	5-55
Figure 5-31	DLS measurement showing reversible transition in size of EL-5F-PEG-2K coupled NPs with change in pH between 3 and 7	5-56
Figure 5-32	Correllogram showing reversible transition in size and aggregation of EL-5F-PEG-2K coupled NPs with change in pH between 3 and 7	5-56
Figure 5-33	DLS measurement showing irreversible aggregation of ethanolamine deactivated NPs at both pH 3 and 7	5-57
Figure 5-34	Correllogram showing aggregation of ethanolamine coupled NPs at both pH 3 and 7	5-58

Figure 5-35 Schematic representation of the explanations for pH dependant size transition of EL-5F and EL-5F-PEG-2K coupled NPs. A) Inter-particle self-assembly of peptide EL-5F at pH 3, B) Aggregation due to lack of repulsive charges at pH 3, C) Intra-particle self-assembly of peptide EL-5F at pH 3 5-59

Figure 5-36 TEM images of A) Native NPs, B) EL-5F coupled NPs at pH 3 , C) EL-5F coupled NPs at pH 7, D) EL-5F-PEG-2K coupled NPs at pH 3, E) EL-5F-PEG-2K coupled NPs at pH 7, F) Ethanolamine coupled NPs at pH 3, G) Ethanolamine coupled NPs at pH 7 5-61

List of Tables

Table 2-1	Charge distribution in different moduli of Type I SAPs	2-4
Table 5-1	Atomic concentration (in %) of C1s, N1s, O1s, Al2p on the blank and modified Anodisc surfaces	5-32
Table 5-2	Area (%) under the deconvoluted XPS peaks of C1s carbon and N1s nitrogen of the Anodisc CMBD-modified and EL-5F-PEG-2K-coupled samples	5-34
Table 5-3	Membrane resistance, R_m (m^{-1}) of the Anodisc blank, $(PAA/PAH)_3$ PAA-modified and $(PAA/PAH)_3$ PAA-modified + EL-5F-PEG-2K coupled membranes (flux, J ($L/H*m^2$), pressure, P (MPa), viscosity, μ = 0.00089 Pa.s)	5-45

Abbreviations

AA	Acrylic acid
AC	3-aminopropionic acid
AMPS	2-acrylamid-2-methylpropanesulfonic acid
AP	2-aminoethyl phosphonic acid
APS	Ammonium persulfate
AS	2-aminoethane-1-sulfonic acid
ATRP	Atom transfer radical polymerization
Boc	N-tert-butoxycarbonyl
CAM	Contact angle measurement
CBD	Carboxy benzene diazonium
CD	Circular dichroism
CMBD	Carboxy methyl benzene diazonium
CMPPESK	Chloromethylated poly(phthalazinone ether sulfone ketone)
DEAEMA	AA/2-(diethylamino)ethyl methacrylate
DHAP	2,5 – dihydroxyacetophenone
DLS	Dynamic light scattering
EDANS	5-[(2-aminoethyl)amino]naphthalene - 1 - sulfonic acid
FWHM	Full widths at half maximum
HA	Hexanoic acid
HCAA	α-cyano-4-hydroxy-cinnamic acid
HPA	Hexyl phosphonic acid
HPMA	Poly[N-(2-hydroxypropyl) methacrylamide]
MALDI-TOF	Matrix-assisted laser desorption/ionization time-of-flight
MF	Microfiltration
MWCO	Molecular weight cut-off
NBD	Nitro benzene diazonium
NCA	N-carboxyanhydride
NF	Nanofiltration

NHS	N-hydroxy succinimide
NP	Nanoparticle
PA	Peptide amphiphiles
PAA	Poly(acrylic acid)
PAH	Poly(allylamine hydrochloride)
PAMPS	Poly(2-acrylamid-2-methylpropanesulfonic acid)
PAN	Poly(acrylonitrile)
PC	Polycarbonate
PEG	Poly(ethylene glycol)
PEGMA	Poly(ethylene glycol) methyl ether methacrylate
PEI	Polyethylenimine
PEM	Polyelectrolyte multilayer
PES	Polyethersulfone
PET	Poly(ethylene terephthalate)
6-PHA	6-phosphono hexanoic acid
PHEMA	Poly(2-hydroxyethyl methacrylate)
pI	Isoelectric point
PLGA	Poly(L-glutamic acid)
PMMA	Poly(methyl methacrylate)
PNIPAAm	Poly(N-isopropylacrylamide)
PNIPAM	Poly(N-isopropylacrylamide)
PPEGMA	Poly(poly(ethylene glycol) methyl ether methacrylate)
PP	Poly(propylene)
PV	Pervaporation
P4VPy	Poly(4-vinylpyridine)
QCM	Quartz crystal microbalance
RATRP	Reverse atom transfer radical polymerization
R_m	Membrane resistance
SAM	Self-assembled monolayer
SAP	Self-assembling peptide
SEC	Size exclusion chromatography
SEM	Scanning electron microscopy

SPR	Surface plasmon resonance
TEM	Transmission electron microscopy
ThT	Thioflavin T
UF	Ultrafiltration
XPS	X-ray photoelectron spectroscopy

CHAPTER-1

INTRODUCTION

1. INTRODUCTION

1.1 BACKGROUND

Membrane technology is a generic term for various characteristic separation processes where the membrane acts as a specific filter to separate substances from a more heterogeneous solution. Two factors that primarily determine the effectiveness of a membrane filtration process are selectivity and productivity. Selectivity represents the retention or separation factor, whilst productivity is expressed as the membrane flux (Lightfoot & Moscariello, 2004). With different kinds of membranes being developed, synthetic membranes have played a very important role in the field of separation science. These membrane phases can be homogeneous or heterogeneous and can also be non-porous solids (e.g. pervaporation membranes), microporous solids (e.g. microfiltration membranes) or nanoporous solids (e.g. ultrafiltration membranes) (Wandera et al., 2010).

Conventional filtration membranes have been well established for separating larger molecules and their applications in the separation of biomolecules range from DNA purification to large-scale protein purification. The difference in size and shape is the main basis of separation through semipermeable membranes. However, achieving 100% cut-off at a fine range of size or shape using any filtration membrane has been a challenge (Figure 1-1).

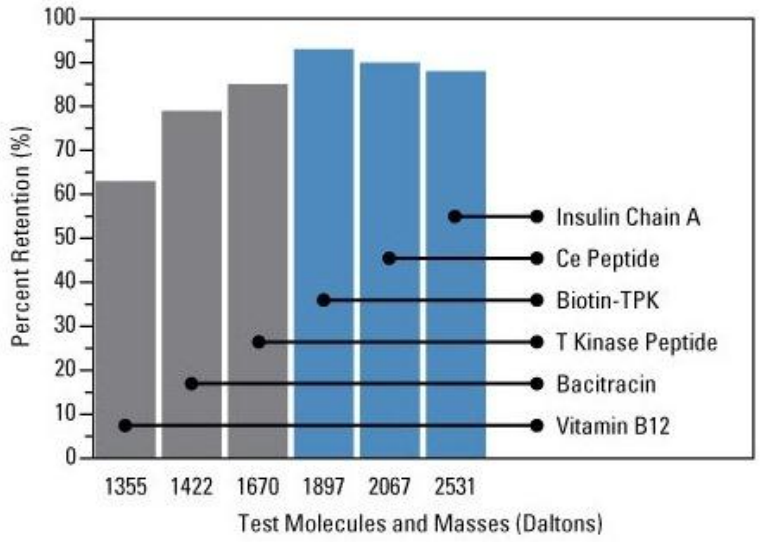

Figure 1-1: A characteristic diagram showing the retention (%) of a 2 kDa nominal molecular weight cut-off dialysis membrane. Image reproduced from (http://www.piercenet.com/previews/2013-articles/separation-characteristics-dialysis-membranes, 23rd Nov, 2014).

Due to these limitations in achieving finer separations that take advantage of more complex molecular properties such as charge, ion-exchange membranes were developed with the incorporation of ion-exchange sites to enhance the separation by selectively differentiating between molecules based on charge as well as size (Xu, 2005). Alternatively, membrane pores were filled with pH-sensitive polyelectrolyte gels, which enhance the selective ion permeability depending on the pH of the permeate (Mika et al., 2002). Various polymers were also incorporated into membrane pores to achieve specific separation goals. For instance, a microporous membrane was rendered pH-sensitive with modification using poly(acrylic acid) (PAA) for membrane mediated synthesis of nanocrystalline ferrihydrite (Winnik et al., 1998). Similarly, poly(L-glutamic acid) (PLGA) was tethered to cellulose membrane to precisely control water flux with changes in pH (Hollman & Bhattacharyya, 2002).

Thus, methods which provide finer control of separation through membranes, in particular through switchable mechanisms, appear to be an attractive approach to develop selective membranes for specific applications. This thesis describes an attempt to develop one such novel membrane, exploiting the pH-driven self-assembly of peptides to control membrane permeability.

1.2 SELF-ASSEMBLING PEPTIDE (SAP) FUNCTIONALIZED MEMBRANES - A NOVEL APPROACH

A number of polymers and/or peptides have been tethered to membranes to act as molecular brushes during specific separation purposes. Membrane pores have also been functionalized with molecular brushes to achieve a variety of objectives. In some applications, brushes were incorporated to extract specific proteins; amphoteric polymer brushes have been attached to membrane surfaces and pores, thus forming an ion-exchange membrane to bind proteins (Iwanade et al., 2007); poly(methacrylic acid) brushes have been grafted to chitosan membranes to adsorb alkaline trypsin (Bayramoglu et al., 2008); poly(2-hydroxyethyl methacrylate) (PHEMA) brushes were attached to alumina membranes to obtain high purity polyhistidine-tagged ubiquitin (HisU) (Jain et al., 2007). Brushes of poly(n-isopropylacrylamide) (PNIPAAm) were grafted to the pores or track-etched poly(ethylene terephthalate) (PET) membranes to achieve a temperature-responsive pore diameter (Friebe & Ulbricht, 2007). Incorporation of pH-sensitive molecular brushes into pores of polymer microcapsule membranes for controlled drug release has been successfully carried out (Lin et al., 2006). Controlling intrapore transport of pure water has been achieved by swelling and shrinking of polyionic gels inside membrane pores (Zhou et al., 2005). Nanocoils of PLGA were adsorbed to the 200 nm pores of a track-etched gold coated membrane and used as a pH dependent “nanovalve” to control the flux of water (Ito et al., 2000). However, the “self-

assembly" claimed by Ito involved only the spontaneous adsorption of thiolated polypeptide onto the gold surface, as distinct from the supramolecular self-assembly that is exploited in this project. Inter-molecular self-assembly of peptides tethered to a membrane surface and the influence of such self-assembly on the permeability of the membrane have not been studied so far.

Despite extensive and widespread research on the development of novel functional membranes, the range of structures possible using SAPs will add a new dimension to transmembrane transport. The side chains of amino acids in peptides, offer a wide range of chemical functionalities that could possibly facilitate the use of different SAPs, to tune membrane permeability using the same principles but under different conditions. Peptide self-assembly is the spontaneous organization of peptide strands into ordered structures through non-covalent interactions (Zhang & Altman, 2001). The versatility of these SAP systems with precise structural and conformational control at the nano scale offers exciting possibilities for the development of novel biomaterials (Zhang, 2003). The ability to undergo structural transitions triggered by external stimuli has been exploited in various applications including drug delivery, tissue engineering and biosensing (Liang et al., 2014; Luo & Zhang, 2012). Rationally designed self-assembling β-strand-forming peptides exhibit an entire hierarchy of structures from twisted tapes through ribbons, fibrils and fibres and can also be switched to α-helix or random coils, depending on solvent conditions (Aggeli et al., 2003; Smeenk et al., 2005; Vandermeulen et al., 2006).

In this study, a SAP was conjugated to poly(ethylene glycol) (PEG) polymer intended to act as a spacer between the peptide and the membrane surface, providing sufficient conformational freedom for the peptides to self-assemble. Research in the past has suggested that the conjugation of synthetic polymers to peptide sequences does not interfere with the

supramolecular self-assembly of the peptides, but tends to form a water-rich shell around the SAPs, limiting uncontrolled lateral aggregation of SAPs (Klok, 2005; Klok et al., 2000).

The intrinsic self-assembling capability of peptides has gained significant attention and has been extensively explored because of its potential for the development of a new class of hybrid biomaterials. However, to my knowledge, self-assembly of peptides or bioconjugates covalently attached to surfaces has not been demonstrated. Thus, in an attempt to achieve this, the work reported in this thesis involves a novel approach aimed at developing a stimuli-responsive membrane functionalized with a SAP and to study the influence of the self-assembly/disassembly of the peptide on the separation properties of the membrane (Figure 1-2). This method is believed to have broad applications in drug delivery and bioseparations.

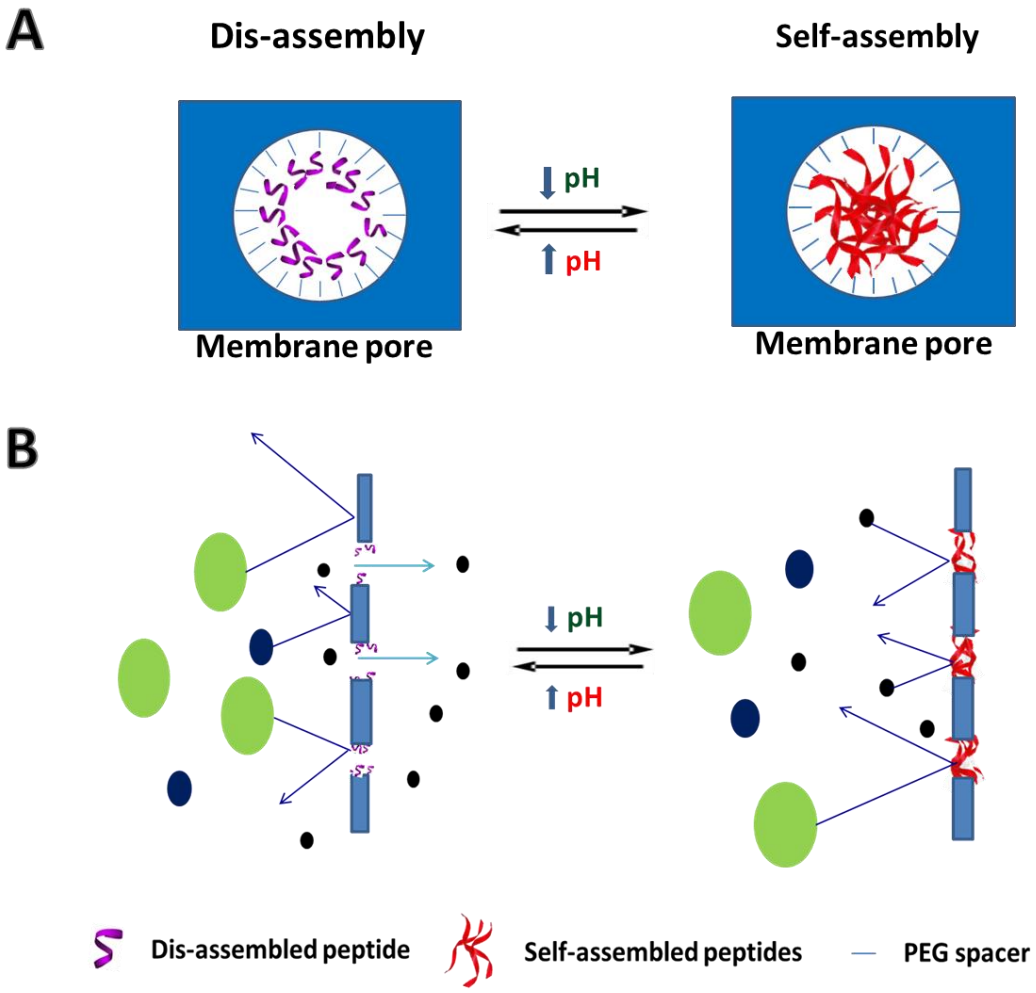

Figure 1-2: Schematic representation showing pH dependent reversible self-assembly of peptides tethered to membrane pores, A) top view, B) cross sectional view.

1.3 SIGNIFICANCE OF THIS RESEARCH

SAPs form structural networks that are ideally suited for various applications, which include tissue scaffolding and biosensors. Moving self-assembly out of the laboratory and into mainstream functional materials applications requires technologies that can exploit nanostructures at macro scale. Membranes are particularly suitable for this because they have macroscopic forms used in industrial separations at large scale (commonly 10^4 m^2 of

membrane area) but ultimately their function with respect to solute separation depends on the nanostructure of membrane pores. This may also carve a new route for controlled release drug delivery systems. Altogether, the attempted proof of concept in this study, could potentially lead to the development of a new generation of functional membranes based on the wide range of properties available in amino acid side-chains that can be combined in peptides, particularly those which self-assemble.

1.4 OBJECTIVES

The primary goal of this research was to develop a novel stimulus responsive membrane utilizing the structural versatility of SAPs to build intrapore networks of molecules and control the permeation of solutes and/or solvents through the membrane. To progress towards this overall goal, the following sub-objectives were addressed.

1. To identify a suitable reversibly SAP and determine the effect of conjugating a polymer spacer on the self-assembly behavior.
2. To functionalise a membrane surface for subsequent tethering of the SAP through the spacer molecule.
3. To tether the SAP to the membrane surface and/or within pores, while retaining self-assembly behaviour.

1.5 THESIS ORGANIZATION

Chapter 2 outlines the background of the research and provides an extensive review of the existing literature related to this study. In the first part of this chapter, the different types of SAPs and their stimuli-responsive features are described in detail. In the second part, the different conjugation strategies used to conjugate peptide and polymer and the self-assembly of such bioconjugates are explained. In the third part, an overview of the various chemistries used to immobilise carboxylate groups on alumina surfaces is given. The final part of this chapter describes the various methods and materials used to modify membranes, thereby making them stimuli-responsive, and the applications of such stimuli-responsive membranes.

Chapter 3 describes the first approach to characterizing one potential candidate SAP, named P11-4, to determine its suitability for use on a membrane. This candidate was subsequently abandoned, because it did not retain self-assembling properties after conjugation to the PEG spacer molecule but the work is included because it provides insights into the behaviour of SAPs after conjugation to other molecules.

Chapter 4 describes the rapid and reversible, pH-regulated self-assembly of peptide ELELELELELF (EL-5F) and its conjugates with 2 and 5 kDa PEG (EL-5F-PEG-2K and EL-5F-PEG-5K). Peptide EL-5F was conjugated to PEG 2K and PEG 5K via amine coupling and the conjugates were purified using size exclusion chromatography. The reversible pH dependent self-assembly of the peptide and its conjugates were confirmed using circular dichroism, transmission electron microscopy and Thioflavin T assay results. The influence of varied salt concentrations on self-assembly is also described.

Chapter 5 elucidates attempts to achieve pH-dependent, reversible self-assembly of EL-5F-PEG-2K when tethered to the surface of the Anodisc membrane. Various strategies carried out for the immobilisation of carboxylate groups on the Anodisc alumina membrane surface

such as i) phosphonic acid chemistry, ii) diazonium chemistry and iii) polyelectrolyte multilayer (PEM) adsorption, are outlined. The characterization of the modified membrane using flux tests and molecular weight cut off experiments at different pH values is presented. Finally, to test the underlying hypothesis that SAPs would retain their self-assembly when tethered to a surface, this chapter also describes additional analyses carried out to study the reversible self-assembly of EL-5F and EL-5F-PEG-2K tethered to nanoparticle surfaces, using dynamic light scattering (DLS) experiments.

An overall set of conclusions and recommendations for further work are presented in Chapter 6.

CHAPTER-2

REVIEW OF LITERATURE

2. REVIEW OF LITERATURE

2.1 INTRODUCTION

The aim of this research was to develop a novel stimuli responsive membrane functionalized with SAP-polymer bioconjugates. The polymer conjugated with the peptide acts as a spacer thereby providing necessary conformational freedom for the peptide to self-assemble. This attempt to tether the SAP and its bioconjugates to membrane surfaces and investigations on the effect of self-assembly on the permeation properties of the membrane pores could potentially have broad applications. To provide the reader with a better understanding of this research, this chapter will first outline the advances in the development of SAPs and various peptide-polymer bioconjugates. An overview of various strategies for conjugation and self-assembly of such bioconjugates is given. Finally, strategies for bioconjugate-membrane tethering and stimuli responsive membranes developed for various applications are also discussed.

2.2 MOLECULAR SELF-ASSEMBLY

Molecular self-assembly is the spontaneous unification of molecules into ordered hierarchical structures through non covalent interactions (Figure 2-1). Molecular self-assembly is pervasive in nature and has emerged as a new strategy in chemical synthesis, polymer science and engineering (Ball, 1994; Lehn, 1993; Whitesides et al., 1991). Two key features in molecular self-assembly are chemical complementarity and structural compatibility through weak and non-covalent interactions (Zhang, 2002), which include hydrogen bonds, ionic bonds and Van der Waal's forces (Pauling, 1960). Though these bonds are weak, their

collective interactions can result in well-defined stable macroscopic structures. Self-assembly occurs spontaneously in nature, for example self-assembly of the lipid bilayer membrane, assembly of proteins into quaternary structures, formation of double helical DNA via hydrogen bonding and assembly of collagen and keratin into ligaments and hair (Zhang, 2002). These natural occurrences formed the basis for design and creation of several useful man made self-assembling molecules.

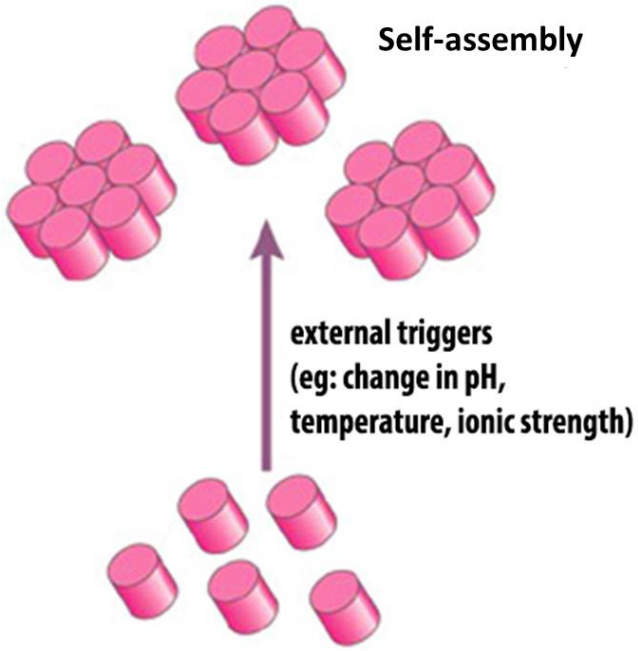

Figure 2-1: Self-assembly (bottom up approach) of molecules under the influence of external stimuli.

2.3 SELF-ASSEMBLING PEPTIDES

Molecular self-assembly has stimulated interest in self-assembling molecules such as peptides. Zhang and his colleagues discovered a new class of peptide based biological materials in yeast from the self-assembly of complementary oligopeptides (Zhang et al., 1993). EAK16-II was the first SAP to be discovered as a repetitive segment in zuotin, a yeast protein that was actually characterized to preferentially bind to left handed Z-DNA (Zhang et

al., 1992). Henceforth, SAPs have been emerging strongly in different directions (Figure 2-2) offering potential applications in diverse fields such as biomedical sciences, biological surface engineering and biosensing (Zhang, 2002). Zhang and co-workers classified the SAPs under four categories (see Section 2.3.1). Aggeli et al. (2001) designed β sheet-forming SAP systems, which form hydrogels upon self-assembly. Peptide nanotubes were found to self-assemble and insert themselves into lipid bilayer membranes, allowing the passage of ions across cell membranes (Bieri et al., 1999).

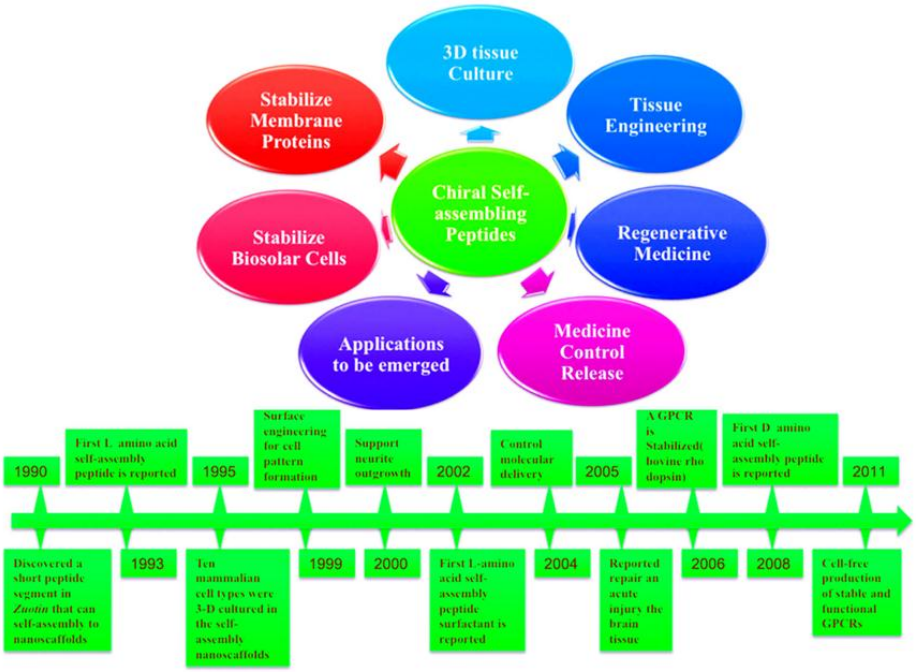

Figure 2-2: Timeline showing the development process and applications of SAPs spanning over 20 years. Image adapted from (Luo & Zhang, 2012).

2.3.1 Type I SAPs

Type I SAPs consist of distinct hydrophilic and hydrophobic sides and thus form β sheet in solutions. These peptides form complementary ionic bonds with regular repeats on the hydrophilic side. The complementary ionic sides are classified into several moduli based on the positive and negative charges of the amino acids on the hydrophilic surface (Table 2-1). This charge configuration plays a crucial role in determining the secondary structure of the peptide (Zhang et al., 1993; Zhang et al., 1995).

Table 2-1: Charge distribution in different moduli of Type I SAPs

Modulus	Arrangement
I	- + - + - + - +
II	- - + + - - + +
IV	- - - - + + + +

2.3.2 Type II SAPs

Type II peptides are known as "molecular switches" due of their ability to change the molecular structure in response to environment changes. DAR16-IV (DADADADARARARARA) and EAK12-d (AEAEAEAEAKAK) are two peptides, which change their conformation from β sheet to α helix upon increase in temperature (Zhang & Rich, 1997). Similar structural transitions can also be induced by changing the pH. DAR16-IV exhibits a helical structure at pH 1-2 and a β sheet at pH 5 or above. Conversely, EAK12-d forms stable β sheet at pH 1-3 and changes to alpha helix upon increasing the pH to 5 (Altman et al., 2000).

Both DAR16-IV and EAK12-d have a cluster of negatively charged residues close to the N-terminus and a cluster of positively charged residues on the C-terminus (Hol, 1985; Hol et al., 1981). Therefore, the secondary structures of such sequences may undergo drastic conformational changes under appropriate conditions. There have also been many other reports on the self-assembly and disassembly or change in conformations of proteins and peptides depending on environmental changes such as pH, temperature or crystal lattice packing (Zhang & Altman, 1999).

These outcomes not only provide insights into protein-protein interactions during protein folding and pathogenesis of some protein conformational diseases such as Parkinson's, and Alzheimer's disease but also can be developed into molecular switches that can be regulated by changing the environmental conditions (Zhang, 2002).

2.3.3 Type III SAPs

Type III SAPs were primarily developed for biological surface engineering. They undergo self-assembly onto surfaces rather than between molecules, which could be described conceptually as a "molecular paint". They form monolayers on surfaces for interaction with other molecules. These peptides consist of a ligand, linker and an anchor. The terminal segment is the ligand, which incorporates diverse functional groups for recognition by different biomolecules. The linker acts as a spacer and allows for flexible interaction at a specified distance away from the surface. The final feature is the anchor, which consists of a functional group aiding the covalent attachment of the peptide to the surface (Zhang, 2002). These peptides can be used for the modification of variety of surfaces in the field of biomedical engineering to study cell-cell communication (Zhang & Altman, 2001) and to form non-fouling self-assembled monolayers (Nowinski et al., 2012). Similar SAP systems,

with a segment of linker for surface anchoring, have also been developed by Whitesides and his group (Chen et al., 1997; Whitesideset al., 1991).

2.3.4 Type IV SAPs

These surfactant-like peptides undergo self-assembly to form nanotubes and nanovesicles with diameters around 30-50 nm (Figure 2-3). Detailed studies of these molecules helped in the design of non-lipid biological surfactants and understanding in depth the subtleties of self-assembly (Vauthey et al., 2002). Each peptide monomer is about 2 nm in length, consisting of seven to eight amino acids. They have a hydrophilic head composed of aspartic acid and a hydrophobic tail involving amino acids such as alanine, valine or leucine. These types of peptides have much in common with biological phospholipids, which also comprise of a hydrophilic head and hydrophobic tail (Zhang, 2002).

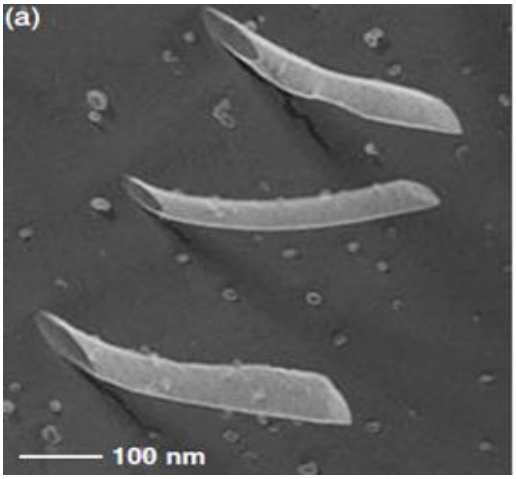

Figure 2-3: TEM image showing surfactant like peptides forming nanotubes with diameter around 30-50 nm. Image reproduced from (Zhang, 2002).

2.3.5 Responsive peptide hydrogels

Over the years, research on hydrogel forming SAPs has gained a lot of attention due to their synthetic accessibility, low cost and high stability. Boden et al. (1997) first reported the discovery of peptide-based hydrogels and suggested that the presence of attractive forces between side chains, lateral interaction between adjacent β sheets and strong adhesion of solvent to the β sheet can facilitate their design. In addition to this they initially identified the responsiveness of some peptide hydrogels to changes in pH. QATNTDGSTDYGILQINSR is a peptide that forms a hydrogel below pH 12 but dissolves when the pH is increased above 12. Boden and his team were motivated by this fact and developed the following series of shorter peptides comprising pH responsive residues such as arginine, glutamic acid and ornithine.

1. **P11-2 (QQRFQWQFEQQ):** P11-2 formed stable nematic gel consisting of fibrils at pH below 5 but increasing the pH led to flocculation. Perhaps this pH sensitivity was due to the overall charge of the peptide. Below pH 5, the glutamic acid residues are protonated, leaving the peptides with a net positive charge (arginine), which stabilizes the fibrillar dispersion. Above pH 5, when the peptide is uncharged, the inter-strand interaction become too strong and leads to flocculation.
2. **P11-3 (QQRFQWQFQQQ):** As the glutamic acid residues had a great effect on the pH sensitivity of the hydrogel, Boden and his co-workers synthesized peptide (P11-3), which is similar to P11-2 except the glutamic acid residue was replaced with glutamine. P11-3 formed nematic gels over a wide pH range, and flocculation was observed only above pH 10 due to the deprotonation of arginine, 2.5 pH units lower than that of free arginine in solution.

3. **P11-4 (QQRFEWEFEQQ):** P11-4 was developed replacing glutamine residues at positions 5, 7 and 9 with glutamic acid in P11-3. This peptide was shown to adopt four different phases depending on pH that include: (*i*) nematic gel (pH< 3.2), (*ii*) flocculated solution (pH 3.2-5), (*iii*) nematic fluid (pH 5-7) and (*iv*) isotropic fluid (pH>7), respectively. The γ-carboxyl groups of the glutamic acid residues are uncharged at pH < 3 and there is one net positive charge per peptide on Arg^+. This aids in the self-assembly of the peptide. At pH > 7, all the carboxyl groups are deprotonated (negatively charged), thus, causing electrostatic repulsion between the adjacent γ-COO^- leading to dissociation of fibrils (Figure 2-4).
4. **P11-5 (QQXFXWXFEQQ):** P11-5 is also a 11 residue peptide containing three ornithine residues at positions 3, 5 and 7 of P11-4 peptide. Converse to P11-4, P11-5 forms a nematic gel at high pH and turns into an isotropic fluid at low pH. The switching occurs between pH 7.4-7.8. Switching between isotropic and nematic phases is reversible in both P11-4 and P11-5 and it takes place in seconds (time). However switching from low pH to high pH and vice versa over three cycles of pH shifts results in buildup of ionic strength due to repeated additions of acid and base, leading to screening of the electrostatic repulsion between fibrils and ultimate flocculation (Aggeli et al., 2003).

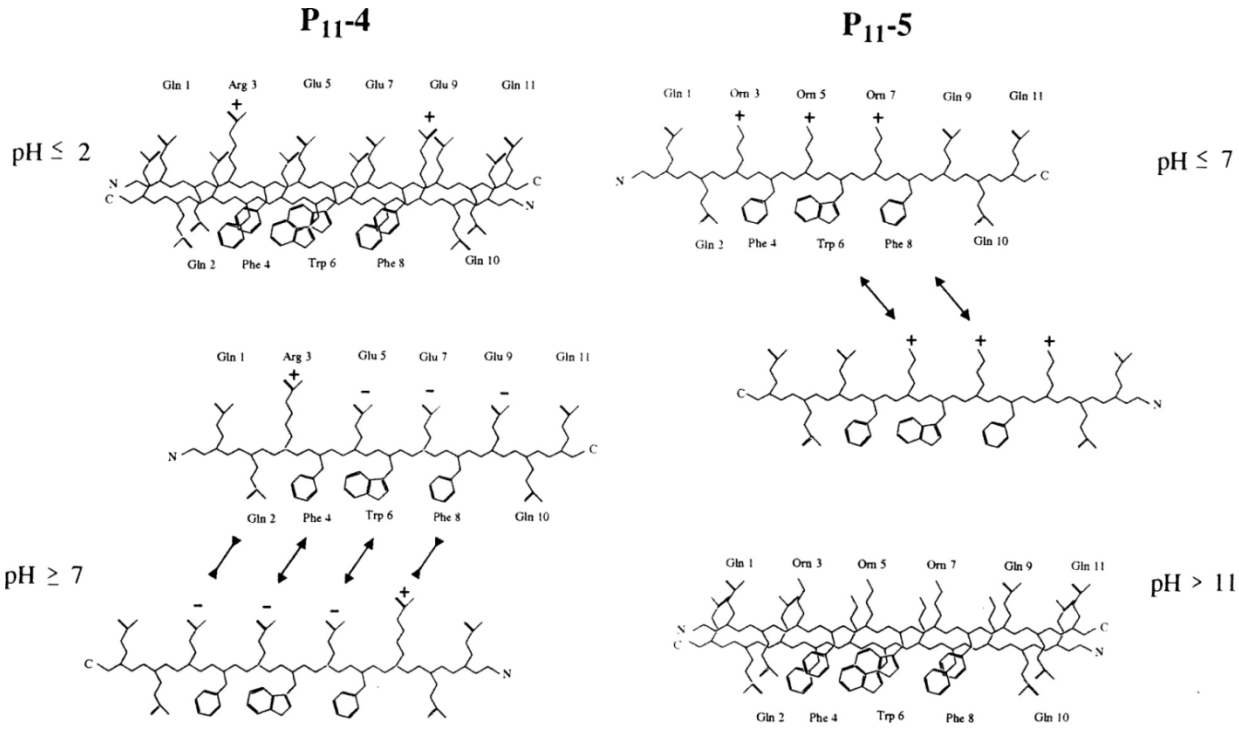

Figure 2-4: The self-assembled and disassembled states of peptides P11-4 and P11-5 at low and high pH values. Image reproduced from (Aggeli et al., 2003).

5. **MAX1 (VKVKVKVKV^{D}PPTKVKVKVKV-NH2):** MAX1 is a hydrogel-forming SAP, developed by Schneider and co-workers, which is entirely based on β hairpins. It contains two eight residue strands of alternating valine and lysine amino acids connected by a tetrapeptide sequence (-**V^{D}PPT**-). MAX1 exists as a random coil below pH 5.5. It cannot self-assemble until controlled solution conditions (pH 9) permit intramolecular folding of the peptide into a β-hairpin conformation. This transition is mainly due to the deprotonation of the lysine residues, which are protonated at low pH, resulting in intra-strand repulsion. Upon deprotonation, the repulsion is relieved and intra-molecular hydrogen bonds are formed, yielding a β hairpin. This β hairpin is characterized by the type II β turn centered at **V^{D}PPT**, which connects the two amphiphilic β strands, resulting in a hairpin with one lysine rich face

and the other hydrophobic, valine rich face. This folded state is prone to intermolecular self-assembly and it is reversible too. As suggested by the authors, the self-assembly of a gel from monomeric hairpins is due to the formation of lateral hydrogen bonds and facial hydrophobic interactions. The control peptide VKVKVKVK-NH_2 did not show any sign of gelation proving that β hairpin formation is essential for gelation to occur. MAX1 hydrogel surfaces exhibit antibacterial activity against E. *coli*, K. *pneumoniae*, S. *aureus*, S. *epidermidis* and S. *pyrogenus*. Co-culture experiments showed that the hydrogel surface inhibited bacterial proliferation but allowed mammalian cell proliferation (Salick et al., 2007).

6. **RATEA 16 (RATARAEARATARAEA):** RATEA 16 is peptide that forms a hydrogel at neutral pH. This exhibits a reversible three phase system; acidic (pH < 3.5) - monomers in solution; neutral (pH 7.4) - hydrogel; basic (pH > 12.5) - precipitate. At pH < 3.5, RATEA 16 existed as monomers due to the protonation of glutamic acid residues resulting in inter strand repulsion. Above pH > 12.5, the arginine residues are deprotonated, leaving the peptide with no net charge. This led to aggregation, promoted by the hydrophobic interactions between the alanine residues. However, at neutral pH, the glutamic acid and arginine residues are all charged, giving rise to electrostatic attraction between them, as well as inter-strand repulsion due to a net charge of +2. This blend of attractive and repulsive forces ensures that the peptides interact and disperse well, respectively (Zhao et al., 2008).

2.3.6 Responsive peptide amphiphiles

Peptide amphiphiles (PA) are a different class of SAPs that possess a hydrophobic tail and a hydrophilic head. Stupp's group pioneered the research in this field (Cui et al., 2009; Cui et al., 2010; Hartgerink et al., 2002). A family of PA's was demonstrated to self-assemble reversibly into nanofiber networks, which resulted in the formation of hydrogels with changes in pH. The PA fibers can also be reversibly polymerized by oxidation/reduction to enhance their stability. Molecules self-assemble to form a hydrogel upon acidification and dissemble at neutral and basic pH. PA's that are oxidized do not self-assemble at acidic pH due to the formation of intra-strand disulfide bonds. This renders the fibers unaffected with changes in pH. Similarly, the supramolecular fibers that are polymerized (oxidized) also lose pH sensitivity and are stable over a wide range of pH. However reduction restored the pH-controlled reversible assembly/disassembly, showing the high degree of control this system permits over the assembly process (Figure 2-5).

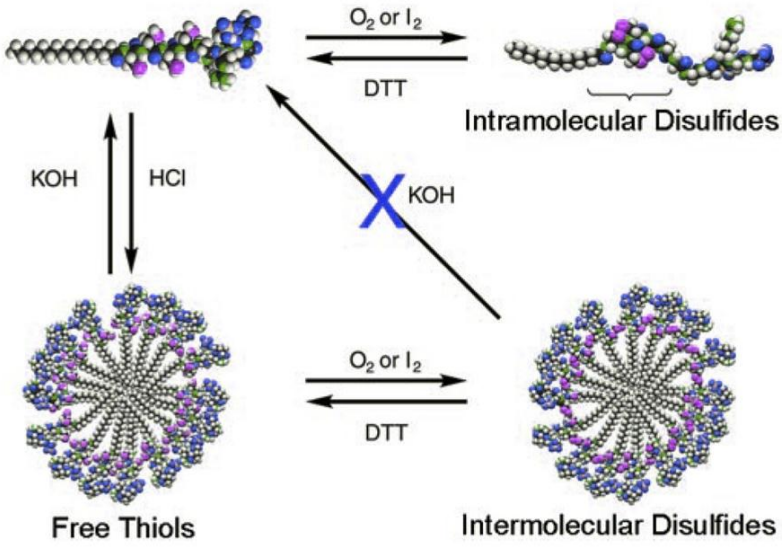

Figure 2-5: Reversible self-assembly of peptide amphiphiles. Image adapted from (Hartgerinket al., 2002).

With a wide range of self-assembling peptide systems available, it becomes critical to choose the appropriate type of peptide suitable for the development of stimuli-responsive membranes. The prerequisite for a robust and reversible membrane is a peptide that can rapidly and reversibly self-assemble in response to external stimuli. However, there have been few demonstrations of rapid and reversible self-assembly of peptides. DAR16-IV and EAK12-d peptides were reported to self-assemble upon changes in pH and temperature but *reversible* self-assembly of these peptides has not been described. P11-4 and P11-5 peptides can be considered promising candidates due to their spontaneous and reversible self-assembly in response to external triggers (e.g., pH, ionic strength). The reversibility in previous work persisted only for 3-4 cycles due to the salt build up in solution. However, it is predicted that this might not potentially limit the incorporation of these peptides onto the membrane surface because the solution passing through the pores is constantly refreshed, preventing salt

accumulation. Furthermore, the use of P11-4 can potentially enable the site-specific conjugation of the polymer spacer to the N terminal amine of P11-4 via amine coupling. This may be difficult to achieve with P11-5, however, because of the presence of amine side chains on the ornithine residues. Thus, in this study, P11-4 was chosen as a promising candidate for the development of peptide-polymer bioconjugates because of its potential to reversibly self-assemble and also because of the capability for its site-specific coupling to polymers.

2.4 PEPTIDE-POLYMER BIOCONJUGATES

The conjugation of synthetic polymers with polypeptides and proteins has given rise to new class of hybrid materials with unique properties. These bioconjugates hold great promise for diverse biomedical applications such as drug delivery (Liang et al., 2014; Qiao et al., 2014), tissue engineering (Luo & Zhang, 2012) and biosensing (Yemini et al., 2004). Peptide-PEG bioconjugates are the most promising candidates belonging to this class of materials. The conjugation of PEG to a peptide can enable retention of self-assembly (Hentschel et al., 2006; Pechar et al., 2002) while preventing aggregation (Collier & Messersmith, 2004; Smeenk et al., 2005) and increasing the stability (Hamley et al., 2005) and biocompatibility of the bioconjugate (Vandermeulen & Klok, 2004)

2.4.1 PEG polymer spacers

Tethering the peptide directly to the membrane surface would restrict its secondary structure transformation and self-assembly. Therefore, it is necessary that the peptide is provided with sufficient conformational freedom to self-assemble. To achieve this, a spacer acting as a linker between the peptide and the membrane surface can potentially aid in the self-assembly

of the peptide. PEG is a widely used spacer. Aminohexanoic acid and hexamine are other well-known spacers.

PEG is a hydrophilic, inert polymer composed of repeating units of CH_2CH_2O. It is widely used to stabilize, immobilize and modify the physical properties of biological molecules. The process of chemically linking proteins and peptides to PEG is known as pegylation. PEG is nontoxic, nonionic and highly flexible. Pegylated proteins and peptides have become increasingly important in therapeutics over the past few decades. Pegylation results in longer therapeutic half-lives, improved circulation, lower immunogenicity and antigenicity compared to that of the native compounds (Veronese & Harris, 2002; Veronese & Pasut, 2005). PEG reduces the tendency for proteins to aggregate, thus increasing solubility and stability (Morar et al., 2006). Pegylation acts as a guard for peptides and proteins and prevents electrostatic and hydrophobic interactions with other proteins and reduces protein adsorption on surfaces. PEG has been used as a linker to immobilize proteins or peptides to surfaces (Nolan et al., 1999). Trau et al., (2005) have used PEG linkers to display antigenic peptides on surfaces of microspheres for diagnostic purposes. In such applications, it is very important that the peptide is accessible to the potential receptor such as the antibody and also that the peptide is free to take its conformation. Thus, in this study, a PEG spacer was conjugated to the peptide to act as a linker between the membrane surface and the peptide and provide sufficient conformational freedom for the peptide to self-assemble.

2.4.2 Strategies for peptide-PEG bioconjugation

In this study, the peptide was conjugated to a PEG spacer prior to tethering onto the membrane surface. A number of strategies are available for peptide-polymer bioconjugation, of which a few prominent strategies are discussed below.

Initially, the methods used to conjugate peptides and polymers resulted in non-specific conjugation, leading to the formation of positional isomers. Later, site-specific conjugation techniques were developed that provided precise control over the peptide/polymer ratio and the site of conjugation without influencing the properties of the polymer and the peptide. Klok (2005) broadly classified these methods into liquid and solid phase synthesis. This was further grouped into convergent and divergent methods. In the convergent method, a pre-synthesized polymer is tethered to a pre-synthesized peptide, usually achieved through site-specific conjugation. However, non-specific conjugation can also be achieved under basic conditions by amine coupling between the N-hydroxy succinimidyl group on the polymer and the ε-amino group of the most prevalent lysine residues of the peptide/protein sequence. In order to achieve site-specific conjugation, the N-terminal amine can be targeted by reductive alkylation using a aldehyde functionalized polymer. The pKa values of the N-terminus amine ranges from 7.6 to 8 and those of lysine residues ranges from 10-10.2. Therefore, under slightly acidic conditions (pH 5), the polymer is selective for the N-terminal amine due to the lower pKa. Kinstler et al. (1996) demonstrated the site specific conjugation of mPEG-propionaldehyde to the α-amine of protein under acidic conditions (pH 5).

Chemoselective conjugation was achieved through thiol coupling to free cysteine groups by using maleimide chemistry (Kopecky et al., 2006). Cysteines usually form disulphide bonds and it is rare to find a free cysteine group. In designed peptides, a single cysteine can be engineered into the sequence to provide a specific conjugation site. This can be done in such

a way that the cysteine residue is located away from the sequence that determines the structural organization of the peptide so that the conjugated polymer does not hinder the self-assembly process. Yang et al. (2008) used this method to form hydrogels by self-assembly. Sato (2002) reported the use of transglutaminase enzyme to catalyse the acyl transfer between the γ-carboxyamide group of glutamine and alkylamines under mild conditions to conjugate PEG to protein.

Carboxylated PEG has been amine coupled via NHS activation to peptides using N,N'-dicyclohexylcarbodiimide (Xu et al., 2007). The reaction of diazonium derivatives to tyrosine has been exploited to link diazo-functional PEG to pentapeptide (D-Ala2) – leucine encephalin (Jones et al., 2012). The reaction of aminooxy end functionalized polymers and levulinyl-modified peptides results in oxime formation (Heredia et al., 2007). This method has been used to conjugate branched PEG to peptides such as anti-HIV protein (Miranda et al., 2007). Cycloaddition click reaction between alkynes and azides has been employed for bioconjugate synthesis (Lutz, 2007). Alkyne functionalized peptidomimetics and diazido-PEG hev been linked using this chemistry (Isimjan et al., 2010).

Reversible conjugation can be achieved through noncovalent chemistries. For example, peptides tagged with hexahistidine motif (as in affinity chromatography) is recognized by complementary nickel-nitriloacetic acid complex on end-modified PEG. This reversible PEGylation method is used to screen therapeutic proteins *in vivo* (Kim et al., 2013).

N-carboxyanhydride polymerization from PEG microinitiators has been successfully used to synthesize peptide-polymer conjugates (Hadjichristidis et al., 2009). This method was used to polymerise L-alanine from amino-terminated PEG (Zhang et al., 2003). Another method uses PEG as a cleavable support to synthesis the peptide (Gravert & Janda, 1997). A range of PEGylated resins are available commercially. PEG chain is connected to the peptide via a

photocleavable, acid or base labile linker (Thumshirn et al., 2003). PEG diols were coupled to Fmoc-amino acids making it compatible with solid phase peptide synthesis and used to synthsize (on resin) a peptide-PEG-folate conjugate (Niculescu-Duvaz et al., 2008). Mono disperse Fmoc-PEG-COOH have been used to prepare conjugate such as PEG-FFKLVFF-COOH (Castelletto et al., 2012). PEG functionalized resins such as Tentagel PAP ^{TM} consists of PEG chains tethered to cross linked polystyrene beads via labile benzyl ether linkages. This method was initially developed to improve the solubility of the synthesized hydrophobic peptides from these PEG supports (Kleine et al., 1994). Mutter et al. (1980) developed liquid phase synthesis of peptides from linear PEG supports.

In contrast to the previously discussed convergent techniques, in the divergent method initiators for polymerization reaction such as atom transfer radical polymerization (ATRP) are incorporated at the peptide termini (Le Droumaguet & Nicolas, 2010). Two different ATRP initiators were tethered to the terminals of model matrix metalloprotease substrate peptide. POEGMA and PNIPAAm were polymerized from the C and N terminals respectively. The self-assembly of this conjugate in an aqueous solution and the enzymatic degradation of the peptide linker were demonstrated successfully (de Graaf et al., 2012).

Earlier methods developed for peptide-PEG conjugation resulted in non-specific coupling. Subsequently, several strategies such as thiol coupling via maleimide chemistry, orthogonal coupling via click chemistry and solid phase supported conjugation were developed for site-specific tethering of peptide and PEG. Despite the high yields possible using some of these techniques, they involve tedious multiple reaction steps and the use of a number of reagents. However, amine coupling of NHS-activated PEG to the peptide could be carried out on the free peptide rather than during its solid-phase synthesis and is simple, rapid and inexpensive compared with the conjugation methods reviewed above.

2.4.3 Self-assembly of peptide-polymer conjugates

A critical determinant of success during the development of a reversible peptide-polymer bioconjugate is the role of the polymer spacer on the self-assembly of the peptide. Because this study involves the development of a peptide-polymer bioconjugate and the subsequent tethering of this bioconjugate onto a membrane surface, it is important that the conjugation of the PEG polymer spacer to the peptide does not hinder the self-assembly process. It has been proven in the past that the conjugation of random coil amphiphilic synthetic polymers to peptides generally does not interfere with the supramolecular self-assembly of the peptides (Figure 2-6). The self-assembly of low molecular weight polymers or high molecular weight block copolymers is forced by non-specific interactions. In the case of peptide-polymer hybrid materials, the assembly process is mediated by specific folding and organization properties of the peptide sequence, which may lead the formation of ordered hierarchical functional structures (Waterhouse & Gerrard, 2004; Zhang, 2003).

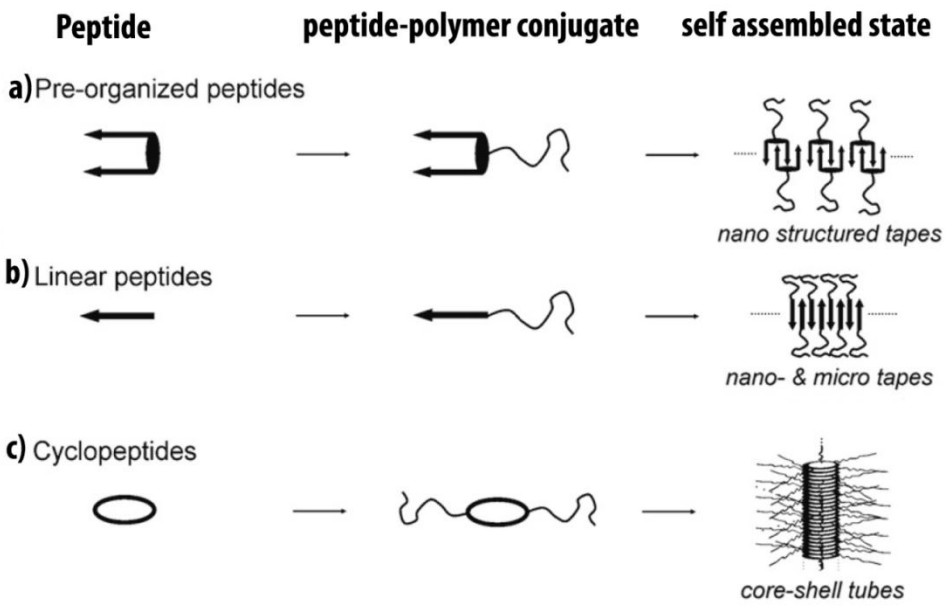

Figure 2-6: Peptide guided self-assembly of peptide-polymer bioconjugates. Image adapted from (Borner, 2009).

Self-assembly of β sheet, α helix and coiled coil peptide–PEG conjugates have been reported in the past. The most prevalent and widely applied β sheet self-assembling bioconjugates have been discussed in detail in the forthcoming section. One of the first to work in this field was Meredith and co-workers. They investigated the aggregation properties of the central domain of a diblock copolymer of β-amyloid peptide and PEG and found that the core of fibrils formed by this diblock copolymer resembled the one formed by the β-amyloid peptide (Burkoth et al., 1998).

A conjugate comprising peptide QQKFQFQFEQQ and PEG 3700 chain self-assembled into β sheet fibrils. Another diblock conjugate of PEG 440 and truncated peptide KFQFQFQ also formed fibrils, although the morphology of the conjugate fibrils differed from that of the native peptide (Collier & Messersmith, 2004). Conjugates comprising of N-terminal alkyl chain and C terminal PEG 3000 tethered to amyloid forming hexapeptide KTVIIE were

shown to form self-assembled fibrils. This could be dismantled by the removal of alkyl chains via UV active photo liable nitrobenzyl group (Meijer et al., 2007).

Castelletto et al. (2010) studied the influence of PEG molar mass on the self-assembly of the conjugate FFKLVFF-PEG. PEG 1000, PEG 2000 and PEG 10000 were tested. It was found that all three FFKLVFF-PEG conjugates formed fibrils retaining the β sheet secondary structure of the peptide in the core. At high concentrations, the conjugates with PEG 1000 and 2000 formed nematic phase, whereas the one with PEG 10000 exhibited a hexagonal columnar phase. The effect of PEG molar mass on the self-assembly of another conjugate FFFF-PEG was also studied. The conjugate with a low molecular weight PEG formed nanotubes consisting of antiparallel β sheets whereas at higher PEG molar mass, fibrils were observed (Tzokova, Fernyhough, et al., 2009). It was also reported that at higher concentrations, the nanotube cross linking led to the formation of soft hydrogels (Tzokova, Fernyhouph, et al., 2009).

The formation of β sheet self-assembled fibrils by conjugate DGRFFF-PEG was reported by Castelletto and co-workers. It was observed that on tissue culture plates, low concentration DGRFFF-PEG films enhanced cell proliferation whereas on low attachment surfaces, no cell proliferation was observed. The PEG shell surrounding the peptide core in the fibril structure hinders access to the RGD motif, thus preventing cell adhesion (Castelletto et al., 2013).

Conjugate comprising PEO68 and a peptide incorporating a $(TV)_4$-ester-VG 'switch' forms β sheet tape structures in an aqueous solution at pH 6.2 because of an O → N acyl switch (Hentschelet al., 2006).

Radu et al. (2009) reported the self-assembly of a bioconjugate formed upon conjugation of peptide P11 (QQRFQWQFEQQ) and poly [N-(2-hydroxypropyl) methacrylamide] (HPMA). It was observed that the peptide P11 self-assembled at pH 2 and disassembled at pH 7 whilst

the conjugate P11-poly(HPMA) retained the random coil structure at both these pH. However, further increase in pH (pH > 11) using 1 M NaOH and subsequent incubation for 10 days resulted in the secondary structure transition towards β-sheet. This was attributed to the presence of Na^+ ions, pH and incubation time. Several other groups have also investigated the self-assembly properties of hybrid diblock and triblock polymers based on various β-strand peptide sequences and PEG. All these studies have confirmed the ability of the peptide to direct the self-assembly of the block copolymers into fibrils or ordered suprastructures (Rosler et al., 2003).

Other approaches involved pH changes to initiate self-assembly in bioconjugates, by the removal of temporarily induced defects in the peptide moiety (Hentschelet al., 2006), protecting group strategies (Yu et al., 2009) and enzymatic approaches (Kühnle & Börner, 2009).

It is important to note that, the above-mentioned methods are all irreversible (Kuhnle & Borner, 2011). Despite achieving great success in conjugation and self-assembly of peptide-polymer segments, repeated use of external triggers to reversibly manipulate the secondary structure of bioconjugates remains a challenge. This study aims at developing a stimuli-responsive membrane for rapidly reversible permeability control. It is important that the tethered bioconjugate can self-assemble rapidly and reversibly on the membrane surface with repeated changes in external stimuli. Thus, a robust and rapidly reversible self-assembling bioconjugate was sought. Recently, Kuhnle et al. (2011) demonstrated the reversible self-assembly of the peptide domain (ELELELELELFG, EL-5FG) in a peptide-PEG bioconjugate using calcium (Ca^{2+}) ions. Ca^{2+} ions bind to the deprotonated carboxylates, thus screening the negative charges and enabling self-assembly. On addition of EGTA, it binds to the Ca^{2+} ions reverting the system back to the disassembled state. The peptide segment, containing an alternating pattern of hydrophilic and hydrophobic amino acids, had a high tendency towards

β sheet formation but the extent of conversion decreased markedly within three cycles of secondary structure shifts, attributed by the authors to increased ionic strength.

2.4.4 Bioconjugate self-assembly on membrane surfaces

Despite the wide range of studies conducted on the self-assembly of peptide-PEG bioconjugates in solution, no attempts have been made in the past to tether SAPs or bioconjugates to membrane surfaces and pores and study the effect of self-assembly on the permeation properties of the membrane. Although, stimuli responsive polymers have been incorporated into membrane pores to control permeation for specific separation purposes, the development of a novel membrane functionalised with SAPs can add a new dimension to membrane transport. Rationally designed SAPs can form a range of structures triggered by external stimuli, which will possibly have a significant influence on the transmembrane permeability. Such membranes would have wide applications in the field of separations, drug delivery and biosensors.

Two main considerations associated with using peptides as functionalization agents in membranes are

i) Cost: Over the years, a number of methods and chemistries have been developed for building peptide chains. In the last ten years, solid phase peptide synthesis (SPPS) has emerged as the most popular method for peptide synthesis. It can be performed using two different techniques, Boc protection chemistry and Fmoc chemistry (Palomo, 2014). The latter one has become popular due to the simplicity of the process and because the use of hazardous hydrogen fluoride can be avoided (Made et al., 2014). The advances in synthetic peptide chemistry, solid support materials and purification technology have brought down the large scale production costs to a great extent (Al-Warhi et al., 2012; Thayer, 2011). One gram of peptide costs around few hundred dollars and only a few grams of peptide will be required

for the modification of a square meter area of a membrane surface. This SAP functionalized membrane is designed to be reusable due to the stimuli responsive reversible self-assembly of the tethered peptide molecules. Fouling on the membrane surface and pores could possibly decrease the efficiency of the membrane after repeated use and therefore it may need to be discarded. As this is a novel membrane based on peptides, further research is needed to optimize the cleaning procedures to check the compatibility of various solvents on the functionality of the membrane and the associated costs. This may further increase the longevity of the membrane. Taking into consideration the low production costs of peptides and reusability of these membranes, the overall costs associated with each purification process should be minimal.

ii) Stability: Peptides are much more stable than proteins because the two factors that affect protein stability do not exist in synthetic peptides. These are tertiary folding and proteinase contamination. They are robust and stable for several weeks even at room temperature (Bell, 1997).

2.5 STIMULI-RESPONSIVE MEMBRANES

The demand for membrane technology in both laboratory and industrial scale applications has been consistently increasing over the past few decades. In the laboratory, membranes are used primarily for purification and separation of proteins and other biomolecules whereas industrial applications include gas separations, medicine, waste water treatment and desalination of drinking water. Membrane technology utilises low energy and works without addition of any chemicals. To precisely control the permeability and separation properties, membranes have been modified using various methods and materials to render them stimuli responsive (Zhao et al., 2011). The growing interest in the synthesis of novel hybrid materials

with switchable physiochemical properties has contributed largely to the development of stimuli responsive membranes whose permeation properties can be tuned using external stimuli such as pH, temperature and ionic strength. In these approaches, either the synthesized stimuli responsive materials have been processed directly into membranes or the existing base membrane is chemically modified to immobilise responsive polymers to the surfaces. The latter has gained importance over the years with modification of membranes with a range of stimuli responsive materials whose structure and conformation under different conditions influence the permeability of the membrane. The two important conditions to be satisfied for successful membrane modification are, i) the properties of the base membrane should be conserved, and ii) successful functionalization of the membrane with responsive molecules (Wandera et al., 2010).

Membrane functionalization is carried out in two ways (Figure 2-7), the 'grafting to' method, which involves tethering preformed, end-functionalized molecules to the surface, and the 'grafting from' method, which is a surface-initiated polymerization technique whereby the polymer chains grow from initiator sites on the membrane by addition of monomers from a solution (Zhao & Brittain, 2000).

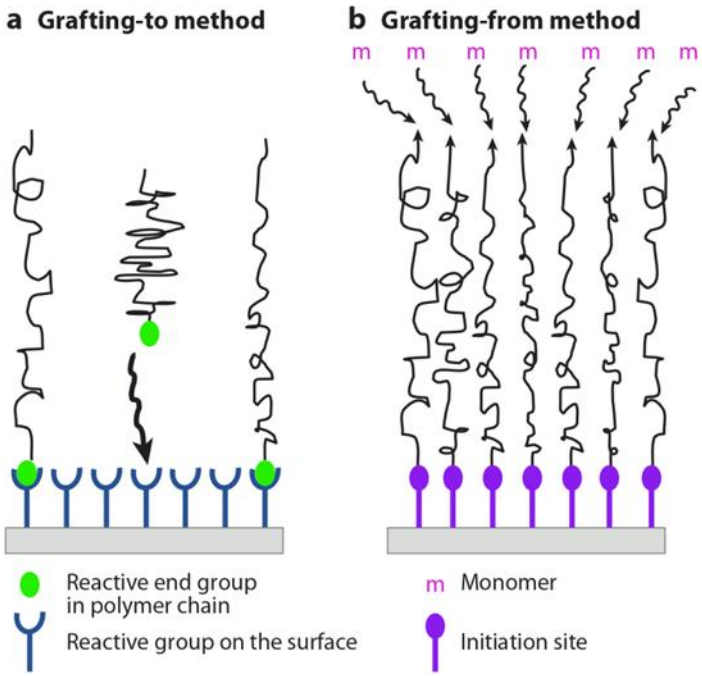

Figure 2-7: Schematic representation of membrane functionalization approaches, a) the grafting-to method, in which the functional end groups in a polymer chain are covalently coupled to active groups on the surface, b) the grafting-from method, in which the polymer chains grow from initiator sites tethered to the surface. Image adapted from (Jain et al., 2009).

2.5.1 Surface-initiated modification

The 'grafting from' method is done in two steps: the first step immobilizes the initiator precursor on to the membrane surface and the second step initiates polymer growth from the immobilized initiator sites by monomer addition. There are several methods employed for surface-initiated modification, of which a few are described below.

I) ATRP: ATRP provides well-ordered growth of polymer chains on the membrane surface. It is carried out in two steps: immobilization of the ATRP initiator on the membrane and catalyst triggered polymerization from the immobilized initiator sites (Friebe & Ulbricht, 2007).

II) Photo-initiated polymerization: In this method a photo initiator such as benzophenone is coated on to the membranes by immersing the membrane in a solution containing the initiator. Then the membrane is dipped into monomer solution for polymerization to occur form the immobilized initiator sites, in the presence of UV light under an inert atmosphere. This method is often used to modify membranes with polymers that respond to pH, temperature, ionic strength and light (Yagci et al., 2010).

III) Redox-initiated polymerization: Chemicals such as persulfate salts and Fenton's reagent are used to produce free radicals and this helps in carrying out graft polymerization in an inert atmosphere. This technique can be used to tether stimuli responsive polymers to membranes and create membranes with sensitivity to pH, temperature, ionic strength and oxidoreduction (Belfer et al., 2004).

IV) Radiation induced polymerization: In this method, the membrane is immersed in an aqueous monomer solution with various concentration of hydrated copper (II) sulfate, bubbled with pure nitrogen and irradiated with ^{60}Co γ-ray radiation (Chen et al., 2006).

V) Plasma graft filling polymerization: Here the membrane is irradiated with argon plasma to create the initiator radicals and then polymer chains grow from these initiator sites (Kai et al., 2000).

2.5.2 'Grafting to' method

In this method membrane surface functionalization is carried out either by physical adsorption or chemical grafting of pre-synthesized polymer chains.

I) Physical adsorption: Here, a membrane is coated with the responsive polymer by immersing it in the polymer solution and then drying it. Annealing the coated

membrane will help in strengthening the polymer coat. Stimuli responsive additives can also be incorporated in the polymer coating that is laid on the membrane, to induce switchable properties after modification (Cheong et al., 2013).

II) Chemical grafting: This method involves tethering pre-formed polymer chains or hydrogels on to a membrane surface and making them sensitive to particular external stimuli (Hollman & Bhattacharyya, 2002; Ito et al., 2000).

2.5.3 pH responsive membranes

This study involves the chemical coupling of pH responsive peptide-PEG bioconjugates on to an alumina membrane surface. Thus, the following sections will review various pH responsive membranes prepared using the 'grafting to' technique. Fabrication of membranes with variable permeation properties whose pore size change in response to pH has been done for various applications such as controlled release of drugs, self-cleaning surfaces and selective filtration.

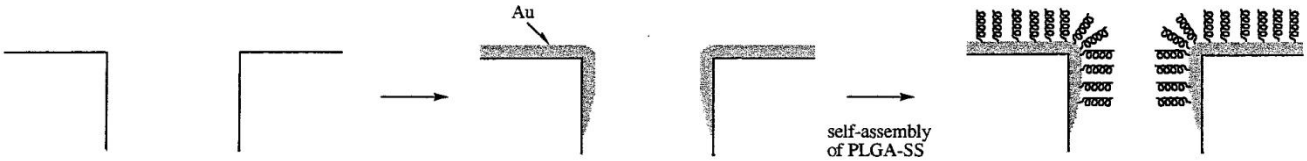

Figure 2-8: Immobilisation of PLGA on gold coated polycarbonate membrane. Image adapted from (Ito et al., 2000).

Ito et al. (2000) developed a pH responsive nanometer pore size membrane by tethering ionizable polypeptide brushes on gold coated, track-etched porous polycarbonate (PC) membranes (Figure 2-8). The membrane was first coated with platinum, then with gold and immersed in an aqueous solution of PLGA for 24 h. It was observed that the water permeation of the modified membrane was dependent on pH while that of an unmodified membrane was independent of pH. At low pH, water permeation was high and at neutral pH it was low. At low pH, the PLGA chains are protonated and have a folded α-helical conformation, whereas at neutral pH, they have a random conformation extending into the solution due to deprotonation of the PLGA chains. These conformational changes affect the membrane permeability, making it pH dependent. The inflection point of the water permeation rate was observed to be pH 4.5-5, which coincides with the isoelectric point (pI) of PLGA (4.58).

Figure 2-9: Immobilisation of poly(acrylic acid) conjugated with cysteamines (PAA-SH) on gold coated PC membrane. Image adapted from (Zhang & Ito, 2001).

Zhang and Ito (2001) produced similar pH responsive porous PC membranes by modifying with self-assembled chains of PAA-SH on gold-coated nanoporous membranes, whose water permeability was pH-controlled (Figure 2-9). Membranes with pore diameter of 200 nm was coated with gold up to 50 nm in thickness and then immersed in an aqueous solution of PAA-SH at different pH and ionic strengths. The water permeation of the unmodified membrane

was independent of pH while that of the modified one was dependent on pH and ionic strength. At low pH, water permeability was high and at neutral pH it was low. An increase in ionic strength at high pH increased the permeability. At high pH, permeability was highly dependent on ionic strength whereas at low pH the effect was minimal. At high ionic strength, permeability becomes less responsive to change in pH. This is because high ionic strength shields the deprotonated polymer segments from electrostatic repulsion.

Hollman and Bhattacharya (2002) demonstrated the effect of chemically tethered PLGA on the water flux of microporous cellulosic supports. The functionalized membranes were prepared in two steps, aldehyde derivatization and PLGA attachment. Permeating PLGA solution through the cellulosic supports at pH 9.2-9.8 resulted in the coupling of terminal amine in PLGA and the aldehyde present on the membrane. The modified membranes exhibited a decrease in water flux at high pH and increased water flux at low pH due to the extended random coil and helix formation of PLGA chains, respectively. This behaviour was reversible.

Nakayama et al. (2003) prepared stimuli responsive membranes for the release of nicotine by applying coating and radiation curing. The same technique was used by Ng et al. (2005) to prepare a pH sensitive PHEMA membrane coated with pH responsive PAA, for the controlled release of model drugs. They later used variable pH responsive polyampholyte coating comprising copolymers of AA/2-(diethylamino)ethyl methacrylate (DEAEMA) to develop pH responsive drug incorporated membranes (Ng & Ng, 2008).

Ghosh et al. (2009) developed biocompatible ionic strength responsive membranes by modifying commercial microporous poly(vinylidene fluoride) (PVDF) membrane with a salt responsive hydrogel composed of poly-N-vinyl-lactams and bisacrylamide cross-linker via in situ thermal polymerization. At low NaCl concentration, the polymer chains had a fully

extended conformation, therefore closing the membrane pores, resulting in low permeability and low protein permeation through the membrane. While at high NaCl concentration, the polymer chains collapse and the permeability is high.

Mika and co-workers developed a new type of pH sensitive polyethylene (PE) porous membrane with the pores filled with polyelectrolyte, poly(4-vinylpyridine) (P4VPy) (Mika et al., 1995). The P4VPy was stabilized on the porous substrate by UV- initiated grafting. The permeability of this modified membrane was dependent on pH. The morphology, physiochemical properties, the effect of crosslinking of the polyelectrolyte on the flux and separation, the effect of polyelectrolyte composition on the membrane performance and other properties were investigated by Childs and his group (Childs et al., 2001; Mika et al., 1997).

Childs et al. (2002) designed pore-filled membranes by coating hydrophobic polyolefinic microfiltration (MF) membrane with polyethylenimine (PEI) to produce a chemically active surface. The coated PEI membrane was cross-linked with naphthalene-1,4-disulfonyl chloride in CCl_4. 4,4'-Azo-bis (4-cyanovaleryl chloride), a heat sensitive radical source was incorporated into the coated membrane and was heated to 75^{o}C in the presence of acrylic acid (AA), 4-(vinylpyridine) or styrene. The membrane exhibited pH dependent flux changes similar to molecular brushes grafted within the membrane pores.

Mika, Childs and co-workers (2006) studied in detail their pore-filled flat sheet pH sensitive membranes and then continued their work with hollow fiber membranes. They prepared a gel filled microporous poly(propylene) (PP) hollow fiber membrane by incorporating poly(4-vinylpyridinium salt) gels into the fiber walls. The gels were anchored in the pores by cross-linking P4VPy with α,α'-dichloro-p-xylene followed by quaternization using benzyl bromide. The flux of the membrane significantly improved when the membrane had a asymmetric

distribution of the gel through the wall of the fibers. These membranes find application in water softening industries.

Hu and Dickson (2007) developed pH responsive membranes by in situ cross-linking of PAA inside PVDF hydrophobic microporous membranes (Figure 2-10). The membranes exhibited a reversible flux variation with pH change between 2.5-7.4. The water flux of this membrane is lower compared to the unmodified substrate even when the polymer chains are in their compact form at low pH. This is because the gel swells in the substrate due to volume exclusion effect. This was the first pH sensitive membrane developed by in situ cross-linking polymerization of AA inside hydrophobic PVDF microporous membranes. The pore sizes of the original membrane decrease after pore filling. Therefore, MF and UF membranes can be converted to nanofiltration (NF) membranes by filling the pores with polyelectrolytes and can be used for various bioseparation applications.

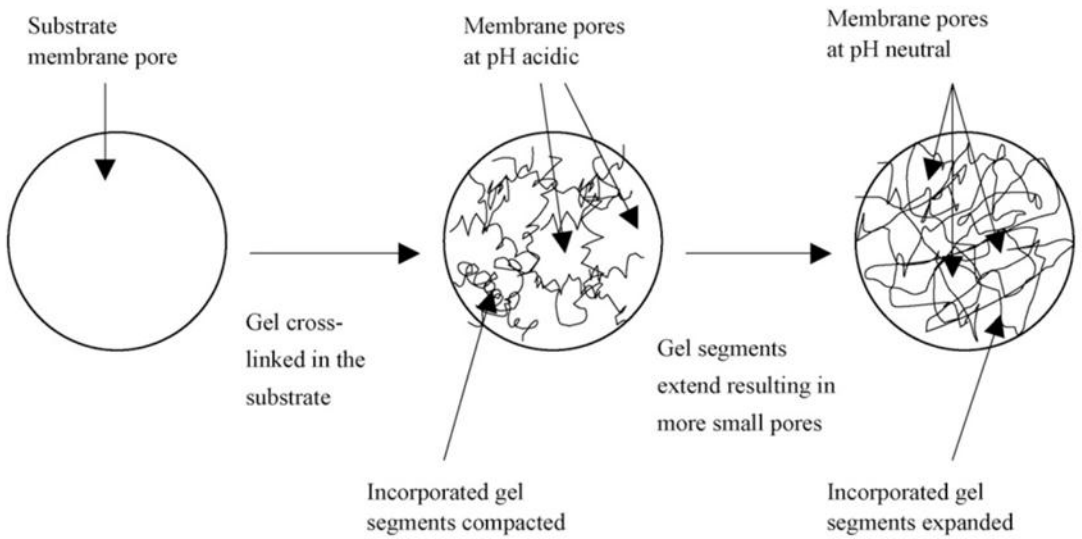

Figure 2-10: Schematic representation of pore-filled membrane showing changes in physical characteristics of the incorporated gel upon change of pH. Image reproduced from (Hu & Dickson, 2007).

In summary, synthetic membrane modifications have been carried out using different polymers such as PAA, P4VPy, PEI and PLGA to develop pH-responsive membranes. These membranes were developed for specific separation purposes and the function of each membrane was based on a specific principle such as size exclusion, ion exchange or hydrophobicity. The choice of the particular pH-responsive polymer used to modify the membrane depends on the final application of the membrane. Therefore, there is a need for the development of a universal stimuli-responsive membrane that could be used for a wide range of applications. Because of their versatile range of chemistries, the use of reversible SAPs to control the membrane selectivity or retention capability could potentially provide a new dimension to membrane transport and increase the feasibility of using membranes for numerous (currently tedious) separation processes. Membranes functionalized using such molecules, possessing unique chemistries, will help exploit both structural motifs (β-sheets, α-helices, nanotube, random coils) and chemical properties (hydrophilicity, hydrophobicity, electrostatic interactions) to control pore transport.

2.5.4 Application of pH-sensitive pore-filled membranes

Pore-filled membranes are generally NF membranes and they can be used for salt separation. MF membranes can be converted to NF membranes after filling their pores with pH-sensitive gels. Mika et al. (2002) investigated the salt separation and hydrodynamic permeability of a pore-filled pH-sensitive membrane. It was found that adding HCl increased the rejection of cations in tap water with the increase in ionization of the incorporated P4VP. Pure water flux decreased reversibly when the pH was changed from 5.5 to 2.6 by addition of HCl. Similar reversible flux changes were obtained when pH adjusted municipal tap water was used. This is due to the microphase transitions taking place in the gel network incorporated in the pores of the support membrane. The majority of the gel polymer is located in the non-draining regions, which results in a high flux in the draining regions due to the low effective

concentration of the gel in this region. Therefore, the fluid moves faster in the heterogeneous gel even if only a part of the volume is accessible. On protonation, charge is introduced, which in turn induces an electrostatic dispersive force, causing the collapsed gel to swell and when the dispersive force outbalances the polymer-polymer interactions, heterogeneity is eliminated and the whole gel swells to the maximum allowed by the support membrane. This process is reversed on deprotonation.

Zhou et al. (2005) prepared pore-filled NF membranes by UV-initiated copolymerization of 2-acrylamid-2-methylpropanesulfonic acid (AMPS) and N,N'-methylenebisacrylamide within the pores of a microporous polypropylene (PP) substrate. These poly(2-acrylamid-2-methylpropanesulfonic acid) (PAMPS) gel filled membranes were readily prepared with controlled amounts of the incorporated gel polymer. The thickness of the membrane changed with PAMPS incorporation. As the thickness increased, the polymer volume fractions of the PAMPS pore filling gels were limited to values between 0.01-0.06, which was low compared to other gel filled membranes based on the same substrate. Darcy permeability of PAMPS membranes was lower than other gel filled membranes studied earlier. This was due to the hydrophilic nature of PAMPS. Some water molecules bind tightly to the polymer chains and become immobilized. This increases the hydrodynamic size of the polymer chains and narrows the channels for water transport.

Winnik et al. (1998) examined the use of PAA pore-filled microporous membranes in membrane mediated synthesis of nanocrystalline ferrihydrite. These membranes displayed a chemical-valve effect of flux in response to change in pH. Treatment of PAA grafted membranes with solution containing ferrous ions resulted in large uptake of iron (> 24% by weight of iron with membrane containing 152% graft yield of PAA). Subsequent alkaline (pH 14) oxidation at 70^{o} C with either oxygen or hydrogen peroxide led to the formation of a superparamagnetic nanocrystalline in the form of ferrihydrite, ($5Fe_2O_3.9H_2O$).

The concept of 'pore-filling' resulted in high performance composite membranes for the separation of different polar organic mixtures by pervaporation (PV) (Ulbricht & Schwarz, 1997). Frahn et al. (2004) developed PV separation phases using pore–filled poly(acrylonitrile) (PAN) UF membranes. Methacrylates, acrylates, and vinylates were pore-filled in situ by heterogeneous photo-initiated graft copolymerization in water. Toluene/n-heptane mixtures and multi-component aromatic/aliphatic mixtures (20/80 weight-ratio; 80^{o}C) were used as feed to test the selectivity of the membranes. It was found that the membranes had good permeate flux and high aromatic hydrocarbon selectivity. This was because of the small effective barrier thickness (<3μm) and the restricted swelling of the graft copolymer caused by the covalent tethering to the pores of the substrate.

2.5.4.1 Extraction of specific proteins

Iwanade et al. (2007) immobilized amphoteric polymer brushes to membrane surfaces and pores to extract specific proteins. A hollow fiber MF membrane was converted into an amphoteric porous hollow fiber membrane by radiation induced graft polymerization of glycidyl methacrylate and subsequent ring-opening of the epoxy group with ampholites. Three types of ampholites, i) 3-aminopropionic acid (AC), ii) 2-aminoethane-1-sulfonic acid (AS) and iii) (2-aminoethyl phosphonic acid) (AP) were immobilized on a poly(glycidyl methacrylate) brush. The amphoteric polymer brush captured proteins such as lactoferrin, cytochrome c and lysozyme during the permeation of protein solution through the pores of the membranes. The proteins were held in multilayers. The proteins adsorbed onto the AC-, AP-, and AS-diol fibers were eluted by passing 1 M NaCl through the pores.

An ion exchange membrane matrix was prepared by Bayramoglu and co-workers (2008) by grafting poly PHEMA (methacrylic acid) to chitosan membranes (chitosan-g-poly(MAA)) for the adsorption of alkaline trypsin. This was done in two steps, in the first step chitosan

membranes were made by phase inversion technique and then epichlorohydrin was used as cross linking agent to increase its chemical stability in acid media; in the second step ammonium persulfate (APS) initiated the graft copolymerization of methacrylic acid onto the chitosan membranes under nitrogen atmosphere. This membrane was found to adsorb trypsin from an aqueous solution. The influence of pH, temperature and ionic strength on the adsorption equilibrium was also investigated. The pH of the medium has a very important effect on the adsorption of trypsin by the chitosan-g-poly(MAA) membrane and the adsorption is maximum at pH 7. With increasing ionic strength, the trypsin adsorption capacity of the membrane was found to decrease. Glutamic acid solution (0.5M, pH 4) was used to elute the adsorbed trypsin. The experimental data obtained for trypsin adsorption fitted well with the Langmuir isotherm model. This chitosan-g-poly(MAA) membrane can be used as an ion exchange adsorbent in the separation of basic proteins from biological fluids.

Affinity membranes containing functionalized polymer brushes for rapid purification of histidine tagged proteins were developed by Jain et al. (2007). A porous alumina membrane was modified with PHEMA brushes derivatized with nitrilotriacetate-Ni^{2+} (NTA-Ni^{2+}) complexes (Figure 2-11). This membrane allows purification of HisU in less than 30 min with a binding capacity of 120 mg of His/cm^3. The brushes can bind upto 23 monolayers of HisU. Gel electrophoresis reveals that the purity of eluted HisU is more than 99%. Thus, reusable membranes modified with PHEMA-NTA-Ni^{2+}brushes are very useful for rapid and selective purification of polyhistidine-tagged proteins.

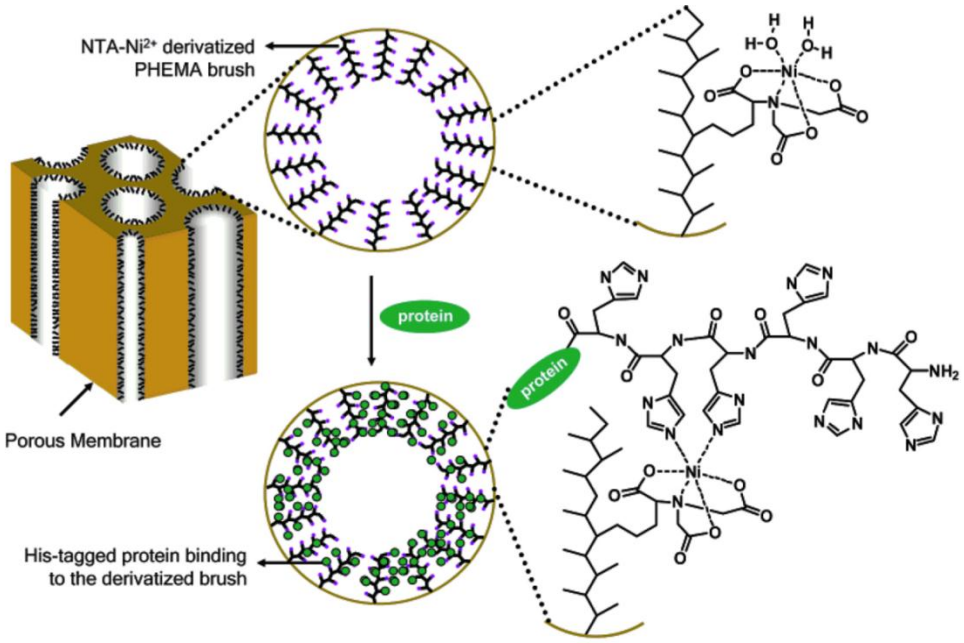

Figure 2-11: Covalent capture of His-tagged protein by NTA-Ni^{2+} derivatised PHEMA brush inside a membrane pore. Image adapted from (Jain et al., 2007).

2.5.4.2 Rejection of proteins

Chen et al. (2007) modified PVDF membranes with polymer brushes to make them more effective in preventing protein fouling. Poly(methyl methacrylate) (PMMA) and poly(poly(ethylene glycol) methyl ether methacrylate) (PPEGMA) were grafted onto UV pretreated PVDF membranes surface and pores by reverse ATRP. With an increase in graft concentration, the pore size of the modified membranes decreased and became uniform and the water flux was found to increase. The increase of pure water flux of the modified membrane indicates the improvement of surface hydrophilicity by PMMA grafting. Protein adsorption and protein solution permeation experiments showed that this membrane exhibited good antifouling properties. Due to the higher hydrophilicity of PPEGMA, the PPEGMA

grafted membrane was more effective in preventing protein fouling than PMMA grafted membrane

Liu et al. (2007) used the same PVDF membrane modifying it using a comb-like polymer brush to improve the fouling resistance. Poly(ethylene glycol) methyl ether methacrylate (PEGMA) was grafted on to the PVDF porous membrane by pre-irradiation of electron beam to form a layer polymer brushes. The pH of the reaction solution significantly affected the degree of grafting. The dynamic adsorption process of a water droplet on the membrane surface confirmed the improved hydrophilicity of the membrane. The pure water flux and BSA solution flux changes indicated the improvement in the filtration performance of the PEGMA grafted PVDF membrane.

P (PEGMA) polymer brushes were tethered to chloromethylated poly(phthalazinone ether sulfone ketone) (CMPPESK) through surface initiated ATRP by Zhu and co-workers (2008). The grafting of hydrophilic P (PEGMA) brushes decreased the pore diameters and increased the solute rejections of the PPESK membrane. Water contact angle measurements indicated that the P (PEGMA) graft chains remarkably promoted the hydrophilicity of the membrane. With reduction in pore size and improvement in membrane hydrophilicity, the pure water flux of the modified membrane initially increased and then decreased with increase in thickness of graft layer. The dynamic anti-fouling experiment results proved the enhancement of fouling resistance of the membrane after grafting of P (PEGMA) polymer brushes.

Polyethersulfone membranes were modified by blending branched amphiphilic polymers with the base material to improve the anti-fouling property of the membrane (Shi et al., 2007). Pegylated polyethersulfone (PES) was prepared via reaction of chlorosulfonated PES with oligomeric PEG. Pegylated PES was then used for fabrication of PES UF membranes. This modified membrane showed improved hydrophilicity and greater resistance to protein

adsorption compared to the unmodified membrane. UF experiments proved that the presence of pegylated PES in the membranes increased water permeability and protein fouling resistance. The improved anti-fouling properties gave the membrane a longer operation lifespan.

Friebe and Ulbricht (2007) grafted PNIPAAm brushes onto the pores of track etched PET membrane by surface initiated ARTP to achieve temperature responsive pore diameter (Figure 2-12). Monomer concentration and reaction time were the parameters used to adjust the degree of grafting. The layer thickness of dry PNIPAAm on the pore walls of PET was 80 nm and temperature induced swelling and shrinking ratio of ~3 was observed. This kind of controlled polymerization can be used to functionalize pores with different macromolecules at varied densities and layer thickness. Such stimuli responsive membranes can be used for controlled release and in microfluidic devices and drug delivery systems.

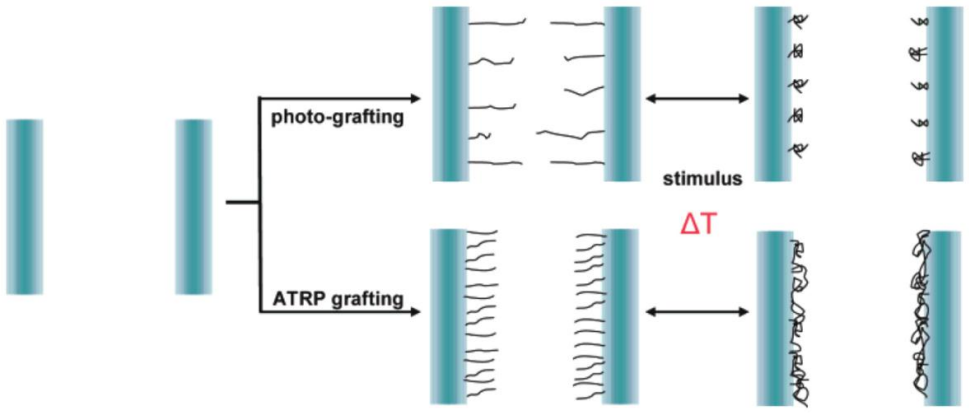

Figure 2-12: Schematic representation of PET membrane pore functionalized with stimuli responsive PNIPAAm via two different methods and the change in effective pore diameter with change in temperature. Image adapted from (Friebe & Ulbricht, 2007).

Polymer-modified membrane systems have been used in the past to control water permeability, desalination, extract specific proteins and enhance fouling resistance. It is predicted that the next generation of stimuli-responsive membranes will be more complex, advanced and capable of mimicking functions in living systems. Therefore, from a long-term perspective, using biomolecules such as peptides rather than synthetic polymers to modify membranes could render the system more representative and compatible with biological systems. Such biomolecule-modified membranes can be used to regulate the transport of drugs in response to biochemical signals in tissue engineering, drug delivery and bioseparations.

2.6 ANODISC^{TM} ALUMINA MEMBRANES

Anodisc ^{TM} alumina membranes manufactured electrochemically have gained popularity mainly due to their simple, low cost fabrication, chemical stability and hardness, organised and uniform pore size (Figure 2-13) and high pore density (Jessensky et al., 1998; Sadasivan et al., 2005). These are commercially available with pore sizes 20, 100 and 200 nm. The circular membrane used in this work had a diameter of 43 mm and was 60 μm thick. The average size of a peptide (~10 mer)-PEG (~ 2 kDa) bioconjugate is expected to be around 24 nm. Thus, the Anodisc ^{TM} alumina membranes of pore size 20 nm represents a suitable candidate to chemically couple the SAP-PEG conjugate to the surface and/or pores, and subsequently investigate the effect of peptide self-assembly and disassembly on the flux properties and permeability of the membrane.

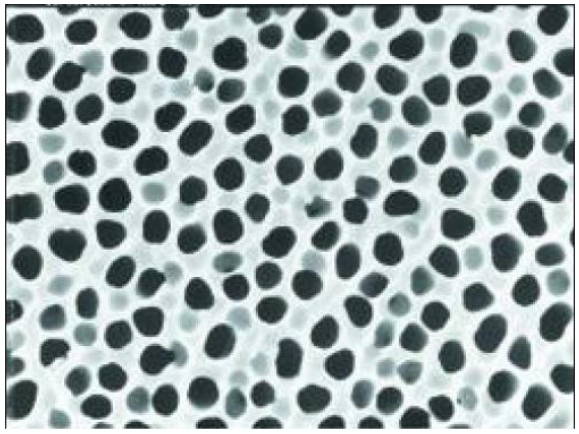

Figure 2-13: Anodisc pore structure. Image reproduced from (http://www.whatman.com/products.aspx?PID=193, 5th May, 2012).

It is desirable to modify the surface properties of the membrane, in order to tether biomolecules on to the surface. The immobilisation of chemically reactive groups such as carboxylates (COOH) on to the alumina surface would enable amine coupling of the peptide-PEG conjugate on to the membranes for biofunctionality. Such modifications can possibly be used as building blocks for generating complex architectures and functions on alumina membranes adding further to their existing applications.

2.7 IMMOBILISATION OF CARBOXYLATE GROUPS (COOH) ON ALUMINA SURFACE

A variety of approaches have been taken to immobilise COOH groups on various surfaces. Some of the most commonly used methods include phosphonic acid chemistry (Hauffman et al., 2008), diazonium chemistry (Mahouche-Chergui et al., 2011) and PEM (Dai et al., 2006).

2.7.1 Phosphonic acid chemistry

The immobilisation of COOH groups on metals and metal oxides has paved the way for grafting various biomolecules for various applications. Gold surfaces have been modified using fatty acids (Radu-Wu et al., 2009), hexanoic acids (Paik et al., 2003), silver using alkanoic acids, alkoxybenzoic acids (Tao et al., 2002), stainless steel using alkanoic acids (Lim et al., 2007), palmitic acids and stearic acid (Shustak et al., 2004) in order to immobilise self-assembled monolayers (SAM's) of carboxylic acids. Despite the modification of oxides of various metals such as zirconium, hafnium, indium using alkanoic acids (Pawsey et al., 2000), stearic acid (Ting et al., 2009), carboxy terminated thiols (Yan et al., 2000) respectively, immobilisation of COOH groups on aluminium oxide surface has been a challenge. There are very few methods reported for modifying alumina surfaces. Aronoff et al. used alkanoic acid to form stable carboxylate films on aluminium oxide surface. Initially, the alumina surface was treated with an alkoxide of zirconium and this enables strong consequent adsorption of the alkanoic acid (Aronoff et al., 1997). Stearic acid (Limet al., 2007) has been used to incorporate carboxylate monolayers on alumina surface. The modification protocols for these methods have been tedious and time consuming. Another method involves using phosphonic acids, which uses a simple procedure to immobilise COOH groups on alumina surface. The polar acidic phosphonate group interacts with diverse metal oxide surfaces such as Al_2O_3, Ta_2O_5 and ZrO_5. The degree of ordering of these films on the surfaces is comparable to that of alkyl thiol SAMs on gold (Hahner et al., 2001). Octylphosphonic acid (Hauffmanet al., 2008), alkane phosphate (Hahneret al., 2001), 3-hydroxyl-3-phosphono-butiric acid tert-butyl ester (Blajiev et al., 2008) are some of the phosphonates used for aluminium oxide modification. In this study, 6-phosphonohexanoic acid (6-PHA) has been used (Figure 2-14). Figure 2-15 shows the chemical structure of another phosphonic acid.

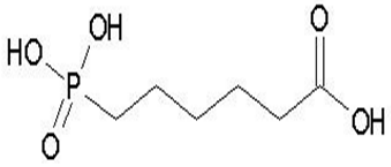

Figure 2-14: Chemical structure of 6-PHA

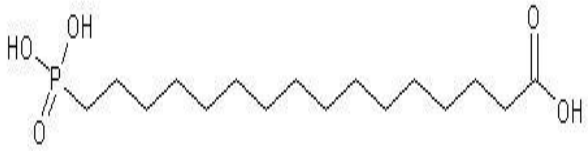

Figure 2-15: Chemical structure of 16-phosphono-hexadecanoic acid

2.7.2 Diazonium chemistry

The second method to immobilise COOH groups on an Anodisc surface involved diazonium chemistry. Diazonium salts are used for surface modification as coupling agents for conjugating biomolecules, polymers and nanoparticles to surfaces. The diazonium group activates nucleophilic aromatic substitutions and makes route for introducing functional groups such as OH, CN and COOH into the aromatic ring leading to the formation of diverse compounds (Figure 2-16) (Mahouche-Cherguiet al., 2011).

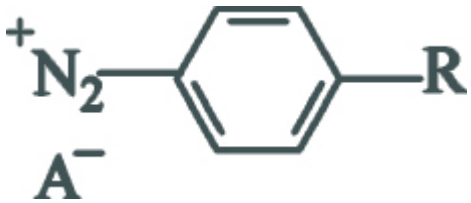

Figure 2-16: General chemical structure of aryl diazonium salts where R refers to range of substituents such COOH, NO_2 etc. and A^- is the counter anion.

The aryl diazonium salt (Figure 2-17) is reduced electrochemically (Bernard et al., 2003) or using reducing agents (Simons et al., 2014) to radicals, which bind with high affinity to a range of surfaces, which includes carbon, metallic and polymers. This helps in immobilising the surface with variety of functional groups (R) such as alkyls (Bernardet al., 2003), halides, carboxylic acid groups and nitro groups (Allongue et al., 1997) (Figure 3).

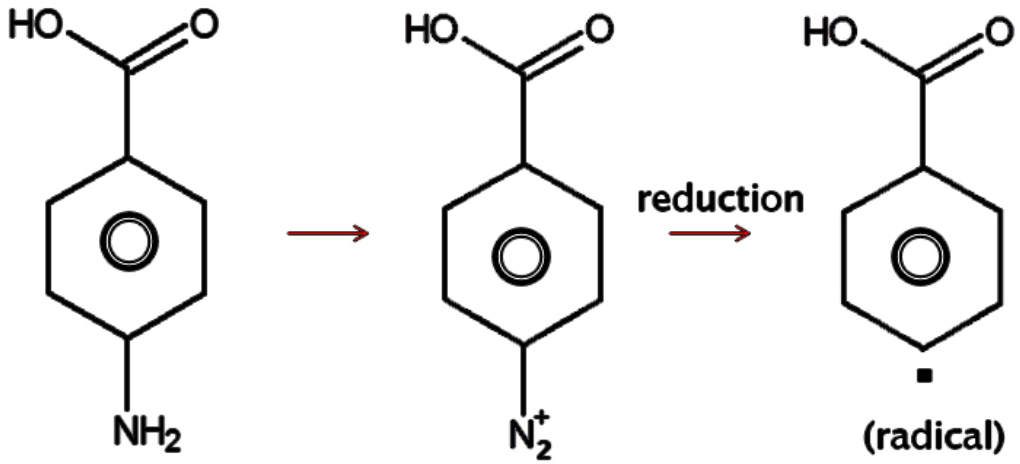

Figure 2-17: The carboxy benzene diazonium (CBD) reduction mechanism forming radical. Reduction is either done electrochemically or using reducing agents.

Polymers such as polymethylmethacrylate (Chehimi et al., 2014), polyaniline (Liu & Freund, 1996), Teflon (Combellas et al., 2003) and metal oxides such as iron oxide, titanium oxide (Griffete et al., 2011) have been modified using diazonium chemistry. This method has not been employed to modify aluminium oxide surfaces. This is the first attempt testing the interaction of diazonium molecules on Anodisc alumina membrane surface.

2.7.3 PEM adsorption

An alternative approach developed to immobilise COOH groups on Anodisc surface involved deposition of PEM's (Figure 2-18) terminating with PAA, which provides the free COOH groups on the surface necessary for further modification (Dai et al., 2006). Layer by layer deposition of alternating polyanion and polycation allows modification of porous membranes (Ai et al., 2003), which can be used for a range of applications including protein microarray analyses because of their high surface area and possible overcoming of mass transport limitations by flowing solutions through small pores (Hollman & Bhattacharyya, 2004). The initial polyanion layer adsorbs to the surface by electrostatic or hydrophobic interaction, thus creating a charged surface or reversing the charge of the surface. Adsorption of subsequent polycation layer reverses the charge on the surface aiding the adsorption of next layer (Schlenoff & Dubas, 2001). Alternate layers of poly(styrene sulfonate) and protonated poly(allylamine hydrochloride) (PSS/PAH) were on poly(ether sulfone) ultrafiltration (UF) membranes to bring about change in the molecular weight cut off of the membrane (Malaisamy & Bruening, 2005). Porous alumina membranes were modified with PAA/PAH multilayers and used as substrates for protein arrays with low non-specific adsorption (Dai et al., 2006). Catalytic membranes were prepared using layer-by-layer deposition of PAH and citrate protected negatively charged gold colloids in porous alumina membrane pores. The same procedure can be applied in modifying nylon and PC membranes as well, indicating the versatility of this method allowing formation of films virtually on any surface (Dotzauer et al., 2006). Studies have shown that the presence of supporting electrolyte such as NaCl increases the thickness of the PEM's (Dubas & Schlenoff, 1999).

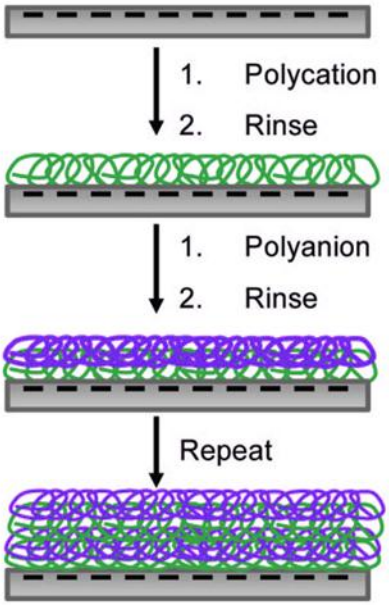

Figure 2-18: Schematic diagram of layer-by-layer adsorption of polyelectrolytes on Anodisc surface. Image adapted from (Bruening et al., 2008).

After the successful immobilisation of COOH groups on the surface, EDC/NHS activation was done and the peptide-PEG conjugate EL-5F-PEG-2K was amine coupled to the surface.

2.8 SUMMARY OF LITERATURE REVIEW

Over the years, conventional synthetic membranes have been used for purification and separation of various biomolecules and chemicals. To further improve the separation properties and have a precise control over permeability, membranes have been modified using a diverse range of polymers (e.g., PAA, PHEMA, P4VPy and PEI), thereby rendering them stimuli-responsive. Despite the development of a number of these polymer-based, pH-responsive membranes, these membranes are typically targeted towards a specific separation process. Thus, this study primarily focuses on the development of a novel, versatile membrane system that can potentially be applicable for a wide range of separations, based on both physical and chemical properties of the separation mixture. To achieve this, because of

their chemical diversity, SAPs was chosen as a suitable alternative to polymers for inducing pH responsiveness through their ability to spontaneously organize into well-ordered structures in response to external stimuli such as pH, temperature and divalent ions. The wide variety of hierarchical structures and properties of amino acid side chains present numerous avenues for the application of such a membrane system. Additionally, the conjugation of a PEG spacer to the peptide is expected to provide the necessary conformational freedom for the peptide to self-assemble. Amongst the different conjugation strategies used in the past, amine coupling, a simple, rapid and inexpensive approach appears to be suitable for coupling the peptide to PEG. Despite numerous successful conjugation and peptide-polymer self-assembly investigations reported in the literature, the repeated use of external triggers to reversibly manipulate the secondary structure of bioconjugates remains a challenge and assembly/disassembly is often subject to slow dynamics in at least one direction. The tethered peptide-PEG conjugate needs to reversibly self-assemble, rapidly, in response to external triggers, to render the membrane switchable.

Anodisc ^{TM} alumina membranes, because of their inert nature and small pore size (20 nm), are suitable for tethering the SAP-PEG conjugate and to further investigate the effect of self-assembly and disassembly on the flux properties and permeability of the membrane. The membrane surface must be functionalized with reactive groups such as carboxylic acids to enable amine coupling of the peptide-PEG bioconjugate to the surface. Phosphonic acid chemistry, which involves a very simple procedure, has been used widely to immobilise COOH groups on alumina surfaces. PEM adsorption is another technique used in the past to incorporate COOH groups onto porous membrane surfaces for various applications. The experimental methods, results and the important findings arising in this thesis as a consequence of the above literature review are presented in the following chapters.

CHAPTER-3

INVESTIGATION OF FACTORS INFLUENCING SELF-ASSEMBLY OF PEPTIDE P11-4-PEG BIOCONJUGATE

3. INVESTIGATION OF FACTORS INFLUENCING SELF-ASSEMBLY OF PEPTIDE-PEG BIOCONJUGATE

3.1 INTRODUCTION

Peptide P11-4 (QQRFEWEFEQQ) was chosen as the candidate for the development of the stimuli responsive membrane. A SAP that could be conjugated to a PEG spacer long enough to allow freedom for the peptide to self-assemble when tethered to a membrane to create switchable permeation was sought. P11-4 was considered ideal for this purpose because of its rapid and reversible pH dependent self-assembly. In this chapter, the self-assembly behaviour of P11-4 is described. Subsequently, the development of a bioconjugate derived via conjugation of P11-4 to PEG 2000 is demonstrated and the factors influencing its self-assembly are reported.

Aggeli et al. (Aggeli et al., 2003) designed and synthesized a number of switchable peptides that self-assemble depending on pH conditions. P11-4 is a peptide that was developed to form self-assembled fibrils at low pH and disassemble at high pH. This peptide was shown to adopt four different phases depending on pH that include: (*i*) nematic gel (pH< 3.2), (*ii*) flocculated solution (pH 3.2-5), (*iii*) nematic fluid (pH 5-7) and (*iv*) isotropic fluid (pH>7), respectively. The γ-carboxyl groups of the glutamic acid residues are uncharged at pH < 3 and there is one net positive charge per peptide on Arg^{+}, stabilizing the dispersion of fibrils and aiding in the self-assembly of the peptide. At pH > 7, all the carboxyl groups are deprotonated (negatively charged), thus causing electrostatic repulsion between the adjacent γ-COO^{-}, leading to dissociation of fibrils. The switching between isotropic and nematic phases is reversible in P11-4 and takes place within seconds of change in pH conditions. However switching from low pH to high pH and vice versa over three cycles of pH shifts

results in buildup of ionic strength due to repeated additions of acid and base, leading to screening of the electrostatic repulsion between fibrils and ultimate flocculation (Aggeli et al., 2003).

Over the years, this intrinsic self-assembling capability of peptides has been extensively explored and led to the development of a new class of hybrid bioconjugates upon conjugation with various synthetic polymers. This promising new class of biomaterials holds great potential for a variety of biomedical and biosensing applications (Borner, 2009). The extensive applicability of such bioconjugates is primarily derived from the ability of the peptide to retain its intrinsic self-assembly within the hybrid bioconjugate (Hentschel et al., 2006; Pechar et al., 2002). Reversible self-assembly of peptides has predominantly been induced using various external stimuli (*e.g.*, pH, temperature, ionic strength, presence of divalent ions) and has been well characterized for a number of peptides. However, the development of self-assembling switchable peptide-polymer bioconjugates has remained quite challenging. Recently, Kühnle et al. demonstrated the reversible self-assembly of a peptide-PEG bioconjugate using Ca^{2+} ions (Kuhnle & Borner, 2011). Despite the successful demonstration of reversible self-assembly in these bioconjugates, the conjugate conversion decreased within three cycles of secondary structure shifts and was attributed to an increase in ionic strength, which shields the charges of the glutamic acid side chains. This increase is difficult to avoid and thus, the development of robust bioconjugates with reproducible structural transitions has remained elusive.

In an attempt to develop a bioconjugate with reproducible structural transitions, peptide P11-4 was conjugated to a PEG chain of molecular weight 2 kDa and the resulting conjugate was purified using a size exclusion chromatography (SEC) column. Subsequently, numerous factors influencing the self-assembly of this conjugate (P11-4-PEG-2K) were investigated. Peptide P11-4 was chosen due to its spontaneous pH-dependent self-assembling property that

can potentially facilitate the development of a stimuli responsive filtration biomembrane. PEG chain conjugated to P11-4 would be expected to act as a spacer to provide conformational freedom for the peptide to self-assemble on the membrane surface and pores. It is important to note that the self-assembly of peptide P11-4 within a hybrid peptide-polymer bioconjugate has not been studied before now.

3.2 EXPERIMENTAL SECTION

3.2.1 Materials The P11-4 peptide was purchased from Genscript (New Jersey, U.S.A). Heterobifunctional PEG reagent N-tert-butoxycarbonyl (Boc)-protected-amino-PEG 2000-carbonate-N-hydroxy succinimide (NHS) was purchased from NOF Corporation (Tokyo, Japan). All other chemicals were purchased from Sigma Aldrich (St. Louis, MO, U.S.A). The Boc-protected amino groups were included to facilitate the tethering of the bioconjugate to membrane.

3.2.2 Conjugation and purification P11-4 peptide was dissolved at 4 mg/mL in 20 mM sodium phosphate buffer (pH 8). NHS-activated PEG 2000 at twice the molar concentration of the peptide was added to the solution and mixed for 2 h at room temperature. The resulting P11-4-PEG-2K conjugate was then separated from unreacted peptide using a Superdex™ peptide 10/300 GL size exclusion column (GE, Healthcare Life Sciences, Uppsala, Sweden). The fractions corresponding to the conjugate peaks were collected, pooled and exchanged into 5 mM HCl (pH 2.5) using the same column.

3.2.3 Effect of ethanolamine on conjugation 200 µL of 1 M ethanolamine hydrochloride was added to NHS-activated PEG 2000 and left to incubate for 5 min. Then P11-4 peptide in 20 mM sodium phosphate buffer (pH 8) was added and mixed for 2 h at room temperature. The concentrations of P11-4 and PEG were similar to that mentioned in Section 3.2.2.

Control conjugation reactions were carried out simultaneously in the absence of ethanolamine. Both the conjugation mixtures, in the presence and absence of ethanolamine were run through the size exclusion column.

3.2.4 Time course experiment P11-4 peptide was dissolved at 4 mg/mL in 20 mM sodium phosphate buffer (pH 8). NHS-activated PEG 2000 at twice the molar concentration of the peptide was added to the solution. 150 µL of sample was collected from this conjugation mixture at time intervals of 0, 1, 2, 3, 4, 5, 15, 30, 60 and 120 min. The sample collected was immediately mixed with 50 µL ethanolamine to quench the NHS reaction. All the samples were run through the size exclusion column.

3.2.5 Electrospray mass spectroscopy High resolution accurate mass samples were analysed on a maXis 3G UHR-Qq-TOF mass spectrometer (Bruker Daltonik GmbH, Bremen, Germany) coupled to a Dionex Ultimate 3000 LC system (ThermoFisher, MA, U.S.A). A 5 µL sample was injected into a flow of 50:50 water (0.5% formic acid):acetonitrile at 0.2 mL/min. 5 µL ESI-L Low Concentration Tuning Mix (Agilent Technologies, CA, U.S.A) was injected after each sample as a calibrant. Data was processed using Compass software (Bruker Daltonik GmbH, Bremen, Germany).

3.2.6 Matrix-assisted laser desorption/ionization time-of-flight (MALDI-TOF) mass spectrometry MALDI-tof mass spectrometry analysis was performed on a Bruker MALDI Ultraflex III TOF TOF using Flex Control version 3.4 software. The samples were diluted using 0.1% TFA to a final concentration of 0.1 mg/mL. 1 µL of the diluted sample was mixed with 1 µL of α-cyano-4-hydroxy-cinnamic acid (HCAA) matrix (saturated HCAA matrix in acetone diluted 1:9 in solvent (6:3:1 ethanol:acetone:0.1% TFA)). 1 µL of the matrix/sample mixture was spotted onto an AnchorChip (Bruker). Pepcal (Bruker) was spotted onto the

adjacent calibration spots and used to calibrate the instrument prior to analysis. The samples were analyzed using the RP_700-3500 method with a range of 700 – 7000 Da.

3.2.7 Circular dichroism spectroscopy Circular dichroism (CD) UV spectra were recorded on a Jasco J-815 CD spectrometer (Oklahoma City, OK, U.S.A) in solution using a sample concentration of 0.8 mg/mL in water. The pH of each sample was adjusted in an Eppendorf tube by dropwise addition of 1 M HCl or NaOH with thorough mixing and the tube centrifuged (5 min, 9000 x g) with an Eppendorf MiniSpin Plus benchtop centrifuge (Eppendorf South Pacific, North Ryde, NSW, Australia). The clear supernatant was then removed by pipette and placed into a 1 mm pathlength quartz cuvette for CD scanning at 1 nm intervals from 250 to 200 nm. Spectra were obtained as an average of three consecutive scans after background subtraction. Samples were removed from the cuvette by pipette and returned to the Eppendorf tube for subsequent pH adjustment and the above process repeated.

3.2.8 Transmission electron microscopy Samples were examined using a Morgagni 268D transmission electron microscope (TEM), FEI (Hillboro, OR, USA) operating at 80 kV, with magnifications of up to 140,000 x. Micrographs were captured using a SIS/Olympus Megapixel III digital camera (Tokyo, Japan) mounted above the phosphor screen. Solutions of native and conjugated EL-5F containing β sheet and random coil structures identified by CD were used for sample preparation. 20 µL of the samples was deposited for 1 min on carbon-coated Formvar 200-mesh copper grids, and then washed twice with water. Negative staining of the samples was achieved by placing the grids wet-side down on top of 20 µL of 1% w/w uranyl acetate solution in water for 1 min. Filter paper was used to remove excess liquid from the grids by blotting, and the grids were then left to dry for several hours before TEM observations.

3.3 RESULTS

3.3.1 Secondary structure characterization of native P11-4

Initially, to investigate the secondary structure transitions of the native peptide P11-4, samples were analysed using CD spectroscopy (see Section 3.2.7). A negative minimum around 215 nm indicated a β sheet structure, whereas a negative minimum around 200 nm is characteristic of a random coil (Greenfield, 2006). It was observed (Figure 3-1) that the native peptide dissolved in 5 mM HCl at pH < 3 had β sheet secondary structure (self-assembly). However, with an increase in pH (pH > 7) a conformational shift from β sheet to random coil was observed and subsequent decrease in pH (pH < 3) resulted in a reverse transition towards β sheet structure. These shifts from β sheet to random coil and vice versa occurred rapidly (within 5 min), with the extent of conversion being constant even after incubation for more than 24 h.

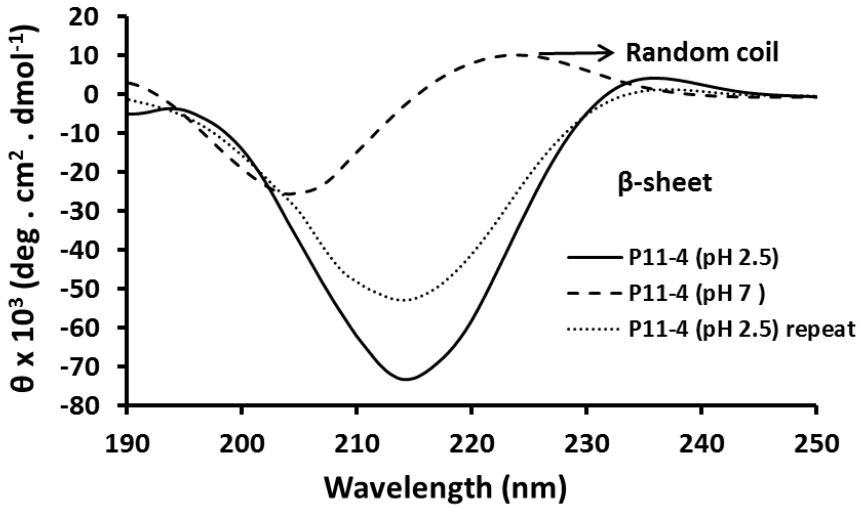

Figure 3-1: CD spectra of native peptide P11-4 showing the repeated conformational shifts between β sheet and random coil upon changing the pH between 2.5 and 7.

TEM analysis of the self-assembled β sheet and random coil secondary structures indicated fibrils of about 10-30 nm wide and several hundred nanometers in length at pH<3 (Figure 3-2). In contrast, no extended fibrils were observed at pH > 7. These observations corroborate with previous secondary structure investigations on P11-4 (Aggeli et al., 2003) and thereby suggest that the peptide self-assembly was robust and spontaneous.

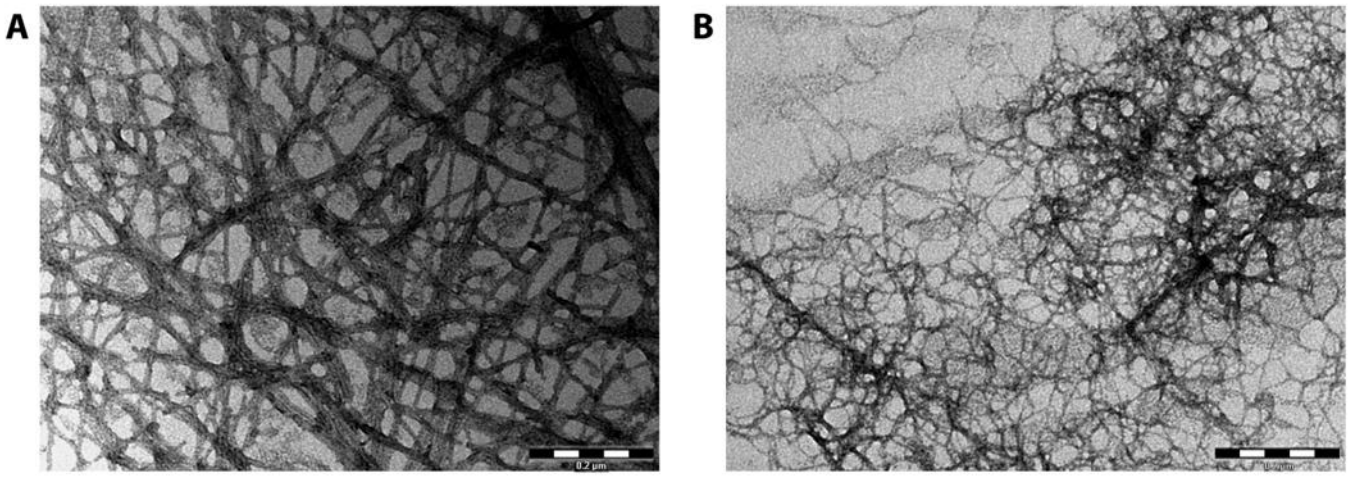

Figure 3-2: TEM images of negatively stained (A) P11-4 at pH < 3, (B) P11-4 at pH > 7.

3.3.2 Conjugation, purification and characterization of conjugate P11-4-PEG-2K

Upon analysing the secondary structure transitions of P11-4, the peptide was then conjugated to the NHS-activated PEG polymer via amine coupling (Klok, 2005). The NHS ester-primary amine reaction was carried out at pH 8, which is within the range (pH 7-8) identified previously as most efficient (Grabarek & Gergely, 1990). Because P11-4 contains only one primary amine at the N-terminus, it enables site-specific conjugation. Thus, the conjugation was carried out on the free peptide rather than during solid-phase synthesis and was simple, quick and inexpensive compared with other conjugation strategies such as orthogonal

coupling via click chemistry (Lutz et al., 2007) and solid phase-supported conjugation (Hentschel & Börner, 2006; Vandermeulen et al., 2003), which involve a number of reagents and multiple reaction steps.

The conjugates were purified using a SEC column (see Section 3.2.2) and corresponding chromatograms of native P11-4, NHS-activated PEG 2000 and EDC/NHS were obtained separately to individually identify the positions of their respective peaks (Figure 3-3).

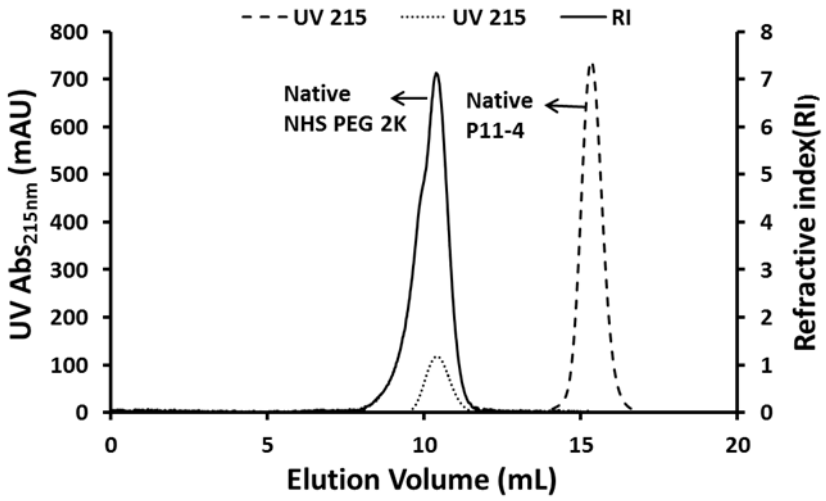

Figure 3-3: Size exclusion chromatograms of native P11-4 and NHS PEG-2K.

Figure 3-4 represents the chromatogram for the column based separation of P11-4-PEG-2K from the conjugation mixture. It is evident that the conjugate P11-4-PEG-2K (Mol. wt. = 3554.6 Da), as the largest component in the mixture, eluted first. This was then followed by the unreacted peptide (Mol. wt. = 1554.6 Da) and the low molecular weight EDC/NHS by-product, respectively. Although one would expect the NHS-PEG to elute closely after and/or partially co-elute with the conjugate, the hydrolysis of NHS-PEG to PEG-OH results in no UV absorbance. So, there would be no visible peak. This indicates that the final conjugate sample is likely to have contained free PEG. Thus, calculations on the area of the individual

peaks suggested approximately 88% conversion from the conjugation reaction. This level of conversion is higher than those achieved previously using other methods for numerous other peptide bioconjugates (Radu et al., 2009; Stutz et al., 2013). Subsequently, sodium phosphate salts were desalted from the purified conjugate in water (Figure 3-5).

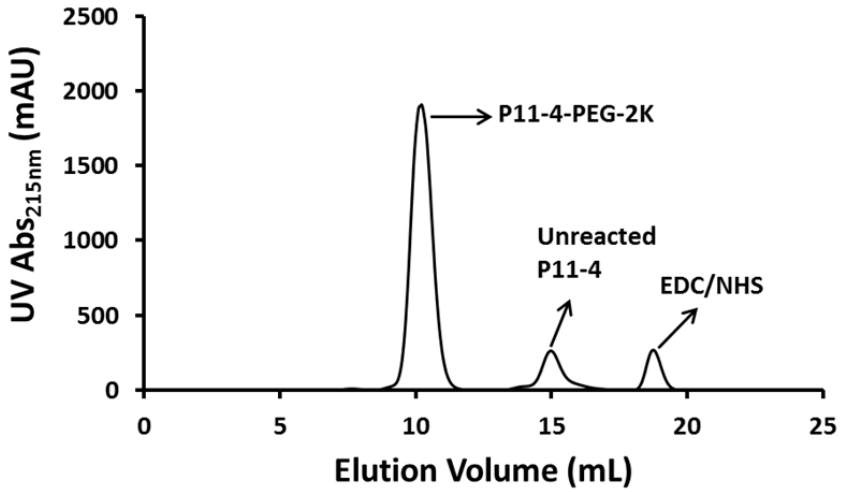

Figure 3-4 Size exclusion chromatogram showing the separation of conjugate P11-4-PEG-2K from the unreacted peptide and EDC/NHS by-product.

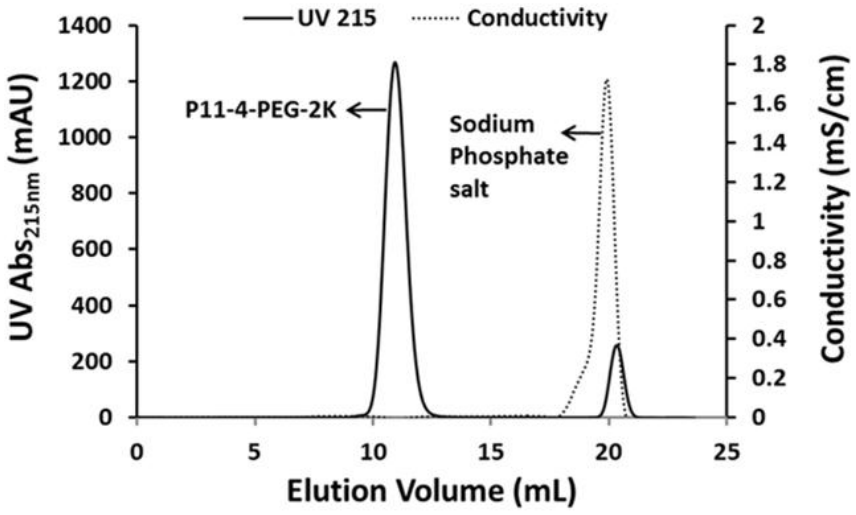

Figure 3-5: Size exclusion chromatogram showing the desalting of sodium phosphate salts from conjugate P11-4-PEG-2K.

The desalted conjugate was then analysed using electrospray mass spectroscopy in order to verify its molecular weight. However, the presence of large and polydisperse unreacted PEG polymer hindered the detection of the conjugate within the spectra (Figure 3-6).

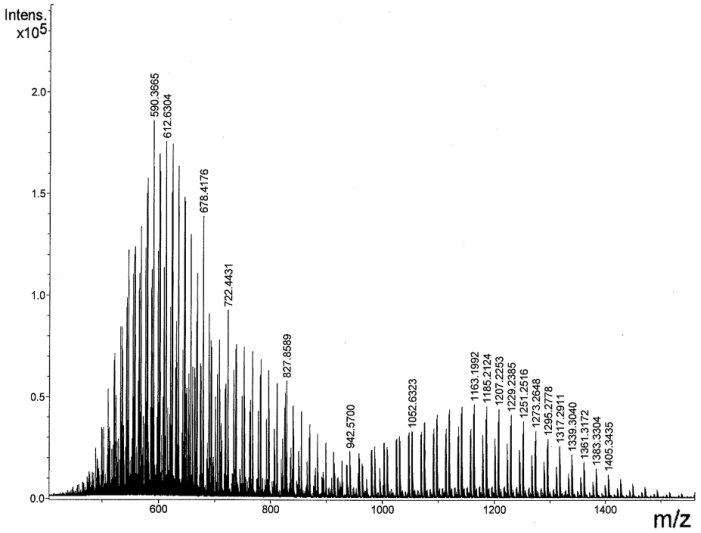

Figure 3-6: Mass spectra of conjugate P11-4-PEG-2K.

Thus, the presence of the conjugate was subsequently confirmed using MALDI-TOF mass spectrometry as evident from the spectra at around 3500 Da (Figure 3-7). The presence of the conjugate was further investigated by performing experiments involving the effect of ethanolamine and time course experiments to monitor the formation of the conjugate over time.

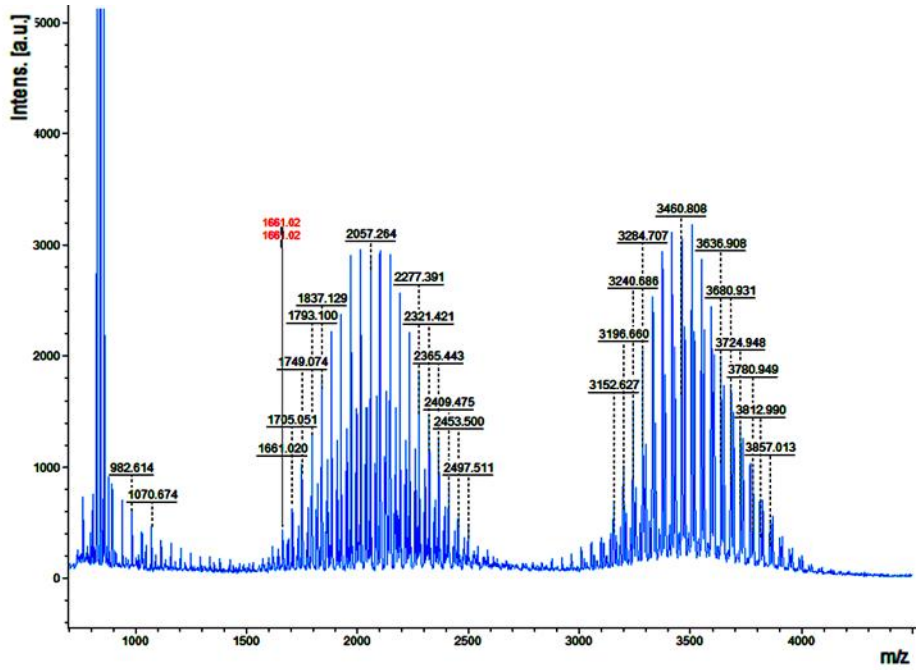

Figure 3-7: Mass spectra of conjugate P11-4-PEG-2K.

3.3.2.1 Effect of ethanolamine on conjugation

The presence of ethanolamine hydrochloride within the conjugation mixture has been known to convert active NHS ester into an inactive hydroxethyl amide (Ghosh et al., 2013), thereby preventing the conjugation reaction. To investigate the effect of ethanolamine on conjugation, the conjugation reaction was carried out in the presence and absence of ethanolamine and the conjugate was then purified using a SEC column. Figure 3-8 represents the chromatogram

for the conjugation reaction in the presence and absence of ethanolamine. It was observed that the presence of ethanolamine did not facilitate the conjugation as evident from the absence of the conjugate and the presence of large amounts of unreacted P11-4 within the eluted samples (Figure 3-8). In contrast, the absence of ethanolamine in the conjugation mixture resulted in the formation of P11-4-PEG-2K bioconjugate. These results indicate that the presence of ethanolamine in the conjugation reaction had a significant effect and prevented the conjugation of P11-4 and PEG.

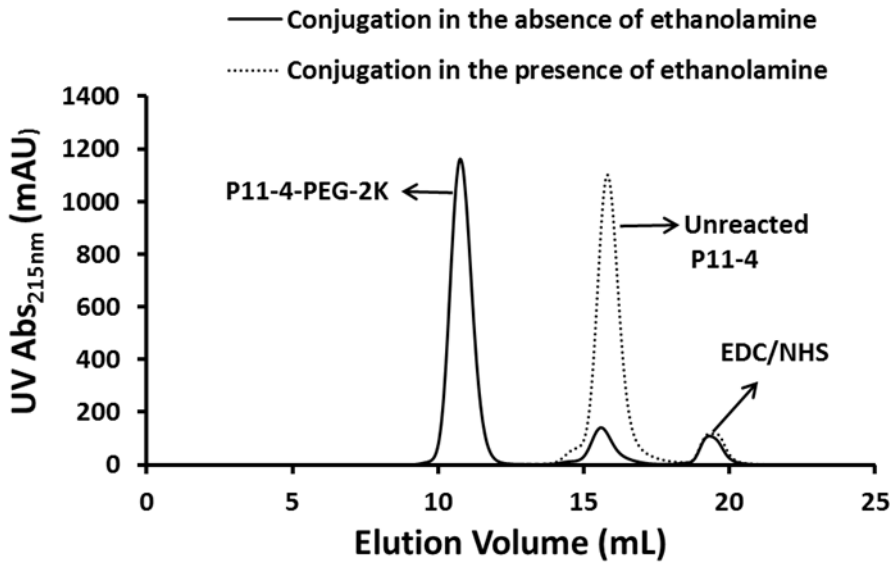

Figure 3-8: Size exclusion chromatogram of conjugation mixtures in the presence and absence of ethanolamine.

3.3.2.2 Time course experiment

To investigate the optimal time intervals for the formation of the P11-4-PEG-2K bioconjugate, the conjugation reaction was carried out at timed intervals (0-120 min) and

subsequently the reaction mixture purified using a SEC column. The conjugation of P11-4 to PEG was a function of time as evident from the increase in the amount of bioconjugate in reaction mixtures obtained from various time intervals (Figure 3-9). The formation of bioconjugate occurred instantly, as observed from the 50% conversion (black; Figure 3-9) from the conjugation mixture collected immediately (0 min sample) after mixing the peptide with NHS-PEG. Furthermore, approximately 80% conversion of the conjugation mixture was observed within 2 min (Figure 3-10), after which the reaction stabilised to obtain a maximum conversion of about 87.5% after 120 min. These results indicate that the conjugation of P11-4 to PEG was rapid and almost maximum conversion was attained within a span of 2 min.

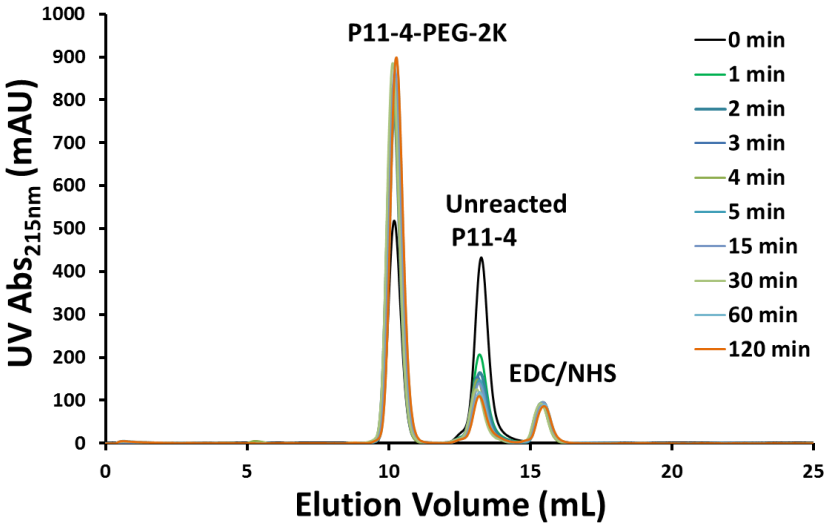

Figure 3-9: Size exclusion chromatogram of conjugation mixtures at different time intervals ranging from 0-120 min.

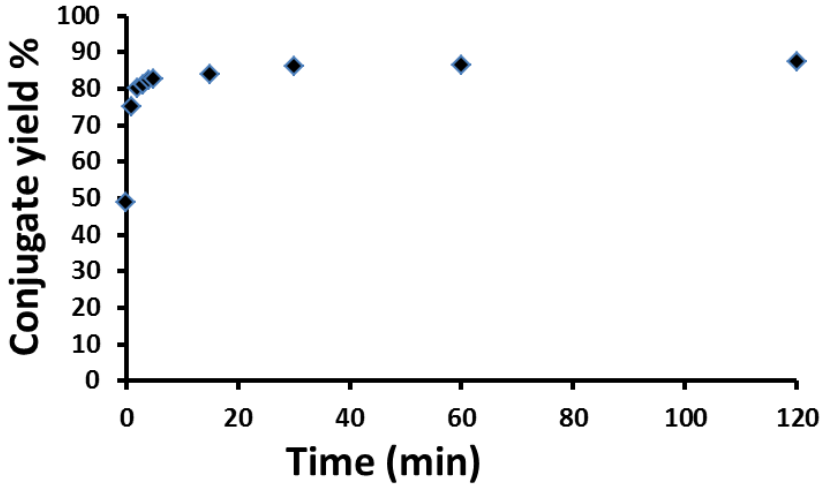

Figure 3-10: Conjugate yield obtained from reaction mixtures obtained at different time intervals ranging from 0-120 min.

3.3.3 Secondary structure characterization of conjugate P11-4-PEG2K

To investigate the secondary structure transitions of the conjugate P11-4-PEG-2K, the purified samples subjected to different pH conditions were analysed using CD spectroscopy. As seen in Figure 3-11, the conjugate had a random coil structure at pH 7 and with a further decrease in pH (pH < 3) the conjugate still retained its random coil conformation. Interestingly, the conjugate retained its random coil structure even after incubation for more than 10 days. Previously, Radu et al. (2009) reported similar observations during the self-assembly of the bioconjugate formed upon conjugation of peptide P11 (QQRFQWQFEQQ) with poly [N-(2-hydroxypropyl)methacrylamide] (HPMA). It was observed that the peptide P11 self-assembled at pH 2 and disassembled at pH 7 whilst the conjugate P11-poly (HPMA) retained the random coil structure at both these pH. However, further increase in pH (pH > 11) using 1 M NaOH and subsequent incubation for 10 days resulted in the secondary structure transition towards β-sheet. This was attributed to the presence of Na^+ ions, pH and

incubation time. Thus, similar experiments were performed using P11-4-PEG-2K bioconjugate. However, the conjugate retained its random coil structure even after incubation at pH 11 for 20 days (data not shown). These results indicate that the conjugate did not self-assemble across various pH and/or incubation periods, thereby encouraging further investigations on various other parameters influencing the self-assembly of P11-4-PEG-2K bioconjugate. Thus, additional experiments were performed to analyse and investigate the effect of the numerous parameters that could possibly have an effect on P11-4-PEG-2K self-assembly.

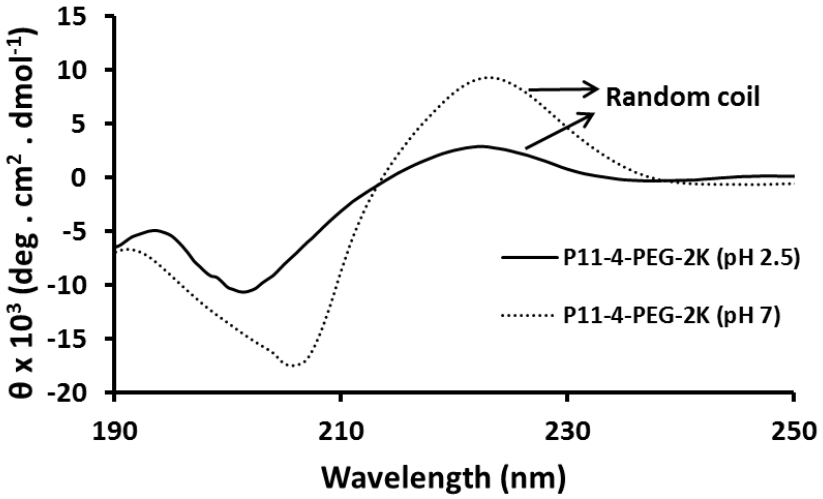

Figure 3-11: CD spectra of conjugate P11-4-PEG-2K showing random coil conformation at both pH 2.5 and 7.

3.3.3.1 Effect of salt (NaCl) on self-assembly of P11-4-PEG-2K

The presence of NaCl in the conjugation solution has been known to promote self-assembly owing to its ability to screen electrostatic repulsion of the peptide strands (Carrick et al., 2007). Thus, to investigate the effect of NaCl on self-assembly, NaCl at concentrations of 130 and 250 mM was added to the P11-4-PEG-2K solution at pH 2.5, 7 and 11, respectively. It was observed that the conjugate retained its random coil conformation (Figure 3-12) even after incubation for 20 days across all tested pH conditions. This indicates that increasing the ionic strength or salt concentration did not induce secondary structure transitions in the case of P11-4-PEG-2K.

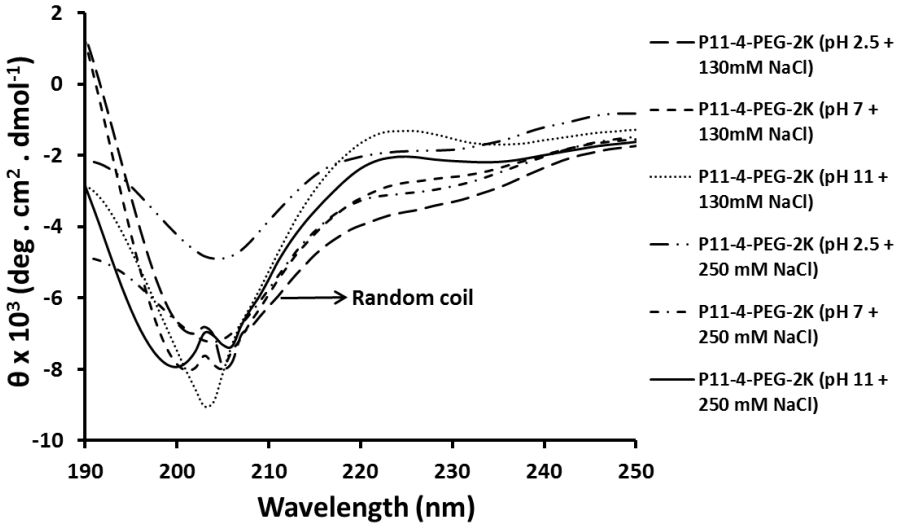

Figure 3-12: CD spectra of conjugate P11-4-PEG-2K showing random coil conformation in the presence of 130 and 250 mM NaCl at pH 2.5, 7 and 11.

3.3.3.2 Effect of free PEG on self-assembly of P11-4

Purification of the conjugation mixture through the column (Section 3.2.2) suggested the presence of small amounts of free unreacted PEG in solution. Thus, to investigate the effect of free PEG on self-assembly of P11-4 in the conjugate, designated concentrations (*e.g.*, 5, 10 and 15 mg/mL) of free PEG-2K were added to P11-4 solution and incubated at pH 2.5 for 24 h. CD spectroscopy suggested the formation of a β sheet structure at pH 2.5 even in the presence of high concentrations (15 mg/mL) of free PEG, as evident by the presence of a negative minimum around 217 nm (Figure 3-13). Furthermore, it was observed that the β sheet content (*e.g.*, β sheet content $\propto \theta_{217\text{nm}}$) remained unchanged despite the increase in concentration of free PEG-2K. The results suggest that free PEG-2K did not have a significant effect on the self-assembly of the conjugate.

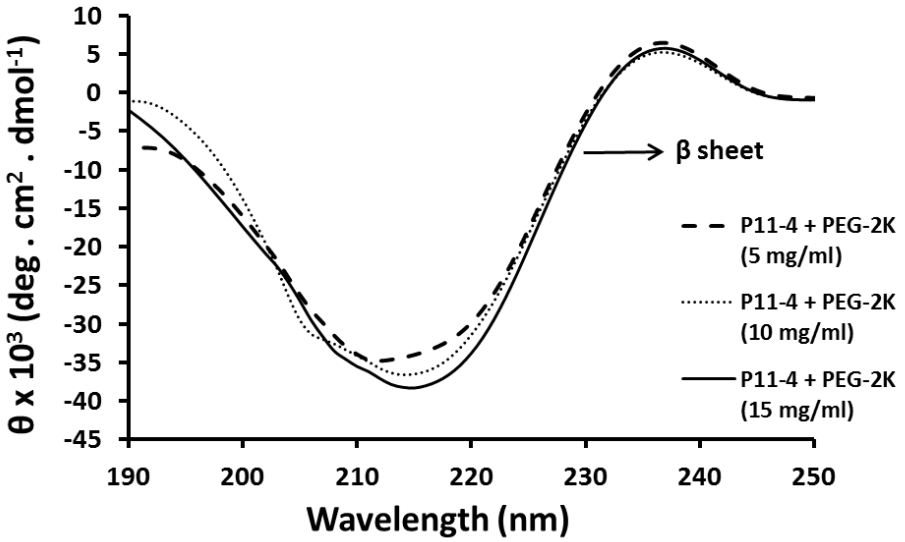

Figure 3-13: CD spectra of peptide P11-4 showing β sheet conformation at pH 2.5 in the presence of PEG-2K at concentrations 5, 10 and 15 mg/mL.

3.3.3.3 Effect of phosphate ions on self-assembly of P11-4

To investigate the effect of sodium phosphate buffer concentration on self-assembly of the peptide P11-4, P11-4 at a concentration of 0.25 mg/mL was dissolved in designated concentrations (3-50 mM) of sodium phosphate buffer. The pH was then adjusted to 2.5 using 1 M orthophosphoric acid and incubated for 2 h. It was observed that P11-4 forms a β sheet structure only in 3 mM buffer, whilst a random coil conformation exists at higher concentrations (Figure 3-14). Subsequently, similar experiments were performed with higher concentration of P11-4 (0.4 mg/mL) with buffer concentration ranging from 3 – 20 mM (Figure 3-15). In this case, it was observed that P11-4 forms a β-sheet structure at all buffer concentrations ranging from 3-20 mM. However, the β sheet intensity around 215 nm was found to decrease with buffer concentration. These results indicate that low concentrations of buffer are sufficient to promote self-assembly of P11-4 and therefore, subsequent experiments on conjugation of P11-4 to PEG were performed using 3 mM sodium phosphate buffer. Previously, a similar effect of phosphate ions on the self-assembly of peptide EMK16-II was observed (Zou et al., 2009). It was observed that 3 mM phosphate buffer promoted self-assembly of the peptide. However at higher concentrations, β sheet content was found to be dependent on both the concentration of the buffer and the peptide.

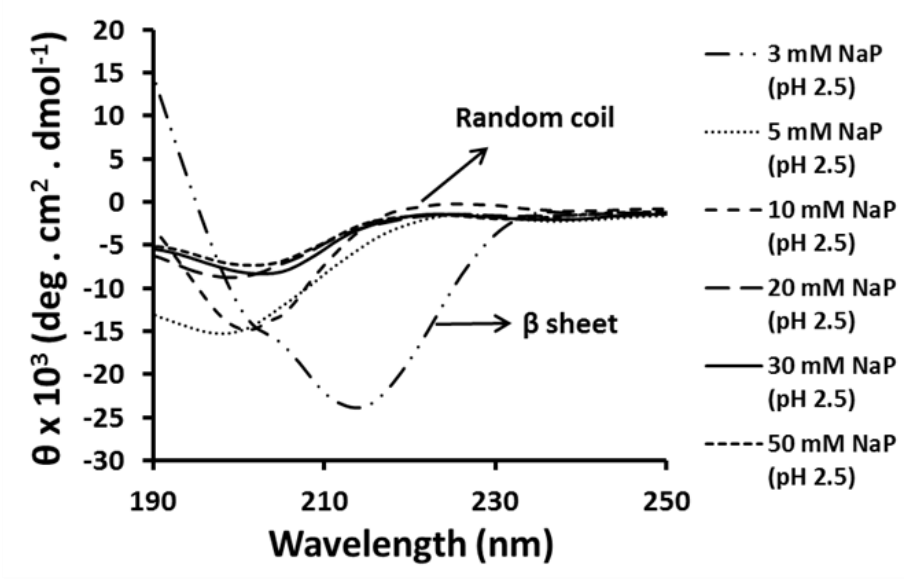

Figure 3-14: CD spectra showing secondary structure conformation of peptide P11-4 (0.25 mg/mL) in different concentrations of sodium phosphate buffer ranging from 3-50 mM at pH 2.5.

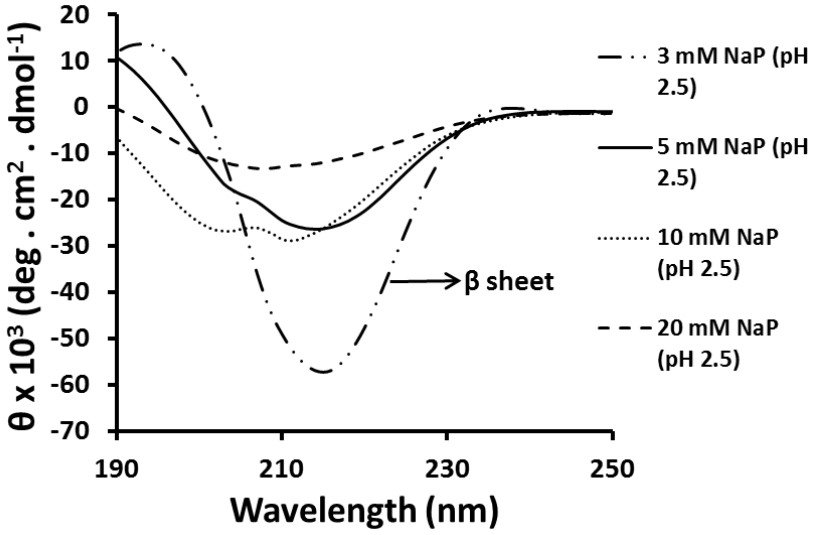

Figure 3-15: CD spectra showing secondary structure conformation of peptide P11-4 (0.4 mg/mL) in different concentrations of sodium phosphate buffer ranging from 3-20 mM at pH 2.5.

3.3.3.4 Conjugation in 3 mM sodium phosphate buffer

Based on previous investigations (Section 3.3.3.3) on the effect of buffer concentrations on self-assembly, conjugation of the P11-4 and NHS-PEG was carried out in 3 mM sodium phosphate buffer (pH 8). The concentrations of the peptide and PEG were similar to that used in previous conjugation experiments. The conjugate and the unreacted P11-4 were separated and desalted into water using the SEC column as described earlier. Control experiments were performed using P11-4 in 3 mM buffer and subjected to similar purification and desalting steps as the conjugate samples. As seen in Figure 3-16, the conjugate yield conversion achieved was reduced to 57% in comparison with 88% conversion achieved using 20 mM sodium phosphate buffer. This is probably due to pH variations with low concentration buffer (*e.g.*, low salt content). It was also observed that at pH 2.5, unreacted P11-4 and the P11-4 control formed β sheet structures, whilst the conjugate retained its random coil conformation (Figure 3-17). These results suggest that a reduction in the buffer concentration did not promote self-assembly of the bioconjugate.

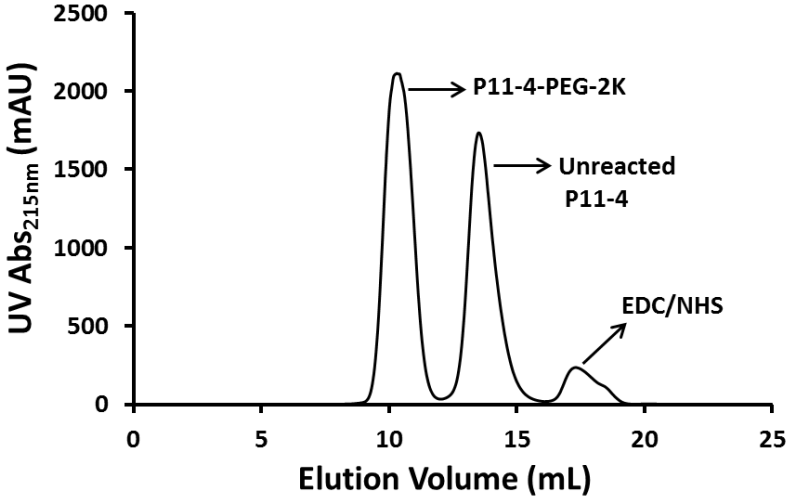

Figure 3-16: Size exclusion chromatogram showing the separation of conjugate P11-4-PEG-2K from the unreacted peptide and EDC/NHS in 3 mM sodium phosphate buffer.

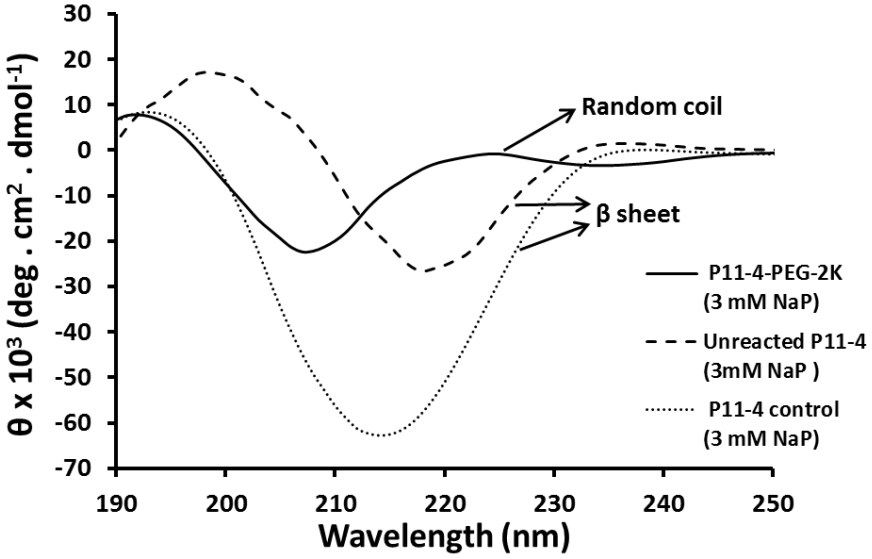

Figure 3-17: CD spectra showing secondary structure conformation of P11-4-PEG-2K, unreacted P11-4 and P11-4 control at pH 2.5.

3.3.3.5 Conjugation in water

As an alternative to varying salt or buffer concentrations, conjugation was also carried out in water by adjusting the pH to 8. Purification of conjugate (Figure 3-18) and unreacted P11-4 was carried out as described earlier and the secondary structure was analysed using CD at pH 2.5. Similar instabilities in pH were observed as in the case of low concentration buffers. Secondary structure analysis (Figure 3-19) at pH 2.5 suggested the formation of β sheet structure in the case of unreacted P11-4, while the conjugate remained in random coil state.

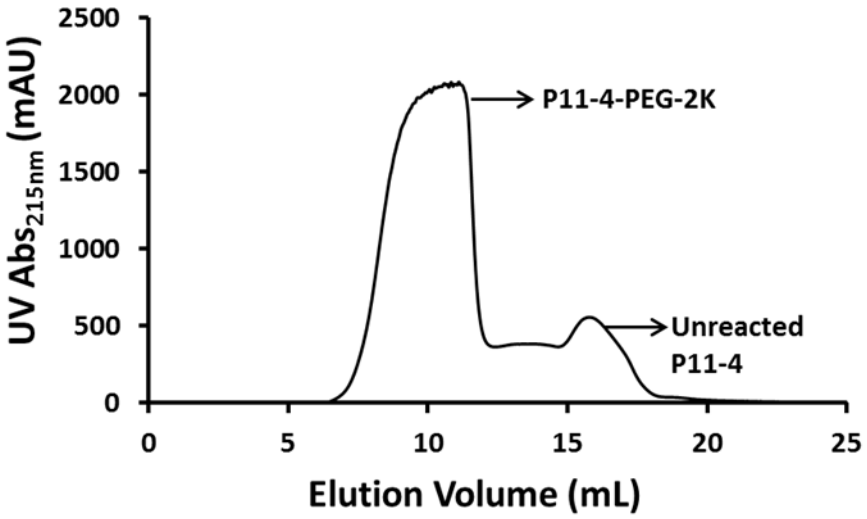

Figure 3-18: Size exclusion chromatogram showing the separation of conjugate P11-4-PEG-2K from the unreacted peptide in water.

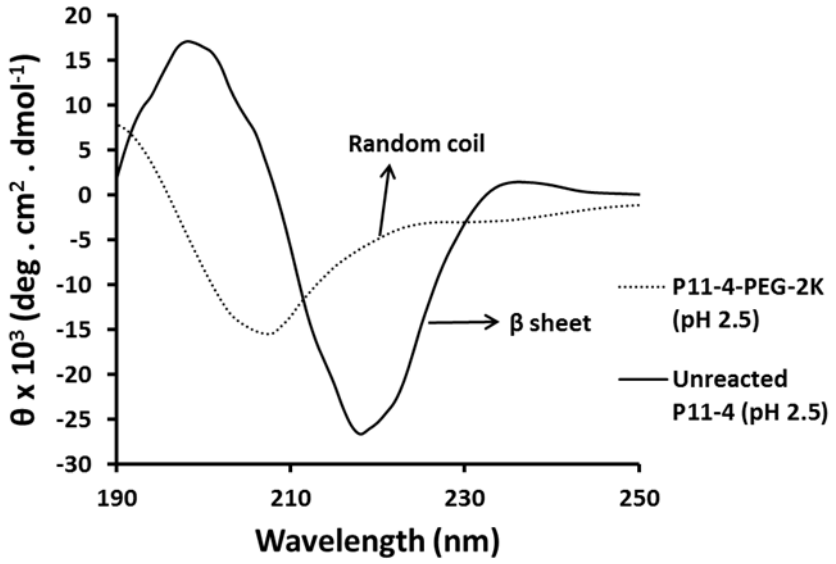

Figure 3-19: CD spectra showing secondary structure conformation of P11-4-PEG-2K and unreacted P11-4 at pH 2.5.

3.3.3.6 Conjugation using equimolar concentrations of P11-4 and PEG

To minimize the unreacted PEG in the conjugate solution, conjugation was performed with NHS-PEG and P11-4 at equal molar concentrations (1:1 ratio) in 3 mM sodium phosphate buffer. This is almost twice the molar concentration of P11-4 used in earlier conjugation experiments. The conjugate was purified (Figure 3-20), desalted in water, and analysed using CD spectroscopy for self-assembly at pH 2.5. Despite an increase in molar concentrations of P11-4, the conjugate retained its random coil structure (Figure 3-21).

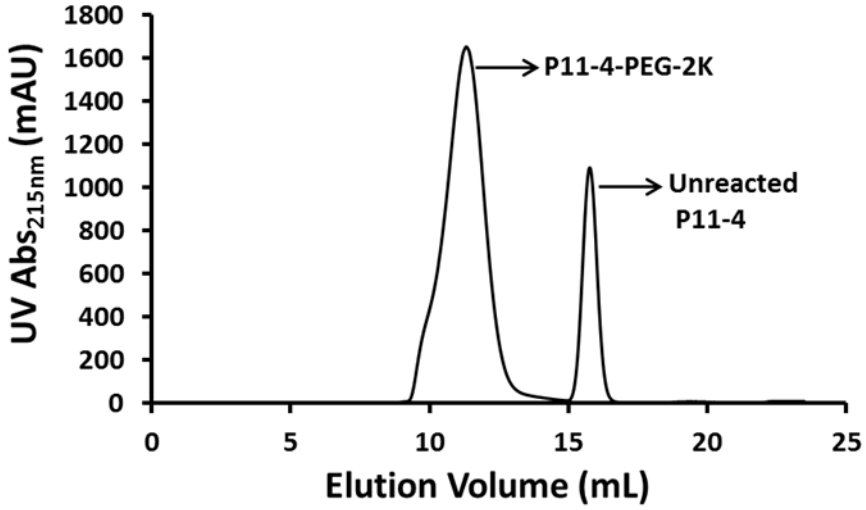

Figure 3-20: Size exclusion chromatogram showing the separation of conjugate P11-4-PEG-2K from the unreacted peptide and EDC/NHS in 3 mM sodium phosphate buffer.

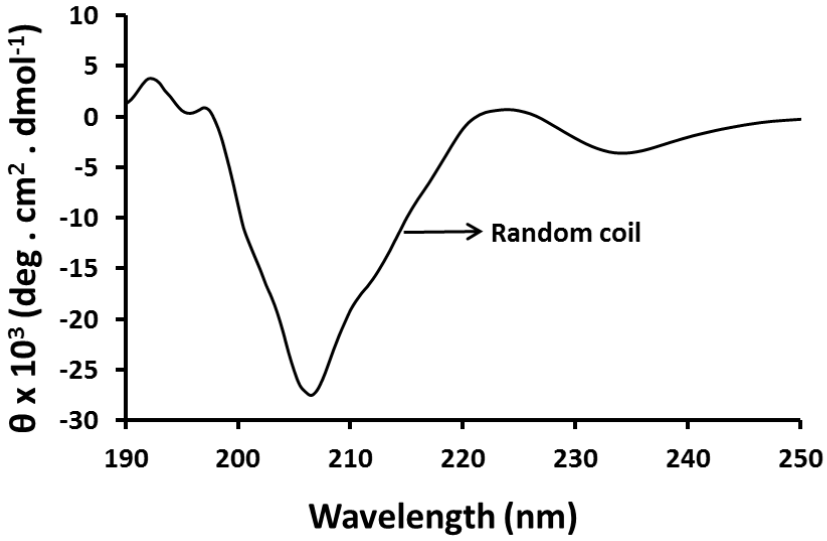

Figure 3-21: CD spectra of P11-4-PEG-2K showing random coil conformation at pH 2.5.

3.3.3.7 Effect of residual by-products of EDC/NHS reaction on the self-assembly of P11-4

Finally, to investigate the effect of the presence of residual by-products of the amine coupling reaction on P11-4 self-assembly, NHS-PEG was dissolved in 3 mM sodium phosphate buffer and left mixing overnight to hydrolyse the NHS esters and prevent the amine coupling reaction with the N-terminal amine of P11-4. Subsequently, P11-4 was dissolved in this upon adjusting the pH to 8 and the mixture was left mixing overnight. This mixture was purified through the SEC column and large amounts of unreacted P11-4 were recovered (Figure 3-22), indicating that there was very little conversion of conjugate in the mixture. Subsequently, unreacted P11-4 was desalted in 5 mM HCl (pH 2.5) and CD spectra analysis suggested the formation of β sheet structure. This indicates that the residual by-products such as succinic acid of EDC/NHS amine coupling reaction do not hinder the self-assembly of P11-4.

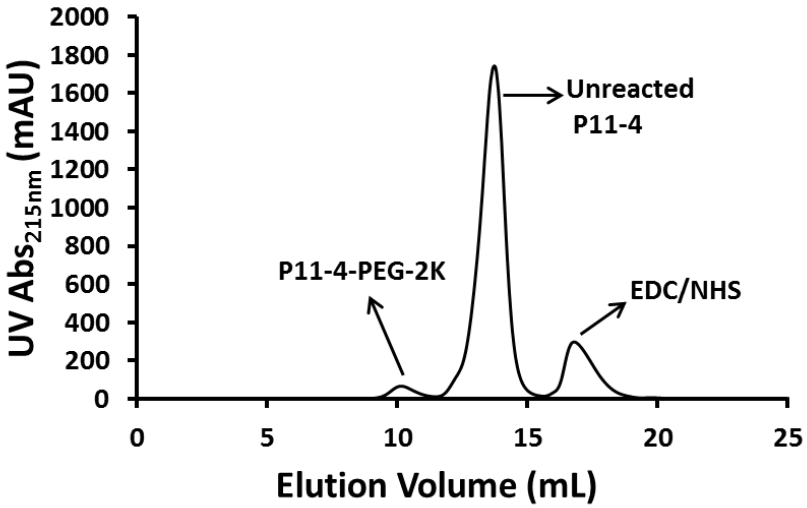

Figure 3-22: Size exclusion chromatogram showing the separation of conjugate P11-4-PEG-2K from the unreacted peptide and EDC/NHS in 3 mM sodium phosphate buffer.

3.4 DISCUSSION AND CONCLUSION

P11-4 a peptide known for its rapid self-assembly (Aggeli et al., 2003) was conjugated with NHS PEG-2K in an attempt to a develop novel peptide-polymer bioconjugate. The conjugation was performed in solution and was purified using a standard SEC column. Conjugation of P11-4 to PEG-2K was confirmed using MALDI-tof spectrometry analysis. The conjugation reaction occurred essentially instantly and the maximum yield was obtained within 2 min of mixing the reagents. However, conjugation of P11-4 to PEG-2K hindered the self-assembly of P11-4 and the conjugate thus remained in random coil conformation at pH < 3, whereas the native P11-4 formed β sheet at that pH. Further, the conjugate retained its random coil structure across wide pH values (pH 2.5, 7 and 11) and incubation periods (2 min to 20 days).

The ability to manipulate the self-assembly processes in artificial systems is largely dependent on the solution parameters (*e.g.*, salt or buffer concentrations) and various experimental (*e.g.*, coupling reaction conditions and incubation periods) conditions. To establish a better understanding of the biochemical and biophysical nature of the self-assembly of P11-4, the effect of solution conditions and conjugation parameters on peptide self-assembly were investigated. Initially, the presence of unreacted free PEG and its effect on P11-4 self-assembly was investigated because PEG-2K would be expected to be present in the purified conjugate mixture. It was observed that even the presence of a large excess of PEG-2K did not prevent self-assembly of P11-4. Further investigations on solution conditions such as concentration of phosphate ions during self-assembly suggested that low concentration buffers (*e.g.*, 3 mM sodium phosphate buffer) were more suitable for promoting self-assembly of P11-4. This was evident from the decrease in β sheet intensity with an increase in concentration of phosphate ions. However, conjugation experiments were carried out using 3 mM sodium phosphate buffer, which did not promote self-assembly because the conjugate retained its random coil structure at pH 2.5. Subsequent conjugation experiments carried out in water resulted in similar behaviour.

Generally, self-assembly is mediated through weak intermolecular bonds (*e.g.*, van der Waals bonds), electrostatic interactions, hydrogen bonds and stacking interactions. The combination of these relatively low energy interactions results in the formation of intact and well-ordered supramolecular structures (Zhang, 2002). Thus, further investigations were based on analysing the effect of conjugation parameters that include (*i*) concentrations of P11-4 and NHS-PEG-2K in the reaction mixture and (*ii*) residual by-products of EDC/NHS reaction. In both cases, the self-assembly of native P11-4 remained unperturbed, whilst the conjugate retained a random coil conformation at pH 2.5. Previous demonstrations of self-assembly of

P11-4 suggest that the presence of one unit of net positive or negative charge per peptide molecule is required for self-assembly (Aggeli et al., 2003). Ideally, at pH < 3, all the γ-carboxyl groups of glutamic acid residues are uncharged and results in only one net positive charge on Arg^+. The positive and negative charges on the N and C terminals cancel one another out. However, in case of P11-4-PEG-2K, PEG is conjugated to P11-4 via the N-terminal amine coupling. This eliminates the positive charge of the N-terminal amine, thereby resulting in a conjugate with Arg^+ and the negatively charged C terminal carboxylate, which can probably counterbalance each other. Thus, the net charge on the conjugate remains neutral. Thus, it can be concluded that the conjugation of PEG to the N-terminal amine of peptide P11-4 via EDC/NHS coupling may prevent the self-assembly of the peptide.

In conclusion, the conjugation of P11-4 to NHS-PEG-2K via N-terminal amine coupling was demonstrated and validated using MALDI-TOF spectrometry. The rapidly synthesized bioconjugate (*e.g.*, < 2 min) did not retain self-assembly and retained a random coil structure at pH < 3. A feasible explanation for this behavior was sought and several investigations of various factors affecting the self-assembly of P11-4 were performed. No conditions were identified that promoted conjugate self-assembly, which made it unsuitable for tethering to a membrane. Therefore, this avenue was abandoned in favour of seeking an alternative peptide that would retain its self-assembling behaviour after conjugation with the PEG spacer. The alternative peptide identified was EL-5F and the detailed characterization of EL-5F and its conjugates is the subject of Chapter 4.

CHAPTER-4

REVERSIBLE AND RAPID SELF-ASSEMBLY OF PEPTIDE-PEG BIOCONJUGATES EL-5F-PEG-2K AND EL-5F-PEG-5K

4. REVERSIBLE AND RAPID SELF-ASSEMBLY OF PEPTIDE-PEG BIOCONJUGATES EL-5F-PEG-2K AND EL-5F-PEG-5K

4.1 INTRODUCTION

This chapter outlines the development of rapid and reversibly self-assembling bioconjugates EL-5F-PEG-2K and EL-5F-PEG-5K synthesized via conjugation of peptide EL-5F (ELELELELELF) with PEG chains of MW 2 and 5 kDa (PEG-2K and PEG-5K) respectively. This work has been published in *Langmuir* journal (Ponnumallayan & Fee, 2014) (See Appendix C). With previous attempts (Chapter 3) to conjugate P11-4 and NHS-PEG-2K resulting in inability of the conjugate to self-assemble, an alternative peptide was identified that had been shown previously to reversibly self-assemble in the presence of divalent ions (Kuhnle & Borner, 2011). Recently, changes in pH (Ghosh et al., 2012; Zimenkov et al., 2006) and the addition/removal of divalent metal ions such as Cu^{2+}, Fe^{2+}, Zn^{2+} and Rh^{2+} have been used to trigger structural transitions in peptides (Pagel et al., 2008; Przybyla & Chmielewski, 2010; Zaykov et al., 2010). Kuhnle et al. successfully demonstrated the reversible self-assembly of the peptide domain (ELELELELELFG, EL-5FG) in a peptide-PEG bioconjugate using Ca^{2+} ions (Kuhnle & Borner, 2011). This peptide segment, containing an alternating pattern of hydrophilic and hydrophobic amino acids, has a high tendency towards β sheet formation but the extent of conversion in Kuhnle & Borner's work decreased markedly within three cycles of secondary structure shifts, which they attributed to increased ionic strength.

In this study, initial results showed that, in my hands, Ca^{2+} was unable to effectively trigger self-assembly so an alternative approach for the regulation of rapid, reversible self-assembly of the peptide EL-5F and its PEG conjugates using changes in pH, is instead described. As

decribed in detail in this chapter, the assembly and disassembly processes are controlled by pH-induced protonation and deprotonation, respectively, of the glutamic acid side chains of the peptide (Figure 4-1), which in turn elicit robust and reproducible structural transitions of the conjugates that are quantitatively related to pH, even at high salt concentrations.

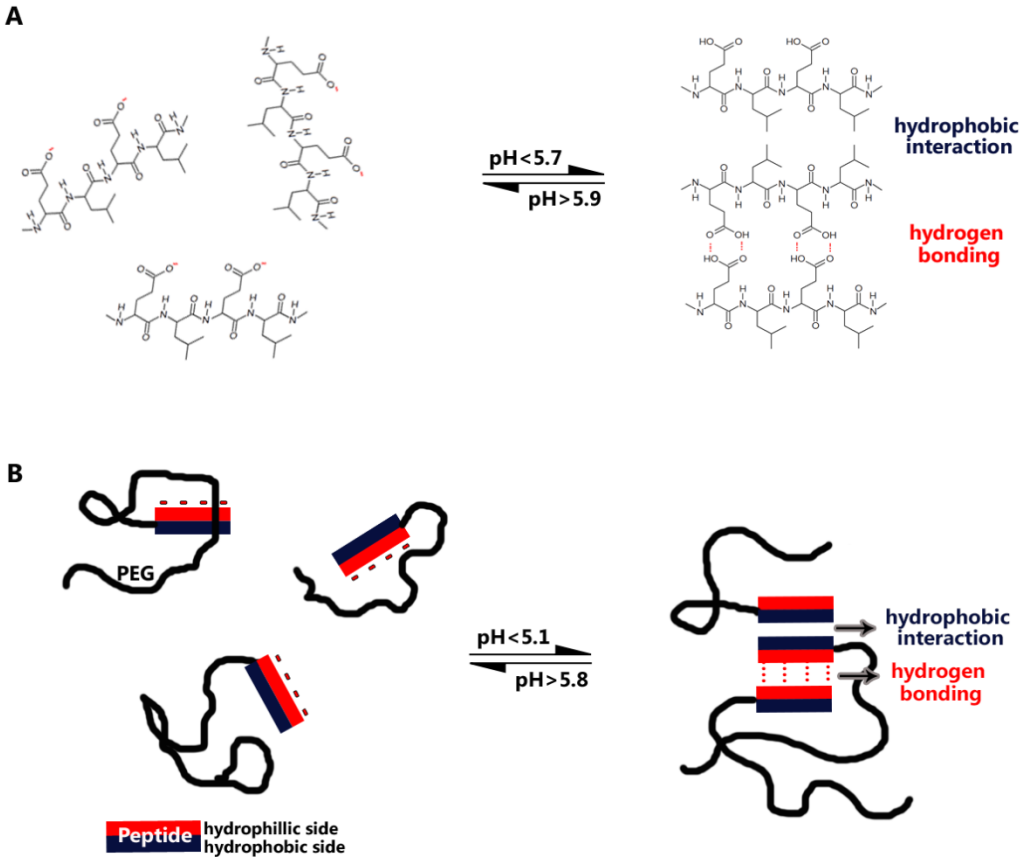

Figure 4-1: Structural view of pH-regulated, reversible self-assembly of (A) peptide EL-5F, (B) EL-5F-PEG conjugates.

4.2 EXPERIMENTAL SECTION

4.2.1 Materials The EL-5F peptide was purchased from Genscript. Heterobifunctional PEG reagents N-tert-butoxycarbonyl (Boc)-protected-amino-PEG 2000-carbonate-N-hydroxy succinimide (NHS) and Boc-protected-amino-PEG 5000-carbonate-NHS were purchased from NOF Corporation. All other chemicals were purchased from Sigma Aldrich. The Boc-protection was removed after peptide-PEG conjugation, to facilitate the tethering of the bioconjugate to membrane and nanoparticle (Chapter 5) surfaces.

4.2.2 EL-5F concentration calibration curve EL-5F peptide was dissolved in 3% ammonia solution at a series of concentrations. UV absorption spectra for each sample (maximum absorbance of EL-5F at 224 nm) was obtained using a Nanodrop UV spectrophotometer (Wilmington, Delaware, U.S.A). A calibration curve of UV 224 absorption against known concentrations was plotted (See Appendix A).

4.2.3 Conjugation and purification EL-5F peptide was dissolved at 4 mg/mL in 20 mM sodium phosphate buffer (pH 8). To synthesize EL-5F-PEG-2K, NHS-activated PEG 2000 at twice the molar concentration of the peptide was added to the solution and mixed for 2 h at room temperature. The resulting conjugate was then separated from unreacted peptide using a Superdex™ peptide 10/300 GL size exclusion chromatography column. The fractions corresponding to the conjugate peaks were collected, pooled and exchanged into water using the same column. Conjugation of NHS-activated PEG 5000 to the peptide and purification of the resultant EL-5F-PEG-5K conjugate was performed using the same procedure.

4.2.4 Matrix-assisted laser desorption/ionization time-of-flight (MALDI-TOF) mass spectrometry

MALDI-TOF mass spectrometry analysis was performed on a Bruker MALDI Ultraflex III TOF TOF using Flex Control version 3.4 software. The conjugate samples were diluted using 0.1% TFA to a final concentration of 0.1 mg/mL. For EL-5F-PEG-2K, 1 µL of diluted sample was mixed with 1 µL of α-cyano-4-hydroxy-cinnamic acid (HCAA) matrix (saturated HCAA matrix in acetone diluted 1:9 in solvent (6:3:1 ethanol: acetone: 0.1% TFA)). 1 µL of the matrix/sample mixture was spotted onto an AnchorChip. The instrument was calibrated with peptide calibration standards for mass spectrometry. EL-5F-PEG-2K was analysed manually in the positive ion reflectron mode between m/z 700–4500. 500 laser shots with a frequency of 200.0 Hz were acquired per spectrum. For EL-5F-PEG-5K, 2 µL of the diluted sample was mixed with 2 µL of 2% v/v TFA then 2 µL of 2,5-dihydroxyacetophenone (DHAP) matrix (7.6 mg of DHAP in 375 µL of ethanol + 125 µL of 5 mg/mL ammonium formate). 0.5 µL of the matrix/sample mixture was then spotted onto a ground steel plate (Bruker). Protein 1 calibration standard (Bruker Daltonics) was spotted onto adjacent calibration spots to calibrate the instrument. EL-5F-PEG-5K was analysed manually in positive ion linear mode between m/z 4040-20,200 Da. 200 laser shots with a frequency of 100.0 Hz were acquired per spectrum.

4.2.5 Circular dichroism spectroscopy CD spectra were recorded on a Jasco J-815 CD spectrometer in solution using a sample concentration of 0.8 mg/mL in water. The pH of each sample was adjusted in an Eppendorf tube by dropwise addition of 1 M HCl or NaOH with thorough mixing and the tube centrifuged (5 min, 9000 x g) with an Eppendorf MiniSpin Plus benchtop centrifuge. The clear supernatant was then removed by pipette and placed into a 1 mm pathlength quartz cuvette for CD scanning at 1 nm intervals from 250 to 200 nm. Spectra were obtained as an average of three consecutive scans after background subtraction.

Samples were removed from the cuvette by pipette and returned to the Eppendorf tube for subsequent pH adjustment and the above process was repeated.

4.2.6 Transmission electron microscopy Solutions of native and conjugated EL-5F containing β sheet and random coil structures identified by CD were used for sample preparation. 20 µL of the samples was deposited for 1 min on carbon-coated Formvar 200-mesh copper grids, and then washed twice with water. Negative staining of the samples was achieved by placing the grids wet-side down on top of 20 µL of 1% w/w uranyl acetate solution in water for 1 min. Filter paper was used to remove excess liquid from the grids by blotting, and the grids were then left to dry for several hours before TEM observations.

4.2.7 Thioflavin T fluorescence binding assay 50 µM thioflavin T (ThT) in water was added to the peptide and conjugate solutions, to obtain final concentrations of 20 µM ThT and 0.5 mg/mL of peptide or conjugate. The fluorescence intensity of the samples was recorded immediately at room temperature. Fluorescence intensity was measured in 100 µL samples in a 96-well plate, with a Molecular Devices SpectraMax M5 fluorimeter (Sunnyvale, U.S.A) equipped with a plate reader. Samples were excited at 450 nm and fluorescence intensity was recorded at 480 nm, using a 25 µM ThT solution in water as a blank. The fluorescence intensity values were obtained as an average of 15 recordings for each sample.

4.2.8 BOC deprotection 50 µL of concentrated TFA was added to 1 mL of 2 mg/mL BOC-protected conjugate EL-5F-PEG-2K solution in water and sonicated (Digitec ultrasonic cleaner, Zwolle, Netherlands) for 2 h. This mixture was lyophilized and reconstituted in D_2O for nuclear magnetic resonance (NMR) analysis (See Appendix B).

4.3 RESULTS AND DISCUSSION

4.3.1 Conjugation and purification EL-5F was conjugated to the NHS-activated PEG polymers via standard amine coupling at pH 8 (Grabarek & Gergely, 1990; Klok, 2005). EL-5F contains only one primary amine, at the N-terminus, enabling site-specific conjugation. Thus, conjugation could be carried out on the free peptide rather than during solid-phase synthesis and was simple, quick and inexpensive compared with other conjugation strategies such as orthogonal coupling via click chemistry (Lutz et al., 2007) and solid phase-supported conjugation (Hentschel & Börner, 2006; Vandermeulen et al., 2003) that involve a number of reagents and multiple reaction steps.

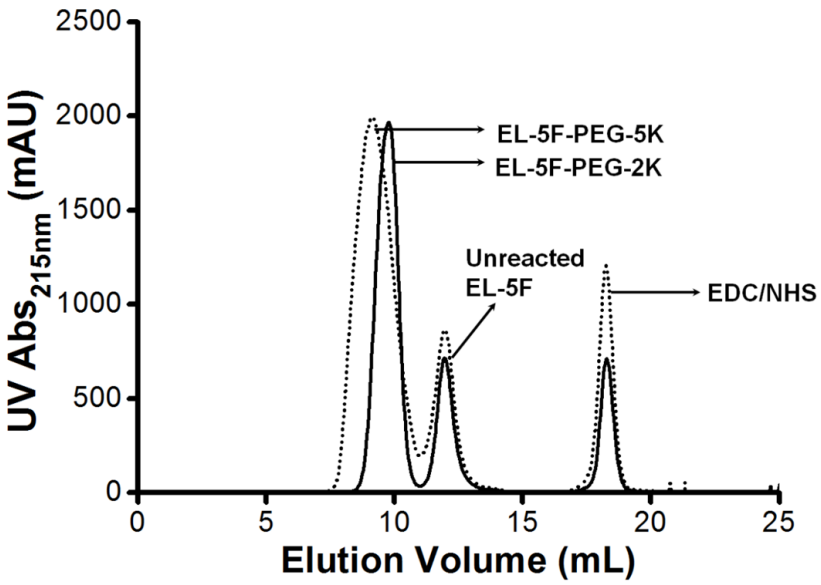

Figure 4-2: Size exclusion chromatogram showing the separation of conjugates EL-5F-PEG-2K and EL-5F-PEG-5K from the unreacted peptide and EDC/NHS.

A Superdex peptide SEC column was used to separate the conjugate from the unreacted peptide and EDC/NHS by products. SEC chromatograms of native EL-5F, NHS-activated

PEG 2000 and 5000 and EDC/NHS were obtained separately to identify the positions of their corresponding peaks. Figure 4-2 shows chromatograms of the conjugation reaction mixtures used to form EL-5F-PEG-2K and EL-5F-PEG-5K. In both cases, the conjugate was the largest component in the mixture (EL-5F-PEG-2K = 3376 Da; EL-5F-PEG-5K = 6376 Da) and was eluted first, followed by the unreacted peptide (1376.55 Da), then the low molecular weight EDC/NHS by-product.

NHS-PEG also undergoes hydrolysis to produce PEG-OH, which has no UV absorbance, so it is not seen in Figure 4-2, although it is expected to follow closely after and partially co-elute with the conjugate peak. The final conjugate sample is therefore likely to have contained free PEG but this apparently did not hinder the self-assembly of the conjugate, as is evident from the CD results described below. Calculating the areas of the individual peaks, it was found that the conversion of the conjugation reaction was around 80%, which is comparable with the highest conversions achieved previously using other methods for other peptides (Kuhnle & Borner, 2011; Radu-Wu et al., 2009; Stutz et al., 2013). The presence of the conjugates after purification was confirmed by MALDI-TOF mass spectrometry as described in Section 4.2.4 (Figures 4-3 and 4-4).

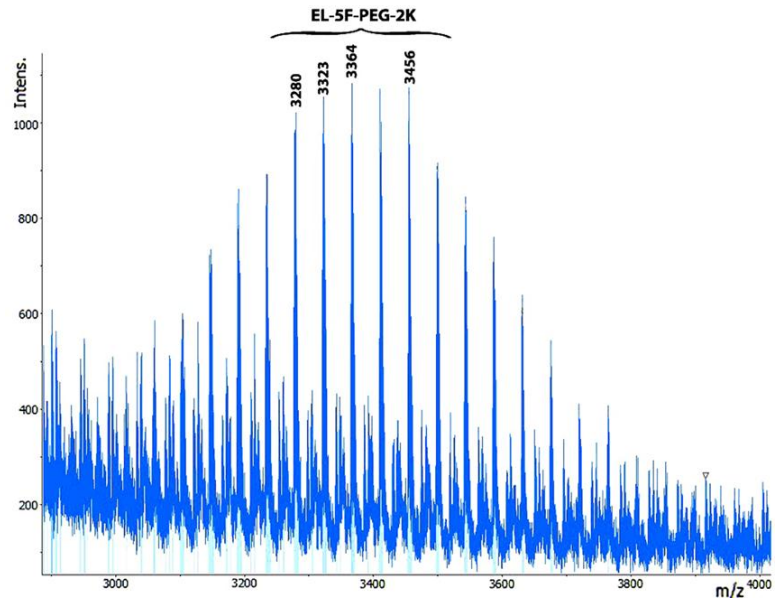

Figure 4-3: MALDI-TOF mass spectrum of the EL-5F-PEG-2K conjugate confirming the successful coupling of peptide EL-5F (1376.5 Da) and PEG 2K.

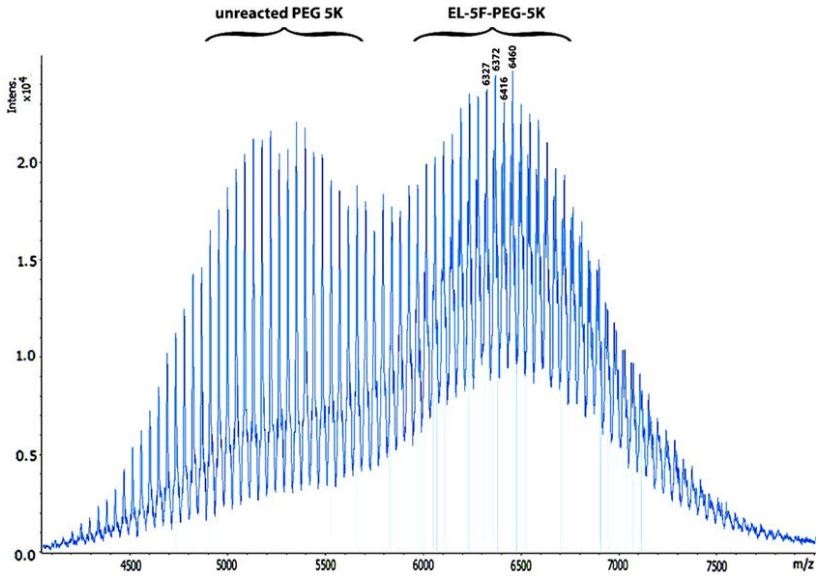

Figure 4-4: MALDI-TOF mass spectrum of the EL-5F-PEG-5K conjugate confirming the successful coupling of peptide EL-5F (1376.5 Da) and PEG 5K.

4.3.2 Secondary structure characterisation The secondary structure transitions of the peptide EL-5F and the conjugates were analysed using CD spectroscopy. A negative minimum around 215 nm and positive maximum near 200 nm indicates a β sheet structure, whereas a negative minimum around 200 nm is characteristic of a random coil (Greenfield, 2006) The native peptide dissolved in water at pH < 5.7 had a β sheet secondary structure (self-assembly) (Figure 4-5A). When the pH was increased to 5.9 and above, there was a conformational shift from β sheet to random coil and this was again reversed to the β sheet conformation by decreasing the pH to 5.7 and below. The shifts from β sheet to random coil and vice versa occurred rapidly (within 5 min), whilst the extent of conversion was constant even after incubation for more than 24 h (Figure 4-6). Similar rapid and reversible transitions between β sheet and random coil with pH change were observed with the conjugates EL-5F-PEG-2K and EL-5F-PEG-5K (Figure 4-5B). This indicates that the PEG chain did not prevent pH-regulated self-assembly of the conjugates (and neither did the presence of the Boc-protected amine terminal of the PEG chain). Furthermore, the length of the PEG chain did not appear to be significant, in contrast to hindrance of bioconjugate self-assembly reported in earlier work with the same peptide conjugate when the molecular weight of the PEG adduct was increased from 0.8 to 3.2 kDa (Kuhnle & Borner, 2011).

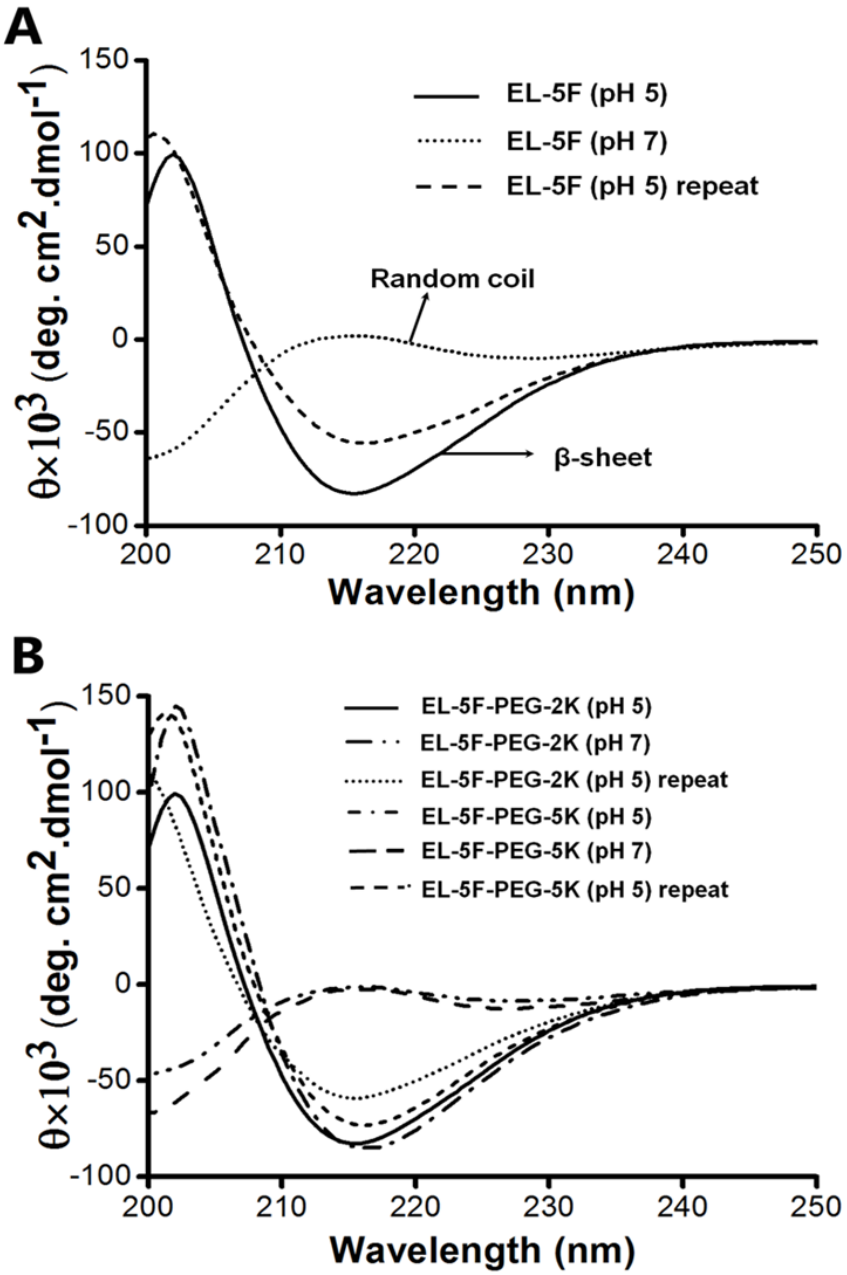

Figure 4-5: CD spectra of (A) native peptide EL-5F, (B) EL-5F-PEG-2K and EL-5F-PEG-5K, showing the repeated conformational shifts between β sheet and random coil upon changing the pH between 5 and 7.

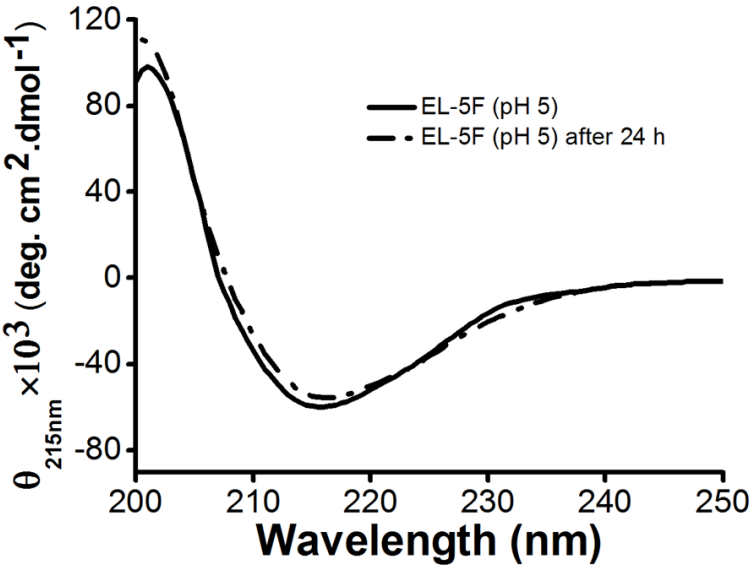

Figure 4-6: CD spectra of native peptide EL-5F, showing similar β sheet intensities before and after 24 h incubation at pH 5.

Another interesting observation was that even after fifteen cycles of pH-regulated shifts between random coil and β sheet, the extent of conversion was reproducible in EL-5F-PEG-2K (Figure 4-7) and EL-5F-PEG-5K (See Appendix C) whereas divalent ion switching of PEG-EL-5FG was demonstrated for only two cycles of self-assembly. It was noted that the final transition took 3 days to reach 70% conversion from β sheet to random coil form, attributed to a build-up of salt (Kuhnle & Borner, 2011). Furthermore, the reported reversible peptide systems by Aggeli et al. became unresponsive within 3 or 4 cycles of pH shifts and this was also attributed to an increase in ionic strength (Aggeli et al., 2003).

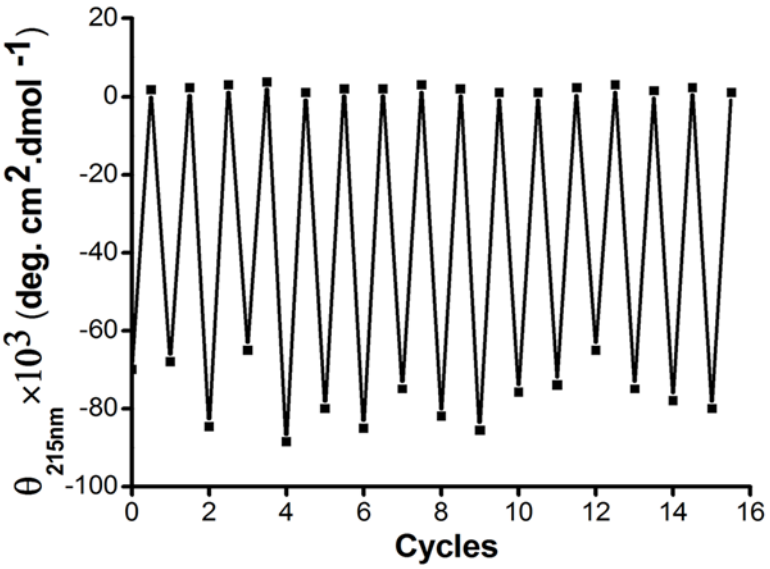

Figure 4-7: CD negative intensity at 215 nm, indicating the extent of β sheet (θ_{215nm} < -60 x 10^3) to random coil ($\theta_{215nm} \approx 0$) transition with 16 repeated secondary structure shifts of EL-5F-PEG-2K, mediated by corresponding changes in pH from below 5 to above 7.

In this study, the concentration of salt formed by the alternating addition of HCl and NaOH for these pH switches was < 20 µM in total. Therefore, the effect of ionic strength on the reversibility of the native EL-5F peptide structural shifts, at NaCl concentrations ranging from 0 to 200 mM was investigated. Note, as described below, that the extent of conversion was directly related to pH, so care was taken here to keep the low pH consistently around 5. It was found that increased ionic strength reduced the conversion of the peptide to β sheet, as evident from the decreased CD intensity at 215 nm, but reversible self-assembly was maintained, even up to the addition of 200 mM NaCl (Figures 4-8 and 4-9). Maximum conversion to β sheet was seen below 50 mM NaCl, with a sharp transition from 50 to 100 mM NaCl to a lower but still evident self-assembly between 100 and 200 mM NaCl (Figure 4-9). The reason for the distinct change in the extent of conversion between 50 and 100 mM

NaCl is not evident to us. However, the trend in Figure 4-9 implies that self-assembly would be sustained at salt concentrations beyond 200 mM. To my knowledge, this robust and rapid repeated reversibility even at high salt concentrations has not been demonstrated previously with any peptide or peptide conjugates.

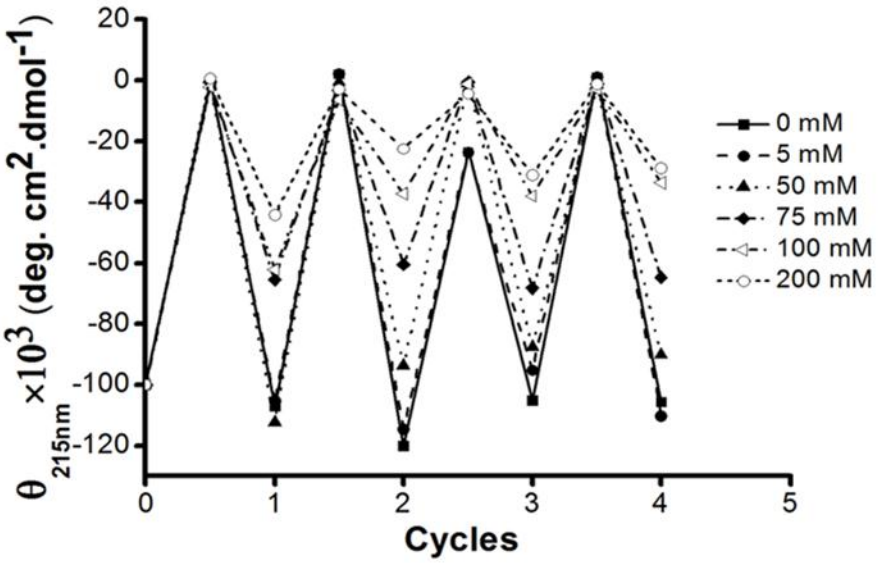

Figure 4-8: CD negative intensity at 215 nm, indicating the extent of β sheet-to-random coil transition of EL-5F after the addition of NaCl at concentrations ranging from 0 to 200 mM mediated by corresponding changes in pH between 5 and 7.

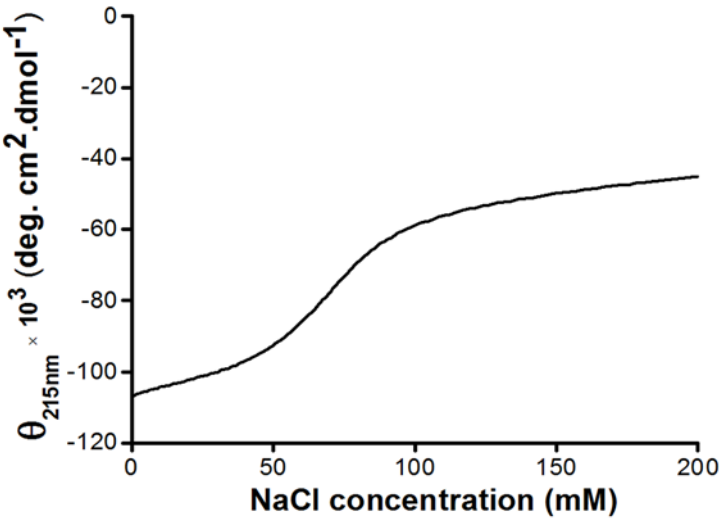

Figure 4-9: The mean β sheet intensity at 215 nm for EL-5F at NaCl concentrations ranging from 0 to 200 mM.

The transitions between β sheet and random coil for EL-5F, EL-5F-PEG-2K, and EL-5F-PEG-5K occurred between pH 5.7–5.9, pH 5.4–5.8 and pH 5.1–5.4, respectively (Figure 4-10). However, while the maximum β sheet intensity for EL-5F was in the pH range 5.3–5.7, just below transition, those for EL-5F-PEG-2K and EL-5F-PEG-5K were shifted to the pH ranges 3.3–3.6 and 3–4.5 respectively. The extent of conversion to β sheet by EL-5F, as measured by CD intensity, increased sharply with the decrease from pH 5.9 to 5.7, and then gradually decreased over the range pH 5.3 to 3. Intuitively, one might expect the conversion to β sheet to *increase*, rather than decrease, with lower pH. It is believed that the observed decrease in CD intensity was caused by a decrease in peptide concentration in solution as a result of reversible precipitation as the pH approached the peptide's isoelectric point (pI 2.9), such that the decrease in concentration more than offset increased β sheet formation in the remaining peptide. This explanation is supported by my observations of increasing cloudiness

and the presence of a pellet in centrifuged samples (prior to CD measurement of the clear supernatant) as pH decreased through this range, both of which disappeared as pH was increased. Decrease in the supernatant EL-5F concentration was detected by Nanodrop absorbance after sample acidification, which was reversed upon pH increase. Conversely, below pH 5.4, the CD adsorption intensity at 215 nm for the self-assembled EL-5F-PEG-2K gradually increased over a similar pH range (5.4–3.3), while EL-5F-PEG-5K showed an increase in intensity over the pH range 5.1–4.5, below which it was stable. It is difficult to compare the absolute intensities for the different native and conjugate samples, because intensity is highly sensitive to concentration but the trend of increasing CD intensity with decreasing pH for the conjugates was possibly caused by the hydrophilic PEG adduct maintaining the solubility of the conjugates at low pH thus allowing an increased β sheet content to increase the CD intensity. In contrast to the native peptide sample, no change in supernatant peptide concentrations was measured between low and high pH values for the conjugated peptide samples.

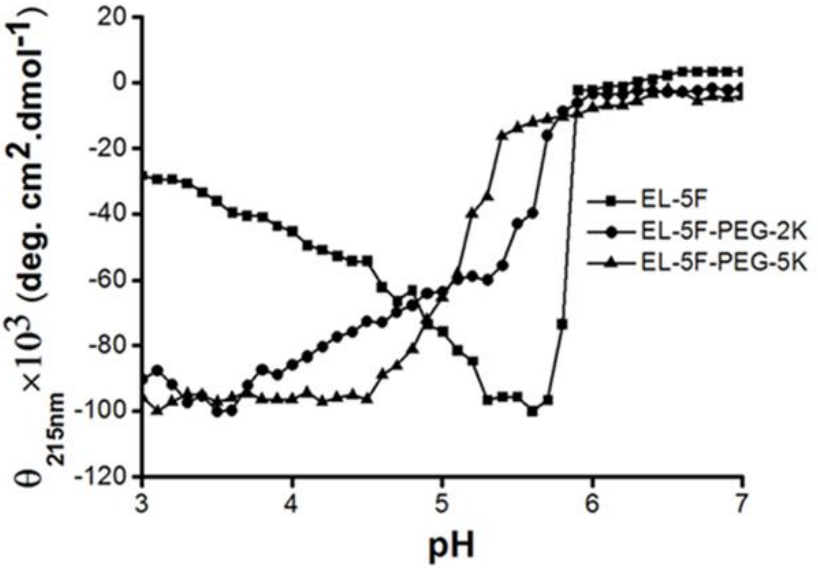

Figure 4-10: Circular dichroism adsorption at 215 nm (values > 0 indicating β sheet formation) for peptide EL-5F and conjugates over the pH range 3–7.

These observations can be used to elucidate the mechanism behind the pH-regulated reversible self-assembly of the EL-5F, EL-5F-PEG-2K and EL-5F-PEG-5K, as illustrated in Figure 4-1. At pH > 5.9, all the carboxyl groups in the peptide are deprotonated (negatively charged) and the resulting repulsive electrostatic forces between adjacent γ-COO^- groups in the neighbouring peptides prevent self-assembly, leading to fibril dissociation. In contrast, at pH < 5.1, the γ carboxyl groups become protonated (uncharged), allowing self-assembly of peptide fibrils. The actual pKa value of γ carboxyl groups (Glu 4.2–4.5) differs slightly from the pH required for self-assembly seen here. However, the pKa values of amino acid side chains in SAPs may differ from the values of the individual amino acids in free solution because of interactions with neighbouring charged side chains (Tang et al., 2011). The slightly lower pH transition range to self-assembly of the conjugates may be caused by mild exclusion of H^+ ions by the heavily hydrated PEG chains, which is supported by the greater

downward shift in transition pH caused by the larger PEG chains in EL-5F-PEG-5K compared with EL-5F-PEG-2K, although the effect was small. The peptide has two distinct sides, with regular repeats of alternating hydrophilic and hydrophobic side chains. During self-assembly, the peptide molecules form β sheets, held together on one side by hydrogen bonding between the uncharged carboxyl group side chains of the glutamic acid residues facing each other and on the other side by hydrophobic interactions between the leucine side chains facing one another.

4.3.3 Self-supporting hydrogelation The peptide EL-5F formed a clear self-supporting gel in water at pH < 5.4 at concentrations as low as 0.2 wt% and, furthermore, this transition appeared to be immediate. The gel did not collapse even when the tube was left inverted for several hours at room temperature. However, the gel disassembled immediately when the pH was increased above 5.8 and the solution became isotropic. Concentration normally plays a critical role in gelation of SAPs. Gel formation occurred only for the "aged" native EL-5FG peptide, at a concentration of 1 wt%, and after a period of several days (Kuhnle & Borner, 2011), whereas in this case, reversible transitions between gel and isotropic liquid with pH change were virtually immediate (< 5 min). Similar gelation behaviour was also observed in EL-5F-PEG-2K (Figure 4-11) and EL-5F-PEG-5K (data not shown). Fletcher et al. reported similar gelation behaviour of native peptides at low concentrations (Fletcher et al., 2011) but there are very few examples of peptide-PEG conjugates forming hydrogels, and in the cases that have been reported, the required concentrations exceeded 3 wt% (Hamley, 2014; Hamley et al., 2011; Jing et al., 2008; Martens et al., 2009; Radu-Wuet al., 2009; Radu et al., 2009). In this case, rapid, reversible pH-regulated hydrogelation of self-assembled conjugates at a 15-fold lower concentration than previously reported was observed. This behaviour can be

attributed to the glutamic acid and leucine side chains, responsible for strong hydrogen bonding and hydrophobic interactions, respectively, as described above (Figure 4-1).

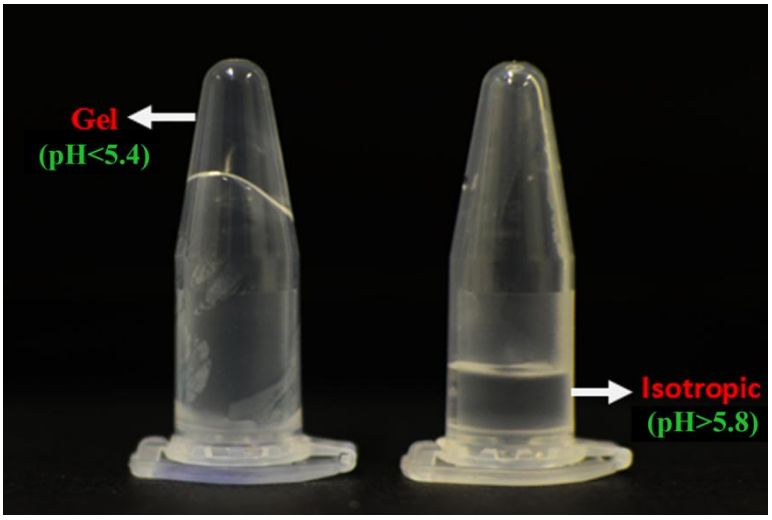

Figure 4-11: Self-supporting hydrogel of EL-5F-PEG-2K at pH < 5.4 (0.2 wt%) and the dissociation of the gel at pH > 5.8.

4.3.4 Characterisation of structural morphology The self-assembled fibrils of EL-5F, EL-5F-PEG-2K and EL-5F-PEG-5K at pH < 5.1 were investigated using TEM. Less rigid and discontinuous structures with no fibrillar extensions were observed at pH > 5.9 in any of the three samples (Figure 4-12B, D and F). However, at pH < 5.1, fibrils several hundred nanometres in length were observed. The native peptide fibrils had a width of around 8–10 nm (Figure 4-12A), while the conjugates formed thinner fibrils, of around 4–6 nm (Figure 4-12C and E), possibly caused by the heavily hydrated PEG chains surrounding the fibrils hindering peptide interactions beyond a certain local PEG density. A similar observation was reported by Messersmith et al. for PEG-conjugated β sheet peptides (Collier & Messersmith, 2004).

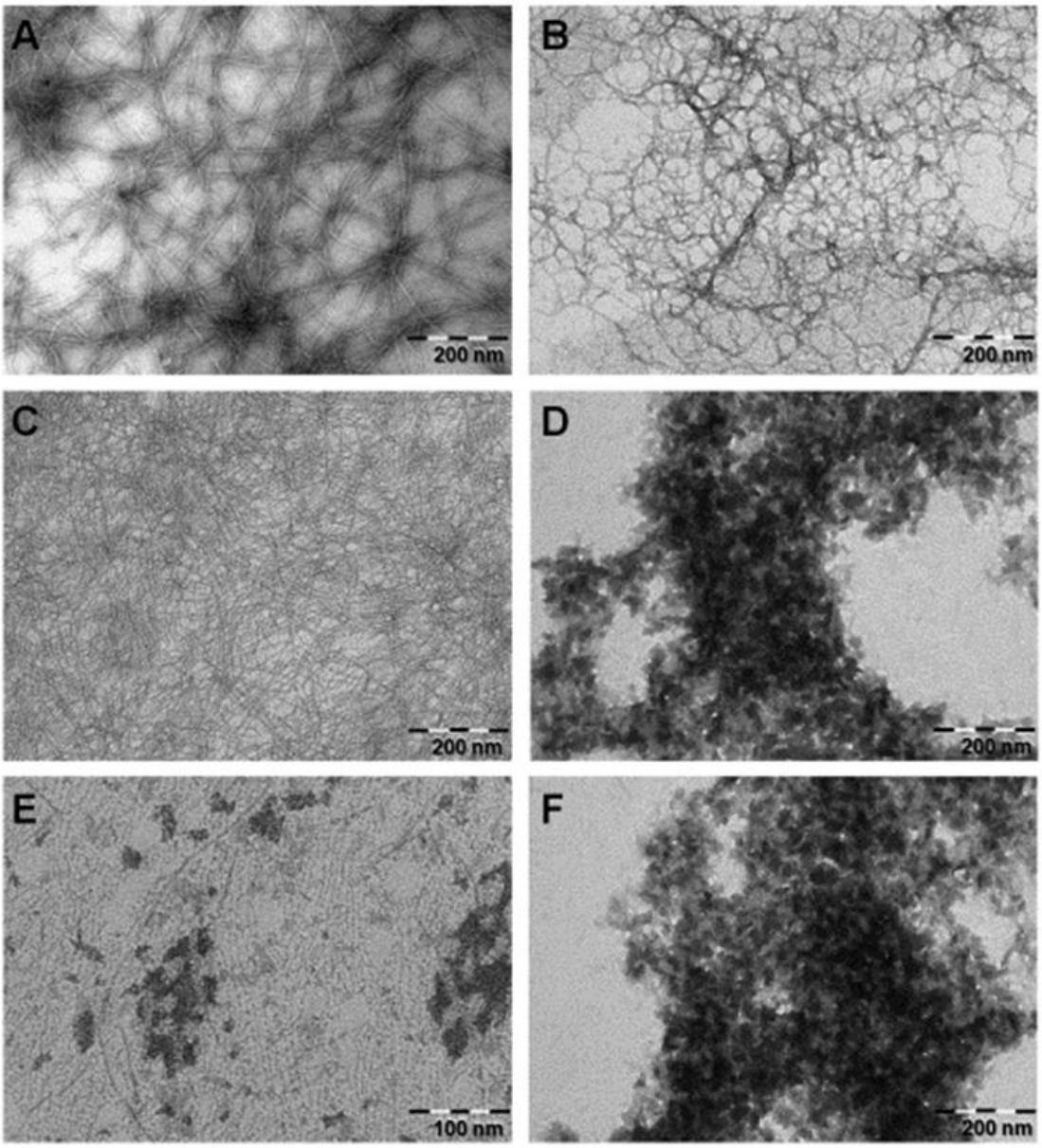

Figure 4-12: TEM images of negatively stained (A) EL-5F at pH < 5.7, (B) EL-5F at pH > 5.9, (C) EL-5F-PEG-2K at pH < 5.4, (D) EL-5F-PEG-2K at pH > 5.8, (E) EL-5F-PEG -5K at pH < 5.1, (F) EL-5F-PEG-5K at pH > 5.4.

4.3.5 ThT binding assay A ThT binding assay was performed to confirm self-assembly of EL-5F and the two PEG conjugates upon change of pH. ThT is a fluorescent benzothiazole dye that preferentially binds to cross-linked β sheet structures of proteins and peptides. This dye has high affinity to fibrils even with only four or five associated β strands because of its small tip-to-tail length (~15 Å) (Biancalana et al., 2009; Foderà et al., 2008), whereas larger dye molecules such as Congo red or Thioflavin S require higher numbers of self-assembled β strands (Radu-Wuet al., 2009).

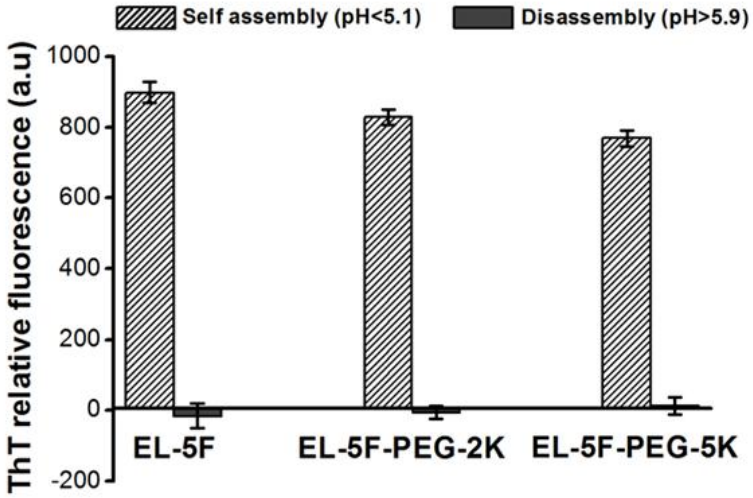

Figure 4-13: ThT binding assay of EL-5F, EL-5F-PEG-2K and EL-5F-PEG-5K at pH < 5.1 and pH > 5.9.

Figure 4-13 shows that the ThT fluorescence intensity was high for EL-5F, EL-5F-PEG-2K and EL-5F-PEG-5K at pH < 5.1, indicating the presence of self-assembled fibrils. The fluorescence intensities of the three samples did not differ greatly from one another, although there is a small trend to lower intensity with increasing PEG molecular weight, perhaps consistent with the PEG chains reducing the final width of the fibrils. It is apparent that conjugation between EL-5F and PEG did not eliminate the crosslinking of the β sheets. Increasing the pH above 5.9 resulted in negligible fluorescence intensity in all the samples,

indicating the dissociation of the β sheet network. This disassembly of fibrils was rapid and occurred within 5 mins of pH change. These results are consistent with the data obtained from CD and TEM and confirm reversible and rapid conformational changes of both the native peptide and its PEG conjugates.

4.4 CONCLUSIONS

Repeated rapid and reversible, pH-regulated, self-assembly of peptide EL-5F and conjugates of this peptide with 2 and 5 kDa PEG was demonstrated successfully. Self-assembly of the peptide and conjugates into β sheet structures upon change of pH was confirmed using CD, TEM and ThT binding analyses. Sustained, reversible self-assembly of the peptide and its PEG conjugates was shown to occur within 5 min for more than 15 cycles of pH shift and the extent of structural conversion was directly related to pH. The presence of PEG chains slightly decreased the pH range over which structural transition occurred, with the 5kDa PEG chains having a greater effect than the 2 kDa chains. The reversibility of secondary structure switching was sustained even at high salt concentrations (200 mM) but the extent of β sheet formation decreased with increasing salt concentration, most markedly between 50 and 100 mM salt. Rapid and reversible hydrogelation through self-assembly of the peptide and its conjugates at concentrations as low as 0.2 wt% was also demonstrated, which is 15-fold lower than the concentrations previously reported for similar systems. This approach to switching the mechanical properties of bioconjugates between β sheets and random coil using external triggers for reversible self-assembly could have broad applications in diverse fields, such as drug delivery, biosensing and bioseparations. The successful demonstration of conjugation and reversible self-assembly of the peptide-polymer bioconjugate enabled subsequent work (Chapter 5) to focus on the development of novel stimuli responsive

membrane using EL-5F-PEG-2K. Further investigation into the self-assembly of EL-5F-PEG-2K tethered to the membrane and its ability to enable switchable membrane permeability are presented in Chapter 5.

CHAPTER-5

DEVELOPMENT OF A NOVEL STIMULI-RESPONSIVE FILTRATION MEMBRANE FUNCTIONALIZED WITH SELF-ASSEMBLING PEPTIDE-PEG BIOCONJUGATE

5. DEVELOPMENT OF A NOVEL STIMULI-RESPONSIVE FILTRATION MEMBRANE FUNCTIONALIZED WITH SELF-ASSEMBLING PEPTIDE-PEG BIOCONJUGATE

5.1 INTRODUCTION

Signal-responsive biomaterials with the capability to undergo transitions upon communication with the external environment have recently drawn attention due to their applications in miniaturized devices, "smart" coatings, and drug-delivery systems (Shu et al., 2013). These materials possess unique capabilities to alter their structure or dimensions when there is a change in the physical or chemical environment. For instance, the development of multifunctional membranes and materials that respond to external stimuli such as pH, temperature, light, biochemicals or magnetic or electrical signals, represents a new dimension in separation science and molecular recognition (Wandera et al., 2010). This chapter focuses on the development of one such stimuli-responsive functional biomembrane achieved upon coupling self-assembling bioconjugate EL-5F-PEG-2K to the surface and pores of a bare nanofiltration membrane. The coupling strategies involved in the immobilisation of bioconjugate to the membrane are outlined. The study also investigates the influence of self-assembly of this tethered EL-5F-PEG-2K conjugate on the permeation properties of the membrane at high and low pH. Finally, the reversible, pH-dependant self-assembly of peptide EL-5F and the conjugate EL-5F-PEG-2K covalently tethered to the surface of nanoparticles (NPs) is also described. This was done primarily to demonstrate the inter-particle self-assembly of EL-5F/EL-5F-PEG-2K tethered to simple surfaces such as NPs.

Over the past two decades, membranes have been modified with a range of stimuli responsive polymers like PAA and P4VPy known to influence the flux properties during various

applications (Wandera et al., 2010). However, there are very few reports on investigations of peptide-modified membrane surfaces and their applications. Ito et al. (2000) immobilised ionizable PLGA polypeptide brushes onto a porous PC membrane and showed that variations in pH causes protonation and deprotonation of the peptide chains, influencing water permeation through the membrane pores. Similarly, Hollman et al. (2002) covalently attached PLGA to microporous cellulosic supports and reported similar observations in pH-responsive water permeation properties.

In parallel to the development of such stimuli responsive membranes, several attempts on the conjugation of engineered peptides and/or peptide-polymer bioconjugates to different surfaces have also been carried out. Despite widespread success in rapid and reversible stimuli responsive self-assembly of peptides and proteins in solution, self-assembly of peptides or bioconjugates covalently attached to surfaces has not been reported to date. Zhang et al. (1999) synthesized peptides that undergo self-assembly on to surfaces rather than among themselves. These were known to form monolayers on surfaces to interact with specific biomolecules. Whitesides and his colleagues (1991) also developed peptide systems that consisted of a linker molecule for surface anchorage. More recently, peptides were anchored to gold surfaces via thiol interaction to form non-fouling self-assembled monolayers (Nowinski et al., 2012). In addition to these, peptides tethered to nanostructures such as quantum dots have been used as intracellular delivery vehicles. Thus, peptides or the bioconjugates tethered to surfaces have merely been used as monolayers or delivery vehicles. However, the inter-molecular self-assembly of those peptides or bioconjugates on surfaces has not been investigated to date.

Anodisc alumina membranes, because they are chemically inert and have uniform and small pore sizes (20 nm), were chosen to tether the self-assembling bioconjugate EL-5F-PEG-2K to the surface and study the effect of reversible self-assembly on the permeation properties of

the membrane. During the course of development of such stimuli responsive biomaterials or membranes, numerous strategies for the immobilisation of peptides or bioconjugates onto membranes or surfaces have also been developed. Particularly, the immobilisation of carboxylic acid (COOH) monolayers on different substrates has provided an effective route for surface modification. Carboxylic acids are useful candidates for enhancing chemical coupling of organic or biomolecules to native metals and metal oxide surfaces due to their accessibility, varying chain length and reactive functionality (Jadhav, 2011). Gold surfaces have been modified using fatty acids (Radu-Wu et al., 2009), hexanoic acids (Paik et al., 2003); silver has been modified using alkanoic acids, alkoxybenzoic acids (Tao et al., 2002); and stainless steel using alkanoic acids (Lim et al., 2007), palmitic acids, stearic acid (Shustak et al., 2004) to immobilise self-assembled monolayers of carboxylic acids. The modification of oxides of various metals such as zirconium, hafnium and indium has been carried out using alkanoic acids (Pawsey et al., 2000), stearic acid (Ting et al., 2009), and carboxy terminated thiols (Yan et al., 2000), respectively. A number of methods on the modification of alumina surface have been reported and include:

(i) Alkanoic (Aronoff et al., 1997) and stearic acid (Limet al., 2007) have been used to incorporate self-assembled monolayers of COOH groups on alumina surface.

(ii) The use of phosphonic acids involve a simple procedure in which the polar acidic phosphonate group interacts with diverse metal oxide surfaces such as Al_2O_3, Ta_2O_5 and ZrO_5. The degree of ordering of these films on the surfaces is comparable to that of alkyl thiol self-assembled monolayers on gold (Hahner et al., 2001). Octylphosphonic acid (Hauffman et al., 2008), alkane phosphate (Hahneret al., 2001), 3-hydroxyl-3-phosphono-butiric acid tert-butyl ester (Blajiev et al., 2008) are some of the phosphonates used for aluminium oxide modification.

In this study, 6–phosphonohexanoic acid (6-PHA) (Figure 5-1), one of the smallest phosphonic acid molecules available, was used.

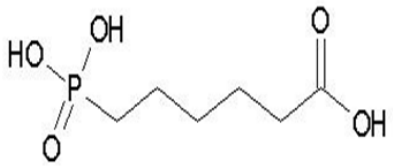

Figure 5-1: Chemical structure of 6-PHA.

(iii) Diazonium salts are widely used for surface modifications as coupling agents for conjugating biomolecules, polymers and nanoparticles to surfaces. The diazonium group activates nucleophilic aromatic substitutions and introduces functional groups such as OH, CN and COOH into the aromatic ring leading to the formation of diverse compounds (Mahouche-Chergui et al., 2011).

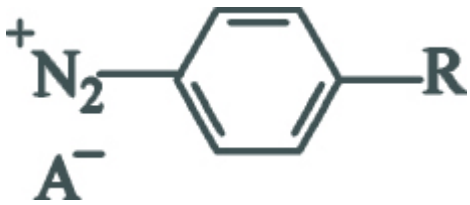

Figure 5-2: General chemical structure of aryl diazonium salts where R refers to range of substituents such as COOH, OH and NO_2 and A^- is the counter anion.

Aryl diazonium salts (Figure 5-2) are reduced electrochemically (Bernard et al., 2003) or using reducing agents (Simons et al., 2014) to radicals that bind with high affinity to a range of surfaces, which includes carbon, metallic and polymeric. This facilitates the immobilisation of the surface with a variety of

functional groups (R) such as alkyls (Bernardet al., 2003), halides, carboxylic acid groups and nitro groups (Allongue et al., 1997) (Figure 5-3).

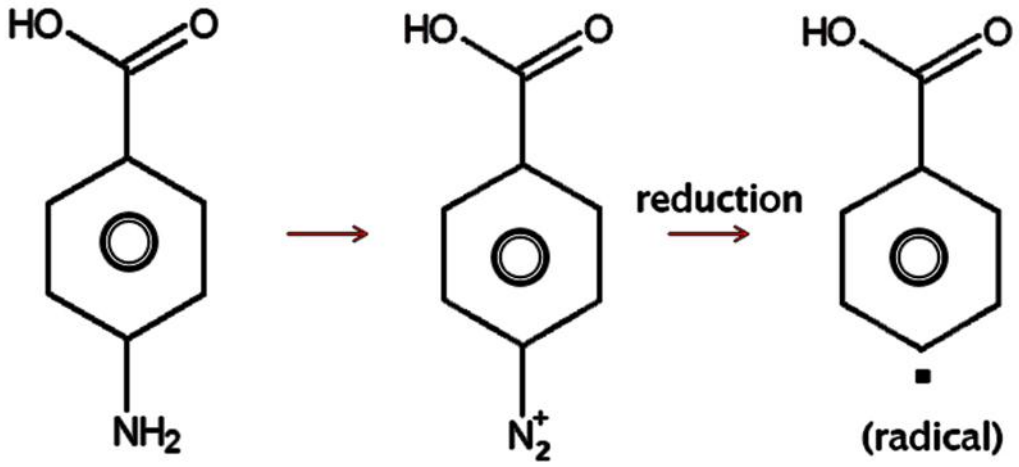

Figure 5-3: CBD reduction mechanism forming radical. Reduction is either done electrochemically or using reducing agents.

Although oxides such as iron oxide and/or titanium oxide have been modified using diazonium chemistry (Griffete et al., 2011), this method has not been employed for the modification of aluminium oxide surfaces. Thus, in this study, for the first time, attempts were made to test the interaction of CBD, nitro benzene diazonium (NBD) (Figure 5-4A) and carboxymethyl benzene diazonium (CMBD) (Figure 5-4B) molecules on an Anodisc alumina membrane surface.

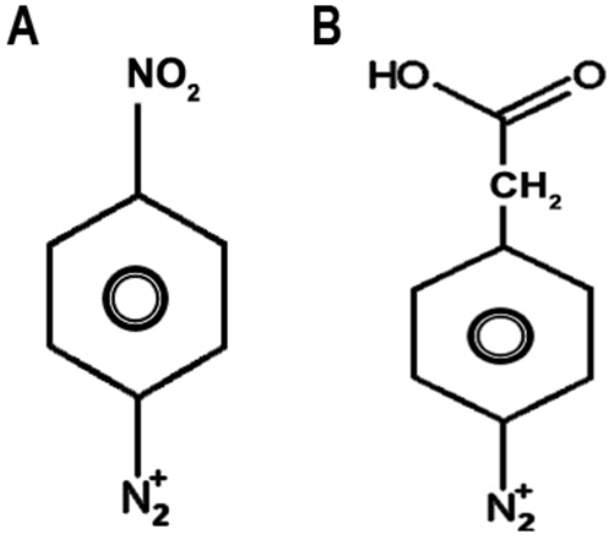

Figure 5-4: General chemical structure of A) NBD and B) CMBD salts.

(iv) Finally, the deposition of PEM's terminating with PAA (Figure 5-5) have also been used to provide free COOH groups on the alumina surface (Dai et al., 2006). Layer by layer deposition of alternating polyanion (PAA) and polycation (PAH) layers allows modification of porous membranes (Ai et al., 2003), which can be used for a range of applications, including protein microarray analyses because of their high surface area and possible ability to overcome mass transport limitations by flowing solutions through small pores (Hollman & Bhattacharyya, 2004). The initial polyanion layer adsorbs to the surface by electrostatic or hydrophobic interaction, thus, creating a charged surface or reversing the charge of the surface. The adsorption of subsequent polycation layer reverses the charge on the surface, aiding the adsorption of the subsequent layer (Schlenoff & Dubas, 2001). Earlier studies have shown that the presence of supporting electrolyte such as NaCl increases the thickness of the PEM's (Dubas & Schlenoff, 1999). Thus, in this study, upon the successful immobilisation of COOH groups on the surface,

EDC/NHS activation was performed to amine couple the peptide-PEG conjugate EL-5F-PEG-2K onto the surface.

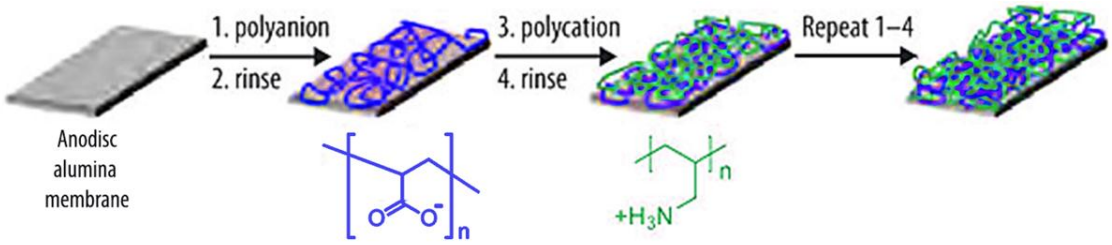

Figure 5-5: Schematic representation of layer-by-layer adsorption of deprotonated PAA and protonated PAH on the Anodisc surface.

To my knowledge, SAPs have not been tethered to membrane surfaces and the effect of self-assembly on the permeability of the membrane pores has also not been investigated. Herein, attempts were made to conjugate the reversible SAP-PEG conjugate EL-5F-PEG-2K to an Anodisc membrane surface using a number of surface modification strategies outlined above. Furthermore the influence of reversible self-assembly on the permeation properties of the membrane upon changes in pH was investigated. PEG-2K acts as a spacer between the peptide and surface, to provide sufficient conformational freedom for the peptides to self-assemble. Finally, the reversible, pH-dependent self-assembly of peptide EL-5F and the conjugate EL-5F-PEG-2K covalently tethered to the surface of NPs was demonstrated using DLS experiments. The results indicated that the self-assembly was between EL-5F/EL-5F-PEG-2K tethered to different particles. Although intra-particle self-assembly is also expected to occur, this will not be detected in the DLS experiments because the instrument cannot detect the small changes in dimension that would occur through molecular rearrangements on the surface.

5.2 EXPERIMENTAL SECTION

5.2.1 Materials The Anodisc alumina membrane (43-mm disks, 20 nm nominal pore size) and Nucleopore track-etched PC membrane (43-mm disks, 15 nm nominal pore size) were purchased from GE Healthcare Life Sciences. The EL-5F peptide was purchased from Genscript. Heterobifunctional PEG reagents N-tert-butoxycarbonyl (Boc)-protected-amino-PEG 2000-carbonate-N-hydroxy succinimide (NHS) was purchased from NOF Corporation. Carboxylated polystyrene nanoparticles (NPs) of mean diameter 118 nm was purchased from Izon (Oxford, U.K). All other chemicals were purchased from Sigma Aldrich.

5.2.2 Immobilisation of carboxylic acid (COOH) groups on the Anodisc membrane surface

The immobilisation of COOH groups on the Anodisc surface was carried out using the following three methods:

i) phosphonic acid chemistry,

ii) diazonium chemistry,

iii) PAA) / PAH multilayers.

5.2.2.1 Phosphonic acid chemistry

The Anodisc membrane was left immersed in 1 mM 6-PHA solution in water (pH 4) for 2 h at room temperature. It was then rinsed with water and vacuum dried for FTIR analysis. The same procedure was used for modification with hexyl phosphonic acid (HPA) and hexanoic acid (HA). The experiment was also performed using ethanol as the solvent.

Quantification of COOH groups on the Anodisc surface using sodium bicarbonate ($NaHCO_3$) vs HCl titration

The 6-PHA-modified membrane and an unmodified membrane (control) were immersed in 10 mL of 20 mM $NaHCO_3$ solution overnight. The $NaHCO_3$ solution of both the modified and control membranes was then titrated against 1 M HCl with methyl orange indicator.

5.2.2.2 Diazonium chemistry

CBD was immobilised on the Anodisc surface in basic and acidic conditions:

Basic condition

35.62 mg of CBD salt (50 mM) was added to the Anodisc membrane in a vial. 3 mL of 0.05 M $NaHCO_3$ buffer (pH 10) was added to it and left in orbital shaker for 1 h. After rinsing with water and ethanol twice, it was vacuum dried overnight. The control reaction was carried out in the absence of CBD salt.

Acid condition

59 mg of CBD or NBD salt (50 mM) was added to the Anodisc membrane in a vial. 5 mL of 0.6 M hypophosphoric acid was added and left in an orbital shaker for 1 h. After rinsing with water and ethanol twice, it was vacuum dried overnight. The control reaction was carried out in the absence of CBD salt.

CMBD was immobilised on the Anodisc surface using *in situ* and *ex situ* method.

In situ modification

Amino phenyl acetic acid was added to the Anodisc membrane. 20 mL of acetonitrile was added and sonicated until it dissolved completely. Tert-butyl nitrile was added and sonicated for an hour. The reaction mixture was decanted and the modified Anodisc was washed with acetone and milli-Q water. The control reaction was carried out in the absence of p-amino phenyl acetic acid.

CMBD _ex situ_ synthesis

4 mL of fluoroboric acid (25%) was added slowly with stirring to 5 mM of aryl amine in an ice bath. A cold solution 5 mM $NaNO_2$ dissolved in water was then added dropwise with stirring to the amine solution in the ice bath. The collected product was then recrystallised from acetonitrile and diethyl ether, dried and stored in a desiccator.

Ex situ modification

In contrast to *in situ* modification, here the synthesized CMBD powder was added directly to the Anodisc membrane. 15 mL of acetonitrile was added and sonicated until the CMBD dissolved completely. Ferrocene dissolved in 5 mL acetonitrile was added to the CMBD solution. This reaction mixture containing the Anodisc was sonicated for 15-20 min. When the bubbling stopped, the reaction was complete. The reaction mixture was decanted and the modified Anodisc was washed with acetone and milli-Q water. The control reaction was carried out in the absence of CMBD salt.

5.2.2.3 PAA / PAH multilayers

The Anodisc membranes were cleaned with a Bioforce Nanosciences UV cleaner (Ames, IA, USA) for 15 min. Polyelectrolyte deposition began with a 5-min immersion of the positively charged substrates into a solution containing 3.5 mM PAA and 0.5 M NaCl at pH 4.0 (pH was adjusted with 1 M NaOH or 1 M HCl). After rinsing with water for 1 min, the substrates were immersed in a 0.01 M PAH, 0.5 M NaCl solution (pH adjusted to 4.0) for 5 min and rinsed with water for 1 min. The procedure was repeated to allow the deposition of $[PAA/PAH]_3$ PAA films and then vacuum dried.

5.2.3 Amine coupling The COOH-modified Anodisc membrane was rinsed with sodium phosphate buffer pH 6 and immersed in a solution containing EDC/NHS (1:1) (0.1 M of each in sodium phosphate buffer pH 6) for 15 min. After activation, the membrane was rinsed with sodium phosphate buffer pH 8 and then immersed in EL-5F-PEG-2K conjugate or EDANS (*5-[(2-aminoethyl)amino]naphthalene-1-sulfonic acid*) fluorescent dye (in sodium phosphate buffer pH 8) solution for 2 hr. The membrane was rinsed with ethanolamine to deactivate the unreacted EDC/NHS esters. It was then rinsed with water for a min and vacuum dried. In case of EDANS dye, the stock solution was prepared in DMSO (1 mg/mL) and then diluted in sodium phosphate buffer (pH 8) for the coupling reaction.

5.2.4 Fluorescence microscopy Samples were examined using a Leica DM500B epifluorescence microscope (Wetzlar, Germany) through UV excitation. Pictures were captured using Leica DFC310 FX digital camera (Wetzlar, Germany) mounted on top of the microscope. The Anodisc membrane piece was placed on a glass slide with a drop of water and then analysed using the microscope.

5.2.5 Attenuated total reflectance - Fourier transform infrared spectroscopy (ATR-FTIR)

The ATR-FTIR spectra were recorded using a Bruker VERTEX-70 FTIR spectrometer (MA, U.S.A) equipped with a horizontal ATR accessory (Bruker, MA, U.S.A). The samples were mounted in a purged sample chamber in transmission geometry at normal incidence. All the spectra were acquired over 256 scans at a resolution of 4 cm^{-1} between 4000 and 630 cm^{-1} spectral region and three different measurements were obtained on the surface at random locations. A small steel plate was used to press the sample firmly against the detector. Background spectra were obtained by using only the steel plate mounted in the same geometry.

5.2.6 Contact angle measurement (CAM) Static CAMs were performed with a 1 µL droplet of water and $NaHCO_3$ buffer (pH 10) imaged 5-10 s after the drop was applied on bare and CBD-modified native aluminum oxide surfaces. Each computed contact angle was obtained by averaging six CAMs and repeating the procedure for a second droplet at a different spot on the surface. Hence, the quoted contact angle for a surface is an average of 12 measurements. The ImageJ open-source software package was used to process the images.

5.2.7 X-ray photoelectron spectroscopy (XPS) The XPS data were collected on a Kratos Axis $Ultra^{DLD}$ X-ray photoelectron spectrometer (Kratos Analytical, Manchester, UK) equipped with a hemispherical electron energy analyser. Spectra were excited using monochromatic Al K_α X-rays (1486.69 eV) with the X-ray source operating at 150W. This instrument illuminates a large area on the surface and then using hybrid magnetic and electrostatic lenses collects photoelectrons from a desired location on the surface. In this case, the analysis area was a 300 by 700 micron spot obtained using the hybrid magnetic and

electrostatic lens, and the slot aperture. Samples were secured to the sample bar using double-sided carbon tape. The measurements were carried out in normal emission geometry. A charge-neutralisation system was used to alleviate surface charge build-up, resulting in a shift of approximately 3eV to lower binding energy. During curve fitting the C 1s binding energy of the adventitious hydrocarbon on the surface was used to correct for this shift, with the saturated hydrocarbon peak set to 284.8 eV. Survey scans were collected with 160eV pass energy, whilst core level scans were collected with a pass energy of 20eV. The analysis chamber was at pressures in the 10^{-9} torr range throughout the data collection. Data analysis was performed using CasaXPS (www.casaXPS.com). Shirley backgrounds were used in the peak fitting. Quantification of survey scans used the relative sensitivity factors supplied with the instrument. Core level data were fitted using Gaussian-Lorentzian peaks (30% Lorentzian).

5.2.8 Atomic force microscopy (AFM) The AFM images were taken using a Digital Instruments Dimension 3100 instrument (Santa Barbara, CA, U.S.A) and Nanoscope IIIa controller (Veeco, New York, U.S.A). Silicon cantilevers (TAP300Al-G series, Budget Sensors, Innovative Solutions Bulgaria Ltd., Sofia, Bulgaria) with a fundamental resonance frequency of 200-400 kHz were used in tapping mode. Topographic images were obtained at a scan rate of 0.4 Hz with the parameters set point, amplitude, scan size and feedback control optimized for each sample. All images were processed using the Digital Instruments software.

5.2.9 Field emission scanning electron microscopy (FESEM) Surface structure and morphology analysis of the membrane samples were conducted using a field emission scanning electron microscope (Hitachi S-4700 FESEM, Tokyo, Japan). The samples were coated with platinum prior to the analysis using a Hitachi E-1030 Ion Sputter Coater. The measurements were performed at an accelerating voltage of 3 kV.

5.2.10 Flux test The flux of the modified and unmodified Anodisc membrane was determined through dead end filtration experiments conducted on AKTAexplorer™ 100 liquid chromatography system (GE Healthcare Life Sciences, Uppsala, Sweden). The AKTA system was used to pump the specified amount of buffer at a controlled rate through the membrane. The circular, unmodified Anodisc membrane of diameter 43 mm was placed in a polypropylene filter holder (GE Osmonics Labstore, Minnetonka, MN) and connected to the chromatography system. The flux test was carried out at pH 8 using 20 mM sodium phosphate buffer and pH 3 using 20 mM sodium acetate buffer. Initially, sodium acetate buffer (pH 3) was passed through the membrane at different flow rates. At each flow rate, the back pressure was noted and permeate was collected for a specific amount of time. Permeate was weighed and the temperature of the permeate was also measured to determine the exact density. With this data, the volumetric flow rate and flux were calculated. This was repeated thrice to obtain the mean flux at each back pressure. The same procedure was repeated for the modified membranes.

5.2.11 Molecular weight cut-off (MWCO) experiment MWCO experiments of the EL-5F-PEG-2K modified membrane was carried out using AKTAexplorer™ 100 liquid chromatography system. As PEG does not have UV absorbance, the permeate was passed

through a refractive index detector (RID) (Shimadzu Corporation, Kyoto, Japan) connected to the chromatography system. This was a dead end filtration experiment carried out at pH 8 using 20 mM sodium phosphate buffer and pH 3 using 20 mM sodium acetate buffer. Initially, a mixture of PEGs of molecular weight 72 and 29 kDa at a concentration of 2.5 mg/mL each was run through S200 10/300 GL size exclusion column (GE Healthcare Life Sciences) to obtain the elution profile. A similar amount of the same PEG mixture was passed through the modified membrane at pH 3. 50 mL of pH 8 buffer was then run through the membrane to remove the PEG retained on the surface. Following this, the PEG mixture at pH 8 was passed through the membrane. The permeate fractions were collected, lyophilized and reconstituted in the corresponding pH buffer (same amount as the feed sample). This was run through the S200 column and the elution profile of the permeate was compared with the elution profile of the feed.

5.2.12 Coupling of EL-5F / EL-5F-PEG-2K to NPs The stock solution of carboxylated NPs (conc. 10^{13}/mL) was diluted to a concentration of 5 x 10^{11}/mL in PBS (pH 7). 200 mM EDC/NHS was added to the diluted NPs and left to mix for 15 min at room temperature. 100 µL of EL-5F solution (in PBS) at a concentration of 2.6 mg/mL was added to the activated NPs and mixed for 2 h at room temperature. To remove the unreacted peptide and EDC/NHS from the mixture, a series of centrifugation (5 min, 9000 x g) with an Eppendorf MiniSpin Plus benchtop centrifuge and sonication (5 min) with a Digitec ultrasonic cleaner steps were carried out. The solution was centrifuged and the supernatant was carefully pipetted out. The sedimented NPs were resuspended in PBS and sonicated. This was again centrifuged and supernatant separated out. The supernatant collected each time was analysed using Nanodrop. Similar procedure was followed to couple EL-5F-PEG-2K to the NPs. The control sample had 100 µL of 1 M ethanolamine hydrochloride added to the EDC/NHS activated NPs to convert active NHS ester into an inactive hydroxethyl amide.

5.2.13 DLS DLS measurements were recorded on a Malvern Zetasizer Nano ZS (Worcestershire, UK). The pH of each sample was adjusted in an Eppendorf tube by dropwise addition of 1 M HCl or NaOH, with thorough mixing, and the tube then sonicated (5 min). The solution was then removed by pipette and placed into a 12 mm square polystyrene cuvette for DLS measurement. Spectra were obtained as an average of three consecutive measurements. Samples were removed from the cuvette by pipette and returned to the Eppendorf tube for subsequent pH adjustment and the above process repeated.

5.2.14 Transmission electron microscopy (TEM) Solutions of native and EL-5F/EL-5F-PEG-2K/ ethanolamine coupled NPs at pH 3 and 7 were used for sample preparation. 20 µL of the samples was deposited for 1 min on carbon-coated Formvar 200-mesh copper grids, and then washed twice with water. Negative staining of the samples was achieved by placing the grids wet-side down on top of 20 µL of 1% w/w uranyl acetate solution in water for 1 min. Filter paper was used to remove excess liquid from the grids by blotting, and the grids were then left to dry for several hours before TEM observations.

5.3 RESULTS AND DISCUSSION

5.3.1 COOH groups immobilisation on the Anodisc surface

5.3.1.1 Phosphonic acid chemistry

i) Quantification of COOH groups on the Anodisc surface using $NaHCO_3$ vs HCl titration

Initially, the use of phosphonic acid chemistry (e.g., 6-PHA) to modify the Anodisc alumina membrane for the conjugation of EL-5F-PEG-2K was investigated. 6-PHA was used for the modification due to the presence of phosphonate group at one end, having high affinity towards the alumina surface and COOH group at the other end that could be coupled to EL-5F-PEG-2K (Figure 5-1). To confirm the immobilization of COOH groups and also quantify the amount of COOH groups on the surface, the Anodisc sample modified with 6-PHA was analysed using acid-base titration (see Section 5.2.2.1). With 10 mL $NaHCO_3$ containing only about 0.2 mM salt concentrations, it was expected that even partial modification of the membrane surface (e.g., 20% modified membrane) using 6-PHA (1 mM), would bring about an appreciable change in $NaHCO_3$ concentration during titration. However, it was observed that the concentration of $NaHCO_3$ solution (20 mM) in both unmodified and modified samples remained unchanged. This suggested that the membrane surface remained unmodified or the modification did not present enough COOH groups on the surface to be quantified using such titration methods. Thus, the modified surface was analysed using FTIR.

ii) Surface characterization using ATR-FTIR

Subsequently, the surface of the 6-PHA modified membrane was analyzed using FTIR but it was observed that the FTIR spectra for the modified and unmodified membrane samples were identical. Thus, to verify the binding of COOH group to the membrane surface, the Anodisc

was modified using 6-PHA (phosphonate and COOH groups), HPA (phosphonate groups only) and HA (COOH groups only). The modification was carried out both in water and ethanol. However, FTIR analysis still suggested identical spectra for both the control and modified samples (Figure 5-6). Also, no bands corresponding to COOH groups were detected. However, the reason for this failure in membrane modification remained unclear.

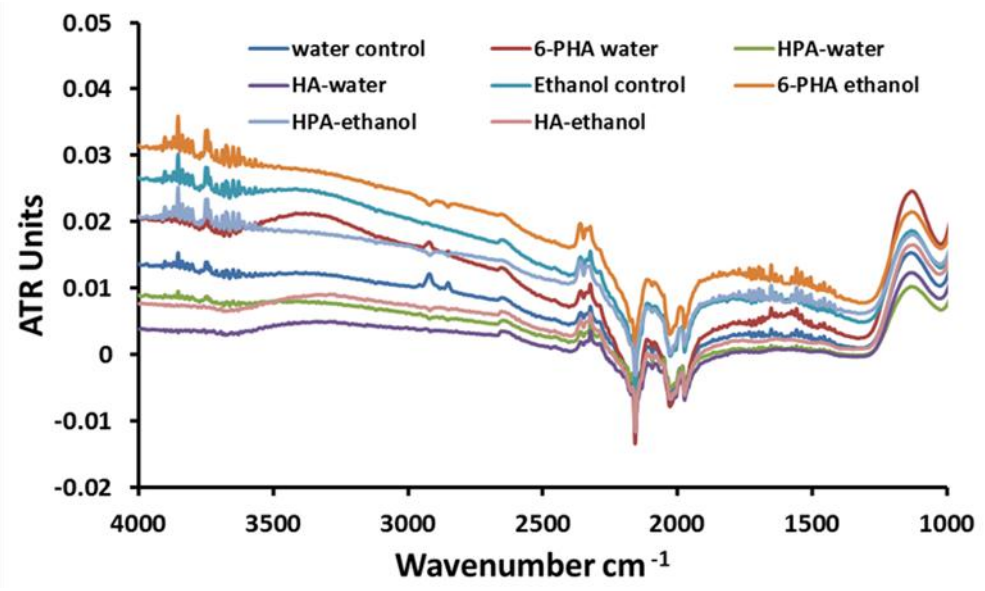

Figure 5-6: FTIR spectra of 6-PHA, HPA and HA modified Anodisc surface in water and ethanol.

5.3.1.2 Diazonium chemistry

i) Surface characterization of CBD/NBD immobilised Anodisc surface using ATR - FTIR

As an alternative approach, the membrane was modified using diazonium chemistry. The CBD-modified Anodisc surface was investigated using FTIR. In the past, diazonium chemistry has been used to modify metal oxides, although not aluminium oxide at high pH (Griffeteet al., 2011). The CBD modification of the Anodisc alumina membrane was carried

out under basic conditions in $NaHCO_3$ buffer (pH 10). It was observed that the FTIR spectra for the modified and unmodified membrane samples were identical (Figure 5-7).

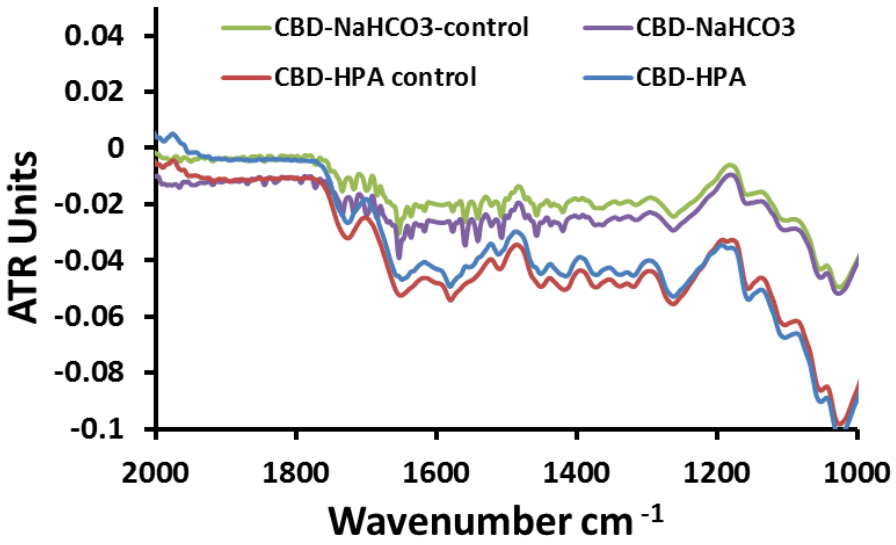

Figure 5-7: FTIR spectra of the CBD-modified Anodisc surface in basic and acidic conditions.

Simons et al. (2014) suggested the use of reducing agents such as hypophosphoric acid for diazonium modification of non-conducting substrates due to their spontaneous reaction mechanism. Thus, CBD modification was also carried out under acidic conditions using hypophosphoric acid as the reducing agent. However, the results were similar to that of the previous experiment (Figure 5-7). It was unclear as to whether the diazonium modification reaction did not occur to completion or the COOH groups were not being detected by FTIR. To clarify this, a diazonium molecule with a different substituent, NBD salt was immobilised on the Anodisc surface using the same procedure under acidic conditions. It was predicted that the presence of corresponding NO_2 bands on the FTIR spectra, could possibly indicate the reaction between the diazonium radical and the alumina surface. However, the results

suggested no differences between the spectra of the control, CBD- and NBD-modified samples (Figure 5-8).

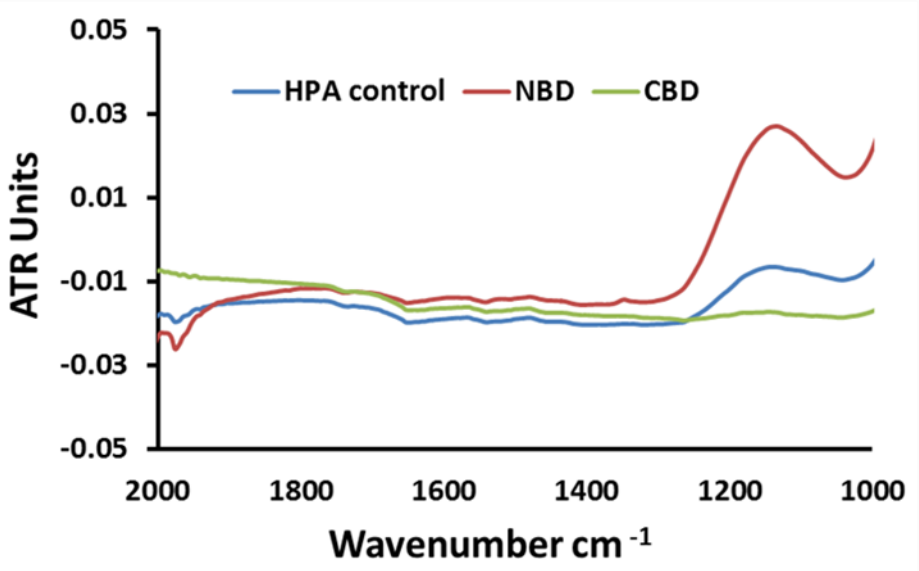

Figure 5-8: FTIR spectra of CBD- and NBD- modified Anodisc surface using hypophosphoric acid as the reducing agent.

Similar results were observed even in the case of powdered Anodisc samples. The modification method was expected to immobilise diazonium molecules only on the surface of the alumina membrane. Therefore, it was predicted that powdering the sample might result in the dominance of unmodified bulk membrane over the modified or sparsely modified membrane surface, which eventually resulted in COOH or NO_2 groups remaining undetected by FTIR. To overcome this, diazonium modification was carried out on powdered Anodisc samples. Powdering the sample prior to the diazonium reaction will result in an increase in surface area, thereby quantitatively increasing the reaction of diazonium molecules on the Anodisc surface. Identical spectra were observed for both the control and CBD-modified sample. However, the NBD-modified sample contained two new bands corresponding to

symmetric and asymmetric stretches of the nitro group at 1348 and 1523 cm^{-1}, respectively (Figure 5-9). This indicated a possible reaction between NBD and the alumina surface. Similar observations were reported by Andrieux et al. (2003), who suggested that radical formation by NBD is easier than with CBD i.e. the nitro substituent is more favourable for radical formation than the carboxylate. In the case of CBD, it was predicted that the competitive binding of COOH and diazonium radical could possibly result in undetected COOH groups in FTIR.

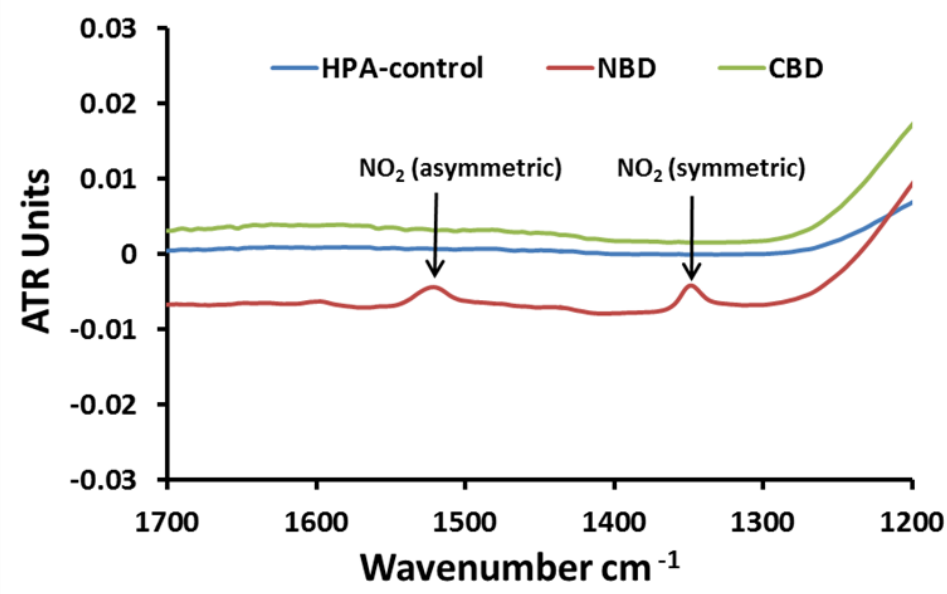

Figure 5-9: FTIR spectra of powdered CBD- and NBD-modified Anodisc membrane using hypophosphoric acid as the reducing agent.

ii) Surface characterization of CBD immobilised native aluminium oxide surface using FTIR and CAMs

To further investigate the reaction of CBD with alumina, the modification procedure was carried out on a native aluminium oxide surface. FTIR spectra suggested similar observations to that observed in the case of the Anodisc membrane. However, CAMs indicated the presence of COOH groups on the surface. Figure 5-10 shows the CAMs of the bare, control and the CBD-modified native alumina surface. The contact angles did not vary much for the bare and control alumina surfaces with water and pH 10 buffer. However, it can be observed that the contact angle markedly decreased by around 50% for the CBD-modified sample at pH 10. This indicates that the surface was more hydrophilic at pH 10 due to the deprotonation of COOH groups on the surface, which in turn made it more polar (Figure 5-11). The conjugate EL-5-PEG-2K was amine-coupled to this surface. However, the FTIR spectra did not contain amide peaks and CAMs were similar to the CBD-modified sample. Therefore, it can be concluded that CBD reaction immobilises COOH groups on the native alumina surface whilst these groups remained unreactive to EDC/NHS activation and subsequent amine coupling of EL-5F-PEG-2K. This may have been due to the orientation of the COOH groups on the surface making it difficult for further reaction to take place.

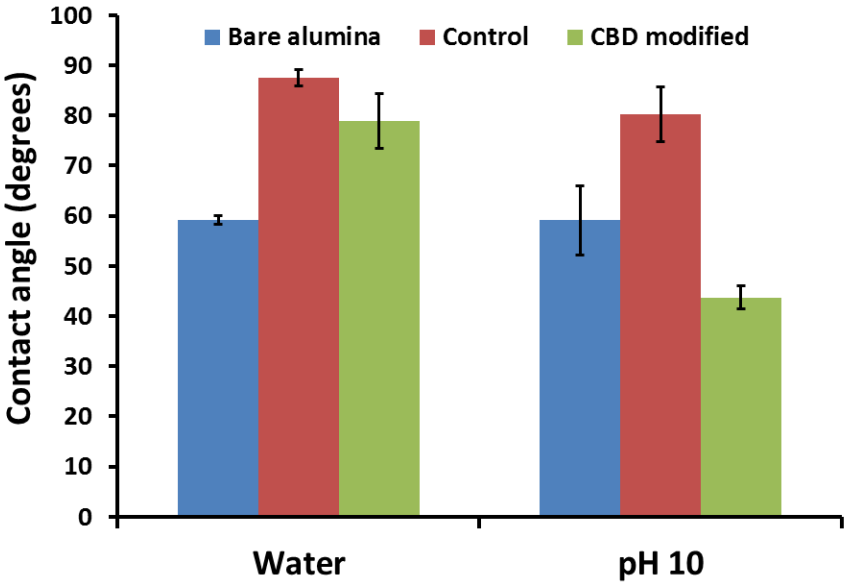

Figure 5-10: CAMs of bare, control and CBD-modified native alumina surface using water and pH 10 buffer.

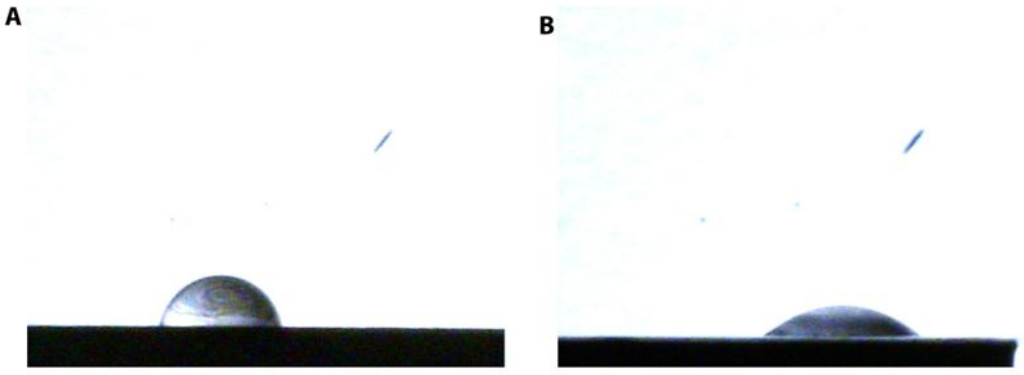

Figure 5-11: CAM images of A) water and B) pH 10 buffer droplet on CBD-modified native alumina surface.

ii) Surface characterization of CBD/NBD-immobilised PC membrane surfaces using ATR-FTIR

In addition to the Anodisc membrane surface, a PC membrane was also subjected to diazonium modification using the same procedure with hypophosphoric acid as the reducing agent. The FTIR spectra showed that there was no difference between the control and the CBD-modified sample, whereas the NBD-modified sample had a prominent peak at 1346 cm^{-1} and a shouldered peak at 1520 cm^{-1} due to symmetric and asymmetric stretches, respectively, of the nitro group (Figure 5-12). This indicates that NBD reacted with the PC surface whereas the CBD molecule did not. As in the case of Anodisc sample, the nitro group is more favourable to radical formation than the carboxylate substituent. Due to these experimental difficulties in immobilising COOH groups on to the surface of PC membrane, further work was done only with the Anodisc membranes.

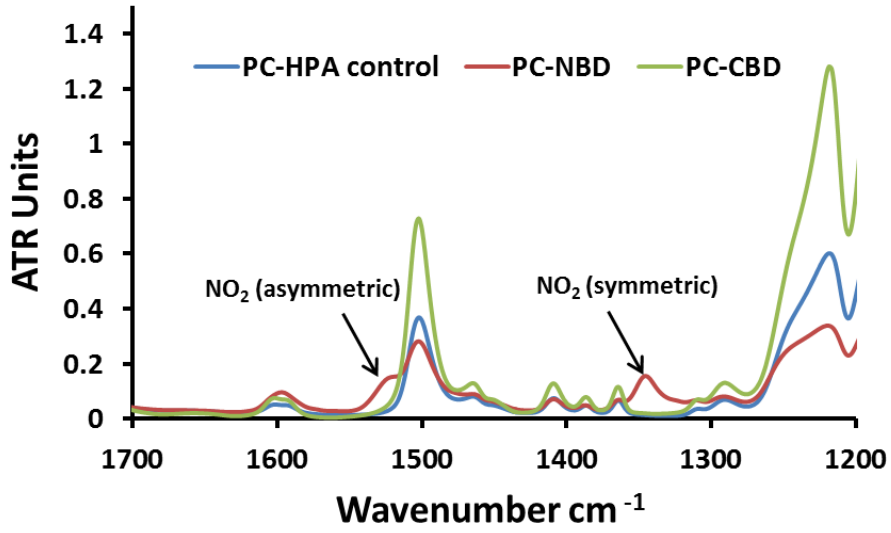

Figure 5-12: FTIR spectra of control, NBD- and CBD-modified PC membrane surfaces using hypophosphoric acid as the reducing agent.

iv) Surface characterization of CMBD immobilised Anodisc surface using ATR - FTIR

As an alternative to CBD-based modification, further investigations on the modification of the Anodisc membrane was carried out using CMBD. The presence of methyl group substituent was expected to favour reduction of diazonium to radicals more than the COOH substituent in the case of CBD and the possibility of amine coupling a molecule to the COOH group in CMBD is rather higher than in CBD. CMBD modifications were carried out using *ex situ* and *in situ* approaches. In the *ex situ* method, previously synthesized CMBD salt was directly added to the reaction mixture and allowed to interact with the Anodisc surface, whereas in the *in situ* approach, the starting material, p-amino phenyl acetic acid, was added to the reaction, which then converted to CMBD salt and modified the Anodisc surface. The EL-5F-PEG-2K conjugate was amine-coupled to the COOH groups on these CMBD-modified Anodisc samples (see Section 5.2.3). The FTIR spectra of CMBD *ex situ* control and modified samples were quite similar (Figure 5-13). There was no clear indication of peaks corresponding to COOH groups in the modified sample. Further, the EL-5F-PEG-2K conjugated samples also resulted in identical spectra, with no additional bands. On the other hand, the CMBD *in situ* modified sample had a broad peak at 1710 cm^{-1} attributed to the acid carbonyl stretch and two other prominent peaks at 1602 cm^{-1} and 1514 cm^{-1} corresponding to benzene rings (Figure 5-13). The membrane appeared coloured due to azo linkages between the aromatic rings on the surface (Figure 5-14). Thus, further experiments on membrane modifications were carried out using the *in situ* approach. Although these results indicated the existence of COOH groups on the *in situ* modified surface, the absence of any new bands in the spectra of EL-5F-PEG-2K coupled sample suggested that the immobilised COOH groups remained unreactive or

that the orientation of COOH groups on the surface did not facilitate the conjugation of EL-5F-PEG-2K.

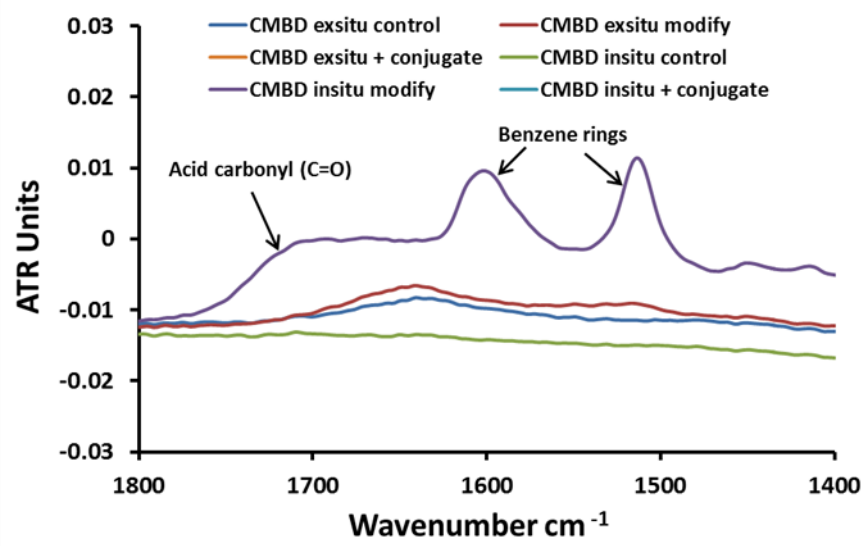

Figure 5-13: FTIR spectra of CMBD ex situ and in situ modified Anodisc surface. Each method had a control sample, only CMBD immobilised sample and conjugate coupled sample.

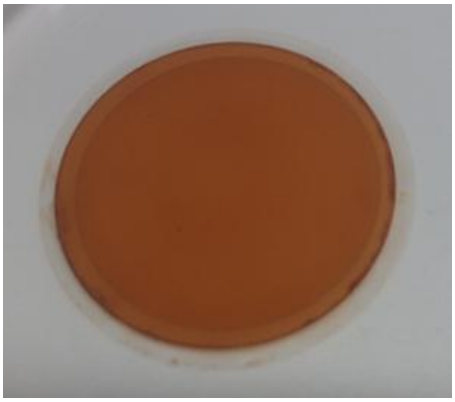

Figure 5-14: The Anodisc membrane appearing coloured due to azo linkages after CMBD in situ diazonium modification.

v) Surface characterization of CBD/CMBD immobilised Anodisc/carbon surface using fluorescence microscopy

To verify the presence of COOH groups on the Anodisc surface, EDANS (*5-[(2-aminoethyl) amino]naphthalene-1-sulfonic acid*) fluorescent dye was amine-coupled to the surface under different conditions and analyzed using fluorescence microscopy (see Section 5.2.4). EDANS dye contains only one primary amine, which can possibly bind to the activated COOH groups on the surface (Figure 5-15).

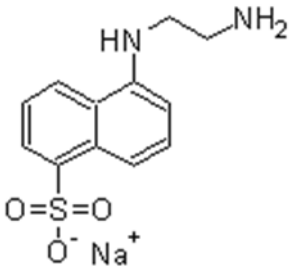

Figure 5-15: Chemical structure of EDANS (5-[(2-aminoethyl)amino]naphthalene-1-sulfonic acid) fluorescent dye.

Experiments were carried out with slight modifications in CBD and CMBD immobilisation procedures and also the amine coupling procedure. Initially, EDANS dye was amine-coupled to the CBD- and CMBD-modified surfaces (see Section 5.2.3). No fluorescence was observed in the EDANS dye-coupled CBD surface (Figure 5-16B) whereas nonspecific adsorption existed in the control sample where the dye was added to the surface without EDC/NHS activation (Figure 5-16A). In case of the CMBD-modified sample, fluorescence spots appeared distributed, whilst no fluorescence (Figure 5-16C) was observed in the control samples. This indicates that (Figure 5-16D) the EDANS dye could possibly be amine-coupled

to the COOH groups and thus, further experiments were carried out using CMBD-modified samples. As the EDANS dye stock was prepared in DMSO, the entire amine coupling reaction was carried out in DMSO without using sodium phosphate (pH 8) buffer, to investigate its effect on amine coupling. However, hazy fluorescence spots were observed in patches across the surface (Figure 5-16F) whilst no fluorescence was observed in the control samples (Figure 5-16E). Thus, the sample was soaked for longer periods during the CMBD modification procedure and subsequently the EDANS dye was amine-coupled. However, similar fluorescence patterns, with hazy patches, were observed. Although indicative of a possible amine coupling, the results were unclear with regard to confirming the presence of COOH groups on the membrane surface. In the past, diazonium modification of carbon surfaces has been achieved successfully. Therefore, it was decided to modify a carbon surface with CMBD and amine-couple EDANS dye to the COOH groups. Amine coupling was carried out in sodium phosphate buffer (pH 8) and DMSO. The control sample contained EDANS dye without EDC/NHS activation. The control sample contained no fluorescence spots (Figure 5-16G), while the amine-coupled samples resulted in a few randomly distributed fluorescence spots (Figure 5-16H and I). Thus, these results do not appear to be conclusive proof of COOH modification of the membrane and/or carbon surface.

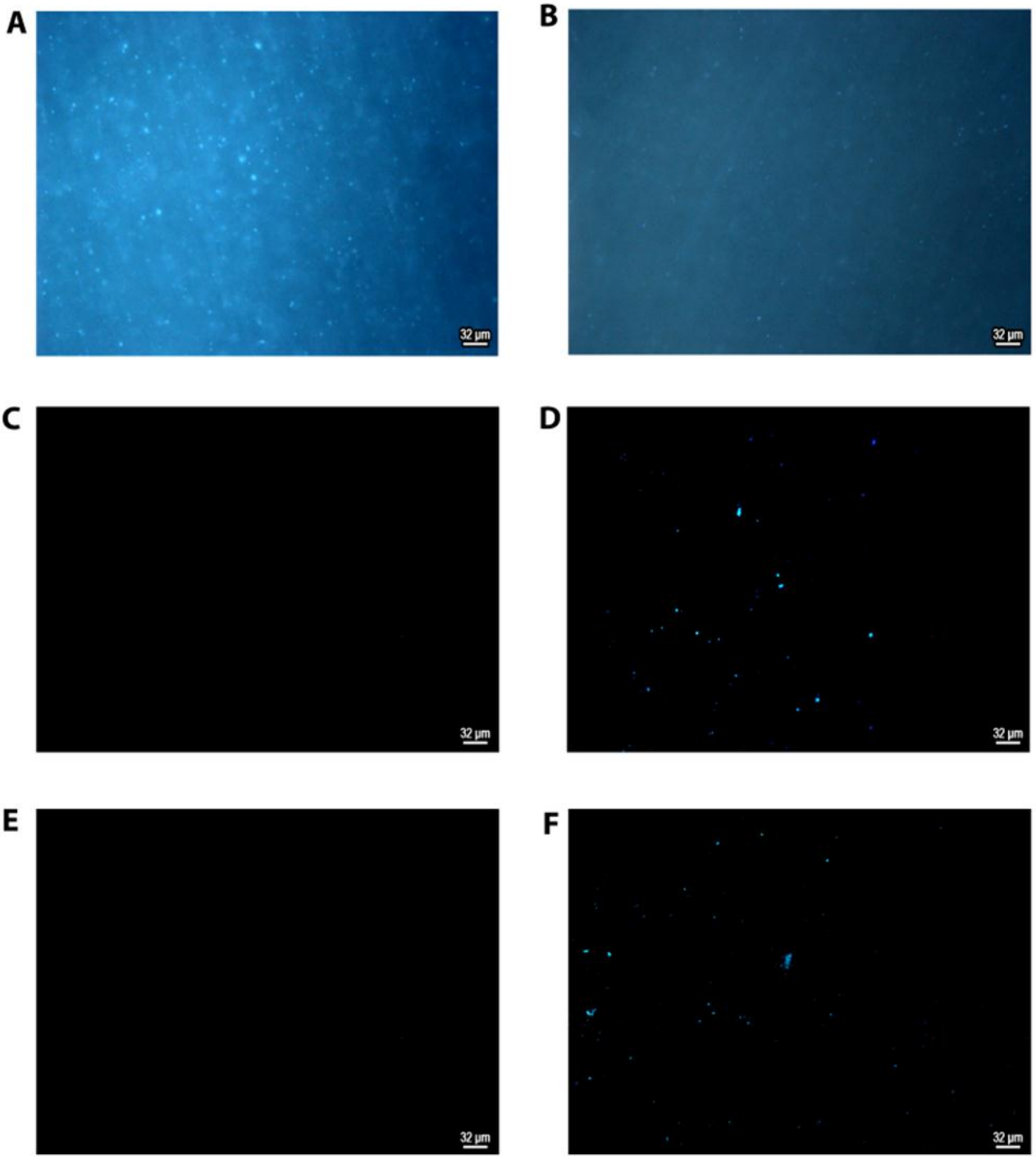
A
32 µm
B
32 µm
C
32 µm
D
32 µm
E
32 µm
F
32 µm

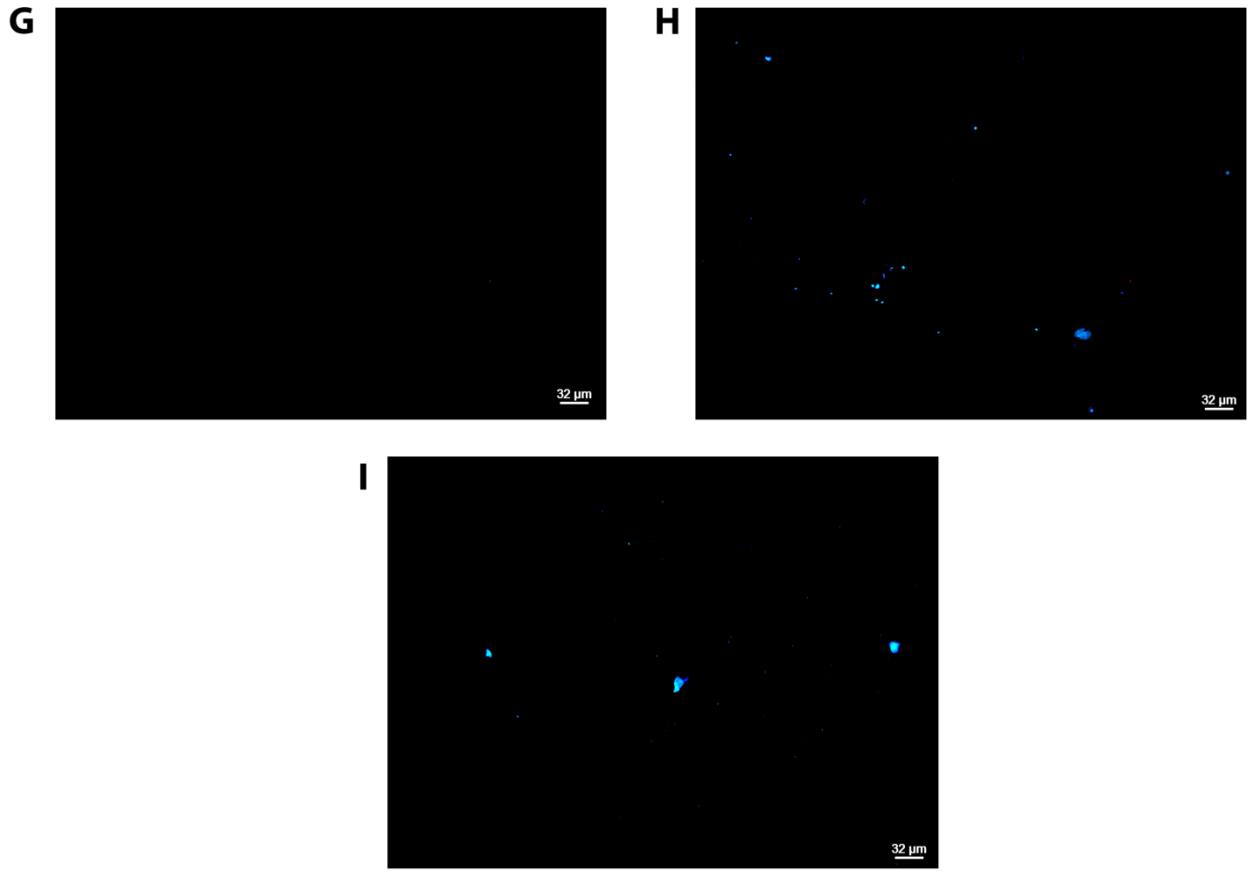

Figure 5-16: Fluorescence microscopy images of EDANS dye coupled Anodisc surface modified using A) CBD control. B) CBD, C) CMBD control, D) CMBD, E) CMBD (DMSO) control, F) CMBD (DMSO). Fluorescence microscopy images of EDANS dye coupled carbon surface modified using G) CMBD control, H) CMBD (DMSO), I) CMBD (sodium phosphate).

vi) Surface characterization of the Anodisc surface using XPS

To further investigate the immobilisation of COOH groups and amine coupling of EL-5F-PEG-2K, the elemental composition of the modified and unmodified Anodisc surfaces were analysed using XPS. In wide-scan XPS measurements, signals arising from aluminium, carbon, oxygen and nitrogen were discerned. The following four different samples were analysed, A) Anodisc blank, B) Anodisc-CMBD modified, C) Anodisc-CMBD + EL-5F-PEG-2K coupled (control), D) Anodisc-CMBD + EL-5F-PEG-2K coupled (Figure 5-17).

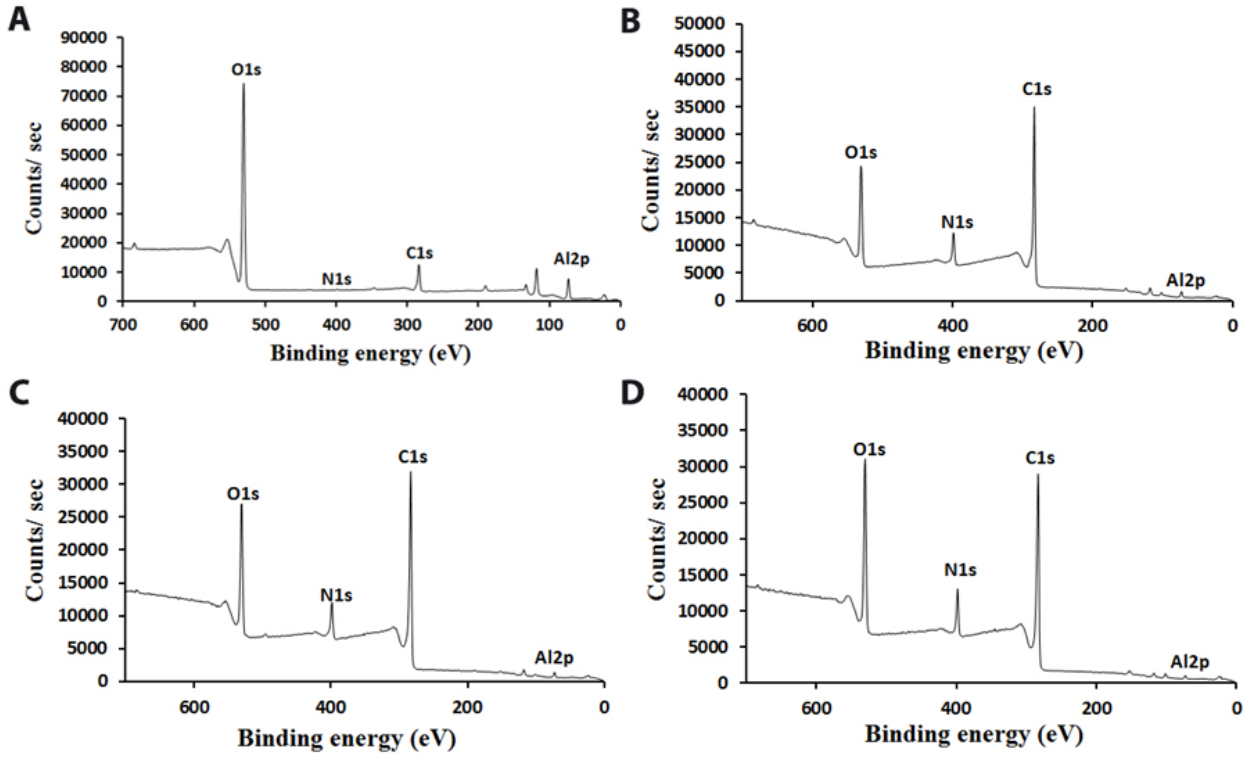

Figure 5-17: Wide scan XPS spectrum of A) Anodisc blank, B) Anodisc–CMBD modified, C) Anodisc–CMBD + EL-5F-PEG-2K coupled (control), iv) Anodisc–CMBD + EL-5F-PEG-2K coupled.

Table 5-1: Atomic concentration (in %) of C1s, N1s, O1s, Al2p on the blank and modified Anodisc surfaces.

Elements	Anodisc Blank	CMBD modified	EL-5F-PEG-2K (control)	EL-5F-PEG-2K coupled
C1s	19.7	73.0	73.2	71.6
N1s	0.2	8.0	7.6	7.6
O1s	45.4	14.3	16.0	18.7
Al2p	26.5	4.3	3.2	1.9
C1s/Al2p	0.7	17.0	22.9	37.3
N1s/Al2p	0.0	1.8	2.4	4.0

Table 5-1 shows the elemental composition (in %) of the modified and blank Anodisc surfaces. It was observed that the C1s composition increased by around 4 fold and Al2p decreased by 6 fold for the CMBD-modified samples compared with the blank. This ratio of C1s/Al2p indicates the successful CMBD modification of the Anodisc membrane surface. Coupling of the conjugate EL-5F-PEG-2K to the COOH groups on the surface further increased the ratio C1s/Al2p by more than 2 times and the N1s/Al2p ratio 2 times, indicating the presence of amine-coupled EL-5F-PEG-2K on the surface. Control experiments were performed by coupling EL-5F-PEG-2K without EDC/NHS activation to verify physical absorption on the surface. Although the control samples suggested an increased C1s/Al2p and N1s/Al2p ratio compared with the CMBD-modified sample, this increase was less significant compared with the EL-5F-PEG-2K amine-coupled sample. Therefore, the survey scan measurements indicate the presence of amine-coupled EL-5F-PEG-2K on the CMBD-modified surface.

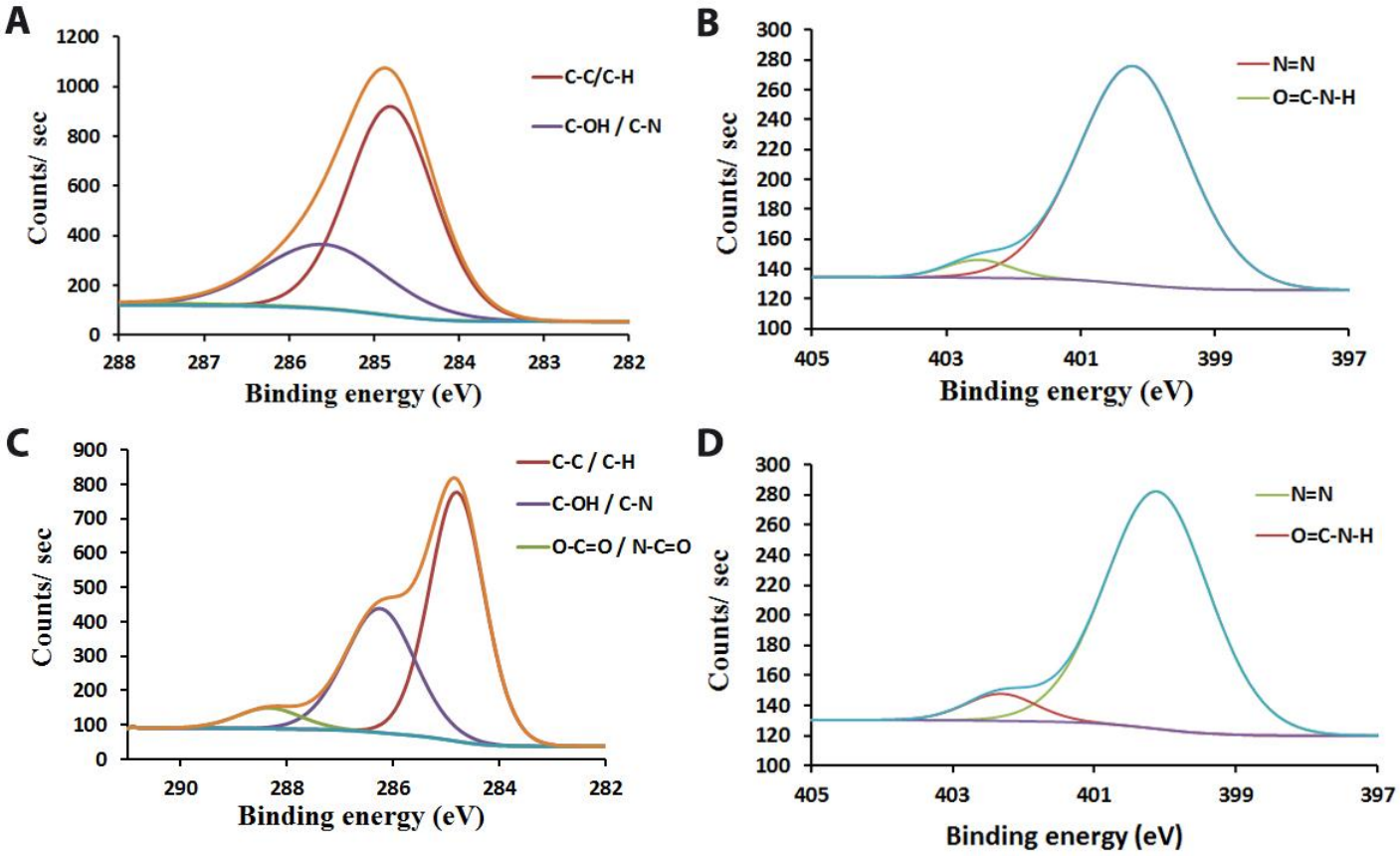

Figure 5-18: Deconvolution of the C1s carbon and N1s nitrogen XPS peaks of Anodisc surface modified with CMBD only (A and B) and CMBD + EL-5F-PEG-2K coupled (C and D) respectively.

To determine the mode of binding of different molecules to the surface, chemical state scans for carbon, nitrogen and oxygen were performed. The deconvoluted C1s and N1s XPS peaks of the Anodisc CMBD-modified (Figure 5-18A and B) and the Anodisc EL-5F-PEG-2K amine-coupled (Figure 5-18C and D) samples were compared. The C1s peak was fitted with three separate components, representing three different chemical environments. Those include carbon atoms in: alkane chains (C-C/C-H), alcohol/ester/ether (C-OH/C-N/C-O-C) groups and acid (0-C=O/N-C=O) groups. All carbon peaks were represented by a mixture of Gaussian (70%) and Lorentzian (30%) shapes. The binding energy of the main carbon component (C-C /C-H) was fixed at 284.8 eV. C-OH /C-O-C was fixed 1.5 eV higher and 0-

C=O/N-C=O was fixed 4.5 eV higher than the main peak. Full widths at half maximum (FWHM) were constrained between 0.2 and 5.

The N1s peak consisted of contributions from the nitrogen atoms in azo linkages (N=N) and peptide bonds (O=C-N-H). FWHM were constrained between 0.2 and 5. All nitrogen peaks were represented by a mixture of Gaussian (70%) and Lorentzian (30%) shapes. Any fitting parameters not mentioned above were free during the minimization procedure.

Table 5-2: Area (%) under the deconvoluted XPS peaks of C1s carbon and N1s nitrogen of the Anodisc CMBD-modified and EL-5F-PEG-2K-coupled samples.

C1s components		CMBD modified	EL-5F-PEG-2K coupled
C1s a	C-C / C-H	66.3	57.9
C1s b	C-OH / C-N	29.6	36.6
C1s c	O-C=O / N-C=O	4.1	5.6
N1s components			
N1s a	N=N	95.3	92.7
N1s b	O=C-N-H	4.7	7.3

It can be observed that the peak area % of C1s c increased by a small amount after EL-5F-PEG-2K coupling, which might be indicative of amide bonds formed between the COOH groups and EL-5F-PEG-2K on the surface (Table 5-2). The increase in peak area % of N1s b further substantiates the formation of amide bonds. However, the changes in peak area % values are not significant; therefore they may have been caused by experimental variations between samples.

Despite the wide scan measurements suggesting the successful coupling of EL-5F-PEG-2K to the COOH groups, inconclusive chemical state scan results suggested the need for further investigations. Thus, a flux test on the modified membrane was carried out under the assumption that EL-5F-PEG-2K was coupled to the COOH groups on the surface. If pH-

switching was subsequently observed, this would give circumstantial evidence that the conjugated peptide was present on the surface.

vii) Determination of flux of CMBD-modified and EL-5F-PEG-2K-coupled Anodisc membranes at pH 3 and 8

The fluxes of the Anodisc CMBD-modified and EL-5F-PEG-2K coupled membranes over a range of back pressures were determined at pH 3 and 8 using dead end filtration experiments (see Section 5.2.10). It can be observed that the flux of the Anodisc CMBD-modified membrane (control) did not change with pH. EL-5F-PEG-2K was amine-coupled to the COOH groups on the surface of the CMBD-modified membrane (Figure 5-19). It was predicted that the membrane coupled EL-5F-PEG-2K would self-assemble at pH 3, increasing the resistance to the flow through the membrane, thereby decreasing the flux, while at high pH, disassembly of EL-5F-PEG-2K should decrease the resistance to flow. However, it was observed that the flux of this membrane remained the same at both the pH values, and was similar to that of the control membrane. This could be due to the following reasons: (i) The surface-coupled EL-5F-PEG-2K becomes unresponsive to pH and does not self-assemble as it does in solution, (ii) There were only very small number of EL-5F-PEG-2K molecules coupled to the surface, lower than the critical concentration of the conjugate needed for self-assembly, (iii) There was no EL-5F-PEG-2K chemically coupled to the membrane surface. Due to the uncertainities relating to both the immobilisation of COOH groups using diazonium chemistry and the amine coupling of EL-5F-PEG-2K, a different method using layer-by-layer deposition of polyelectrolytes to immobilise COOH groups on the Anodisc surface was carried out.

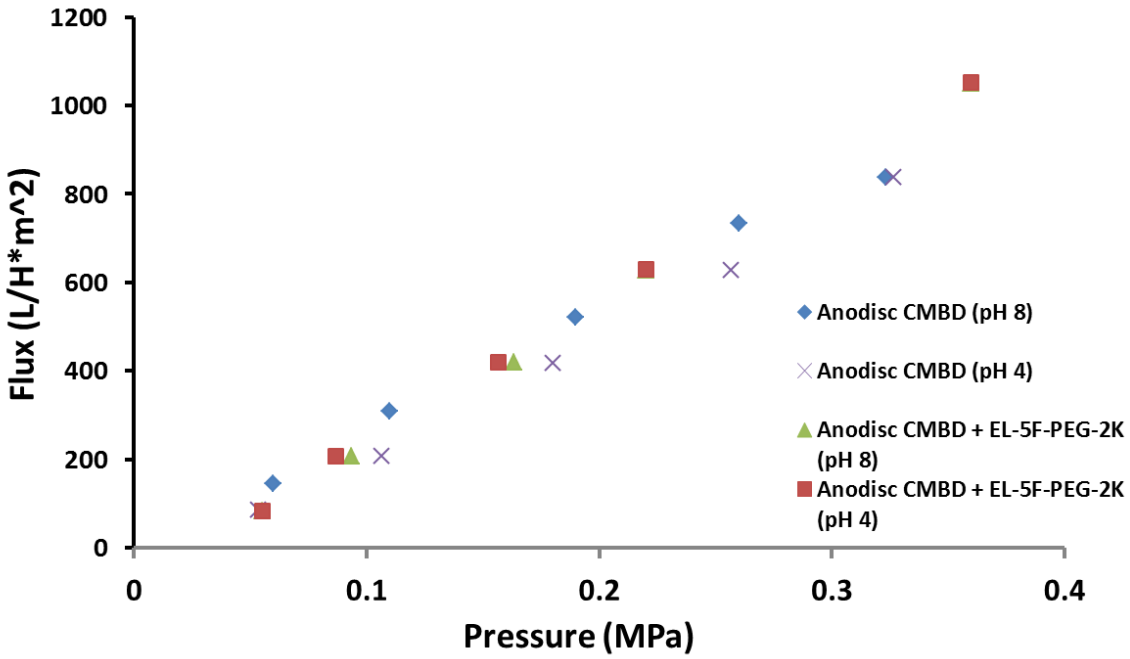

Figure 5-19: Flux data over a range of back pressures of the Anodisc modified using CMBD and CMBD + EL-5F-PEG-2K coupled at pH 3 and 8.

5.3.1.3 PEM adsorption

i) Surface characterization of PAA/PAH-modified and EL-5F-PEG-2K coupled Anodisc surfaces using ATR-FTIR

The Anodisc membrane was alternatively exposed to PAA (polyanion) and PAH (polycation) solutions, with rinsing with water to remove unadsorbed polymer after each deposition step (see Section 5.2.2.3). After $[PAA/PAH]_3PAA$, the layer-by-layer deposition of complementary polymers resulted in free COOH groups on the surface. This $[PAA/PAH]_3$ PAA immobilised surface was characterized using ATR-FTIR. Figure 5-20 shows that the PAA/PAH-modified sample has a peak at 1705 cm^{-1}, corresponding to acid carbonyl stretch. After amine coupling of EL-5F-PEG-2K to the surface COOH groups, this acid carbonyl

peak disappeared and an amide I absorbance band at 1642 cm^{-1} (C=O) appeared. This peak at 1642 cm^{-1} was not present in the previous sample. Generally, conjugation moves absorption to lower wavenumbers. The amide II (N-H) band at 1550 cm^{-1} overlaps with the carboxylate stretch. But, it is clearly evident that the intensity at 1550 cm^{-1} is higher in EL-5F-PEG-2K coupled sample than the PAA/PAH-modified sample. Therefore, the appearance of amide I and amide II absorbance peaks and the disappearance of the acid carbonyl stretch confirmed the amine coupling of EL-5F-PEG-2K to the COOH groups on the PAA/PAH modified membrane.

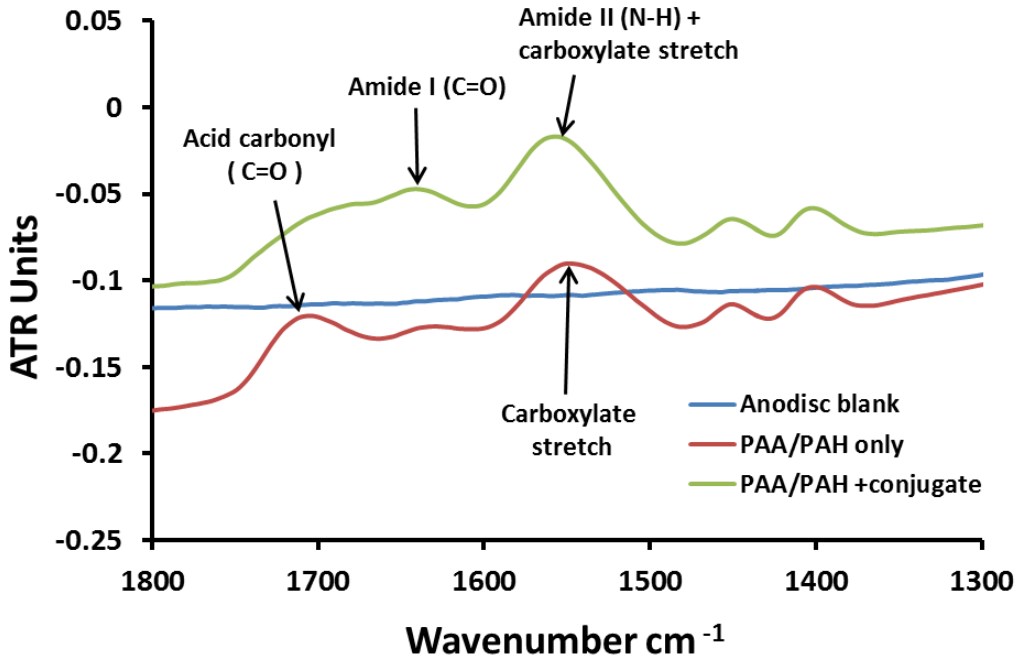

Figure 5-20: FTIR spectra of blank, PAA/PAH modified and PAA/PAH modified + EL-5F-PEG-2K coupled Anodisc surface.

An additional study was done to determine the effect of varying the number of layers in PAA/PAH deposition on the concentration of COOH groups on the surface (Figure 5-21).

Although FTIR spectra are unreliable for quantification purposes, this was done assuming that the intensity is directly proportional to the concentration of molecules immobilised on the surface. It can be observed that the intensity of the peak due to acid carbonyl stretch at 1705 cm^{-1} did not vary much with one or two layers of PAA but increased significantly for $[PAA/PAH]_2$ PAA and $[PAA/PAH]_3$ PAA. The peak intensity corresponding to the carboxylate stretch at 1550 cm^{-1} also increased for three and four layers of PAA. This tentatively suggests that the amount of COOH groups on the surface was directly proportional to the number of PAA layers. Therefore, it was decided to continue with $[PAA/PAH]_3$ PAA deposition for all subsequent work.

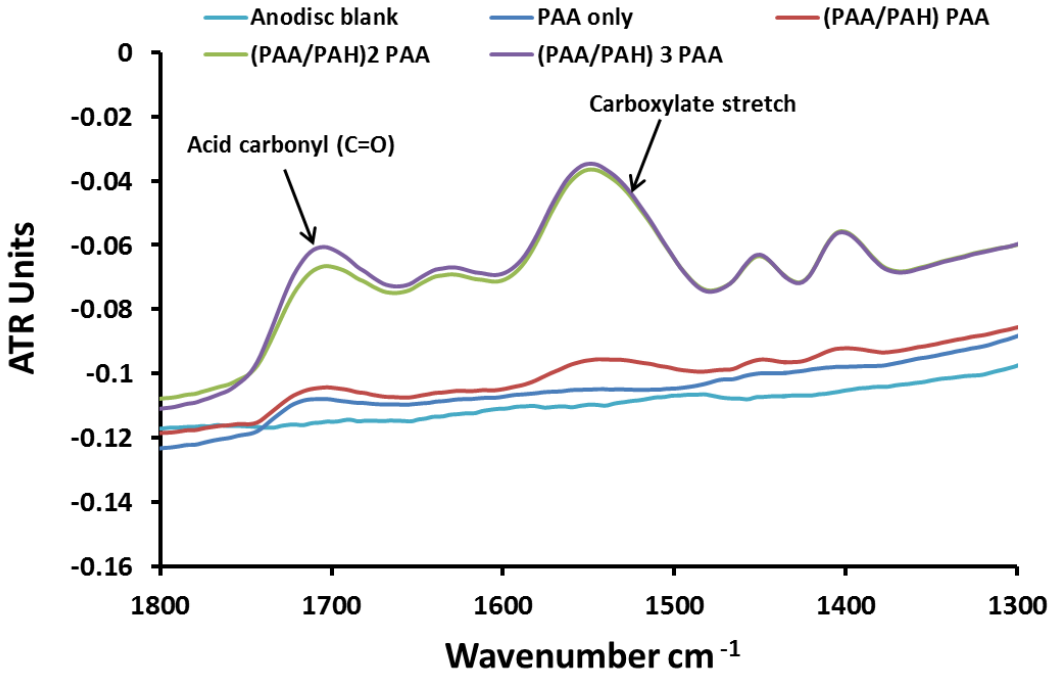

Figure 5-21: FTIR spectra of PAA, (PAA/PAH), $(PAA/PAH)_2$ PAA and $(PAA/PAH)_3$ PAA-modified Anodisc surfaces.

ii) Surface characterization of a PAA/PAH-modified Anodisc surface using AFM

The surface topography of the Anodisc blank and PAA/PAH-modified membrane was investigated using AFM. Due to the porous and fragile nature of the sample, many difficulties were faced during the imaging process. Some of the AFM images of the Anodisc membrane before and after modification are shown in Figure 5-22. The saw-like pore walls protruding from the membrane surface revealed the greater surface roughness present in the Anodisc membrane. The Anodisc alumina membrane has two distinct sides: the filtrate side has a skin layer of 20 nm diameter pores and the permeate side has 100 nm diameter pores. Although the filtrate side is the one of interest here, the permeate side was also analysed. It was observed that the surface roughness was about 150 ± 25 nm and 75 ± 25 nm for the permeate (Figure 22A and B) and filtrate sides (Figure 22E), respectively. This difference could be attributed to the difference in pore size of the respective sides. The high surface roughness values caused difficulties in differentiating between the Anodisc blank and the PAA/PAH-modified membranes and determining the thickness of the PAA/PAH layers on the surface. It was observed that the modified membranes were identical to the blank membrane in AFM analysis, with similar surface roughness values (Figure 22C, D and F). This indicates that the PAA/PAH layers on the surface could have a thickness of few nanometers, within the error range. The purpose of this study was to test for any difference in thickness with an increase in the number of layers of PAA (samples analysed using FTIR in Figure 5-21). As no difference in thickness was observed between the Anodisc blank and $[PAA/PAH]_3$ PAA-modified (4 layers of PAA) membranes, due to high surface roughness values, the other samples with 1, 2 and 3 layers of PAA were not analysed using AFM.

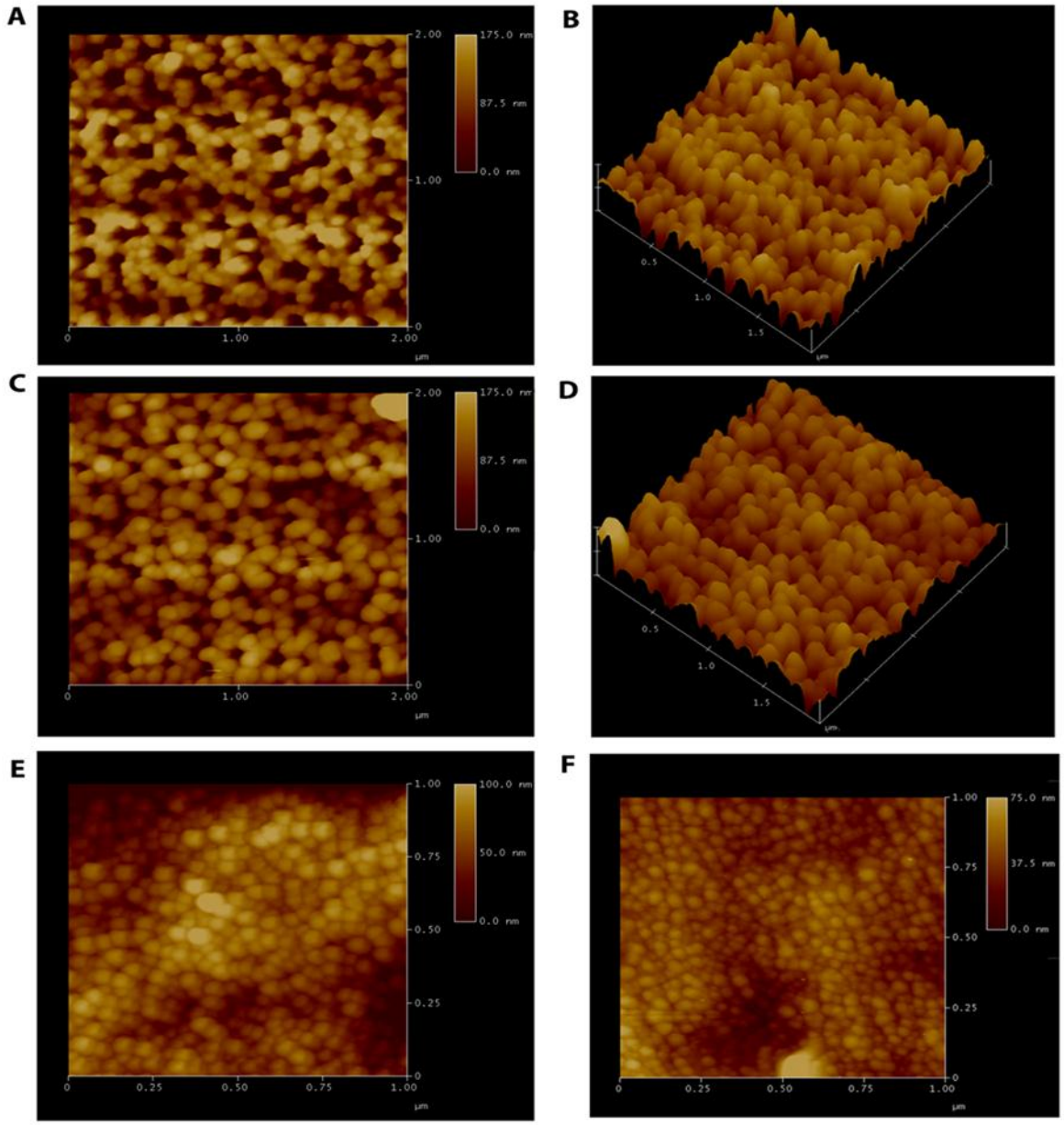

Figure 5-22: AFM images of permeate sides of the Anodisc blank membrane (A and B) and $(PAA/PA)_3$ PAA-modified membrane (C and D), filtrate sides of the Anodisc blank membrane (E) and $(PAA/PA)_3$ PAA-modified membrane (F).

iii) Surface characterization of PAA/PAH modified and EL-5F-PEG-2K coupled Anodisc surface using FE-SEM

The morphology of the bare and modified Anodisc membranes was examined using FE-SEM. Although the filtrate side was the one of interest, the permeate side was also analysed. The bare membrane had pores of size ~ 25 nm on the filtrate side (Figure 5-23A) and ~ 100 nm on the permeate side (Figure 5-23B). Figure 5-23C shows the filtrate side of a $(PAA/PAH)_3$ PAA-modified membrane. It can be observed that the pore size looks smaller (~ 15 nm) than on the Anodisc blank. This indicates that the $(PAA/PAH)_3$ PAA forms a layer of 5-10 nm on the surface and within pores. As the pore size on the permeate side were large, the decrease in size due to the $(PAA/PAH)_3$ PAA layer was insignificant (Figure 5-23D). Figure 5-23E and G shows the filtrate sides of the Anodisc coupled with EL-5F-PEG-2K and dried at pH 8 and 3, respectively. It can be observed that the surface morphology of EL-5F-PEG-2K coupled membrane at pH 3 and 8 were identical. Both these images look similar to Figure 23C. No self-assembled fibrils of EL-5F-PEG-2K at pH 3 are visible. The permeate sides of EL-5F-PEG-2K coupled membrane at pH 3 and 8 (Figure 5-23F and H) were identical to those shown in Figure 23D. Although few close-range tethered EL-5F-PEG-2K are expected to stack together to form fibrils of few nanometers, it might be not possible for the surface-tethered EL-5F-PEG-2K to form fibrils of several hundred nanometers as it does in solution. Another possible reason might be that SEM analysis is not suitable for this purpose. As the Anodisc alumina is non-conducting, it was coated with platinum prior to SEM analysis. There is a possibility that this coating could have hindered the visibility of EL-5F-PEG-2K fibrils, which are only a few nanometers in dimensions. All these reasons made surface characterization using SEM difficult. TEM analysis was used to study the morphology of self-assembled fibrils of EL-5F-PEG-2K in solution. However, because of

the chemical coupling of EL-5F-PEG-2K to the surface and the Anodisc thickness (~ 60 μm), it is not feasible to use TEM analysis.

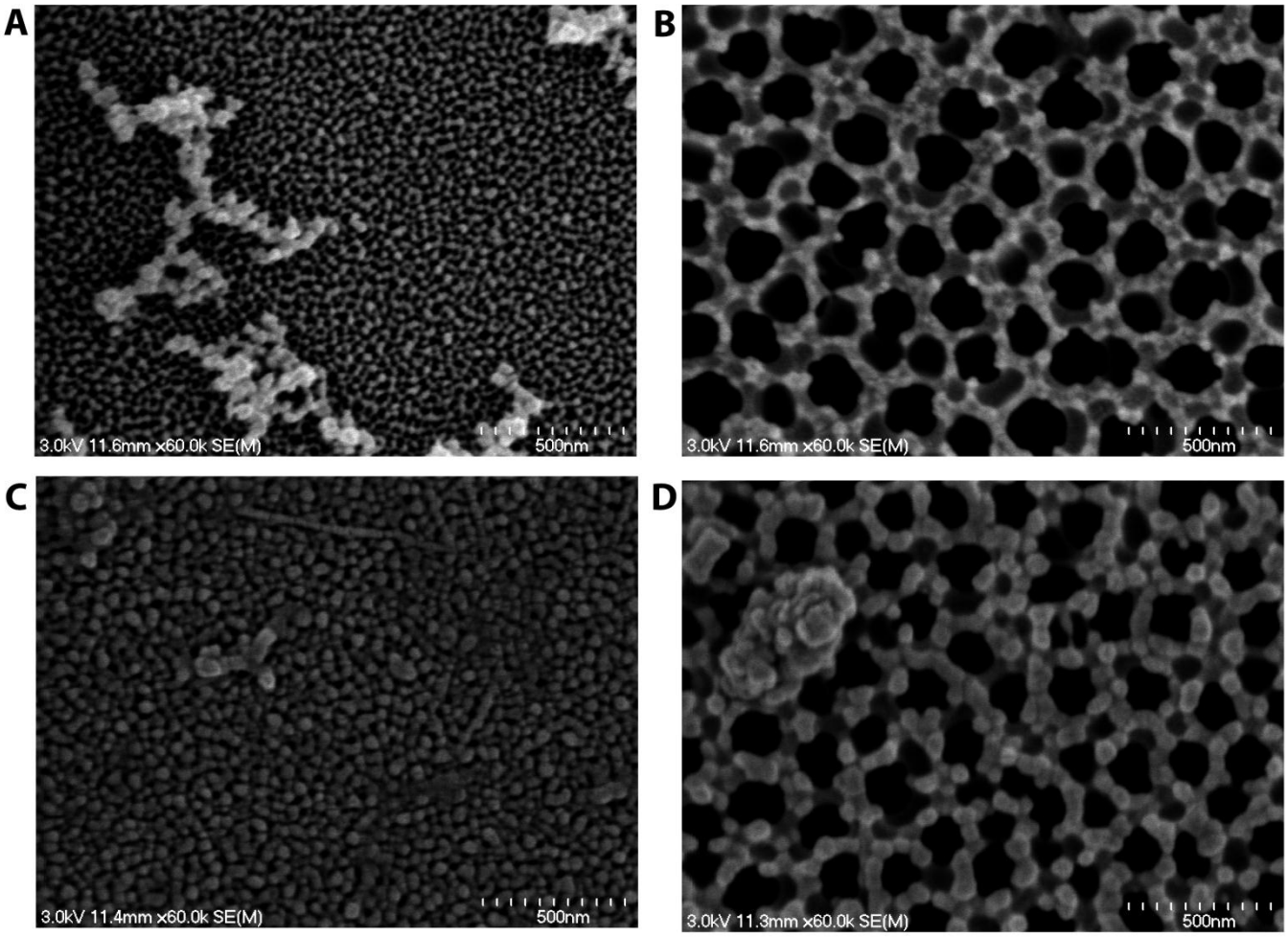

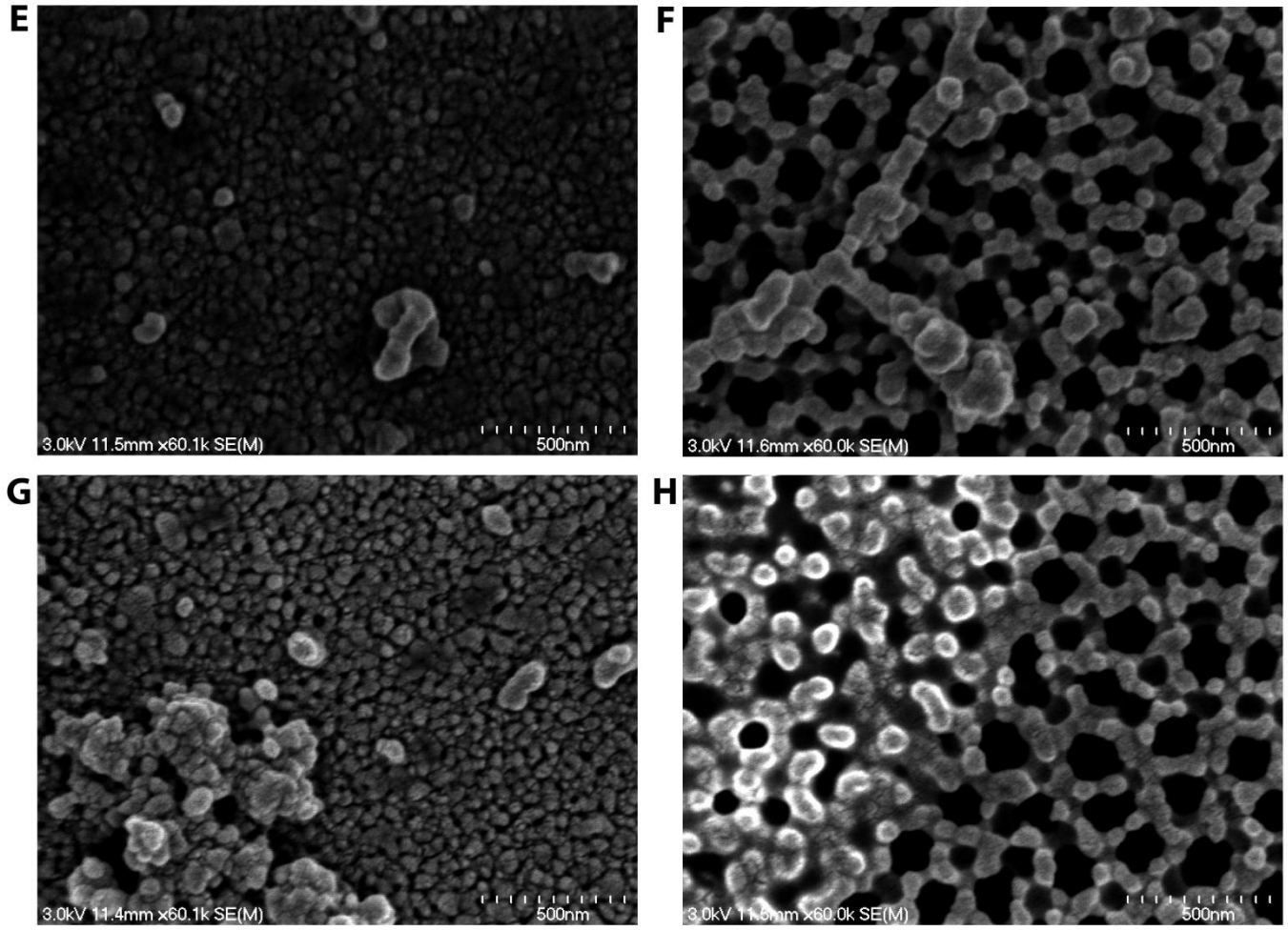

Figure 5-23: FE-SEM images of filtrate and permeate sides of the Anodisc blank (A and B), $(PAA/PAH)_3$ PAA-modified (C and D), $(PAA/PAH)_3$ PAA-modified + EL-5F-PEG-2K coupled (pH 8) (E and F) and $(PAA/PAH)_3$ PAA-modified + EL-5F-PEG-2K coupled (pH 3) (G and H) membranes respectively.

5.3.2 Determination of flux of blank, PAA/PAH-modified and EL-5F-PEG-2K coupled Anodisc membranes at pH 3 and 8

The flux of the Anodisc PAA/PAH modified and EL-5F-PEG-2K coupled membranes over a range of back pressures were determined at pH 3 and 8 using dead end filtration experiments (see Section 5.2.10). The trend line shows the flux trend over a range of back pressures for the Anodisc blank, Anodisc PAA/PAH modified and the Anodisc coupled with EL-5F-PEG-2K. Initial experiments were carried out with the Anodisc blank membrane to check the effect of pH changes on the flux of the membrane. As predicted, it was observed that there was no difference in flux with changes in pH from 3 to 8 (Figure 5-24). The immobilisation of PAA/PAH layers on the Anodisc surface increased the resistance of the membrane by about 10-fold (Table 5-3) but it was observed that pH changes had no effect on the flux of this modified membrane (Figure 5-24).

EL-5F-PEG-2K was amine-coupled to the COOH groups on the surface of the PAA/PAH modified membrane. The resistance of the EL-5F-PEG-2K coupled membrane increased by about 4-fold compared with the PAA/PAH modified membrane. This indicates that EL-5F-PEG-2K on the surface and within pores causes obstruction to the permeability of the membrane. However, it was observed that varying the pH of the buffer from 3 to 8 had no effect on the resistance of the membrane. This was repeated twice to check for reversibility of self-assembly of EL-5F-PEG-2K coupled to the surface. The flux of the membrane remained in similar range for both the pH values. This could be due to the following reasons, i) the resistance offered by the self-assembled EL-5F-PEG-2K (pH 3) in the pores of the membrane was similar to that offered by the disassembled EL-5F-PEG-2K strands (pH 8), ii) the surface coupled EL-5F-PEG-2K becomes unresponsive to pH and does not self-assemble as in solution, iii) there is very little EL-5F-PEG-2K coupled to the surface, which is lower than the critical concentration of the conjugate needed for self-assembly to occur.

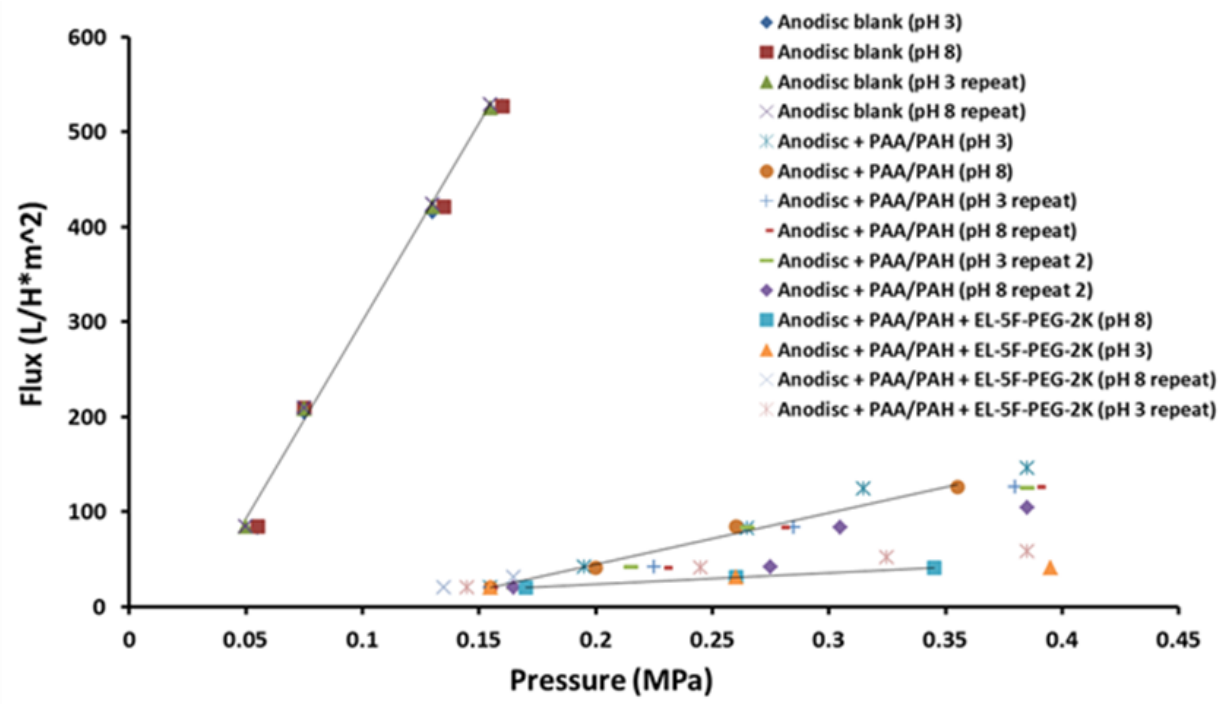

Figure 5-24: Flux data over a range of back pressures of the Anodisc blank, $(PAA/PAH)_3$ PAA-modified and $(PAA/PAH)_3$ PAA-modified + EL-5F-PEG-2K coupled membranes at pH 3 and 8.

Table 5-3: Membrane resistance, R_m (m^{-1}) of the Anodisc blank, $(PAA/PAH)_3$ PAA-modified and $(PAA/PAH)_3$ PAA-modified + EL-5F-PEG-2K coupled membranes (flux, J ($L/H*m^2$), pressure, P (MPa), viscosity, μ = 0.00089 Pa.s).

	J.μ/P	Rm
Anodisc blank	3.7	0.3
Anodisc + PAA/PAH	0.5	2.1
Anodisc + PAA/PAH + EL-5F-PEG-2K	0.1	9.3

The change in resistance of the membrane with self-assembly and disassembly at pH 3 and 8 respectively could be insignificant to bring about change in the (low molecular weight) buffer flux but could perhaps affect macromolecule permeation. This was tested below by passing a neutral solute molecule, PEG, through the membrane pores at pH 3 and 8, and analyzing the change in retention capacity of the membrane with change in pH.

5.3.3 Determination of MWCO of EL-5F-PEG-2K coupled Anodisc membrane at pH 3 and 8

Earlier investigations on the EL-5F-PEG-2K coupled membrane suggest the need for further investigations to obtain more consistent and conclusive evidence for the self-assembly of tethered EL-5F-PEG-2K. MWCO experiments still remain the most convenient and universally applied means of choosing and differentiating between membranes for different applications. Thus, a MWCO experiment to measure the membrane selectivity for solute molecules of different molecular weights (MWs) was performed via dead end filtration (Figure 5-25). A mixture of different molecular weight PEG molecules ranging from 72 to 29 kDa was run through a Superdex S200 size exclusion column to check the individual elution profiles of each PEG in the mixture. It was observed that only PEG 72 and 29 kDa had distinct elution peaks. Therefore, a mixture of PEG 72 and 29 kDa at concentrations of 2.5 mg/mL each was used for the MWCO experiments.

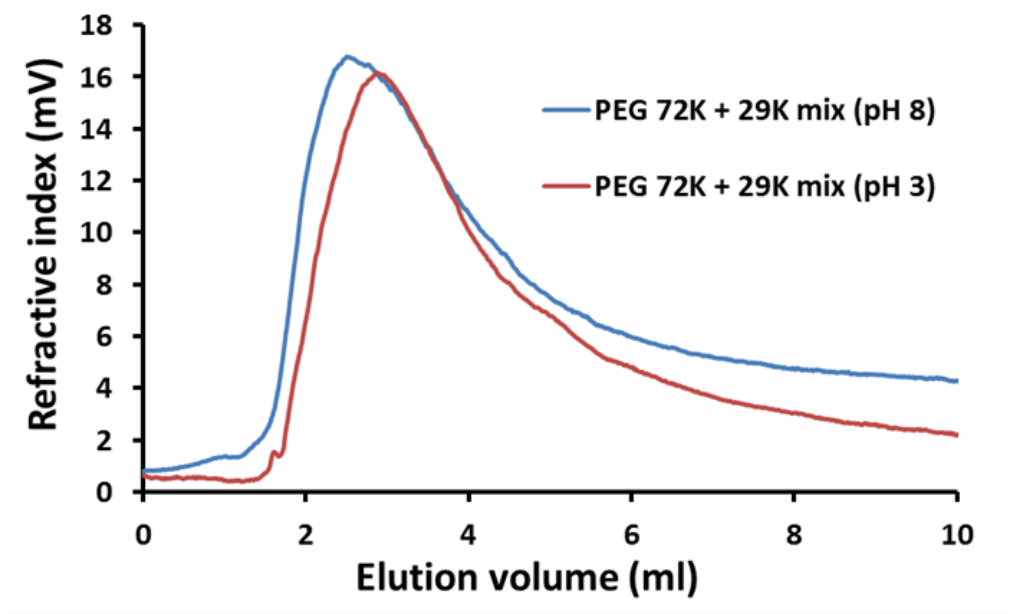

Figure 5-25: The permeation of PEG 72 kDa + 29 kDa mixture (2.5 mg/mL) through $(PAA/PAH)_3$ PAA-modified + EL-5F-PEG-2K coupled Anodisc membrane at pH 3 and 8.

Figure 5-26A represents the elution profile of permeate at pH 3 and 8 in comparison with the elution profile of the feed. It was assumed that the concentration of PEG is directly proportional to the RID intensity (mV). It can observed that there is a significant decrease in the RID intensity (mV) for the permeate samples at both the pH values. This indicates that a large amount of the PEG mixture was retained on the membrane surface. The ratios of area under the peak of PEG 72 and 29 kDa in the feed and permeate was determined and the retention % was calculated. It can be seen that 90% of PEG 72 kDa was retained in the membrane at pH 3 compared with 60% at pH 8 and 81.5% of PEG 29 kDa was retained at pH 3 compared with 53.5% at pH 8 (Figure 5-26B).

The enhanced retention of PEG at pH 3 in comparison with pH 8 is consistent with the notion that the self-assembly of EL-5F-PEG-2K to form β-sheet structures, thereby increasing PEG

retention. In contrast, it is believed that the disassembly of EL-5F-PEG-2K at pH 8 results in a greater amount of PEG permeating through the pores. To validate the reversibility of this self-assembly process, the experiment was repeated at pH 3. However, it was observed that the permeation of PEG through the pores decreased markedly, probably because of fouling on the surface, evident from the very low RID intensity (mV). Control experiments were performed using a bare Anodisc membrane. A comparison on the elution profiles at pH 3 and pH 8 were performed by calculating the area under the peaks as in the case of modified membrane and it was found that the retention % was similar at both the pH values.

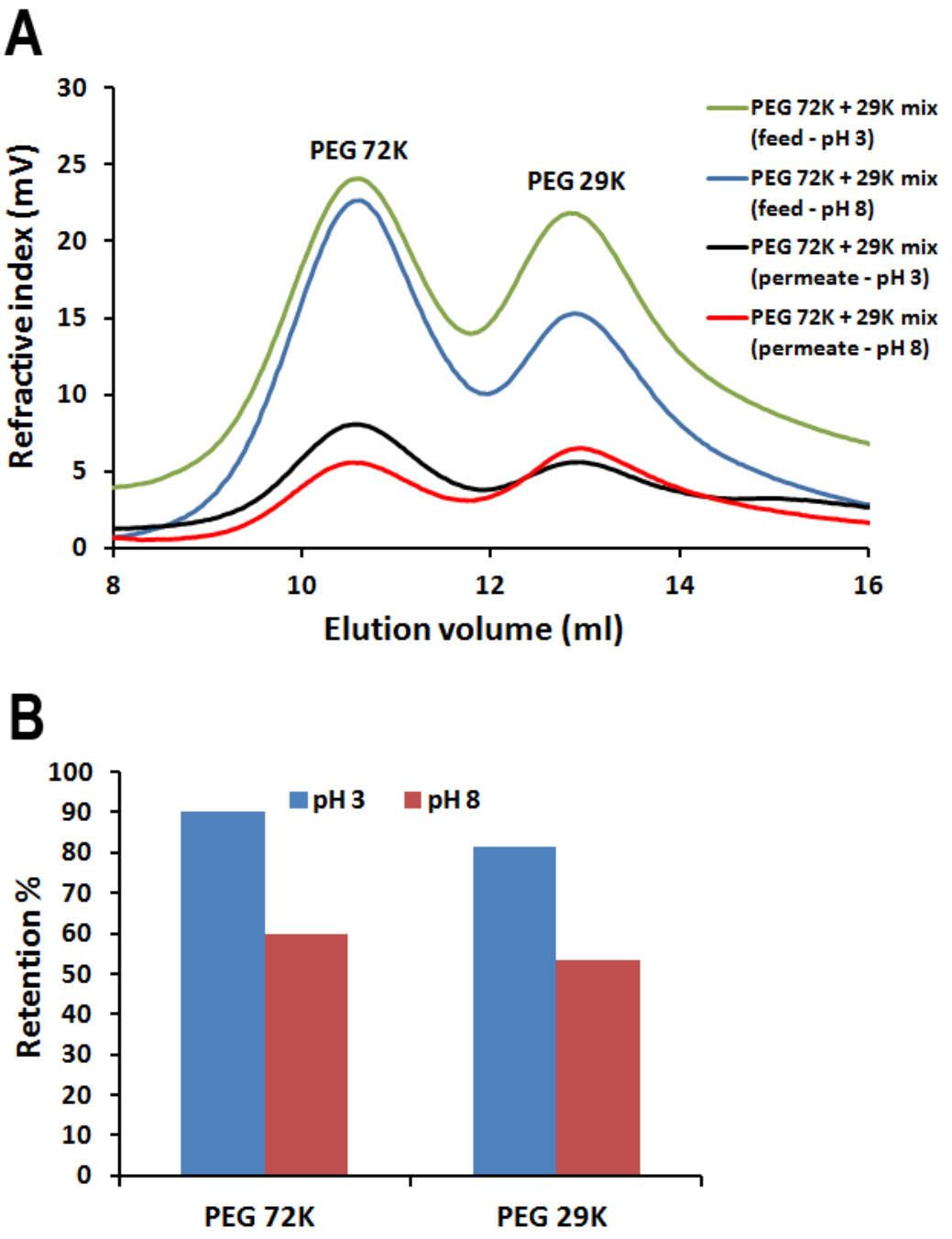

Figure 5-26: A) Size exclusion chromatogram showing the distinct peaks of PEG 72 and 29 kDa in the feed and permeate samples at pH 3 and 8, B) The retention (%) of PEG 72 and 29 kDa from the feed mixture by the $(PAA/PAH)_3$ PAA-modified + EL-5F-PEG-2K coupled Anodisc membrane at pH 3 and 8.

To further investigate the reproducibility of the self-assembly process, two fresh EL-5F-PEG-2K coupled membranes were prepared and the experiment was repeated on both these membranes with the same PEG mixture feed sample (Figure 5-27). Figure 5-28A shows the elution profile of permeate at pH 3 and 8 in comparison with the elution profile of the feed. Calculations indicated that 77.2% of PEG 72 kDa was retained in the membrane at pH 3 whereas it was 60% in the case of pH 8 and 85.2% of PEG 29 kDa was retained at pH 3 compared with 48% at pH 8 (Figure 5-28B). These results corroborate with the previous observations, suggesting the reversible self-assembly of the membrane tethered EL-5F-PEG-2K.

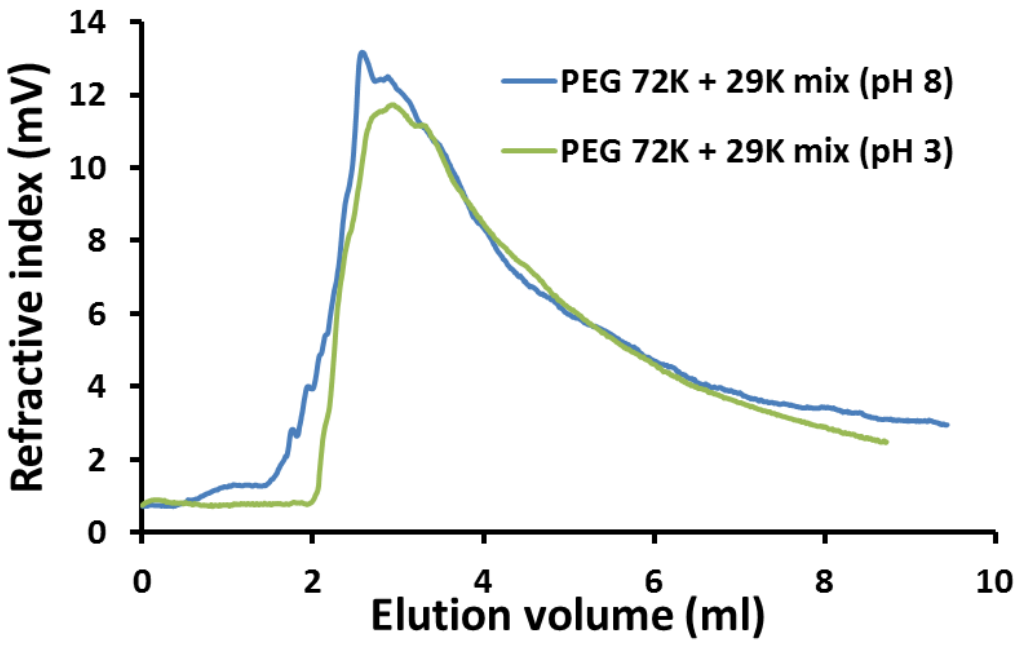

Figure 5-27: The permeation of PEG 72 kDa + 29 kDa mixture (2.5 mg/mL) through $(PAA/PAH)_3$ PAA-modified + EL-5F-PEG-2K coupled Anodisc membrane at pH 3 and 8.

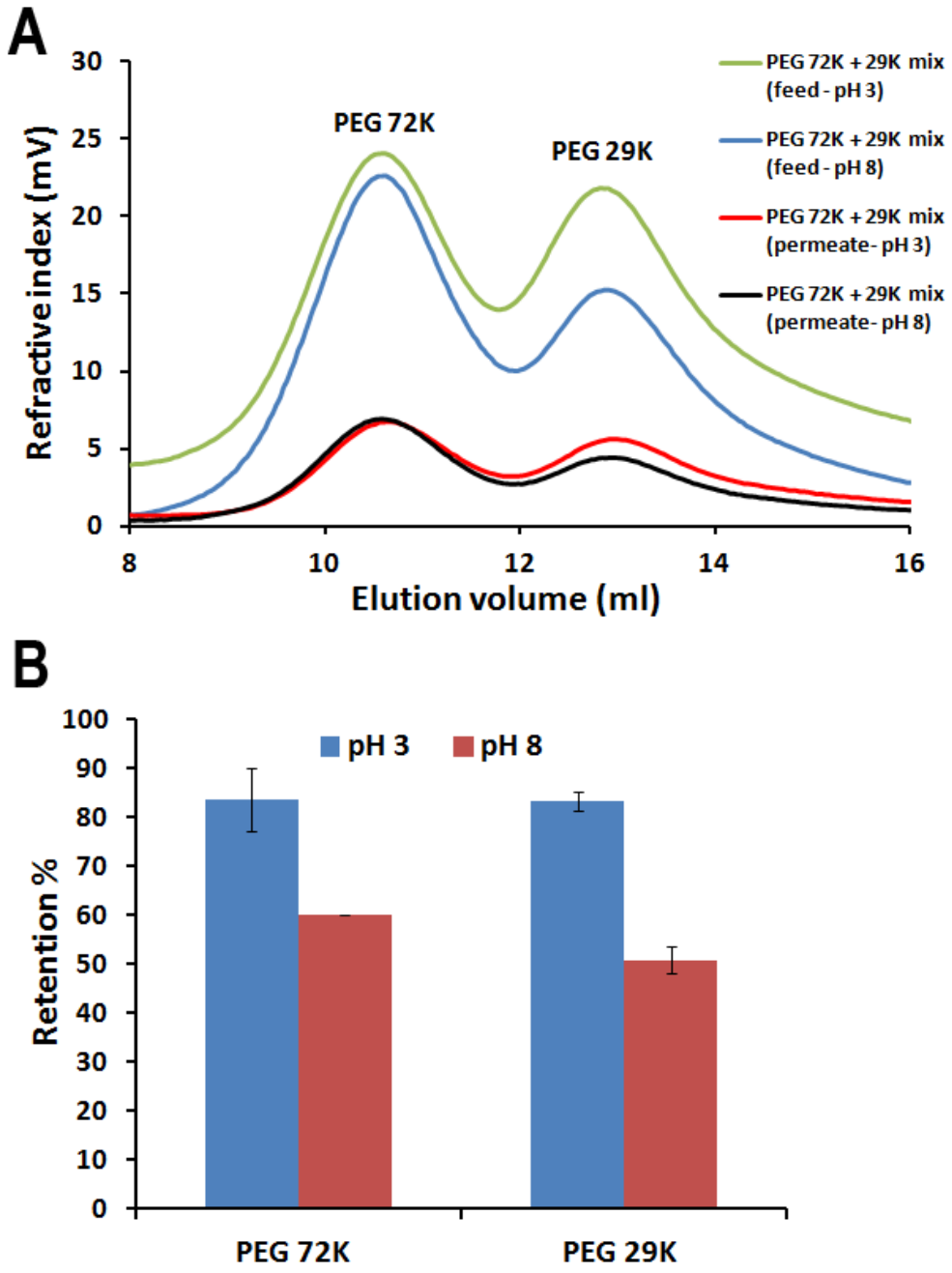

Figure 5-28: A) Size exclusion chromatogram showing the distinct peaks of PEG 72 and 29 kDa in the feed and permeate samples at pH 3 and 8, B) The mean retention (%) of PEG 72 and 29 kDa from the feed mixture by the $(PAA/PAH)_3$ PAA-modified + EL-5F-PEG-2K coupled Anodisc membrane at pH 3 and 8.

However, an additional trial on a newly modified membrane, showed different behavior with the retention of the PEG mixture being higher at pH 8 than at pH 3 (data not shown). This is believed to be due to extensive fouling on the surface at pH 3, thereby increasing the membrane resistance and causing further decrease in permeation of PEG at pH 8. Fouling on surfaces is generally associated with dead end filtration procedures (van der Sman et al., 2012) and requires extensive modification approaches to avoid membrane fouling. Thus, the use of cross-flow filtration could be an effective alternative. Despite this issue, it can be observed that the results are indicative of reversible self-assembly of membrane tethered EL-5F-PEG-2K. Due to time constraints, the effect of reversible self-assembly of EL-5F-PEG-5K on the permeability of the membrane could not be tested. The presence of an extended spacer (PEG-5K) in EL-5F-PEG-5K compared with EL-5F-PEG-2K, might have added increased steric flexibility aiding self-assembly of the peptide.

Other analytical tools to probe molecular changes on surface

Quartz crystal microbalance (QCM) and surface plasmon resonance (SPR)

QCM and SPR are two widely used techniques to study inter-molecular interaction and interaction of molecules with surfaces. Both these techniques detect changes in the amount of adsorbed material on the surface (Paulo et al., 2013). They have been used to demonstrate stimuli-induced attachment/detachment of peptides on a surface and detect changes in the viscoelastic properties of the adsorbed material, thus providing information about the conformational changes (Truong et al., 2010). QCM was also used to monitor viscoelastic changes of multilayer amyloid deposition in situ (Hovgaard et al., 2007; Knowles et al., 2007). On the other hand, SPR was used analyze the influence of alkaloids on aggregation of amyloid-β peptide (Krazinski et al., 2011). With these characterization techniques available to investigate peptide molecules on surface, the challenge lies in using these techniques to

study the peptide structure on a membrane surface. Both QCM and SPR involves using specific chip surfaces and the adsorption/desorption of molecules to this surface is examined. The research reported in this thesis was aimed at investigating the self-assembly of peptide molecules tethered to a membrane surface. Direct characterization of a modified membrane surface using these techniques may be challenging. Alternatively, peptide-PEG bioconjugates can be tethered to QCM/SPR chip surfaces made of similar materials to that of the membranes (for example, Al_2O_3) and the peptide conformation on the chip surface could then be studied. Although the surface topography of this chip differs from that of a (porous) membrane, this study could provide useful insights into tethered peptide structure.

5.3.4 Conjugation of EL-5F/EL-5F-PEG-2K to NPs

5.3.4.1 Coupling and purification

With the conjugation of EL-5F-PEG-2K onto the membrane surface and the predicted self-assembly as evident from MWCO experiments, alternate experiments were carried out to demonstrate the inter-particle reversible self-assembly of EL-5F/ EL-5F-PEG-2K tethered to simple surfaces such as nanoparticles, eliminating the complex membrane features (Figure 5-35A). To conjugate peptide EL-5F or the bioconjugate EL-5F-PEG-2K onto the surface of a polystyrene nanoparticles, the carboxyl groups present on the surface of the NPs were activated by the addition of EDC/NHS. The N-terminus primary amine of EL-5F was coupled to the NHS-activated carboxyl groups via amine coupling. The NHS ester-primary amine reaction was carried out at pH 7, which is within the range 7–8 identified previously as most efficient (Grabarek & Gergely, 1990). The washing steps (see Section 5.2.12) resulted in the separation of unreacted EL-5F and EDC/NHS from the EL-5F coupled NPs. The concentration of unreacted EL-5F in subsequent supernatant's collected after each wash step was measured using Nanodrop. It was observed that the concentration of unreacted EL-5F decreased with each wash step and became almost negligible after four washes as evident from a clear PBS solution. This indicates that the sample is devoid of any free EL-5F and consisted of only EL-5F coupled NPs and negligible amounts of native NPs. Similar amine coupling and purification procedures were carried out to couple EL-5F-PEG-2K to the NPs. In this case, the free amine of the PEG was conjugated to the NHS activated carboxyl groups of the NPs. The control sample consisted of ethanolamine hydrochloride added to the NHS-activated NPs to change the active NHS ester into an inactive hydroxethyl amide. This would render the removal of charged carboxyl groups, thereby making the NPs insensitive to pH changes and also eliminate unintended covalent links during subsequent interactions.

5.3.4.2 Particle size characterisation

To investigate the reversible self-assembly of EL-5F/EL-5F-PEG-2K-conjugated NPs, size transitions potentially indicative of self-assembly at pH 3 and 7 were analysed using DLS measurements. DLS experiments are generally performed to examine the size of particles in solution. In this study, the inter-particle self-assembly of EL-5F/EL-5F-PEG-2K at pH 3 was expected to cause aggregation of NPs and the disassembly at pH 7 would result in no aggregation. Therefore, this pH dependant size variation of the NPs was detected using DLS measurements.

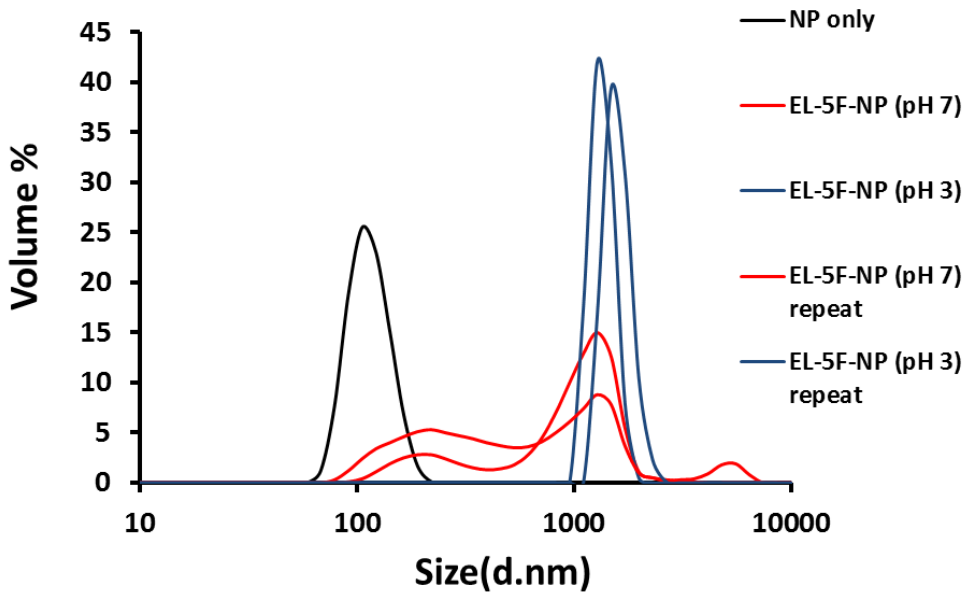

Figure 5-29: DLS measurement showing reversible transition in size of EL-5F coupled NPs with change in pH between 3 and 7.

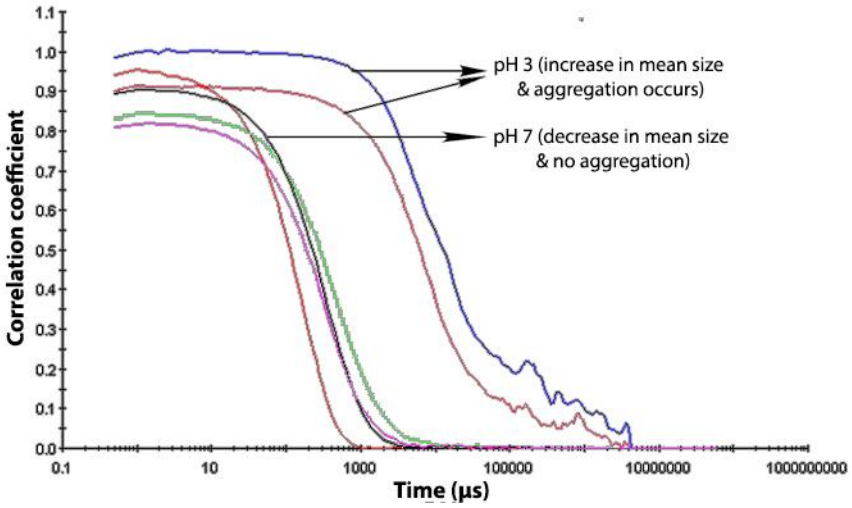

Figure 5-30: Correllogram showing reversible transition in size and aggregation of EL-5F coupled NPs with change in pH between 3 and 7.

Figure 5-29 shows the particle size transition of EL-5F conjugated NPs. It was observed that the native NPs demonstrated a mean size of 125 nm at pH 7. The coupling of EL-5F peptide to the NPs slightly increased the mean size of the particle at pH 7. With decrease in pH to 3, aggregation of the NPs occurred, causing the mean size to markedly increase by around 20 times, as evident from the correllogram (Figure 5-30). This change in size and aggregation was rapid and reversible upon changes in pH (pH 3 to pH 7 and vice versa). Similar results were obtained in case of EL-5F-PEG-2K coupled NPs (Figure 5-31 and 5-32).

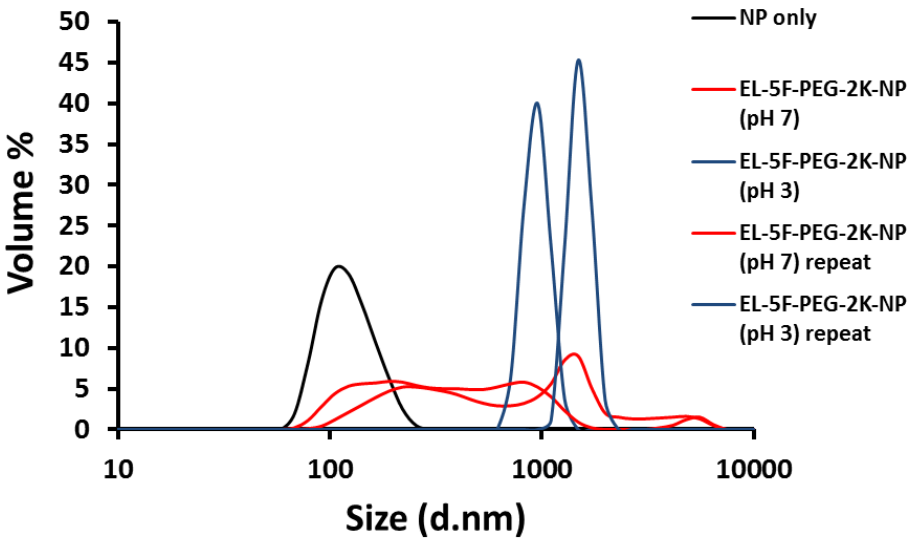

Figure 5-31: DLS measurement showing reversible transition in size of EL-5F-PEG-2K coupled NPs with change in pH between 3 and 7.

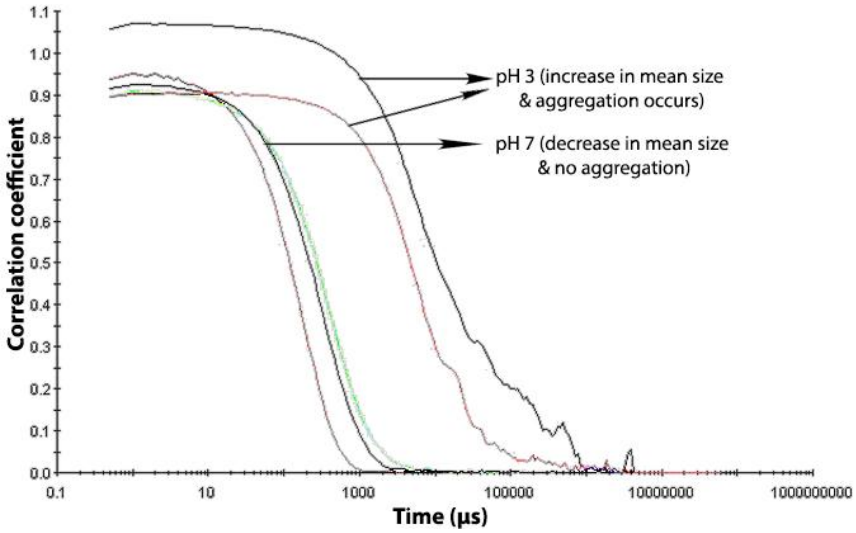

Figure 5-32: Correllogram showing reversible transition in size and aggregation of EL-5F-PEG-2K coupled NPs with change in pH between 3 and 7.

In contrast, the control samples indicated no size transitions with respect to changes in pH. Furthermore, ethanolamine deactivated NPs were found to aggregate and form similar large sized particles at both pH 3 and 7 (Figure 5-33 and 5-34). The particles being small and devoid of any repulsive charges can be accounted as the possible reasons for this agglomeration. Ethanolamine blocks the NHS activated carboxyl groups, thereby eliminating charged moieties and making the NPs insensitive to pH changes.

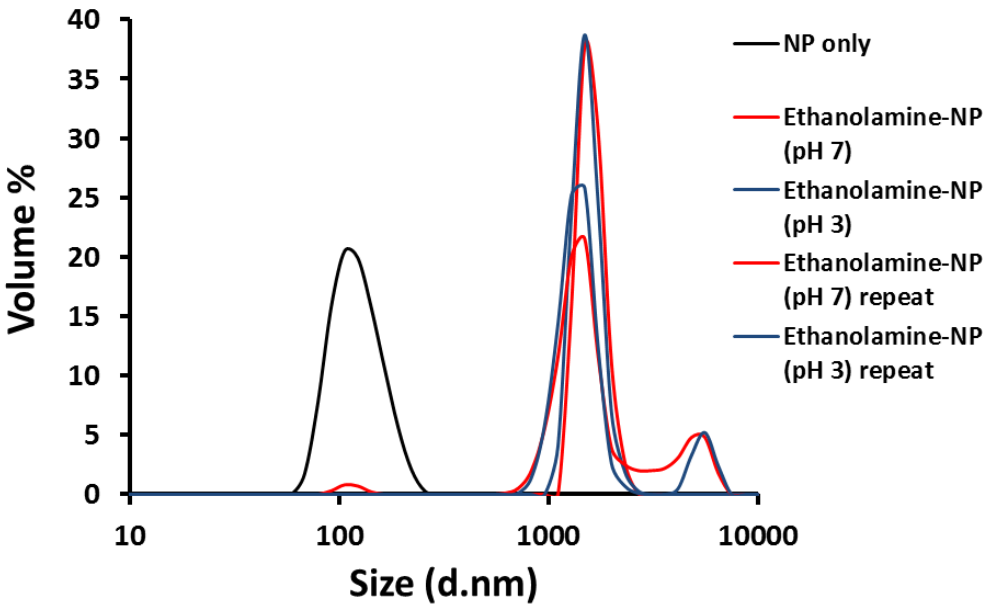

Figure 5-33: DLS measurement showing irreversible aggregation of ethanolamine deactivated NPs at both pH 3 and 7.

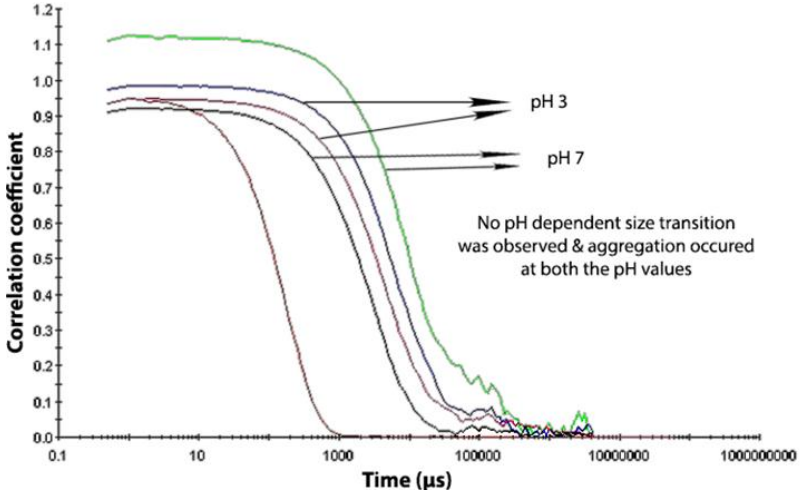

Figure 5-34: Correllogram showing aggregation of ethanolamine coupled NPs at both pH 3 and 7.

These data suggest that the reversible aggregation of the NPs conjugated with peptide EL-5F/ conjugate EL-5F-PEG-2K is potentially due to the reversible self-assembly of EL-5F or EL-5F-PEG-2K on adjacent particles, upon changes in pH (Figure 5-35A). The mechanism of this pH dependent self-assembly of EL-5F and EL-5F-PEG-2K has been elucidated in the previous chapter. However, based on these observations, a few other possible reasons for this pH-dependant size transition of NPs were hypothesized, which include: (i) At pH 3, the carboxyl groups of the glutamic acid side chains of EL-5F are protonated (COOH). Thus, the lack of any repulsive charges as in the case of the control experiment might essentially result in NP aggregation. Similarly, with increase in pH (pH 7) the carboxyl groups become charged (COO^-) resulting in repulsive forces, which prevent aggregation (Figure 5-35B). (ii) Another important factor that requires consideration is the inter-particle and intra-particle self-assembly of the peptide. The mean size change and reversible aggregation as shown by the DLS measurement are potentially due to inter-particle self-assembly of the peptide (Figure 35A). In contrast, although intra-particle self-assembly (Figure 5-35C) of the peptide

is expected to occur to a large extent, it is predicted that this will neither cause any pH dependant size transitions nor aggregation of the NPs.

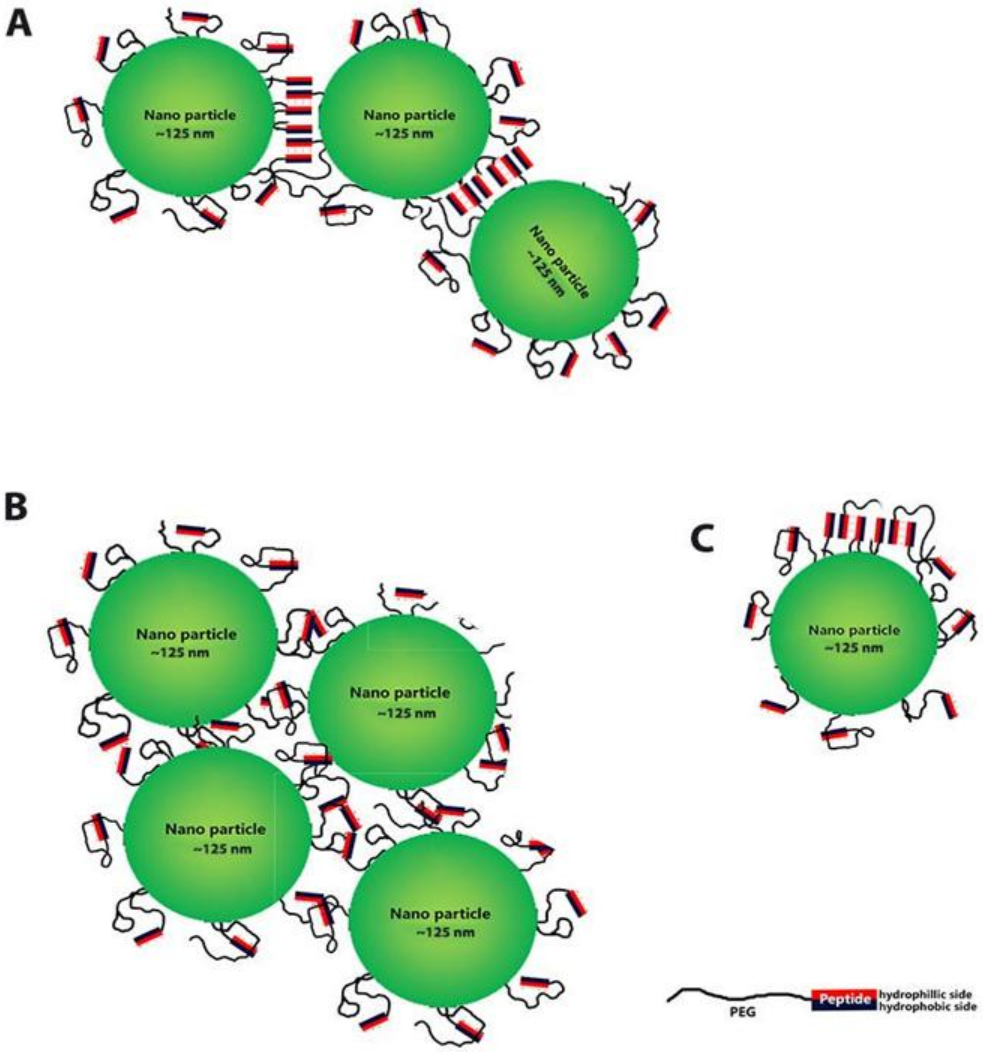

Figure 5-35: Schematic representation of the explanations for pH dependant size transition of EL-5F and EL-5F-PEG-2K coupled NPs. A) Inter-particle self-assembly of peptide EL-5F at pH 3, B) Aggregation due to lack of repulsive charges at pH 3, C) Intra-particle self-assembly of peptide EL-5F at pH 3.

5.3.4.3 Characterisation of structural morphology

The physical morphology of the native and EL-5F/EL-5F-PEG-2K/ethanolamine coupled NPs were investigated using TEM. Figure 5-36A shows the native NPs having a diameter of around 125 nm. Figure 5-36B and C shows the EL-5F coupled NPs at pH 3 and 7 respectively. It can be observed that the NPs aggregated at pH 3 and disaggregate at pH 7. Figures 5-36D and E show the aggregation and disaggregation of EL-5F-PEG-2K coupled NPs at pH 3 and 7 respectively. However, no fibrillar structures were observed in both cases and is believed to be due to the interference from PBS salts in the sample, which appear as dark spots in the images. As predicted, the ethanolamine coupled NPs (control) aggregated irrespective of pH due to lack of repulsive forces (Figure 5-36F and G). The lack of fibrillar structures with change in pH renders these results to be inconsistent and it is believed that these do not substantiate the previous findings using DLS measurements.

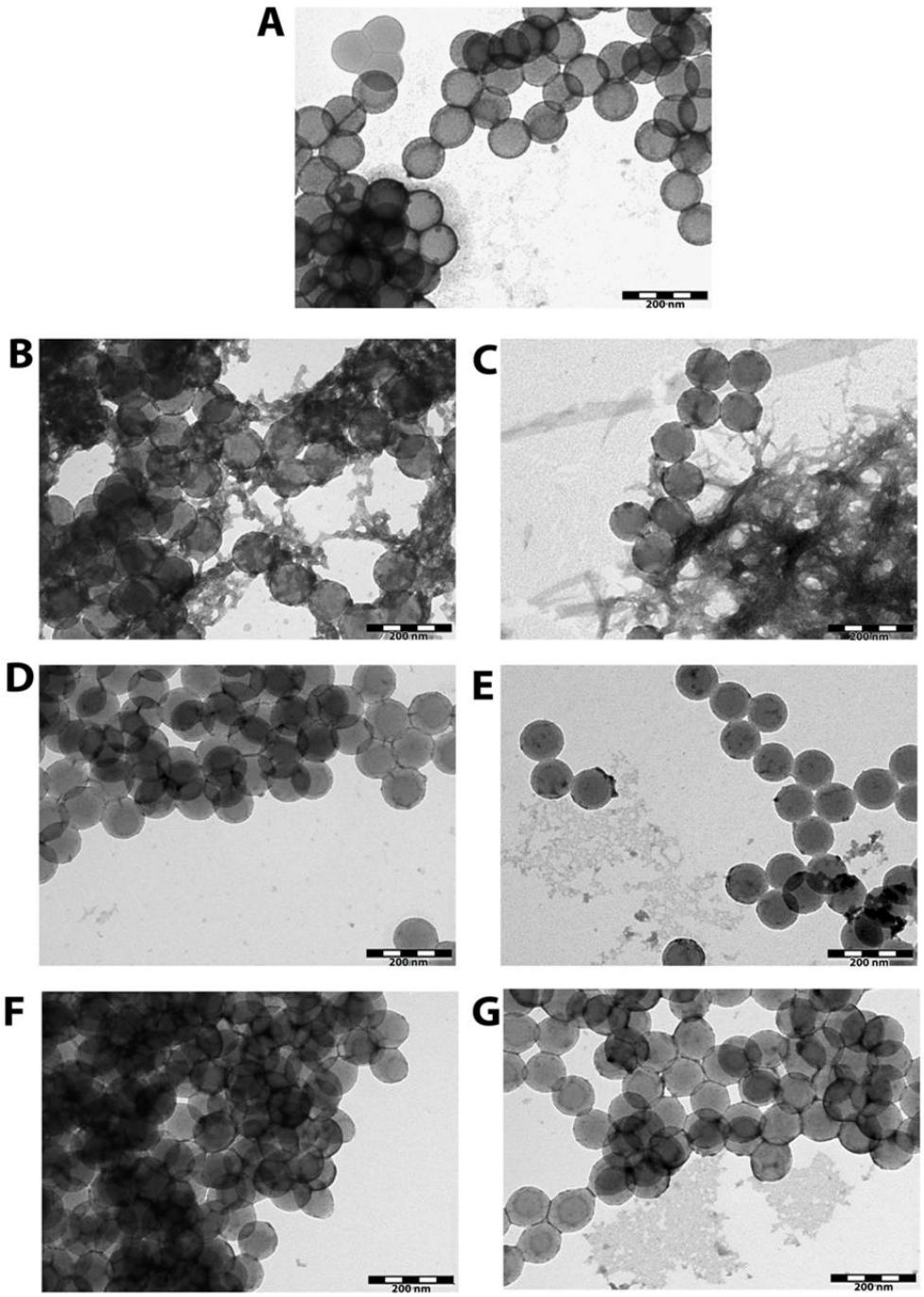

Figure 5-36: TEM images of A) Native NPs, B) EL-5F coupled NPs at pH 3, C) EL-5F coupled NPs at pH 7, D) EL-5F-PEG-2K coupled NPs at pH 3, E) EL-5F-PEG-2K coupled NPs at pH 7, F) Ethanolamine coupled NPs at pH 3, G) Ethanolamine coupled NPs at pH 7.

5.4 CONCLUSIONS

This chapter describes work aimed at the development of a method to enable pH-regulated self-assembly of peptide-PEG conjugate EL-5F-PEG-2K tethered to the Anodisc surface, to control membrane permeability. A variety of approaches were attempted to immobilise COOH groups on the membrane surface for the coupling of peptide-PEG conjugate EL-5F-PEG-2K, which include (i) phosphonic acid, (ii) diazonium chemistry and (iii) multilayer deposition of PAA and PAH. With the attempts to immobilise COOH groups on membranes using phosphonic acid and diazonium chemistry being inconclusive, multilayer deposition of polyelectrolytes PAA and PAH was carried out. EL-5F-PEG-2K was then successfully amine-coupled to the COOH groups and this was confirmed using ATR-FTIR.

Subsequent flux tests indicated no pH-dependant variation in flux properties of the EL-5F-PEG-2K modified membrane. However, MWCO experiments using PEG 72 and 29 kDa were consistent with reversible self-assembly of tethered EL-5F-PEG-2K upon changes in pH, affecting macromolecule permeation. Additionally, studies were carried out on the reversible, pH-regulated self-assembly of peptide EL-5F and conjugate EL-5F-PEG-2K tethered to polystyrene nanoparticle surfaces. This reversible self-assembly on NP surfaces was confirmed from the size transitions and aggregation with changes in pH. These observations warrant further investigations by optimization of protocols, use of alternative conjugation methods and/or characterization approaches. Overall, some of the results are tentatively consistent with possible self-assembly of the peptide on the membrane surface, but further work is needed to confirm this outcome and also to quantitatively increase the levels of tethered peptide to the surface.

CHAPTER-6

CONCLUSIONS AND RECOMMENDATIONS FOR FUTURE WORK

6. CONCLUSIONS AND RECOMMENDATIONS FOR FUTURE WORK

This thesis describes an attempt to develop a stimuli-responsive membrane with its surface and pores functionalized with pH-driven SAP's. The overall findings of this study are elaborated below.

6.1 FACTORS AFFECTING SELF-ASSEMBLY OF BIOCONJUGATE P11-4-PEG-2K

P11-4 was conjugated to NHS-PEG-2K via N-terminal amine coupling and the conjugate P11-4-PEG-2K was purified using size exclusion chromatography. The presence of P11-4-PEG-2K was confirmed using MALDI-TOF spectrometry method. The rapidly synthesized bioconjugate (*e.g.*, < 2 min) did not retain the self-assembly of peptide P11-4 and in contrast to the native peptide, the conjugate displayed a random coil structure at pH < 3. Further, the conjugate retained its random coil structure across various pH conditions (pH 2.5, 7 and 11) even for prolonged incubation periods (up to 20 days). Investigations on the effect of the presence of unreacted free PEG on P11-4 self-assembly indicated that the presence of free PEG in solution did not hinder self-assembly. Further, conjugation carried out in 3 mM sodium phosphate buffer and water, resulted in P11-4-PEG-2K retaining its random coil structure at pH 2.5. Other conjugation parameters such as concentrations of P11-4 and NHS-PEG-2K in the reaction mixture and the effect of residual by-products of EDC/NHS coupling reaction were analysed. It was found that in all cases, the self-assembly of native P11-4 remained unaffected, whereas the conjugate displayed a random coil conformation at pH 2.5. It is evident that the conjugation of PEG to the N-terminal amine of peptide P11-4 via EDC/NHS coupling left the conjugate with no net charge, thus preventing the self-assembly

of the peptide. This rendered P11-4 unsuitable for the intended purpose (creation of a pH-responsive membrane).

Recommendations for future work on P11-4

- Conjugating P11-4 to a low molecular weight PEG. This will give information on the effect of PEG molecular weight on the self-assembly of P11-4.
- Conjugation of PEG to the N terminal of the peptide and protecting the C terminal carboxylate should leave P11-4-PEG-2K with one net positive charge (Arg^+), similar to that of native peptide. This might retain self-assembly of P11-4-PEG-2K.

6.2 RAPID AND REVERSIBLE SELF-ASSEMBLY OF BIOCONJUGATES EL-5F-PEG-2K AND EL-5F-PEG-5K

Rapid, repeated and reversible, pH-regulated, self-assembly of peptide EL-5F and conjugates of this peptide with 2 and 5 kDa PEG was demonstrated. Self-assembly of the peptide and conjugates into β sheet structures upon change of pH was confirmed using CD, TEM and ThT binding analyses. Sustained, reversible self-assembly of the peptide and its PEG conjugates was shown to occur within 5 min for more than 15 cycles of pH shift and the extent of structural conversion was directly related to pH. The presence of PEG chains slightly decreased the pH range over which structural transition occurred, with the 5 kDa PEG chains having a greater effect than the 2 kDa chains. The reversibility of secondary structure switching was sustained even at high salt concentrations (200 mM). Rapid and reversible hydrogelation through self-assembly of the peptide and its conjugates at concentrations as low as 0.2 wt% was also demonstrated, which is 15-fold lower than the concentrations previously reported for similar systems. The successful demonstration of reversible self-assembly of peptide-PEG conjugate, aided subsequent work on the development of stimuli responsive membrane functionalised with SAP's.

Recommendations for future work on EL-5F-PEG conjugates

- The physicochemical properties such as tensile strength, viscosity and thermo sensitivity of the hydrogel formed due to the self-assembly of EL-5F can be characterized. This will give us a better understanding on the use of this pH-dependent hydrogel for various applications such as tissue engineering, drug delivery vehicles and templates for nanofabrication.

6.3 STIMULI RESPONSIVE MEMBRANE FUNCTIONALISED WITH SAP-PEG BIOCONJUGATE

This study focused on the development of a novel stimuli-responsive membrane using the pH-regulated self-assembly of peptide-PEG conjugate EL-5F-PEG-2K tethered to an Anodisc membrane surface. COOH groups were successfully bound to the membrane surface using multilayer deposition of polyelectrolytes, PAA and PAH. EL-5F-PEG-2K was then amine coupled to the COOH groups and this was confirmed using ATR-FTIR. Subsequent flux tests indicated no pH-dependant variation in buffer flux rates of the EL-5F-PEG-2K modified membrane. However, MWCO experiments using 72 and 29 kDa PEG were consistent with control of solute permeability through pH-dependent reversible self-assembly of tethered EL-5F-PEG-2K. Tests with polystyrene nanoparticles with surface tethered EL-5F and EL-5F-PEG-2K showed size transitions and aggregation of NPs with changes in pH, suggesting reversible self-assembly on the NP surface. Overall, this study indicates that the peptide can self-assemble when tethered on the membrane surface, but further work must be carried out to validate these outcomes.

Recommendations for future work on pH-responsive membranes

- The influence of reversible self-assembly with tethered EL-5F-PEG-5K on the permeability of the membrane should be tested. The presence of the longer spacer

(PEG-5K) in EL-5F-PEG-5K compared with EL-5F-PEG-2K, might provide increased steric flexibility, enabling self-assembly of the peptide.

- The protocol for COOH group immobilization should be optimized and quantified using other characterization techniques to achieve maximum surface density. Increased concentration of peptide coupled to the surface will potentially increase the effect of self-assembly on the permeability of the membrane.
- The bioconjugates can potentially be coupled to alternative membranes such as PC, polysulfone and cellulose, and the effect of self-assembly on the permeability of these membranes can be compared with that of the currently tested Anodisc membrane.
- Current work focused primarily on the tethering of SAPs on the membrane surface rather than within the pores. However, an alternative approach to influence membrane permeability would be to tether SAPs within the membrane pores rather than on the surface. This is expected to cause differences in membrane permeability for a wide range of solutes. A possible method to achieve this would be to perform NHS activation of COOH groups immobilised on membrane surface and block the NHS esters with ethanolamine in the absence of transmembrane flow. Subsequent, NHS activation and amine coupling of peptide-polymer bioconjugate under transmembrane flow can potentially result in the intrapore tethering of the bioconjugates.
- MWCO experiments can be carried out in a cross-flow filtration system and with an alternative molecular weight standard species (e.g. dextran) to decrease the effect of fouling on the permeability of the membrane.

REFERENCES

REFERENCES

Aggeli, A., Bell, M., Boden, N., Carrick, L. M., & Strong, A. E. (2003) Self-assembling peptide polyelectrolyte beta-sheet complexes form nematic hydrogels. *Angewandte Chemie-International Edition, 42*(45), 5603-5606.

Aggeli, A., Bell, M., Boden, N., Keen, J. N., Knowles, P. F., McLeish, T. C. B., Pitkeathly, M., & Radford, S. E. (1997) Responsive gels formed by the spontaneous self-assembly of peptides into polymeric beta-sheet tapes. *Nature, 386*(6622), 259-262.

Aggeli, A., Bell, M., Carrick, L. M., Fishwick, C. W. G., Harding, R., Mawer, P. J., Radford, S. E., Strong, A. E., & Boden, N. (2003) pH as a trigger of peptide β-sheet self-assembly and reversible switching between nematic and isotropic phases. *Journal of the American Chemical Society, 125*(32), 9619-9628.

Aggeli, A., Nyrkova, I. A., Bell, M., Harding, R., Carrick, L., McLeish, T. C. B., Semenov, A. N., & Boden, N. (2001) Hierarchical self-assembly of chiral rod-like molecules as a model for peptide beta-sheet tapes, ribbons, fibrils, and fibers. *Proceedings of the National Academy of Sciences of the United States of America, 98*(21), 11857-11862.

Ai, S. F., Lu, G., He, Q., & Li, J. B. (2003) Highly flexible polyelectrolyte nanotubes. *Journal of the American Chemical Society, 125*(37), 11140-11141.

Allongue, P., Delamar, M., Desbat, B., Fagebaume, O., Hitmi, R., Pinson, J., & Saveant, J. M. (1997) Covalent modification of carbon surfaces by aryl radicals generated from the electrochemical reduction of diazonium salts. *Journal of the American Chemical Society, 119*(1), 201-207.

Altman, M., Lee, P., Rich, A., & Zhang, S. G. (2000) Conformational behavior of ionic self-complementary peptides. *Protein Science, 9*(6), 1095-1105.

Al-Warhi, T. I., Al-Hazimi, H. M. A., & El-Faham, A. (2012) Recent development in peptide coupling reagents. *Journal of Saudi Chemical Society, 16*(2), 97-116.

Andrieux, C. P., & Pinson, J. (2003) The standard redox potential of the phenyl radical/anion couple. *Journal of the American Chemical Society, 125*(48), 14801-14806.

Aronoff, Y. G., Chen, B., Lu, G., Seto, C., Schwartz, J., & Bernasek, S. (1997) Stabilization of self-assembled monolayers of carboxylic acids on native oxides of metals. *Journal of the American Chemical Society, 119*(2), 259-262.

Ball, P. (1994) Materials science - polymers made to measure. *Nature, 367*(6461), 323-324.

Bayramoglu, G., Erdogan, H., & Arica, M. Y. (2008) Studies of adsorption of alkaline trypsin by poly(methacrylic acid) brushes on chitosan membranes. *Journal of Applied Polymer Science, 108*(1), 456-465.

Belfer, S., Fainshtain, R., Purinson, Y., Gilron, J., Nyström, M., & Mänttäri, M. (2004) Modification of NF membrane properties by in situ redox initiated graft polymerization with hydrophilic monomers. *Journal of Membrane Science, 239*(1), 55-64.

Bell, L. N. (1997) Peptide stability in solids and solutions. *Biotechnology Progress, 13*(4), 342-346.

Bernard, M. C., Chausse, A., Cabet-Deliry, E., Chehimi, M. M., Pinson, J., Podvorica, F., & Vautrin-Ul, C. (2003) Organic layers bonded to industrial, coinage, and noble metals through electrochemical reduction of aryldiazonium salts. *Chemistry of Materials, 15*(18), 3450-3462.

Biancalana, M., Makabe, K., Koide, A., & Koide, S. (2009) Molecular mechanism of thioflavin-T binding to the surface of β-rich peptide self-assemblies. *Journal of Molecular Biology, 385*(4), 1052-1063.

Bieri, C., Ernst, O. P., Heyse, S., Hofmann, K. P., & Vogel, H. (1999) Micropatterned immobilization of a G protein-coupled receptor and direct detection of G protein activation. *Nature Biotechnology, 17*(11), 1105-1108.

Blajiev, O. L., Ithurbide, A., Hubin, A., Van Haesendonck, C., & Terryn, H. (2008) XPS study of the assembling morphology of 3-hydroxy-3-phosphono-butiric acid tert-butyl ester on variously pretreated Al surfaces. *Progress in Organic Coatings, 63*(3), 272-281.

Borner, H. G. (2009) Strategies exploiting functions and self-assembly properties of bioconjugates for polymer and materials sciences. *Progress in Polymer Science, 34*(9), 811-851.

Bruening, M. L., Dotzauer, D. M., Jain, P., Ouyang, L., & Baker, G. L. (2008) Creation of functional membranes using polyelectrolyte multilayers and polymer brushes. *Langmuir, 24*(15), 7663-7673.

Burkoth, T. S., Benzinger, T. L. S., Jones, D. N. M., Hallenga, K., Meredith, S. C., & Lynn, D. G. (1998) C-terminal PEG blocks the irreversible step in beta-amyloid(10-35) fibrillogenesis. *Journal of the American Chemical Society, 120*(30), 7655-7656.

Carrick, L. M., Aggeli, A., Boden, N., Fisher, J., Ingham, E., & Waigh, T. A. (2007) Effect of ionic strength on the self-assembly, morphology and gelation of pH responsive beta-sheet tape-forming peptides. *Tetrahedron, 63*(31), 7457-7467.

Castelletto, V., Cheng, G., Furzeland, S., Atkins, D., & Hamley, I. W. (2012) Control of strand registry by attachment of PEG chains to amyloid peptides influences nanostructure. *Soft Matter, 8*(20), 5434-5438.

Castelletto, V., Gouveia, R. J., Connon, C. J., & Hamley, I. W. (2013) Self-assembly and bioactivity of a polymer/peptide conjugate containing the RGD cell adhesion motif and PEG. *European Polymer Journal, 49*(10), 2961-2967.

Castelletto, V., Newby, G. E., Zhu, Z., Hamley, I. W., & Noirez, L. (2010) Self-Assembly of pegylated peptide conjugates containing a modified amyloid beta-peptide fragment. *Langmuir, 26*(12), 9986-9996.

Chehimi, M. M., Lamouri, A., Picot, M., & Pinson, J. (2014) Surface modification of polymers by reduction of diazonium salts: polymethylmethacrylate as an example. *Journal of Materials Chemistry C, 2*(2), 356-363.

Chen, C. S., Mrksich, M., Huang, S., Whitesides, G. M., & Ingber, D. E. (1997) Geometric control of cell life and death. *Science, 276*(5317), 1425-1428.

Chen, J., Asano, M., Yamaki, T., & Yoshida, M. (2006) Preparation and characterization of chemically stable polymer electrolyte membranes by radiation-induced graft copolymerization of four monomers into ETFE films. *Journal of Membrane Science, 269*(1–2), 194-204.

Chen, Y. W., Deng, Q., Mao, J. C., Nie, H. R., Wu, L. C., Zhou, W. H., & Huang, B. W. (2007) Controlled grafting from poly(vinylidene fluoride) microfiltration membranes via reverse atom transfer radical polymerization and antifouling properties. *Polymer, 48*(26), 7604-7613.

Cheong, S. I., Kim, B., Lee, H., & Rhim, J. W. (2013) Physical adsorption of water-soluble polymers on hydrophobic polymeric membrane surfaces via salting-out effect. *Macromolecular Research, 21*(6), 629-635.

Childs, R. F., Mika, A. M., Pandey, A. K., McCrory, C., Mouton, S., & Dickson, J. M. (2001) Nanofiltration using pore-filled membranes: effect of polyelectrolyte composition on performance. *Separation and Purification Technology, 22-3*(1-3), 507-517.

Childs, R. F., Weng, J. F., Kim, M., & Dickson, J. M. (2002) Formation of pore-filled microfiltration membranes using a combination of modified interfacial polymerization and grafting. *Journal of Polymer Science Part a-Polymer Chemistry, 40*(2), 242-250.

Collier, J. H., & Messersmith, P. B. (2004) Self-assembling polymer-peptide conjugates: Nanostructural tailoring. *Advanced Materials, 16*(11), 907-910.

Combellas, C., Kanoufi, F., Mazouzi, D., Thiebault, A., Bertrand, P., & Medard, N. (2003) Surface modification of halogenated polymers. 4. Functionalisation of poly(tetrafluoroethylene) surfaces by diazonium salts. *Polymer, 44*(1), 19-24.

Cui, H., Muraoka, T., Cheetham, A. G., & Stupp, S. I. (2009) Self-assembly of giant peptide nanobelts. *Nano Letters, 9*(3), 945-951.

Cui, H. G., Webber, M. J., & Stupp, S. I. (2010) Self-assembly of peptide amphiphiles: From molecules to nanostructures to biomaterials. *Biopolymers, 94*(1), 1-18.

Dai, J. H., Baker, G. L., & Bruening, M. L. (2006) Use of porous membranes modified with polyelectrolyte multilayers as substrates for protein arrays with low nonspecific adsorption. *Analytical Chemistry, 78*(1), 135-140.

de Graaf, A. J., Mastrobattista, E., Vermonden, T., van Nostrum, C. F., Rijkers, D. T. S., Liskamp, R. M. J., & Hennink, W. E. (2012) Thermosensitive peptide-hybrid ABC block copolymers obtained by ATRP: Synthesis, self-assembly, and enzymatic degradation. *Macromolecules, 45*(2), 842-851.

Dotzauer, D. M., Dai, J. H., Sun, L., & Bruening, M. L. (2006) Catalytic membranes prepared using layer-by-layer adsorption of polyelectrolyte/metal nanoparticle films in porous supports. *Nano Letters, 6*(10), 2268-2272.

Dubas, S. T., & Schlenoff, J. B. (1999) Factors controlling the growth of polyelectrolyte multilayers. *Macromolecules, 32*(24), 8153-8160.

Elrahman, S. A., Anzinger, H., & Mutter, M. (1980) Relationship between conformation and physicochemical properties of polypeptides.1.Synthesis of homo-oligopeptides and co-oligopeptides by the liquid-phase method. *Biopolymers, 19*(1), 173-187.

Fletcher, N. L., Lockett, C. V., & Dexter, A. F. (2011) A pH-responsive coiled-coil peptide hydrogel. *Soft Matter, 7*(21), 10210-10218.

Foderà, V., Groenning, M., Vetri, V., Librizzi, F., Spagnolo, S., Cornett, C., Olsen, L., van de Weert, M., & Leone, M. (2008) Thioflavin T hydroxylation at basic pH and its effect on amyloid fibril detection. *The Journal of Physical Chemistry B, 112*(47), 15174-15181.

Frahn, J., Malsch, G., Matuschewski, H., Schedler, U., & Schwarz, H. H. (2004) Separation of aromatic/aliphatic hydrocarbons by photo-modified poly(acrylonitrile) membranes. *Journal of Membrane Science, 234*(1-2), 55-65.

Friebe, A., & Ulbricht, M. (2007) Controlled pore functionalization of poly(ethylene terephthalate) track-etched membranes via surface-initiated atom transfer radical polymerization. *Langmuir, 23*(20), 10316-10322.

Ghosh, A., Haverick, M., Stump, K., Yang, X. Y., Tweedle, M. F., & Goldberger, J. E. (2012) Fine-tuning the pH trigger of self-assembly. *Journal of the American Chemical Society, 134*(8), 3647-3650.

Ghosh, N., Gupta, G., Boopathi, M., Pal, V., Singh, A. K., Gopalan, N., & Goel, A. K. (2013) Surface plasmon resonance biosensor for detection of Bacillus anthracis, the causative agent of Anthrax from soil samples targeting protective antigen. *Indian Journal of Microbiology, 53*(1), 48-55.

Grabarek, Z., & Gergely, J. (1990) Zero-length crosslinking procedure with the use of active esters. *Analytical Biochemistry, 185*(1), 131-135.

Gravert, D. J., & Janda, K. D. (1997) Organic synthesis on soluble polymer supports: Liquid-phase methodologies. *Chemical Reviews, 97*(2), 489-509.

Greenfield, N. J. (2006) Using circular dichroism spectra to estimate protein secondary structure. *Nature Protocols, 1*(6), 2876-2890.

Griffete, N., Herbst, F., Pinson, J., Ammar, S., & Mangeney, C. (2011) Preparation of water-soluble magnetic nanocrystals using aryl diazonium salt chemistry. *Journal of the American Chemical Society, 133*(6), 1646-1649.

Hadjichristidis, N., Iatrou, H., Pitsikalis, M., & Sakellariou, G. (2009) Synthesis of well-defined polypeptide-based materials via the ring-opening polymerization of alpha-amino acid N-carboxyanhydrides. *Chemical Reviews, 109*(11), 5528-5578.

Hahner, G., Hofer, R., & Klingenfuss, I. (2001) Order and orientation in self-assembled long chain alkanephosphate monolayers adsorbed on metal oxide surfaces. *Langmuir, 17*(22), 7047-7052.

Hamley, I. W. (2014) PEG-Peptide Conjugates. *Biomacromolecules, 15*(5), 1543-1559.

Hamley, I. W., Ansari, I. A., Castelletto, V., Nuhn, H., Rösler, A., & Klok, H. A. (2005) Solution self-assembly of hybrid block copolymers containing poly(ethylene glycol) and amphiphilic β-strand peptide sequences. *Biomacromolecules, 6*(3), 1310-1315.

Hamley, I. W., Cheng, G., & Castelletto, V. (2011) A thermoresponsive hydrogel based on telechelic PEG end-capped with hydrophobic dipeptides. *Macromolecular Bioscience, 11*(8), 1068-1078.

Hartgerink, J. D., Beniash, E., & Stupp, S. I. (2002) Peptide-amphiphile nanofibers: A versatile scaffold for the preparation of self-assembling materials. *Proceedings of the National Academy of Sciences of the United States of America, 99*(8), 5133-5138.

Hauffman, T., Blajiev, O., Snauwaert, J., van Haesendonck, C., Hubin, A., & Terryn, H. (2008) Study of the self-assembling of n-octylphosphonic acid layers on aluminum oxide. *Langmuir, 24*(23), 13450-13456.

Hentschel, J., & Börner, H. G. (2006) Peptide-directed microstructure formation of polymers in organic media. *Journal of the American Chemical Society, 128*(43), 14142-14149.

Hentschel, J., Krause, E., & Borner, H. G. (2006) Switch-peptides to trigger the peptide guided assembly of poly(ethylene oxide)-peptide conjugates into tape structures. *Journal of the American Chemical Society, 128*(24), 7722-7723.

Hentschel, J., Krause, E., & Börner, H. G. (2006) Switch-peptides to trigger the peptide guided assembly of poly(ethylene oxide)-peptide conjugates into tape structures. *Journal of the American Chemical Society, 128*(24), 7722-7723.

Heredia, K. L., Tolstyka, Z. P., & Maynard, H. D. (2007) Aminooxy end-functionalized polymers synthesized by ATRP for chemoselective conjugation to proteins. *Macromolecules, 40*(14), 4772-4779.

Hol, W. G. J. (1985) The role of the alpha-helix dipole in protein function and structure. *Progress in Biophysics & Molecular Biology, 45*(3), 149-195.

Hol, W. G. J., Halie, L. M., & Sander, C. (1981) Dipoles of the alpha-helix and beta-sheet - their role in protein folding. *Nature, 294*(5841), 532-536.

Hollman, A. M., & Bhattacharyya, D. (2002) Controlled permeability and ion exclusion in microporous membranes functionalized with poly(L-glutamic acid). *Langmuir, 18*(15), 5946-5952.

Hollman, A. M., & Bhattacharyya, D. (2004) Pore assembled multilayers of charged polypeptides in microporous membranes for ion separation. *Langmuir, 20*(13), 5418-5424.

Hovgaard, M. B., Dong, M. D., Otzen, D. E., & Besenbacher, F. (2007) Quartz crystal microbalance studies of multilayer glucagon fibrillation at the solid-liquid interface. *Biophysical Journal, 93*(6), 2162-2169.

Hu, K., & Dickson, J. M. (2007) Development and characterization of poly(vinylidene fluoride)-poly (acrylic acid) pore-filled pH-sensitive membranes. *Journal of Membrane Science, 301*(1-2), 19-28.

Huang, R., Kostanski, L. K., Filipe, C. D. M., & Ghosh, R. (2009) Environment-responsive hydrogel-based ultrafiltration membranes for protein bioseparation. *Journal of Membrane Science, 336*(1-2), 42-49.

Isimjan, T. T., de Bruyn, J. R., & Gillies, E. R. (2010) Self-assembly of supramolecular polymers from beta-strand peptidomimetie-poly(ethylene oxide) hybrids. *Macromolecules, 43*(10), 4453-4459.

Ito, Y., Park, Y. S., & Imanishi, Y. (2000) Nanometer-sized channel gating by a self-assembled polypeptide brush. *Langmuir, 16*(12), 5376-5381.

Iwanade, A., Umeno, D., Saito, K., & Sugo, T. (2007) Protein binding to amphoteric polymer brushes grafted onto a porous hollow-fiber membrane. *Biotechnology Progress, 23*(6), 1425-1430.

Jadhav, S. A. (2011) Self-assembled monolayers (SAMs) of carboxylic acids: an overview. *Central European Journal of Chemistry, 9*(3), 369-378.

Jain, P., Baker, G. L., & Bruening, M. L. (2009). Applications of polymer brushes in protein analysis and purification *Annual Review of Analytical Chemistry* (Vol. 2, pp. 387-408).

Jain, P., Sun, L., Dai, J. H., Baker, G. L., & Bruening, M. L. (2007) High-capacity purification of his-tagged proteins by affinity membranes containing functionalized polymer brushes. *Biomacromolecules, 8*(10), 3102-3107.

Jessensky, O., Muller, F., & Gosele, U. (1998) Self-organized formation of hexagonal pore structures in anodic alumina. *Journal of the Electrochemical Society, 145*(11), 3735-3740.

Jing, P., Rudra, J. S., Herr, A. B., & Collier, J. H. (2008) Self-assembling peptide-polymer hydrogels designed from the coiled coil region of fibrin. *Biomacromolecules, 9*(9), 2438-2446.

Jones, M. W., Mantovani, G., Blindauer, C. A., Ryan, S. M., Wang, X. X., Brayden, D. J., & Haddleton, D. M. (2012) Direct peptide bioconjugation/pegylation at tyrosine with linear and branched polymeric diazonium salts. *Journal of the American Chemical Society, 134*(17), 7406-7413.

Kai, T., Yamaguchi, T., & Nakao, S. (2000) Preparation of organic/inorganic composite membranes by plasma-graft filling polymerization technique for organic-liquid separation. *Industrial & Engineering Chemistry Research, 39*(9), 3284-3290.

Kim, T. H., Swierczewska, M., Oh, Y., Kim, A., Jo, D. G., Park, J. H., Byun, Y., Sadegh-Nasseri, S., Pomper, M. G., Lee, K. C., & Lee, S. (2013) Mix to validate: A facile, reversible pegylation for fast screening of potential therapeutic proteins invivo. *Angewandte Chemie-International Edition, 52*(27), 6880-6884.

Kinstler, O. B., Brems, D. N., Lauren, S. L., Paige, A. G., Hamburger, J. B., & Treuheit, M. J. (1996) Characterization and stability of N-terminally pegylated rhG-CSF. *Pharmaceutical Research, 13*(7), 996-1002.

Kleine, B., Rapp, W., Wiesmuller, K. H., Edinger, M., Beck, W., Metzger, J., Ataulakhanov, R., Jung, G., & Bessler, W. G. (1994) Lipopeptide-polyoxyethylene conjugates as mitogens and adjuvants. *Immunobiology, 190*(1-2), 53-66.

Klok, H. A. (2005) Biological-synthetic hybrid block copolymers: Combining the best from two worlds. *Journal of Polymer Science Part a-Polymer Chemistry, 43*(1), 1-17.

Klok, H. A., Langenwalter, J. F., & Lecommandoux, S. (2000). *Macromolecules, 33*(21), 7819.

Knowles, T. P. J., Shu, W. M., Devlin, G. L., Meehan, S., Auer, S., Dobson, C. M., & Welland, M. E. (2007) Kinetics and thermodynamics of amyloid formation from direct measurements of fluctuations in fibril mass. *Proceedings of the National Academy of Sciences of the United States of America, 104*(24), 10016-10021.

Kopecky, E. M., Greinstetter, S., Pabinger, I., Buchacher, A., Romisch, J., & Jungbauer, A. (2006) Effect of oriented or random pegylation on bioactivity of a factor VIII inhibitor blocking peptide. *Biotechnology and Bioengineering, 93*(4), 647-655.

Krazinski, B. E., Radecki, J., & Radecka, H. (2011) Surface plasmon resonance based biosensors for exploring the influence of alkaloids on aggregation of amyloid-beta peptide. *Sensors, 11*(4), 4030-4042.

Kühnle, H., & Börner, H. G. (2009) Biotransformation on polymer–peptide conjugates: A versatile tool to trigger microstructure formation. *Angewandte Chemie International Edition, 48*(35), 6431-6434.

Kuhnle, R. I., & Borner, H. G. (2011) Calcium ions to remotely control the reversible switching of secondary and quaternary structures in bioconjugates. *Angewandte Chemie-International Edition, 50*(19), 4499-4502.

Le Droumaguet, B., & Nicolas, J. (2010) Recent advances in the design of bioconjugates from controlled/living radical polymerization. *Polymer Chemistry, 1*(5), 563-598.

Lehn, J. M. (1993) Supramolecular chemistry. *Science, 260*(5115), 1762-1763.

Liang, J., Wu, W. L., Xu, X. D., Zhuo, R. X., & Zhang, X. Z. (2014) pH Responsive micelle self-assembled from a new amphiphilic peptide as anti-tumor drug carrier. *Colloids and Surfaces B-Biointerfaces, 114*, 398-403.

Lightfoot, E. N., & Moscariello, J. S. (2004) Bioseparations. *Biotechnology and Bioengineering, 87*(3), 259-273.

Lim, M. S., Feng, K., Chen, X. Q., Wu, N. Q., Raman, A., Nightingale, J., Gawalt, E. S., Korakakis, D., Hornak, L. A., & Timperman, A. T. (2007) Adsorption and desorption of stearic acid self-assembled monolayers on aluminum oxide. *Langmuir, 23*(5), 2444-2452.

Lin, Y., Swan, J. E., & Fee, C. J. (2006) pH responsive microcapsules for controlled release. *33rd Annual meeting of the controlled release society, Vienna*.

Liu, F., Du, C. H., Zhu, B. K., & Xu, Y. Y. (2007) Surface immobilization of polymer brushes onto porous poly(vinylidene fluoride) membrane by electron beam to improve the hydrophilicity and fouling resistance. *Polymer, 48*(10), 2910-2918.

Liu, G., & Freund, M. S. (1996) Nucleophilic substitution reactions of polyaniline with substituted benzenediazonium ions: A facile method for controlling the surface chemistry of conducting polymers. *Chemistry of Materials, 8*(6), 1164-&.

Luo, Z., & Zhang, S. (2012) Designer nanomaterials using chiral self-assembling peptide systems and their emerging benefit for society. *Chemical Society Reviews, 41*(13), 4736-4754.

Lutz, J., Börner, H. G., & Weichenhan, K. (2007) 'Click' bioconjugation of a well-defined synthetic polymer and a protein transduction domain. *Australian Journal of Chemistry, 60*(6), 410-413.

Lutz, J. F. (2007) 1,3-dipolar cycloadditions of azides and alkynes: A universal ligation tool in polymer and materials science. *Angewandte Chemie-International Edition, 46*(7), 1018-1025.

Made, V., Els-Heindl, S., & Beck-Sickinger, A. G. (2014) Automated solid-phase peptide synthesis to obtain therapeutic peptides. *Beilstein Journal of Organic Chemistry, 10*, 1197-1212.

Mahouche-Chergui, S., Gam-Derouich, S., Mangeney, C., & Chehimi, M. M. (2011) Aryl diazonium salts: a new class of coupling agents for bonding polymers, biomacromolecules and nanoparticles to surfaces. *Chemical Society Reviews, 40*(7), 4143-4166.

Malaisamy, R., & Bruening, M. L. (2005) High-flux nanofiltration membranes prepared by adsorption of multilayer polyelectrolyte membranes on polymeric supports. *Langmuir, 21*(23), 10587-10592.

Martens, A. A., Portale, G., Werten, M. W. T., de Vries, R. J., Eggink, G., Stuart, M. A. C., & de Wolf, F. A. (2009) Triblock protein copolymers forming supramolecular nanotapes and pH-responsive gels. *Macromolecules, 42*(4), 1002-1009.

Meijer, J. T., Henckens, M., Minten, I. J., Lowik, D., & van Hest, J. C. M. (2007) Disassembling peptide-based fibres by switching the hydrophobic-hydrophilic balance. *Soft Matter, 3*(9), 1135-1137.

Mika, A. M., Childs, R. F., & Dickson, J. M. (2002) Salt separation and hydrodynamic permeability of a porous membrane filled with pH-sensitive gel. *Journal of Membrane Science, 206*(1-2), 19-30.

Mika, A. M., Childs, R. F., Dickson, J. M., McCarry, B. E., & Gagnon, D. R. (1995) A new class of polyelectrolyte-filled microfiltration membranes with environmentally controlled porosity. *Journal of Membrane Science, 108*(1-2), 37-56.

Mika, A. M., Childs, R. F., Dickson, J. M., McCarry, B. E., & Gagnon, D. R. (1997) Porous, polyelectrolyte-filled membranes: Effect of cross-linking on flux and separation. *Journal of Membrane Science, 135*(1), 81-92.

Miller, C. R., Vogel, R., Surawski, P. P. T., Corrie, S. R., Ruhmann, A., & Trau, M. (2005) Biomolecular screening with novel organosilica microspheres. *Chemical Communications*(38), 4783-4785.

Miranda, L. P., Shao, H. Y., Williams, J., Chen, S. Y., Kong, T., Garcia, R., Chinn, Y., Fraud, N., O'Dwyer, B., Ye, J., Wilken, J., Low, D. E., Cagle, E. N., Carnevali, M., Lee, A., Song, D., Kung, A., Bradburne, J. A., Paliard, X., & Kochendoerfer, G. G. (2007) A chemical approach to the pharmaceutical optimization of an anti-HIV protein. *Journal of the American Chemical Society, 129*(43), 13153-13159.

Morar, A. S., Schrimsher, J. R. L., & Chavez, M. D. (2006) PEGylation of proteins: A structural approach. *Biopharm International, 19*(4), 34-+.

Nakayama, H., Kaetsu, I., Uchida, K., Oishibashi, M., & Matsubara, Y. (2003) Intelligent biomembranes for nicotine releases by radiation curing. *Radiation Physics and Chemistry, 67*(3-4), 367-370.

Ng, L. T., Nakayama, H., Kaetsu, I., & Uchida, K. (2005) Photocuring of stimulus responsive membranes for controlled-release of drugs having different molecular weights. *Radiation Physics and Chemistry, 73*(2), 117-123.

Ng, L. T., & Ng, K. S. (2008) Photo-cured pH-responsive polyampholyte-coated membranes for controlled release of drugs with different molecular weights and charges. *Radiation Physics and Chemistry, 77*(2), 192-199.

Niculescu-Duvaz, D., Getaz, J., & Springer, C. J. (2008) Long functionalized poly(ethylene glycol)s of defined molecular weight: Synthesis and application in solid-phase synthesis of conjugates. *Bioconjugate Chemistry, 19*(4), 973-981.

Nolan, J. P., Lauer, S., Prossnitz, E. R., & Sklar, L. A. (1999) Flow cytometry: a versatile tool for all phases of drug discovery. *Drug Discovery Today, 4*(4), 173-180.

Nowinski, A. K., Sun, F., White, A. D., Keefe, A. J., & Jiang, S. (2012) Sequence, structure, and function of peptide self-assembled monolayers. *Journal of the American Chemical Society, 134*(13), 6000-6005.

Pagel, K., Seri, T., von Berlepsch, H., Griebel, J., Kirmse, R., Böttcher, C., & Koksch, B. (2008) How metal ions affect amyloid formation: Cu2+- and Zn2+-sensitive peptides. *ChemBioChem, 9*(4), 531-536.

Paik, W. K., Han, S. B., Shin, W., & Kim, Y. S. (2003) Adsorption of carboxylic acids on gold by anodic reaction. *Langmuir, 19*(10), 4211-4216.

Palomo, J. M. (2014) Solid-phase peptide synthesis: an overview focused on the preparation of biologically relevant peptides. *Rsc Advances, 4*(62), 32658-32672.

Pauling, L. (1960). Nature of the chemical bond and the molecular crystals: An introduction to model chemistry: Cornell University: Ithaca, NY.

Paulo, T. d. F., de Sousa, T. P., de Abreu, D. S., Felício, N. H., Bernhardt, P. V., de F. Lopes, L. G., Sousa, E. H. S., & Diógenes, I. C. N. (2013) Electrochemistry, surface plasmon resonance, and quartz crystal microbalance: An associative study on cytochrome c adsorption on pyridine tail-group monolayers on gold. *The Journal of Physical Chemistry B, 117*(29), 8673-8680.

Pawsey, S., Yach, K., Halla, J., & Reven, L. (2000) Self-assembled monolayers of alkanoic acids: A solid-state NMR study. *Langmuir, 16*(7), 3294-3303.

Pechar, M., Kopečková, P., Joss, L., & Kopeček, J. (2002) Associative diblock copolymers of poly(ethylene glycol) and coiled-coil peptides. *Macromolecular Bioscience, 2*(5), 199-206.

Ponnumallayan, P., & Fee, C. J. (2014) Reversible and rapid pH-regulated self-assembly of a poly(ethylene glycol)-peptide bioconjugate. *Langmuir, 30(47), 14250-14256.*

Przybyla, D. E., & Chmielewski, J. (2010) Metal-triggered collagen peptide disk formation. *Journal of the American Chemical Society, 132*(23), 7866-7867.

Qiao, Z.-Y., Qiao, S.-L., Fan, G., Fan, Y.-S., Chen, Y., & Wang, H. (2014) One-pot synthesis of pH-sensitive poly(RGD-co-[small beta]-amino ester)s for targeted intracellular drug delivery. *Polymer Chemistry, 5*(3), 844-853.

Radu-Wu, L. C., Yang, J., Wu, K., & Kopecek, J. (2009) Self-assembled hydrogels from poly N-(2-hydroxypropyl)methacrylamide grafted with beta-sheet peptides. *Biomacromolecules, 10*(8), 2319-2327.

Radu, L. C., Yang, J. Y., & Kopecek, J. (2009) Self-assembling diblock copolymers of poly N-(2-hydroxypropyl)methacrylamide and a beta-sheet peptide. *Macromolecular Bioscience, 9*(1), 36-44.

Rosler, A., Klok, H. A., Hamley, I. W., Castelletto, V., & Mykhaylyk, O. O. (2003) Nanoscale structure of poly(ethylene glycol) hybrid block copolymers containing amphiphilic beta-strand peptide sequences. *Biomacromolecules, 4*(4), 859-863.

Sadasivan, V., Richter, C. P., Menon, L., & Williams, P. F. (2005) Electrochemical self-assembly of porous alumina templates. *Aiche Journal, 51*(2), 649-655.

Salick, D. A., Kretsinger, J. K., Pochan, D. J., & Schneider, J. P. (2007) Inherent antibacterial activity of a peptide-based beta-hairpin hydrogel. *Journal of the American Chemical Society, 129*(47), 14793-14799.

Sato, H. (2002) Enzymatic procedure for site-specific pegylation of proteins. *Advanced Drug Delivery Reviews, 54*(4), 487-504.

Schlenoff, J. B., & Dubas, S. T. (2001) Mechanism of polyelectrolyte multilayer growth: Charge overcompensation and distribution. *Macromolecules, 34*(3), 592-598.

Shi, Q., Su, Y. L., Zhu, S. P., Li, C., Zhao, Y. Y., & Jiang, Z. Y. (2007) A facile method for synthesis of pegylated polyethersulfone and its application in fabrication of antifouling ultrafiltration membrane. *Journal of Membrane Science, 303*(1-2), 204-212.

Shu, J. Y., Panganiban, B., & Xu, T. (2013) Peptide-polymer conjugates: From fundamental science to application. *Annual Review of Physical Chemistry, Vol 64, 64*, 631-657.

Shustak, G., Domb, A. J., & Mandler, D. (2004) Preparation and characterization of n-alkanoic acid self-assembled monolayers adsorbed on 316L stainless steel. *Langmuir, 20*(18), 7499-7506.

Simons, B. M., Lehr, J., Garrett, D. J., & Downard, A. J. (2014) Formation of thick aminophenyl films from aminobenzenediazonium ion in the absence of a reduction source. *Langmuir, 30*(17), 4989-4996.

Smeenk, J. M., Otten, M. B. J., Thies, J., Tirrell, D. A., Stunnenberg, H. G., & van Hest, J. C. M. (2005) Controlled assembly of macromolecular beta-sheet fibrils. *Angewandte Chemie-International Edition, 44*(13), 1968-1971.

Stutz, C., Meszynska, A., Lutz, J. F., & Borner, H. G. (2013) Convenient routes to efficiently N-pegylated peptides. *Acs Macro Letters, 2*(8), 641-644.

Suryanarayan, S., Mika, A. M., & Childs, R. F. (2006) Gel-filled hollow fiber membranes for water softening. *Journal of Membrane Science, 281*(1-2), 397-409.

Tang, C., Ulijn, R. V., & Saiani, A. (2011) Effect of glycine substitution on Fmoc–diphenylalanine self-assembly and gelation properties. *Langmuir, 27*(23), 14438-14449.

Tao, Y. T., Huang, C. Y., Chiou, D. R., & Chen, L. J. (2002) Infrared and atomic force microscopy imaging study of the reorganization of self assembled monolayers of carboxylic acids on silver surface. *Langmuir, 18*(22), 8400-8406.

Thayer, A. M. (2011) Improving peptides. *Chemical & Engineering News Archive, 89*(22), 13-20.

Thumshirn, G., Hersel, U., Goodman, S. L., & Kessler, H. (2003) Multimeric cyclic RGD peptides as potential tools for tumor targeting: Solid-phase peptide synthesis and chemoselective oxime ligation. *Chemistry-a European Journal, 9*(12), 2717-2725.

Ting, G. G., Acton, O., Ma, H., Ka, J. W., & Jen, A. K. Y. (2009) Study on the formation of self-assembled monolayers on sol-gel processed hafnium oxide as dielectric layers. *Langmuir, 25*(4), 2140-2147.

Truong, M. Y., Dutta, N. K., Choudhury, N. R., Kim, M., Elvin, C. M., Hill, A. J., Thierry, B., & Vasilev, K. (2010) A pH-responsive interface derived from resilin-mimetic protein Rec1-resilin. *Biomaterials, 31*(15), 4434-4446.

Tzokova, N., Fernyhough, C. M., Butler, M. F., Armes, S. P., Ryan, A. J., Topham, P. D., & Adams, D. J. (2009) The effect of PEO length on the self-assembly of poly(ethylene oxide)-tetrapeptide conjugates prepared by "click" chemistry. *Langmuir, 25*(18), 11082-11089.

Tzokova, N., Fernyhouph, C. M., Topham, P. D., Sandon, N., Adams, D. J., Butler, M. F., Armes, S. P., & Ryan, A. J. (2009) Soft hydrogels from nanotubes of poly(ethylene oxide)-tetraphenylalanine conjugates prepared by click chemistry. *Langmuir, 25*(4), 2479-2485.

Ulbricht, M., & Schwarz, H. H. (1997) Novel high performance photo-graft composite membranes for separation of organic liquids by pervaporation. *Journal of Membrane Science, 136*(1-2), 25-33.

van der Sman, R. G. M., Vollebregt, H. M., Mepschen, A., & Noordman, T. R. (2012) Review of hypotheses for fouling during beer clarification using membranes. *Journal of Membrane Science, 396*, 22-31.

Vandermeulen, G. W. M., Kim, K. T., Wang, Z., & Manners, I. (2006) Metallopolymer-peptide conjugates: Synthesis and self-assembly of polyferrocenylsilane graft and block copolymers containing a beta-sheet forming Gly-Ala-Gly-Ala tetrapeptide segment. *Biomacromolecules, 7*(4), 1005-1010.

Vandermeulen, G. W. M., & Klok, H.-A. (2004) Peptide/protein hybrid materials: Enhanced control of structure and improved performance through conjugation of biological and synthetic polymers. *Macromolecular Bioscience, 4*(4), 383-398.

Vandermeulen, G. W. M., Tziatzios, C., & Klok, H.-A. (2003) Reversible self-organization of poly(ethylene glycol)-based hybrid block copolymers mediated by a de novo four-stranded α-helical coiled coil motif. *Macromolecules, 36*(11), 4107-4114.

Vauthey, S., Santoso, S., Gong, H. Y., Watson, N., & Zhang, S. G. (2002) Molecular self-assembly of surfactant-like peptides to form nanotubes and nanovesicles. *Proceedings of the National Academy of Sciences of the United States of America, 99*(8), 5355-5360.

Veronese, F. M., & Harris, J. M. (2002) Preface - Introduction and overview of peptide and protein pegylation. *Advanced Drug Delivery Reviews, 54*(4), 453-456.

Veronese, F. M., & Pasut, G. (2005) PEGylation, successful approach to drug delivery. *Drug Discovery Today, 10*(21), 1451-1458.

Wandera, D., Wickramasinghe, S. R., & Husson, S. M. (2010) Stimuli-responsive membranes. *Journal of Membrane Science, 357*(1-2), 6-35.

Waterhouse, S. H., & Gerrard, J. A. (2004) Amyloid fibrils in bionanotechnology. *Australian Journal of Chemistry, 57*(6), 519-523.

Whitesides, G. M., Mathias, J. P., & Seto, C. T. (1991) Molecular self-assembly and nanochemistry - A chemical strategy for the synthesis of nanostructures. *Science, 254*(5036), 1312-1319.

Winnik, F. M., Morneau, A., Mika, A. M., Childs, R. F., Roig, A., Molins, E., & Ziolo, R. F. (1998) Polyacrylic acid pore-filled microporous membranes and their use in membrane-mediated synthesis of nanocrystalline ferrihydrite. *Canadian Journal of Chemistry-Revue Canadienne De Chimie, 76*(1), 10-17.

Xu, J. Z., Moon, S. H., Jeong, B., & Sohn, Y. S. (2007) Thermosensitive micelles from pegylated oligopeptides. *Polymer, 48*(13), 3673-3678.

Xu, T. W. (2005) Ion exchange membranes: State of their development and perspective. *Journal of Membrane Science, 263*(1-2), 1-29.

Yagci, Y., Jockusch, S., & Turro, N. J. (2010) Photoinitiated polymerization: Advances, challenges, and opportunities. *Macromolecules, 43*(15), 6245-6260.

Yan, C., Zharnikov, M., Golzhauser, A., & Grunze, M. (2000) Preparation and characterization of self-assembled monolayers on indium tin oxide. *Langmuir, 16*(15), 6208-6215.

Yang, J., Wu, K., Konak, C., & Kopecek, J. (2008) Dynamic light scattering study of self-assembly of HPMA hybrid graft copolymers. *Biomacromolecules, 9*(2), 510-517.

Yemini, M., Reches, M., Rishpon, J., & Gazit, E. (2004) Novel electrochemical biosensing platform using self-assembled peptide nanotubes. *Nano Letters, 5*(1), 183-186.

Yu, T.-B., Bai, J. Z., & Guan, Z. (2009) Cycloaddition-promoted self-assembly of a polymer into well-defined β sheets and hierarchical nanofibrils. *Angewandte Chemie, 121*(6), 1117-1121.

Zaykov, A. N., Popp, B. V., & Ball, Z. T. (2010) Helix induction by dirhodium: Access to biocompatible metallopeptides with defined secondary structure. *Chemistry-a European Journal, 16*(22), 6651-6659.

Zhang, G. L., Ma, J. B., Li, Y. H., & Wang, Y. N. (2003) Synthesis and characterization of poly(L-alanine)-block-poly(ethylene glycol) monomethyl ether as amphiphilic biodegradable co-polymers. *Journal of Biomaterials Science-Polymer Edition, 14*(12), 1389-1400.

Zhang, H. J., & Ito, Y. (2001) pH control of transport through a porous membrane self-assembled with a poly(acrylic acid) loop brush. *Langmuir, 17*(26), 8336-8340.

Zhang, S. G. (2002) Emerging biological materials through molecular self-assembly. *Biotechnology Advances, 20*(5-6), 321-339.

Zhang, S. G. (2003) Fabrication of novel biomaterials through molecular self-assembly. *Nature Biotechnology, 21*(10), 1171-1178.

Zhang, S. G., & Altman, M. (1999) Peptide self-assembly in functional polymer science and engineering. *Reactive & Functional Polymers, 41*(1-3), 91-102.

Zhang, S. G., & Altman, M. (2001). *Self-assembling peptide systems in biology and biomedical engineering*. Dordrecht: Springer.

Zhang, S. G., Holmes, T., Lockshin, C., & Rich, A. (1993) Spontaneous assembly of a self-complementary oligopeptide to form a stable macroscopic membrane. *Proceedings of the National Academy of Sciences of the United States of America, 90*(8), 3334-3338.

Zhang, S. G., Holmes, T. C., Dipersio, C. M., Hynes, R. O., Su, X., & Rich, A. (1995) Self-complementary oligopeptide matrices support mammalian-cell attachment. *Biomaterials, 16*(18), 1385-1393.

Zhang, S. G., Lockshin, C., Herbert, A., Winter, E., & Rich, A. (1992) Zuotin, a putative z-DNA binding-protein in saccharomyces-cerevisiae. *Embo Journal, 11*(10), 3787-3796.

Zhang, S. G., & Rich, A. (1997) Direct conversion of an oligopeptide from a beta-sheet to an alpha-helix: A model for amyloid formation. *Proceedings of the National Academy of Sciences of the United States of America, 94*(1), 23-28.

Zhao, B., & Brittain, W. J. (2000) Polymer brushes: surface-immobilized macromolecules. *Progress in Polymer Science, 25*(5), 677-710.

Zhao, C. S., Nie, S. Q., Tang, M., & Sun, S. D. (2011) Polymeric pH-sensitive membranes-A review. *Progress in Polymer Science, 36*(11), 1499-1520.

Zhao, Y., Yokoi, H., Tanaka, M., Kinoshita, T., & Tan, T. W. (2008) Self-assembled pH-responsive hydrogels composed of the RATEA16 peptide. *Biomacromolecules, 9*(6), 1511-1518.

Zhou, J. S., Childs, R. F., & Mika, A. M. (2005) Pore-filled nanotiltration membranes based on poly(2-acrylamido-2-methylpropanesulfonic acid) gels. *Journal of Membrane Science, 254*(1-2), 89-99.

Zhu, L. P., Dong, H. B., Wei, X. Z., Yi, Z., Zhu, B. K., & Xu, Y. Y. (2008) Tethering hydrophilic polymer brushes onto PPESK membranes via surface-initiated atom transfer radical polymerization. *Journal of Membrane Science, 320*(1-2), 407-415.

Zimenkov, Y., Dublin, S. N., Ni, R., Tu, R. S., Breedveld, V., Apkarian, R. P., & Conticello, V. P. (2006) Rational design of a reversible pH-responsive switch for peptide self-assembly. *Journal of the American Chemical Society, 128*(21), 6770-6771.

Zou, D. W., Tie, Z. X., Qin, M., Lu, C. M., & Wang, W. (2009) Effect of Phosphate on the Self-Assembly of Peptide EMK16-II. *Chinese Physics Letters, 26*(8).

APPENDICES

APPENDIX A: EL-5F CONCENTRATION CALIBRATION CURVE

A calibration curve was plotted using absorbance at 224 nm for known concentrations of EL-5F (Figure A-1), with the absence of aromatic amino acids tryptophan or tyrosine resulting in no UV absorbance at 280 nm. This calibration curve was used to determine unknown concentrations of EL-5F and the bioconjugates in forthcoming experiments (see Section 4.2.2).

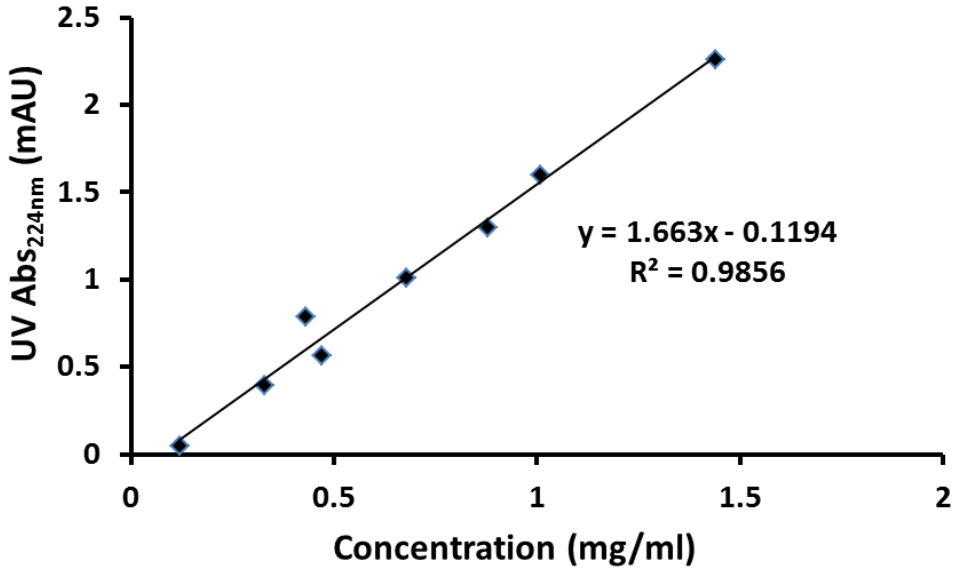

Figure A-1: EL-5F calibration curve.

APPENDIX B: BOC DEPROTECTION OF EL-5F-PEG-2K

The BOC deprotection on the primary amine at the free end of the PEG-2K of conjugate EL-5F-PEG-2K was confirmed using NMR analysis. The disappearance of peak at 1.3 ppm indicates the removal of BOC (Figure B-1). This can potentially enable the coupling of free amine in EL-5F-PEG-2K to the COOH groups on different substrates or membrane surfaces.

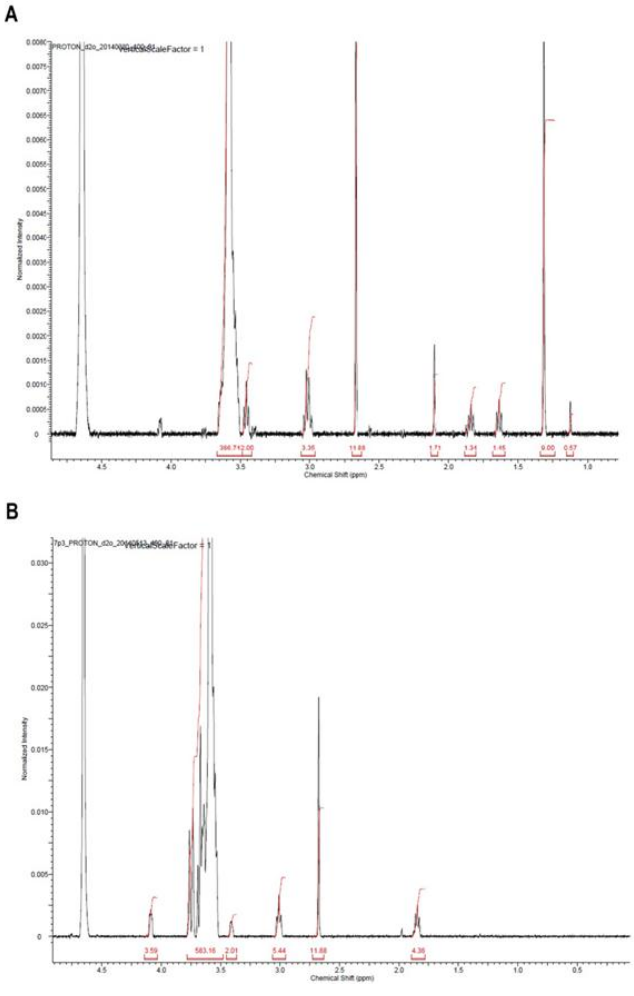

Figure B-1: Proton NMR of A) starting material, EL-5F-PEG-2K with BOC (peak seen at 1.3 ppm), B) product EL-5F-PEG-2K after the complete removal of BOC (peak disappears at 1.3 ppm).

APPENDIX C: REVERSIBLE CONFORMATIONAL SHIFT OF BIOCONJUGATE EL-5F-PEG-5K

Similar to the peptide EL-5F and bioconjugate EL-5F-PEG-2K, sustained pH-regulated shifts between random coil and β sheet was observed in EL-5F-PEG-5K as well (Figure C-1).

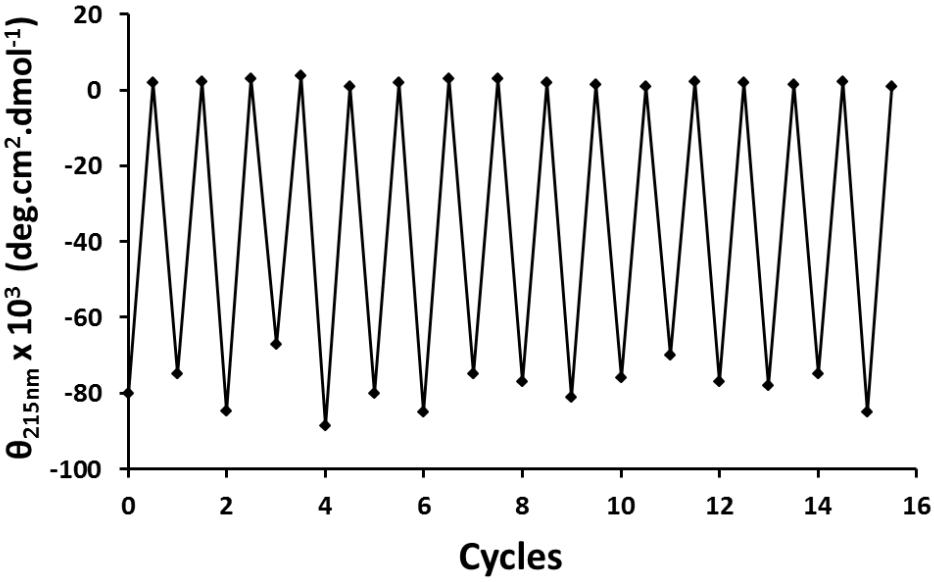

Figure C-1: CD negative intensity at 215 nm, indicating the extent of β sheet (θ_{215nm} < -60 x 10^3) to random coil ($\theta_{215nm} \approx 0$) transition with 16 repeated secondary structure shifts of EL-5F-PEG-5K, mediated by corresponding changes in pH from below 5 to above 7.

APPENDIX D

Reversible and rapid pH-regulated self-assembly of a poly(ethylene glycol)-peptide bioconjugate – *Langmuir*

Chapter 4 in this thesis is extracted from co-authored work, Ponnumallayan, P., Fee, C.J. (2014). Reversible and Rapid pH-Regulated Self-Assembly of a Poly(Ethylene Glycol)-Peptide Bioconjugate, *Langmuir, 30(47),14250-14256* .